Doctoral Thesis
2013

Adaptive Sensor Networks for Mobile Target Localization and Tracking

David Moreno Salinas
Engineer in Automatic Control and Electronics

Departamento de Informática y Automática
E.T.S.I. Informática, UNED

Advisors: Joaquín Aranda Almansa
António M. Pascoal

Departamento de Informática y Automática
Escuelta Técnica Superior de Ingeniería Informática

Adaptive Sensor Networks for Mobile Target Localization and Tracking

David Moreno Salinas
Engineer in Automatic Control and Electronics

Advisors: Joaquín Aranda Almansa
António M. Pascoal

Es mi deseo agradecer en primer lugar a mis directores Joaquín Aranda y Antonio Pascoal por el apoyo y ayuda para la realización de este trabajo, así como todo el tiempo que me han dedicado siempre que lo he necesitado y su orientación, sin la que no hubiera sido posible realizar esta tesis.
También quiero agradecer a todos los compañeros del Departamento de Informática y Automática por todo el tiempo y los buenos momentos pasados juntos durante todos estos años. De igual manera también quisiera mostrar mi agradecimiento a la gente del Instituto Superior Técnico de Lisboa, que siempre me hicieron sentir como uno más en cada una de las ocasiones en que he podido visitarlos.
Finalmente, que no en último lugar, quiero agradecer a mi familia su apoyo duante todos estos años de estudio, y en especial a Nuria, que ha estado apoyándome en todo lo que he necesitado, ayudándome a superar los momentos más duros, gracias por estar siempre a mi lado.
Muchas gracias a todos.

ABSTRACT

Worldwide, there has been increasing interest in the use of Autonomous Underwater Vehicles (AUVs) to drastically change the means available for ocean exploration and exploitation. These vehicles are becoming ubiquitous due in part to the flexibility and versatility that a number of them display in the execution of individual and cooperative tasks. These characteristics, coupled with the fact that their use avoids placing human lives at risk, makes them quite attractive in a number of missions that include pipeline inspection, seabed surveying, and archaeological research, to name but a few. Central to the operation of some classes of AUVs is the availability of good underwater positioning systems to localize one or more vehicles simultaneously based on information received on-board a support ship or a set of autonomous surface vehicles. In an interesting operational scenario the AUV/s is/are equipped with an acoustic pinger and the set of surface vehicles carry a network of acoustic receivers that measure the ranges between the emitter and each of the receivers.

Motivated by these considerations, in this work we address the problem of determining the optimal geometric configuration of sensor networks, in 2D and 3D, that will maximize the range/bearing-related information available for single or multiple target positioning. It is assumed that the range/bearings measurements are corrupted by white Gaussian noise, the variance of which is distance-dependent. Furthermore, we also assume that an initial estimate of the target position is available, albeit with uncertainty. The Fisher Information Matrix and the maximization of its determinant or the minimization of the trace of the CRLB matrix are used to determine the sensor configuration that yields the most accurate "expected" positioning of the target, which is expressed by a probabilistic distribution. It is shown that the optimal configurations lend themselves to interesting geometrical interpretations and that the "spreading" of the sensor configuration depends explicitly on the intensity of the measurement noise, and on the probabilistic distribution that defines the target position. The scenario of underwater target positioning by a surface sensor network is studied along this work as an example of application of the methodology developed. Moreover, the special and particular scenario of a single surface sensor is studied separately due to the growing importance of this problem in the last few years.

RESUMEN

Actualmente, existe un creciente interés en el uso de vehículos autónomos submarinos (AUVs) para cambiar de forma drástica los medios disponibles para la exploración y explotación de los océanos. Esta clase de vehículos está presente en múltiples aplicaciones debido a la flexibilidad y versatilidad que éstos demuestran en la ejecución de numerosas tareas, tanto individuales como colectivas. Estas características, junto con el hecho que su uso evita poner vidas humanas en peligro, hacen que su uso resulte muy atractivo en múltiples actividades, como pueden ser la inspección de tuberías, el estudio del fondo marino, la investigación arqueológica, por nombrar algunas. Para el correcto funcionamiento de diferentes clases de AUVs es fundamental la disponibilidad de buenos sistemas de posicionamiento submarinos con los que localizar uno o más vehículos de forma simultánea mediante información recibida a bordo de un barco de soporte o de un conjunto de vehículos autónomos de superficie. En un escenario operacional interesante, el AUV o AUVs pueden estar equipados con un emisor acústico de modo que el conjunto de vehículos de superficie, que transporta una red de sensores acústicos, mida las distancias entre emisor o emisores y cada uno de los sensores.

De acuerdo a estas consideraciones, en este trabajo se estudia el problema de determinar la configuración geométrica óptima de una red de sensores, tanto en 2D como en 3D, que maximice la información existente en medidas de distancias o ángulos para realizar el posicionamiento de uno o varios objetivos. Se asume que las medidas de distancias y ángulos están corruptas por ruido blanco Gausiano cuya varianza es dependiente de la distancia. Además, se asume que la posición del objetivo se conoce inicialmente, aunque con incertidumbre. La Matriz de Información de Fisher (FIM) y la maximización de su determinante o la minimización de la traza del CRLB se usarán para determinar las configuraciones de los sensores que proporcionan una estimación de la posición de los objetivos más precisa. La posición de estos objetivos vendrá expresada por una distribución de probabilidad. Se muestra a lo largo del trabajo cómo las configuraciones óptimas permiten una interesante interpretación geométrica y cómo la distribución de los sensores depende explícitamente de la intensidad del ruido de medida y de la distribución de probabilidad que define a cada uno de los objetivos. El escenario de posicionamiento de objetivos submarinos por una red de sensores de superficie se ha estudiado a lo largo del trabajo como ejemplo de aplicación de la metodología desarrollada. Es más, el caso especial y particular de un único sensor de superficie se estudia de forma separada debido al creciente interés en este problema a lo largo de los últimos años.

Contents

List of Figures

List of Tables

Chapter 1

INTRODUCTION

Water is the largest component of the surface of our planet so that 70 per cent of the planet is covered by this liquid element that appears in different forms like rivers, lakes and, mainly, oceans. Despite the above, the oceans are the least known part of the surface of our planet, and they harbour the most important mineral, energy, and food resources, and play a key role in the regulation of the climate. For this reason, in recent years, the way in which the oceans are explored and exploited is changing drastically to afford new methods and tools for sampling and interacting with the marine environment in scientific and commercial areas. Recent advances in marine robotics, sensors, computers, communications, and information systems are being applied to develop sophisticated technologies that will lead to safer, faster, and far more efficient ways of exploring the ocean frontier, especially in hazardous conditions. As part of this trend, there has been a surge of interest worldwide in the development of autonomous underwater vehicles (AUVs) capable of roaming the oceans freely, collecting relevant data at an unprecedented scale and reacting to on-line detected events. The areas in which the marine robots are spreading their use, due to the versatility and good performance they show in many demanding tasks at sea, cover a wide range of applications that goes from gas and oil pipeline inspection to biological investigation, and even in a number of areas pertaining to the preservation of the underwater cultural heritage. Namely, in the detection and mapping of shipwrecks or submerged human-made structures. One of the most interesting and challenging applications of marine robots its their use in collaborative tasks between a number of robots, even in interaction with humans. In the latter case the robots play the role of guardians in charge of guiding humans underwater and/or acting as carriers of equipment to be delivered upon request. It is indeed the moment in which the oceans and their resources can be understood and exploited as never before and at the same time afford policy makers the instruments that are needed for a holistic governance of the oceans.

The technical requirements for the marine robots, and thus the requirements to the developers of these systems, together with the mission that they must carry out, are very demanding. These technical challenges are determined by multitude of factors such as operation over extended periods of time in hazardous conditions, tasks on harsh environments, stringent communication constraints, to name but a few. The latter is one of the most important problems because the common communication systems are useless, and the important task of finding out a robot or a diver in a 3 dimensional space while they are carrying a mission becomes one of the hardest problems to solve.

The problem at hand is coupled with the fact that nowadays there has been a significant change in the paradigm of marine robot operations because the emphasis is no longer on the operation of single, bulky robots equipped with a multitude of sensors, but rather on the deployment and cooperation of relatively light and easy to deploy robots acting in cooperation towards the execution of common tasks at sea, and even interacting with humans during these demanding tasks.

The extremely fast development of Global Positioning Systems (GPS) related technologies and their common use in multitude of consumers products as GPS receivers, compasses, and accelerometers in mobile phones, cars, or computer gaming controls may drive to think that the positioning problem is almost solved and it may be only a real problem in very reduced cases. However, as abovementioned, there exist many practical scenarios where the common GPS systems are useless:

- Indoor: GPS signals are usually blocked inside buildings, [47], [73].
- Urban: GPS signals are not reliable and usually blocked by surrounding buildings or totally lost in tunnels, [20].
- Caves: Either on land or underwater, [27] .
- Space: Although there has been some experimental work on using GPS signals on extra-terrestrial navigation, GPS signals are usually not available in space, [60].
- Underwater: where GPS signals are blocked by the water surface, [51], [46].

From the above, it is clear that the problem of source localization in those areas in which the common GPS systems are useless has become increasingly important in the recent years. The localization of a source (or sources) is done through given signals obtained by a sensor array conveniently designed. Our aim is to determine the sensor positions of the array for which the information obtained about the source or sources is maximized, it is, the sensor placement for which the positioning accuracy is the largest possible. The source position will be defined with the information received by the sensor nodes. There may exist some constraints that the sensor positions must achieve, for example, in a surface sensor placement for underwater target positioning the sensors are restricted to lie at the sea surface, or the sensor may need to keep a safe distance with respect to the target to avoid sensor or target damage, to name but a few.

The importance of an accurate target positioning is clear in several application scenarios such as radar, sonar, mobile wireless communications, radio astronomy, seismology, acoustics, geophysics, to name some examples. The accuracy of the estimation of the target or source position can be tested considering the closeness of the estimated position with respect to the actual one. There exist multitude of algorithms to estimate this source position. Localization techniques depend on the information available for the sensor network and this information could be power-level information that consists in measuring the power-level of a signal sent between sensors and source, known as Received Signal Strength (RSS) [71], [18], Time Difference of Arrival (TDOA) and Time of Arrival (TOA) [58], [46], [88], [3], [11]; Angle of Arrival (AOA) [10], Bearings Information (BI) [36], [53], [64], or Range Measurements (RM) [4], [42], [6], [61], [62]. These localization techniques require an accurate knowledge of the sensor positions, since any error on these positions is directly translated to errors on the source estimated position.

In this work, as in most of the works available in literature, the optimal sensor placement is determined by minimizing the Cramer-Rao Lower Bound (CRLB), that is a lower bound on estimate variance that provides a gauge of source position estimator accuracy, or equivalently, optimizing any

indicator of the Fisher Information Matrix (FIM), because $CRLB = FIM^{-1}$. Stated in simple terms the Fisher information is a way of measuring the amount of information that an observable random variable, in this work range or bearing, carries about an unknown parameter, the target position, upon which the probability of the observable random variable depends. Therefore, the sensors must be placed in positions such that the information recovered by them maximizes as much as possible the accuracy with which the target position is estimated. There exist some optimality criteria constructed over the FIM to maximize such information, [85]:

- Maximization of $\log|FIM|$ (also called D-optimum design).
- Minimization of $tr(FIM^{-1})$ (also called A-optimum design).
- Maximization of the smallest eigenvalue of the FIM (also called E-optimum design).

The optimization of any of the above criteria is an effective tool to determine the appropriate location of the sensor nodes to maximize the accuracy of the target position estimation.

This Ph.D. thesis is focused on the problem of underwater target positioning. This problem is of the utmost importance for the development of positioning systems with which multiple underwater targets may be positioned with large accuracy. These sensor nodes must be able to track the targets movements to keep the large positioning accuracy required for many demanding tasks at sea. For the sake of simplicity, the determinant of the FIM is used for the computation of an indicator of the performance that can be achieved (by proper choice of an estimator) with a given sensor configuration. Maximizing this indicator, as proposed in the so-called the *D-optimum design* strategy [85], yields the most appropriate sensor formation geometry for the single target positioning problem. The D-optimality criteria for the design of optimal sensor placement is commonly used in the literature of 2D designs. The A or E-optimality indicators are also very popular. The D-optimality criteria minimizes the volume of the uncertainty ellipsoid for the target estimate, whereas the A-optimality criteria, that consists in minimizing the trace of the CRLB matrix, suppresses the average variance of the estimate, and the E-optimality design, that consists in minimizing the largest eigenvalue of the CRLB matrix, minimizes the length of the largest axis of the same ellipsoid, [85].

An important advantage of D-optimality is that it is invariant under scale changes in the parameters and linear transformations of the output, whereas A-optimality and E-optimality are affected by these transformations. However, if the global optimal is not obtained the D-optimality criteria can yield to some errors, because the information in one dimension can be improved rapidly, while we can have no information in others. This problem can be avoided with the A-E-optimality criteria, [80]. Despite the above, the D-optimality criteria will be used in this work due to simplicity reasons because the A-E-optimality criteria imply the inverse of the FIM. Furthermore, we search for global optimal sensor configurations, that imply the best possible estimate, and the global optimal solutions must optimize any of the above optimality indicators as it will be seen throughout this work. This is true with the exception of Chapter 6 in which the minimization of the trace of the CRLB matrix will be used instead of the determinant of the FIM because the AE-measurements enter the FIM in such a way as to render its determinant extremely large for certain trigonometric configurations. However, the large value of the determinant is misleading since it corresponds to close-to-singular configurations of the network for the reason mentioned above.

1.1 Underwater acoustic navigation and positioning systems

Applications of underwater acoustic navigation and positioning systems include a wide range of scientific and commercial activities, such as biological and archaeological surveys, marine habitat

mapping, gas and oil pipeline inspections, to name but a few. Central to the operation of some classes of AUVs is the availability of reliable underwater positioning systems capable of positioning one or more vehicles/divers simultaneously, based on information received on-board a support ship or an autonomous surface vehicle. The info thus obtained can be used to follow the state of progress of a particular mission or, if reliable acoustic modems are available, to relay it as a navigation aid to the navigation systems existent on-board the AUV. Identical comments apply to a new generation of positioning systems to aid in the tracking of one or more human divers, as proposed in the context of the EC CO3AUVs project [9]. There is a great diversity of systems, suited for different tasks and navigation accuracies, most of them based on computing ranges or bearings (azimuth and elevation angles) to acoustic sources with known positions by measuring the times of arrival (TOA) or time differences of arrival (TDOA) of acoustic signals [58], [46], [88] , [3], [11]. For the sake of completeness the most common systems are commented.

- Ultra Short Baseline System, USBL.

Ultra Short Baseline (USBL) systems are one of the most widely employed underwater tracking systems. This system is based on a transceiver mounted on the hull of a ship and a transponder attached to an underwater target to be followed. An acoustic pulse is emitted by the transceiver and received by the transponder that replies back to the former one. It is possible to measure the elapsed time, TOA, and compute the respective range. The term USBL is due to the fact that the transceiver is composed by an array of three or more transducers that are separated by short distances from each other (less than 10cm). By measuring the phase delays of the acoustic signals arriving at the transceiver, the bearing and elevation of the transponder can also be computed. The accuracy with which the transponder position can be obtained is highly dependent on the installation and calibration of the transceiver, as well as on the accuracy with which the inertial position of the ship can be determined using for example a GPS system.

In this sense, advanced signal processing techniques are required in these systems. The actual position and attitude of the USBL transducer head must be known accurately to compute the absolute position of the target. Typically these units contain an INS, together with the input of a GPS receiver, whose antenna position with respect to the transducer head is known in advance. The correct calibration of the system is a crucial element because any error due to a bad calibration is automatically translated into the target position estimation errors.

There is an alternative configuration named inverted USBL in which the vehicle carries the USBL transducer head, and navigates by using an acoustic pinger with known position, [65], [89].

USBL systems are widely used because they are simple to operate and have relatively moderate prices as compared to other systems. The resulting position estimation errors are usually greater that in other longer baseline systems, very sensible to attitude errors on the transducer head, and increase with the slant range. One can achieve relatively good navigation and repeatability, for instance when several pingers are tracked simultaneously or if one pinger is used as a homing reference for the other, but the system can generate big absolute position errors.

- Short Baseline System, SBL.

The hydrophones of this kind of systems are separated by baselines of 1-100meters rigidly mounted on the hull of a ship and a pinger carried by the underwater target, [81]. The hydrophones emit an acoustic pulse that reaches the pinger and travels back to the hydrophones. The ranges are calculated and the relative position of the target is determined. The baseline on this kind of systems is much smaller than the distance from the hydrophones to the target. An exact positioning of the

hydrophones leads to better localization results. In larger ships it is possible to have bigger baselines between the hydrophones and therefore to improve the TOA measurement quality.

This kind of systems provides only relative position estimates between the SBL hydrophones and the vehicle. For absolute position estimates, the absolute position and orientation of the structure (usually a support vessel) where the hydrophones are mounted must be known accurately in advance.

- Long Baseline System, LBL.

These classical positioning systems yield to the most accurate underwater acoustic positioning system from the three yet mentioned. Moreover, this system is the most widely used for underwater target positioning and it is composed by a set of beacons that are fixed at the bottom of the ocean separated by long baselines (a few kilometres). The target carries a transponder that interrogates the beacons sequentially, the beacons reply to the target and the elapsed time is measured, [38], [13]. Typically, LBL systems are used for relatively long range and wide area coverage navigation and the position of the target can be estimated from the TOA measurement. The precision is dependent on the operation frequency, although a precision of a few meters can be obtained. The typical interrogation cycles are of 10 seconds or longer. There are, however, some high frequency LBL systems employed for short range precision positioning such as the EXACT [96], [92], that are claimed to provide centimetric accuracy. These high frequency systems have been used for drilling operations as well as precise archaeological mapping. As in the USBS systems the calibration errors of the beacon position are translated directly on estimation errors of the target position. The operational costs of a mission involving a LBL system are considerable, including the deployment, calibration and recovery of the beacons, which stresses the need for improved underwater navigation solutions.

- GPS Intelligent Buoys System, GIB.

The most important features of a common GPS system are its wide area coverage, the capability of providing navigation data seamlessly to multiple vehicles, relatively low power requirements, miniaturization of receivers, and environmental friendly in the sense that its signals do not interfere significantly with the ecosystem. Typical acoustic underwater positioning systems are quite the opposite: reduced area coverage, do not usually scale well as to serve for multiple vehicle navigation, high power requirements, and moderated to high impact on the environment in terms of acoustic pollution. Thus the search for a GPS-like underwater system is a quite active research area.

It was against this backdrop of ideas that the GPS Intelligent Buoys (GIB) was developed commercially. The brief explanation that follows is essentially adapted from [4] and the original idea was introduced in [97]. The GIB system consists of a set of surface buoys with GPS receivers, submerged hydrophones, and radio modems. The times of arrival of the acoustic signals emitted by a pinger installed on-board an underwater target (synchronized with GPS time prior to system deployment) are recorded by the buoys and sent in real time through the radio link to a control unit [5], (e.g. on-board a support vessel, where the data are processed and a position fix is computed). Note that, unlike in a LBL system, the position information is only available at the control unit and therefore the system cannot be directly applied for vehicle navigation. The GIB and alike systems are basically used to track underwater platforms. If one wishes to use them as a real-time underwater vehicle navigation aid, the need arises to use an acoustic modem to inform the vehicle about its own position. This type of systems is also referred as an inverted LBL since, in this case, the sea bottom fixed transponders have been replaced by surface buoys and the information now is somehow opposite as compared to a classic LBL. The advantage of this kind of systems is that the operational costs are reduced because they eliminate the need to deploy, calibrate and recover a set of sea bottom

transponders, while providing good accuracy on the order of a few meters. Typically, the surface buoys are free drifting or moored, but there are also systems with self propelled buoys which allow for the execution of basic station keeping and underwater platform tracking without the need of a mooring line or when operating at large depths.

1.2 State of the art and report outline

Next we will give a brief overview of the topics addressed in this Ph.D. thesis, the contents of its chapters, and the papers in which the results were published. The reader is referred to the introductions at the beginning of each chapter for more details, bibliographical references, and precise problem formulations.

1.2.1 Sensor networks for single target localization with acoustic range measurements

Inspired by similar developments in ground robotics, we address the problem of single target positioning based on measurements of the ranges between the target and a set of sensors, obtained via acoustic ranging devices in 2D and 3D scenarios in **Chapter 2** and **Chapter 4**, respectively. In particular, and speaking in loose terms, we are interested in determining the optimal configuration (formation) of a sensor network that will, in a well defined sense, maximize the range-related information available for target positioning, with especial emphasis in **Chapter 4** for the application scenario of underwater target positioning. To this effect, we assume that the range measurements are corrupted by white Gaussian noise the covariance of which may be distance-dependent. The application scenario studied focuses on a system for underwater target localization that is similar to GIB, whereby the Autonomous Surface Vessels (ASVs) play the role of surface buoys. However, in order to overcome the problem of having to synchronize the clocks of all acoustic systems involved, the underwater unit only broadcasts an acoustic signal when prompted to do so upon interrogation by one of the ASVs. This renders the system far more robust and its implementation cheaper. The actual computation of the target position may be done by resorting to trilateration algorithms. See for example [4], [3], [7], and the references therein for an introduction to this circle of ideas, covering both theoretical and practical aspects.

Given a target positioning problem, the optimal sensor configuration can be ascertained by examining the corresponding Cramer-Rao Bound (CRB) or Fisher Information Matrix (FIM), [87]. In the present work, the FIMs corresponding to 2D and 3D scenarios are computed to derive the sensor configurations that yield the best precision with which the position of a target can possibly be estimated, considering a distance-dependent variance of the noise model. To this effect, the determinant of the FIM is used as an indicator of the performance that is achievable with a given sensor configuration. Maximizing this quantity yields the most appropriate sensor formation geometry. Moreover, in striking contrast to what is customary in the literature, where zero mean Gaussian processes with fixed variances are assumed for the range measurements, the variances are now allowed to depend explicitly on the ranges themselves. This allows us to capture the fact that measurement noise may increase in a non-linear manner with the distances measured.

For a given target positioning problem, the optimal geometry of the sensor configuration depends strongly on the constraints imposed by the task itself (e.g. maximum number and type of sensors that can be used) and the environment (e.g. ambient noise). In fact, an inadequate sensor configuration may yield large positioning errors. It is interesting to remark that in spite of the importance and relevance of the optimal sensor placement problem, the topic is far from being studied exhaustively.

At this point, it is important to point out that following what is commonly reported in the literature, we start by addressing the problem of optimal sensor placement given an assumed position for the target. It may be argued that this assumption defeats the purpose of devising a method to compute the target position, for the latter is known in advance. The rationale for the problem at hand stems from the need to first fully understand the simpler situation where the position of the target is known and to characterize, in a rigorous manner, the types of solutions obtained for the optimal sensor placement problem. In a practical situation, the position of the target is only known with uncertainty and this problem must be tackled directly. However, in this case it is virtually impossible to develop a general analytical characterization of the optimal solutions, and one must resort to numerical search methods. At this stage, an in-depth understanding of the types of solutions obtained for the ideal case is of the utmost importance to compute an initial guess for the optimal sensor placement algorithm adopted. These issues are rarely discussed in the literature, notable exceptions include [39]. The organization of the Chapters reflects this circle of ideas in that it effectively establishes the core theoretical tools to address and solve the case when there is uncertainty in the position of the target.

Therefore in **Chapter 2** and **Chapter 4** we address the problem of finding the optimal geometric configuration of a sensor formation for the positioning of a target in 2D and 3D scenarios respectively, based on target-to-sensor range measurements only. In contrast to what has been published so far in the literature, in **Chapter 4** we address explicitly the positioning problem in 3D with the sensor array in 3D. The special scenario where the sensor array is located in a plane (2D) is studied as a particular example of the methodology developed; this application scenario arises for example in the case where an underwater target is positioned by an ocean surface sensor network. Moreover with the solutions obtained, the relationship between 3D and 2D scenarios (commonly exploited in land robotics) where the target and the sensor network lie in the same plane becomes clear.

Some of the results in these chapters appear in the authors publications [61] and [62].

1.2.2 Sensor networks for multiple target localization with acoustic range measurements

Once the solution for single target positioning is well established, the *multiple target positioning problem* in **Chapter 3** for 2D scenarios and in **Chapter 5** for 3D scenarios is studied. This problem is of the utmost importance because it is easy to envision different practical situations in which several AUVs and/or divers are working in collaborative and cooperative tasks, and they must be localized with the largest possible accuracy. Clearly, there will be tradeoffs involved in the precision with which each of the targets can be localized; to study them, we resort to techniques that borrow from estimation theory and Pareto optimization. For the latter, the reader is referred to [45], [22], [90]. See also Appendix B for a very short review of some key concepts and results. Stated briefly, we avail ourselves of concepts on Pareto-optimality and maximize convex combinations of the logarithms of the determinants of the FIMs for each of the targets in order to compute the Pareto-optimal surface that gives a clear image of the tradeoffs involved in the multiobjective optimization problem. We thus obtain a powerful tool to determine the sensor configuration that yields, if possible, a proper tradeoff for the accuracy with which the position of the different targets can be computed.

It is important to remark that, for the multiobjective optimization problem, the logarithms of the determinants of the FIMs will be used instead of the determinants themselves. This makes the functions to be maximized jointly convex in the search parameter space, thus justifying the use of scalarization techniques in the computation of the Pareto-optimal surface, as described in Appendix

B. For a discussion of the convexity of the functions adopted, see for example [12], Chapter 3 and the work in [85] on the D-optimality criterion. This issue will be studied in depth in the corresponding Chapters.

For a multi-target localization problem, similarly to the single target positioning problem, the optimal geometry of the sensor configuration depends strongly on the constraints imposed by the task itself (e.g. maximum number and type of sensors that can be used), the environment (e.g. ambient noise), the number of targets and their configuration, and the possibly different degrees of precision with which their positions should be estimated. An inadequate sensor configuration may yield large localization errors for some of the targets, so it is very important to determine the tradeoffs involved in the multi-target positioning problem.

Therefore in **Chapter 3** and **Chapter 5** the multiple target positioning problem with range measurements is studied in 2D and 3D scenarios, respectively. Analytical solutions are derived for the 2-dimensional scenario, and numerical solutions for the 3-dimensional scenario. In this latter case the application scenario of a surface sensor network that must localize several underwater targets is studied in detail. The range measurements are considered to be corrupted by white Gaussian noise, the variance of which is distance-dependent. Moreover the results obtained for the 2D and 3D scenarios are extended to the situation in which the positions of the targets are known with uncertainty that is described by a probabilistic distribution function.

These results appear in the authors publication [63].

1.2.3 Sensor networks for single target localization with acoustic bearings measurements

In **Chapter 6** the problem of single target positioning based on measurements of the azimuth (bearings, in 2D scenarios) and elevation angles between an underwater target and a set of sensors at the sea surface is studied as a natural extension of the previous analysis. In what follows we will refer to these measurements in 3D as AE (azimuth-elevation) measurements or, for simplicity, with an obvious abuse of notation, simply as bearings measurements. We assume again that the AE measurements are corrupted by white Gaussian noise, the variance of which is distance-dependent. The computation of the target position may be done by resorting to triangulation algorithms, based on the nature of the measurements. We recall that the triangulation problem has been widely studied in the computer vision field, and that there exist many examples of algorithms to compute the position of a target using angle measurements; see for instance [34] and [43] for an example of the design of motion-planning and sensor assignment strategies to track multiple targets with a mobile sensor network by resorting to triangulation.

The problem of determining the optimal sensor placement for target localization with AE-only measurements is of special interest because its solution does not require the exchange of information between the target and the sensor network. Thus, AE-only measurements allow for the sensor network to observe without being detected itself. A problem of this type was studied in [57] for an unmanned underwater vehicle tracking an underwater target while avoiding detection. Given a localization strategy, the optimal sensor configuration can be ascertained by examining the corresponding Fisher Information Matrix (FIM) or its inverse, the so-called Cramer-Rao Bound (CRB) matrix. In **Chapter 6**, the trace of the CRB matrix is used as an indicator of the performance that is achievable with a given sensor configuration. Minimizing this quantity yields the most appropriate sensor formation geometry. It is important to remark that in many studies published in the literature on ground and marine robots, as well as in the previous Chapters of this work, the determinant of the FIM is often used as an indicator of the type of positioning performance that can

be achieved. For the problem that we tackle in **Chapter 6** this indicator is not adequate, as it will be shown. This is a simple consequence of the fact that the AE measurements enter the FIM in such a way as to render its determinant extremely large for certain trigonometric configurations. However, the large value of the determinant is misleading for it corresponds to close-to-singular configurations of the network. This issue does not arise in 2D applications, see [10]. Related

The results appear in the authors publication [64].

1.2.4 Single tracker for single target localization with acoustic range measurements

The systems previously commented exploit the geometric configuration of acoustic sensors in order to define the position of an underwater target from range or bearings measurements. These ranges or bearings are measured at different locations that make it possible to determine the target position. However, in **Chapter 7**, an alternative approach is used, a single sensor that employs both the spatial and temporal diversity in order to extract position information.

There is a great interest in reducing the number of beacons involved in the acoustic navigation systems, as they usually involve deployment, calibration and recovery time which is money and time consuming. A recurrent question arises: what is the minimum number of beacons that can be used to perform a navigation task? A single range measurement does not contain enough information to uniquely determine a position, but instead, it defines a whole circle (in 2 dimensions) or a sphere (in 3 dimensions) of possible positions. This does not mean, of course, that this information is not useful, but rather that this information alone is not enough to compute a position fix. If the vehicle carries an on-board navigation system capable of performing DR (Dead Reckoning) one can use the ranges collected over a time interval in order to correct the DR navigation errors. The locations at which the ranges are acquired act as elements of a virtual beacon array. This suggests the name of Virtual Baseline (VBL) navigation. Of course there are several limitations of this method, including the need of rich and spatially diverse vehicle trajectories, and the need of an accurate DR navigation system. The concept of underwater navigation using ranges to a single beacon/transponder has received increasing attention in the marine robotics community. An early reference can be found in [8] where the target motion analysis (TMA) with unknown marine systems using sonar measurements is discussed, i.e., the estimation of the position and velocity of a target ship, given a sequence of measurements, is studied; or [83] where the observability requirements are obtained for three-dimensional maneuvering target tracking with bearings-only measurements. Another early work on this trend is the work of Larsen who came up with the term Synthetic Long Baseline navigation [49], [50].

A dual to this problem is the tracking of an underwater target with a single range measuring device. Instead of a static surface sensor network, one could think of a surface vehicle that, by moving in convenient trajectories, exploits its spatial diversity while measuring ranges to the underwater platform in order to determine its position. The number of ranges needed to determine the position of a target is of the utmost importance, in the most general scenario, 3 non-collinear ranges in 2 dimensional scenarios, and 4 non-coplanar ranges in 3 dimensional scenarios, are needed to determine a position fix. In a practical situation, as the underwater target positioning with surface sensors, the target is known to be under the sea surface, so 3 non-collinear range measurements are enough. Therefore in **Chapter 7** the study of the optimal trajectories that a single sensor must follow, in order to maximize the accuracy with which a target is localized, is tackled. The problem is studied with two different approaches with which the trajectory of the surface sensor is planned in order to maximize the FIM determinant and thus the positioning accuracy. The difference between

these approaches lies in how the sensor trajectory is planned, by studying just the next movement of the sensor or by planning a given number of future measurements and then following a preplanned trajectory.

1.3 Report main contributions

It is interesting to comment at this point that all chapters have a similar structure and that the contents are explained in a way such that each of the chapters is self contained and it can be read independently of the rest. This allows the reader to pay attention to the chapters in which he/she is interested. The main contributions corresponding to each of the chapters are:

Chapter 2: Single target positioning in 2D scenarios.

- Derivation and definition of the optimal Fisher Information Matrix, with distance-dependent covariance error, that maximizes the logarithm of the FIM determinant.
- Derivation of the design conditions that the optimal sensor formation must achieve to provide the maximum logarithm of the FIM determinant.
- Description of analytical and numerical methods to compute optimal sensor configurations.
- Extension to the more realistic problem where the target position is known with uncertainty. This uncertainty can be defined by any probabilistic distribution function, and the kind of function used determines in high degree the optimal sensor formation.

Chapter 3: Multiple target positioning in 2D scenarios.

- Initial study of the multiple target positioning problem for constant covariance measurement error. An analytical solution that provides the maximum FIM determinant for each of the targets is presented for simple target configurations.
- Use of Pareto optimization techniques for the maximization of convex combinations of the logarithms of the determinants of the FIMs for each of the targets because for complex target configurations and/or distance-dependent covariance error an analytical solution cannot be computed and the optimal sensor configuration must be defined resorting to numerical optimization methods.
- Extension of previous results to the more realistic problem where the target positions are known with uncertainty.

Chapter 4: Single target positioning in 3D scenarios with noisy range measurements.

- Characterization of the solutions to the problem of optimal acoustic sensor placement for target positioning in 3D space, with special emphasis on the underwater target positioning by a surface sensor network.
- Derivation of conditions under which a sensor network maximizes the range-related information available for positioning.
- The core result obtained is an analytic characterization of the conditions that must be met by a generic n sensor network in 3D in order for it to be optimal.

- It is further shown that the optimal sensor configuration lends itself to an interesting geometrical interpretation and that the spreading of the sensor configuration depends explicitly on the intensity of the range measurement noise and the probabilistic distribution that defines the prior uncertainty in the target position.

Chapter 5: Multiple target positioning in 3D scenarios with acoustic range measurements.

- The localization problem in 3D using a sensor array located in 3D space is explicitly addressed. The special scenario of a surface sensor network (2D) is studied as an application scenario.
- Definition of optimal configurations of sensor networks that will, in a well defined sense, maximize the range-related information available for multiple underwater target positioning.
- In depth study of the tradeoffs that are inherent to a multiple target localization problem.
- The situation in which the target positions are known with an uncertainty described by a probabilistic distribution is again studied.

Chapter 6: Surface sensor networks for underwater vehicle positioning with bearings-only measurements.

- The problem of determining the optimal configuration of a sensor network that maximizes the AE (azimuth-elevation)-related information available for target positioning is addressed. The application scenario of surface sensor networks is studied in detail.
- The Fisher Information Matrix and the minimization of the trace of the CRB matrix are used to determine the optimal sensor configuration.
- Presentation of explicit analytical results for both distance-dependent and distance-independent noise.
- Extension to the more realistic scenario in which the target position is known with uncertainty.

Chapter 7: Single tracker for underwater vehicle positioning with acoustic range measurements.

- The problem of determining the optimal trajectory of a surface sensor that maximizes the range-related information available for underwater target positioning is addressed for different speeds $V(t)$ and sampling times Δt between measurements.
- Use of the Fisher Information Matrix and the maximization of its determinant to determine the optimal sensor trajectory.
- This scenario is only studied for a constant covariance error.
- Explicit analytical and numerical results are obtained for two different approaches. The first one when we already have a number of measurements and we want to know the immediate next range measurement (or measurement point) that maximizes the accuracy, considering a limited memory, so as the oldest range measurement is not used for the computation of the new FIM. The second one when a trajectory to follow by the sensor is planned for the next n measurement points and the FIM determinant is maximized for these n points, so an optimal trajectory is preplanned.
- Extension to the situation in which the target moves in straight line with constant velocity.

Chapter 2

SINGLE TARGET POSITIONING IN 2D SCENARIOS WITH RANGE MEASUREMENTS

2.1 Introduction

Motivated by multiple developments in ground robotics, in this chapter we address the problem of single target positioning in two-dimensional scenarios based on measurements of the ranges between the target and a set of sensors obtained via acoustic ranging devices. The optimal configuration (formation) of a sensor network that will, in a well defined sense, maximize the range-related information available for single target positioning is derived. To this effect, we assume the range measurements are corrupted by white Gaussian noise, the variance of which is distance-dependent. The computation of the target position may be done by resorting to trilateration algorithms, [4], [3], [7]. This chapter can be seen as an introductory step for the more complex problem of single target positioning in 3-dimensional scenarios studied in Chapter 4.

Given a target positioning problem, the optimal sensor configuration can be ascertained by examining the corresponding Cramer-Rao Bound (CRB) or Fisher Information Matrix (FIM). See [87] for a lucid presentation of this subject in the context of estimation theory. In the present chapter, the FIM corresponding to a 2D scenario is computed to derive the sensor configuration that yields the best precision with which the position of a target can possibly be estimated considering a distance-dependent variance of the noise model. In the same way, in [84] the Cramer-Rao Bound is derived for a distance-dependent error model for Time of Arrival (TOA) based localization in the two-dimensional (2D) space, showing that an error model with distance-dependent covariance has an important impact on the geometric configuration of nodes on the localization accuracy. To this effect, the determinant of the FIM is used as an indicator of the performance that is achievable with a given sensor configuration. Maximizing this quantity yields the most appropriate sensor formation geometry. The work in this chapter is greatly inspired by the work reported in [55] and in [11] on optimal ranging sensor placement to improve the accuracy in the localization of ground robots.

Interesting results in the area go back to the work of [1], where the Cramer-Rao Bound is used as an indicator of the accuracy of source position estimation and a simple geometric interpretation of this bound is offered. In the same reference, the authors describe a solution to the problem of finding the sensor arrangements that minimize the bound, subject to geometric constraints. In particular, "Carter's optimal arrays yielding minimum range, bearing and position bound variance subject to the constraint that the sensors lie along a line segment are determined without tedious algebraic manipulations". In [52], the problem of target positioning in two-dimensional (2-D) scenarios is examined. The author shows explicitly what is the lowest possible geometric dilution of precision (GDOP) attainable from range or pseudo-range measurements to N optimally located points and determines the corresponding regular polygon-like sensor configuration. In [6] the authors study optimal sensor placement and motion coordination strategies for mobile sensor networks. For a target tracking application with range sensors, they investigate the determinant of the FIM and compute it in the 2D and 3D cases. They further characterize the global minimum in the 2D case. In [42], an iterative algorithm that places a number of sensors so as to minimize the position estimation error bound is developed, yielding configurations for the optimal formation subject to several complex constraints. [10] and [11] characterize the relative sensor-target geometry for positioning problems that exploit bearing-only, time-of-arrival, and time-difference-of-arrival strategies in $\Re^2$. Finally, in [39], the authors address the problem of localizing a source in $\Re^2$ from noisy time-of-arrival measurements by seeking an extreme of the FIM for truncated, radially-symmetric source distributions that characterize prior uncertainty in the target location. Similar conclusions are found in other interesting works such as [25] and [44], where the optimality conditions for the sensor placement in 2D are derived for TDOA.

Some other interesting works that deal with the problem of optimal sensor placement for different application areas are [98] or [59]. In [98] seismic network configurations are derived to maximize the precision with which the location of earthquakes is determined. The maximization of the logarithm of the FIM determinant is used as optimality criteria. In [59] an swarm of sensors is employed in a health monitoring system for structures like bridges, where the optimal placement of the sensors is defined using a swarm intelligence technique called Particle Swarm Optimization (PSO). Another interesting reference is [16], in which a sensor network with a large number of nodes is used for surveillance.

Motivated by previous works, we address the problem of finding the optimal geometric configuration of a sensor formation for the localization of a single target, based on target-sensor range measurements only. The expression of the optimal Fisher Information Matrix that provides the maximum possible information about a target is defined, and from its analytical form, the optimal sensor configurations are derived. Moreover, in contrast to what is customary in the literature of ground robotics, where Gaussian error with constant covariance is considered, we consider the measurement error to be distance-dependent in a non-linear manner.

At this point, it is important to point out that following what is commonly reported in the literature, we start by addressing the problem of optimal sensor placement given an assumed position for the target. It may be argued that this assumption defeats the purpose of devising a method to compute the target position, for the latter is known in advance. The rationale for the problem at hand stems from the need to first fully understand the simpler situation where the position of the target is known and to characterize, in a rigorous manner, the types of solutions obtained for the optimal sensor placement problem. In a practical situation, the position of the target is only known with uncertainty and this problem must be tackled directly. However, in this case it is virtually impossible to develop a general analytical characterization of the optimal solutions, and one must resort to numerical search methods. At this stage, an in-depth understanding of the types of solutions

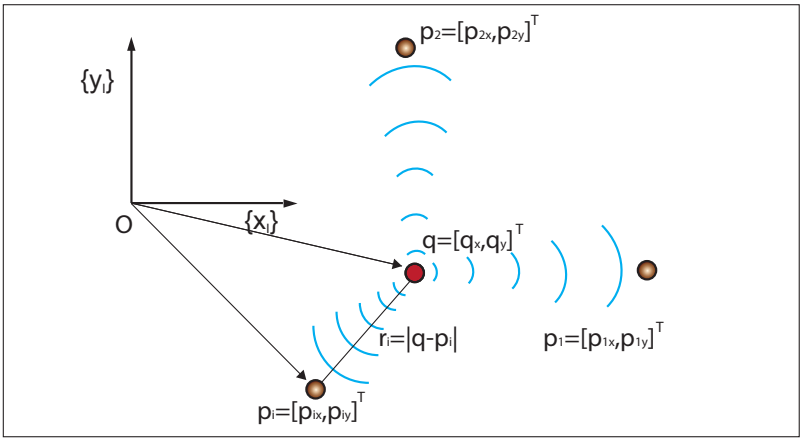

Figure 2.1: Target localization problem set-up.

obtained for the ideal case is of the utmost importance to compute an initial guess for the optimal sensor placement algorithm adopted. These issues are rarely discussed in the literature, a notable exception being [39]. The organization of the chapter reflects this circle of ideas in that it effectively establishes the core theoretical tools to address and solve the case when there is uncertainty in the position of the underwater target.

The present chapter is divided in the following sections. In Section 2.2 the FIM is derived considering distance-dependent measurement error. In Section 2.3 the optimal sensor configurations are defined for Gaussian error with constant covariance. The optimal sensor configurations for Gaussian error with distance dependent covariance (a more realistic assumption for large sensor networks) are studied in Section 2.4. In Section 2.5 the uncertainty in the target location is considered, and optimal sensor configurations for arbitrary probabilistic distributions are defined. Conclusions are commented in Section 2.6.

2.2 Fisher Information Matrix with range-only measurements

Let $\{I\}$ be an inertial reference frame with unit axis $\{x_I\}, \{y_I\}$, and let $q = [q_x, q_y]^T$ be the position of the target to be positioned in $\{I\}$. Further denote by $p_i = [p_{ix}, p_{iy}]^T$; $i = 1, 2, .., n$, the position of the $i - th$ acoustic ranging sensor, also in $\{I\}$. Let $r_i(q) = |q - p_i|$ (abbv. r_i) be the distance (range) between the target q and the $i - th$ sensor, where $|\cdot|$ denotes the Euclidean norm. The variables and the set-up that will be used are illustrated in Figure 2.1 for the case of one target and three sensors.

We denote by z_i the measurement of the actual range $r_i(q)$, corrupted by additive noise ω_i. With the above notation, the measurement model adopted is given by

$$z_i = |q - p_i| + \omega_i = r_i(q) + \omega_i \tag{2.1}$$

Range measurements between two objects are plagued with errors that depend on a multitude of effects: speed of propagation of sound, physical propagation barriers, ambient noise, and degrading signal-to-noise ratio as the distance between the two objects increases, to name but a few. For analytical tractability, it is commonly assumed that the measurement errors can be captured by

Gaussian, zero mean, additive noise with constant covariance. See for example [99], where different noise covariances are taken for different sensors, but the covariances are constant. Clearly, this assumption is artificial in view of the simple fact that the "level of noise" is distance dependent. In an attempt to better capture physical reality, we assume that the measurement noise can be modelled by a zero-mean Gaussian process where the covariance depends on the distance between the two objects that exchange range data. A similar error model is considered in [42]. Stated mathematically,

$$\omega = (I + \eta\delta(r(q)^{\gamma})) \cdot \omega_0 \tag{2.2}$$

where $r(q)$ is the vector of actual ranges, η and γ are the modelling parameters for the distance-dependent noise component, and $\omega = [\omega_1 \cdots \omega_n]^T$ is measurement noise assuming that all noise sources ω_i are independent, and the vector ω_0 is a zero mean Gaussian process $N(0, \Sigma_0)$ with $\Sigma_0 = \sigma^2 \cdot I$, where I is the identity matrix. In the above, δ is the operator *diag*, that either converts a square matrix into a vector consisting of its diagonal elements, or converts a vector into a square diagonal matrix whose diagonal components are the array elements. With these assumptions, the measurement noise covariance matrix is given by

$$\Sigma = \sigma^2 (I + \eta\delta(r(q)^{\gamma}))^2 = \delta\left(\sigma^2 \cdot \left(1 + \eta r_1^{\gamma}\right)^2, \cdots, \sigma^2 \cdot \left(1 + \eta r_n^{\gamma}\right)^2\right) \tag{2.3}$$

In what follows, we assume that the reader is familiar with the concepts of Cramer-Rao Lower Bound (CRLB) and Fisher Information Matrix (FIM); see for example [87]. Stated in simple terms, the FIM captures the amount of information that measured data provide about an unknown parameter (or vector of parameters) to be estimated. Under known assumptions, the FIM is the inverse of the Cramer-Rao Bound matrix (abbv. CRB), which lower bounds the covariance of the estimation error that can possibly be obtained with any unbiased estimator. Thus, "minimizing the CRB" may yield (by proper estimator selection) a decrease of uncertainty in the parameter estimation. Formally, let $\hat{q}(z)$ be any unbiased estimator of q, that is, a mapping $\hat{q} : \Re^n \to \Re^2$ between the observations z and the target position space such that $E\{\hat{q}\} = q$ for all $q \in \Re^2$, where $E\{\cdot\}$ denotes the average operator. Let $p_q(z)$ be the likelihood function that defines the probability of obtaining the observation z given that the true target position is q. It is well known that under some regularity conditions on $p_q(z)$ the following inequality holds:

$$Cov\{\hat{q}\} \geq FIM(q)^{-1} = CRB(q) \tag{2.4}$$

where

$$Cov\{\hat{q}\} = E\{(\hat{q} - q)(\hat{q} - q)^T\}, \tag{2.5}$$

FIM (q) (often abbreviated simply as FIM) is the Fisher Information Matrix defined as

$$FIM(q) = E\left\{(\nabla_q \log p_q(z))(\nabla_q \log p_q(z))^T\right\}, \tag{2.6}$$

and $CRB(q)$ is the Cramer-Rao Bound matrix. In the above, $\nabla_q \log p_q$ denotes the gradient of the log of the likelihood function with respect to the unknown parameter q. Taking the trace of both sides of the covariance inequality yields

$$var\{\hat{q}\} := tr(Cov\{\hat{q}\}) = tr(E\{(\hat{q} - q)(\hat{q} - q)^T\}) \geq tr(FIM(q))^{-1} \tag{2.7}$$

that sets a lower bound on the mean-square error of any unbiased estimator.

Equipped with the above notation and tools of estimation theory we now address the optimal sensor placement problem by solving a related equivalent optimization one: given the FIM for the

problem at hand, maximize its determinant by proper choice of the acoustic sensor coordinates. This strategy for sensor placement underlies much of the previous work available in the literature; see for example [55] , [39] and the references therein. Following standard procedures, the FIM corresponding to the problem of range-based single target positioning can be computed from the likelihood function $p_q(z)$ given by

$$p_q(z) = \frac{1}{(2\pi)^{\frac{n}{2}}|\Sigma|^{\frac{1}{2}}} \exp\left\{-\frac{1}{2}\left(z - r(q)\right)^T \Sigma^{-1}\left(z - r(q)\right)\right\} \tag{2.8}$$

where n is the number of receivers, $z = [z_1, z_2, ..., z_n]^T$ consists of n measured ranges, and $r(q)$ are the actual ranges. Taking the logarithm of (2.8), computing its derivative with respect to q, and then its expected value, the FIM is defined as

$$FIM = C(\delta(r)\Sigma\delta(r))^{-1}C^T \tag{2.9}$$

where $C = (q1_n^T - p) \in \Re^{2xn}$, $1_n \in \Re^{nx1}$ is a vector of 1s, and p is the vector of sensor positions, the latter being defined in $\Re^{2xn}$. For more details about the computation of the FIM see Appendix A. The FIM is constructed by allowing the measurement error to be distance-dependent. Note that Σ depends on the actual range distances, not the measured ones, so its derivative with respect to the estimation parameters of q must not be computed in (2.9). Once the FIM is defined, the Cramer Rao Bound matrix is computed as $CRB = FIM^{-1}$. In this context, the optimal sensor placement strategy for a single vehicle localization problem is obtained by maximizing the determinant of the FIM, which must be computed explicitly. To this effect, we start by expanding (2.9) to obtain

$$FIM = \sum_{i=1}^{n} \begin{pmatrix} (u_{ix})^2 & \left(u_{iy}\right)(u_{ix}) \\ (u_{ix})\left(u_{iy}\right) & \left(u_{iy}\right)^2 \end{pmatrix} \tag{2.10}$$

where

$$u_i = [u_{ix}, u_{iy}]^T = \begin{bmatrix} \frac{\partial|q-p_i|}{\partial q_x}\Gamma_i, & \frac{\partial|q-p_i|}{\partial q_y}\Gamma_i \end{bmatrix}^T; \tag{2.11}$$

and $\Gamma_i = 1/\left(1 + \eta r_i^{\gamma}\right)$ for $i \in \{1, ..., n\}$. Clearly, the expression of the FIM considering a distance-dependence covariance error is well defined.

Actually, the 2D problem is a particular case of the more general problem of target positioning in 3D scenarios, but it is adequate to introduce the 2D problem first to shed light on the more complex target positioning problem in 3D. There is a wide number of works that deal with the 2D target positioning problem as commented in 2.1. The optimal solutions given in these works are recovered in this chapter with a novel methodology, and the results are extended for distance-dependent covariance error and uncertainty in the target location. Furthermore, the optimal formations are not explicitly defined, the optimality conditions that the formation must achieve to minimize the measurement error are defined instead, so any possible optimal configuration may be derived from them. Some examples of optimal sensor placement are shown at the end of each section to illustrate the methodology developed.

2.3 Gaussian error with constant covariance

In this section the optimal sensor placement problem with constant covariance measurement error is studied. The aim of this section is to recover the results on optimal sensor placement defined in the

literature but with a novel methodology with which the optimality conditions for the optimal sensor configurations can be defined in a fast and simple manner.

2.3.1 Optimal Fisher Information Matrix

It was introduced that the FIM captures the amount of information that measured data provide about an unknown parameter (or vector of parameters) to be estimated, and that the determinant of the FIM is used for the computation of an indicator of the performance that is achievable with a given sensor configuration.

As abovementioned, let $q = [q_x, q_y]^T$ be the position of an arbitrary target, $p_i = [p_{i,x}, p_{i,y}]^T$; $i = 1, 2, .., n$, the position of the *i-th* acoustic ranging sensor, and ω_i the corresponding measurement noise defined in (2.2) with $\eta = 0$. Further let r_i be the actual distance between target q and the *i-th* sensor. For the sake of simplicity and without loss of generality the target is considered to be placed at the origin of the inertial coordinate frame. Therefore, (2.10) becomes

$$FIM = \frac{1}{\sigma^2}\sum_{i=1}^{n}\begin{pmatrix} \cos^2(\alpha_i) & \cos(\alpha_i)\sin(\alpha_i) \\ \cos(\alpha_i)\sin(\alpha_i) & \sin^2(\alpha_i) \end{pmatrix} \tag{2.12}$$

where α_i is the angle that the *i-th* range vector forms with the $\{x_I\}$ axis of the inertial coordinate frame. At this point, it is convenient to introduce the vectors X, and Υ in $\Re^n$ (where n is the number of sensors involved in the target positioning task) defined as

$$\begin{aligned} \mathrm{X} &= \begin{bmatrix} u_{1x} & \dots & u_{nx} \end{bmatrix} = \begin{bmatrix} \frac{p_{1x}}{r_1} & \dots & \frac{p_{nx}}{r_n} \end{bmatrix} \\ \Upsilon &= \begin{bmatrix} u_{1y} & \dots & u_{ny} \end{bmatrix} = \begin{bmatrix} \frac{p_{1y}}{r_1} & \dots & \frac{p_{ny}}{r_n} \end{bmatrix}. \end{aligned} \tag{2.13}$$

As a consequence, the FIM is parametrized by 2 vectors in $\Re^n$ instead of n vectors in $\Re^2$. It is also convenient to view these vectors as elements of the Hilbert space with elements in $\Re^n$, endowed with an inner product structure. The latter, as it is well known, allows for computation of the length of a vector and also for the angle between two vectors. The dot product between two vectors can be rewritten as the product of the norms of those vectors times the cosine of the angle between them. Simple computations allow us to rewrite (2.12) as

$$FIM = \frac{1}{\sigma^2}\begin{pmatrix} \mathrm{X}\cdot\mathrm{X} & \mathrm{X}\cdot\Upsilon \\ \mathrm{X}\cdot\Upsilon & \Upsilon\cdot\Upsilon \end{pmatrix} = \frac{1}{\sigma^2}\begin{pmatrix} |\mathrm{X}|^2 & |\mathrm{X}||\Upsilon|\cos(\theta_{\mathrm{X}\Upsilon}) \\ |\mathrm{X}||\Upsilon|\cos(\theta_{\mathrm{X}\Upsilon}) & |\Upsilon|^2 \end{pmatrix} \tag{2.14}$$

The determinant of (2.14) yields

$$|FIM| = \frac{1}{\sigma^4}|\mathrm{X}|^2|\Upsilon|^2\left(1-\cos^2(\theta)\right) \tag{2.15}$$

where θ is the angle formed by vectors X and Υ.

To determine the conditions for which $|FIM|$ is maximum (and consequently the optimal sensor configuration), one simply computes the derivatives of the logarithm of (2.15) with respect to the norms of the vectors and with respect to the angle that appears explicitly in $|FIM|$ and equals the result to 0. Setting this derivative with respect to θ equal to 0 yields the first necessary condition of optimality.

$$\frac{\partial\log(|FIM|)}{\partial\theta} = \frac{\partial|FIM|}{|FIM|} = -\frac{2\cos(\theta)\sin(\theta)}{1-\cos^2(\theta)} = 0 \tag{2.16}$$

Clearly $\sin(\theta) = 0$ provides an indetermination, that from the L'Hopital rule, the limit of (2.16) tends to infinite (moreover, $|FIM| = 0$), so this solution can be discarded. Then the only feasible solution is $\cos(\theta) = 0$. This solution implies that $\theta = k \cdot \pi/2$ where k is any odd number, and then the vectors X and Υ are orthogonal. Hence, a necessary condition (to obtain the optimal sensor network that maximizes the FIM determinant) is that these two vectors must form an orthogonal system. This condition leads to a diagonal FIM.

$$FIM = \frac{1}{\sigma^2} \begin{pmatrix} |\mathrm{X}|^2 & 0 \\ 0 & |\Upsilon|^2 \end{pmatrix} \tag{2.17}$$

Now the focus is on the derivatives of the logarithm of (2.15) with respect to the norms of the vectors. Because

$$\frac{p_{ix}^2}{r_i^2} + \frac{p_{iy}^2}{r_i^2} = 1 \tag{2.18}$$

it follows that

$$|\mathrm{X}|^2 + |\Upsilon|^2 = \sum_{i=1}^{n} \frac{p_{ix}^2}{r_i^2} + \sum_{i=1}^{n} \frac{p_{iy}^2}{r_i^2} = n \tag{2.19}$$

so (2.17), together with (2.19), can be rewritten as,

$$FIM = \frac{1}{\sigma^2} \begin{pmatrix} n - |\Upsilon|^2 & 0 \\ 0 & |\Upsilon|^2 \end{pmatrix} \tag{2.20}$$

The logarithm of the determinant of the FIM can be written now as

$$\log(|FIM|) = \log\left(\frac{1}{\sigma^4} |\Upsilon|^2 \left(n - |\Upsilon|^2\right)\right) \tag{2.21}$$

Thus, the derivative of (2.21) with respect to the norm of the vector Υ, after some simplifications, yields

$$\frac{\partial \log(|FIM|)}{\partial |\Upsilon|} = |\Upsilon| \left(n - |\Upsilon|^2\right) - |\Upsilon|^3 = 0 \rightarrow |\Upsilon|^2 = \frac{n}{2} \tag{2.22}$$

and it is clear from (2.19) that $|\mathrm{X}|^2 = n/2$, so $|\mathrm{X}|^2 = |\Upsilon|^2$. Therefore the expression of the Fisher Information Matrix that provides the maximum (logarithm of the) determinant possible yields,

$$FIM_{opt} = \frac{1}{\sigma^2} \begin{pmatrix} \frac{n}{2} & 0 \\ 0 & \frac{n}{2} \end{pmatrix} \tag{2.23}$$

and the value of the determinant of (2.23) is

$$\left|FIM_{opt}\right| = \frac{n^2}{4\sigma^4} \tag{2.24}$$

It is interesting enough to comment that (2.24) provides the optimal FIM determinant defined in [11] and [55]. Comparing the optimal FIM in (2.23) with the generic one in (2.10) gives an implicit characterization of the conditions that must be satisfied by the sensor network in order for it to be optimal:

$$\sum_{i=1}^{n} \frac{p_{ix}^2}{r_i^2} = \frac{n}{2}$$

$$\sum_{i=1}^{n} \frac{p_{iy}^2}{r_i^2} = \frac{n}{2} \tag{2.25}$$

$$\sum_{i=1}^{n} \frac{p_{ix}p_{iy}}{r_i^2} = 0$$

Thus, all the possible optimal sensor configurations do not depend on the distance between target and sensors, the angles that the range vectors formed between them define the optimality conditions (2.25) and thus, these angles characterize the optimal configurations. From (2.23) it is obvious that the optimal FIM (2.24) is diagonal and its eigenvalues are equal. Therefore, the optimality conditions derived maximize not only the determinant of the FIM but also its minimum singular value. In the forthcoming sections some examples of optimal configurations are shown.

It is important to remark at this point that it is possible to define configurations with equivalent FIM determinant which in practice provide different measurement accuracy. To avoid this problem, it is useful to study the condition number of the FIM to choose the sensor configuration for a given determinant that provides the minimum condition number. This problem does not arise with optimal configurations, because these always provide the minimum condition number (it is clear from the fact that the optimal FIM is a diagonal matrix with all eigenvalues being equal).

2.3.2 Optimal sensor configurations

The optimal formations can be obtained analytically from the system (2.25). It is interesting to notice that this problem, as it will be seen in the next section, is equivalent to the distance-dependent covariance problem when sensors are constrained to be placed at the same distance from the target, it is, they are placed over a circumference centred at the target position. The analysis and solution of the latter problem is equivalent to the global analysis and solution for the constant covariance problem. The only difference between the solutions of both scenarios is that for the distance-dependent covariance case the sensors must be placed at a given distance, as close as possible to the target, whereas in the constant covariance case the sensors can be placed at any distance from the target while the optimal angles be kept, i.e., the distance between target and sensors does not condition the optimal solution. This issue is studied in Section 2.4

For the problem at hand the system (2.25) can be rewritten in polar coordinates as follows:

$$\sum_{i=1}^{n} \frac{p_{ix}^2}{r_i^2} = \sum_{i=1}^{n} \cos^2(\alpha_i) = \frac{n}{2}$$

$$\sum_{i=1}^{n} \frac{p_{iy}^2}{r_i^2} = \sum_{i=1}^{n} \sin^2(\alpha_i) = \frac{n}{2} \tag{2.26}$$

$$\sum_{i=1}^{n} \frac{p_{ix}p_{iy}}{r_i^2} = \sum_{i=1}^{n} \sin(\alpha_i)\cos(\alpha_i) = 0$$

The two first conditions of (2.26) can be combined in $\sum_{i=1}^{n}\left(\cos^2(\alpha_i)-\sin^2(\alpha_i)\right)=0$, and therefore the sensor formation must achieve:

$$\begin{aligned}\sum_{i=1}^{n}\left(\cos^2(\alpha_i)-\sin^2(\alpha_i)\right)&=\sum_{i=1}^{n}\cos(2\alpha_i)=0\\ \sum_{i=1}^{n}\cos(\alpha_i)\sin(\alpha_i)&=\sum_{i=1}^{n}\frac{\sin(2\alpha_i)}{2}=0\end{aligned}\tag{2.27}$$

Using by now classical terminology, the sensor formation must be first and second moment balanced. Then, from (2.27) all the necessary conditions to determine an optimal formation are defined.

Clearly, in order for the information about the optimal configurations to be useful, one must check if the logarithm of the determinant of the FIM meets desired specifications. To this effect, and for comparison purposes, the determinant of the FIM obtained for a number of hypothetical target points (based on a fixed optimal sensor configuration corresponding to a well-defined scenario) will at times be computed by allowing these points to be on a grid in a finite spatial region $\mathcal{D}$. This will allow us to evaluate how good the sensor formation is in terms of yielding accurate localization of the real target, in comparison with the performance localization accuracy that is possible for any hypothetical target (different from the real one) positioned anywhere in $\mathcal{D}$. For the sake of clarity, and with an obvious abuse of notation, we will refer to that determinant, viewed as a function of its argument in $\mathcal{D}$, simply as $|FIM|_{\mathcal{D}}$. In this chapter, $\mathcal{D}$ will always be a rectangle in $\Re^2$.

One simple and intuitive configuration arises noticing the orthogonality relations for sines and cosines from Fourier analysis [37].

$$\begin{aligned}\sum_{i=0}^{n-1}\cos^2\left(\tfrac{2\pi}{n}\cdot n\right)&=\frac{n}{2}\\ \sum_{i=0}^{n-1}\sin^2\left(\tfrac{2\pi}{n}\cdot i\right)&=\frac{n}{2}\\ \sum_{n=0}^{n-1}\cos\left(\tfrac{2\pi}{n}\cdot i\right)\sin\left(\tfrac{2\pi}{n}\cdot i\right)&=0\\ \sum_{i=0}^{n-1}\cos\left(\tfrac{2\pi}{n}\cdot i\right)&=0\\ \sum_{i=0}^{n-1}\sin\left(\tfrac{2\pi}{n}\cdot i\right)&=0\end{aligned}\tag{2.28}$$

Thus, a maximum FIM determinant is achieved with the sensor network regularly distributed around the target projection. Obviously, an infinite number of solutions are obtained by rotating the sensors rigidly along the circumferences, that is, by allowing the above angles to become $2\pi i/n+\alpha_s; i=0,1,...,n-1$, where α_s is a fixed but arbitrary angle in $[0,2\pi]$. In the following examples we have considered a regular formation around the target position and $\sigma=0.1\ m$. It is important to remark on one important feature of the optimal solutions that can be computed based on the analysis explained above. If two disjoint sets of n and m sensors each are optimally placed, the resulting formation of $n+m$ sensors is also optimal. Therefore, new higher order optimal solutions can be obtained by combining reduced order optimal configurations.

Example 2.1

In Figure 2.2 an optimal sensor formation of 5 sensors regularly distributed around the target is shown, with $\sigma = 0.1\ m$ and $\eta = 0$ (constant covariance). It can be noticed how the maximum FIM determinant is obtained at the target position (lighter regions, larger accuracy), taking the theoretical maximum value, $n^2/(\sigma^4 \cdot 4) = 6.25 \cdot 10^4\ m^{-4}$. In Figure 2.2 (b) it is shown the value taken at each point by the FIM determinant in $\mathcal{D}$.

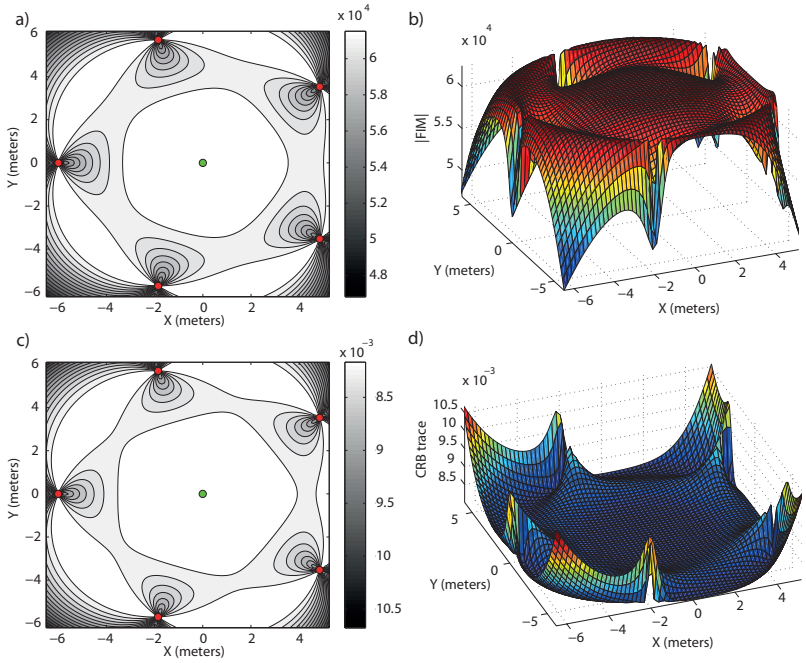

Figure 2.2: Optimal sensor placement for 5 sensors. In (a) $|FIM|_{\mathcal{D}}$ is shown (lighter regions, larger accuracy) and in (b) the FIM determinant value in $\mathcal{D}$. In (c) $tr(CRB)_{\mathcal{D}}$ is shown (lighter regions, larger accuracy) and in (d) the value of the trace of the CRB in $\mathcal{D}$.

In Figure 2.2 (c) and (d) the level curves of $tr(CRB)_{\mathcal{D}}$ (lighter regions, larger accuracy) and the representation of its magnitude in 3D for $\mathcal{D}$ are shown, respectively. This shows the correspondence between maximum determinant and minimum CRB trace. It can be checked how the minimum trace of the CRB is obtained at the target position achieving its theoretical minimum value too, $tr(CRB) = \sigma^2 \cdot 4/n = 0.08\ m^2$. This correspondence between the minimum trace of the CRB and the maximum FIM determinant is clear from the fact that the optimal FIM is a diagonal matrix with all the eigenvalues being equal. ■

Example 2.2

An optimal sensor formation for 3 sensors regularly distributed around the target position is shown in Figure 2.3. The theoretical maximum FIM determinant (and minumum CRB trace, $tr(CRB) = \sigma^2 \cdot 4/n\ m^2$) is obtained at the target position, $|FIM| = n^2/(\sigma^4 \cdot 4) = 2.25 \cdot 10^4\ m^{-4}$.

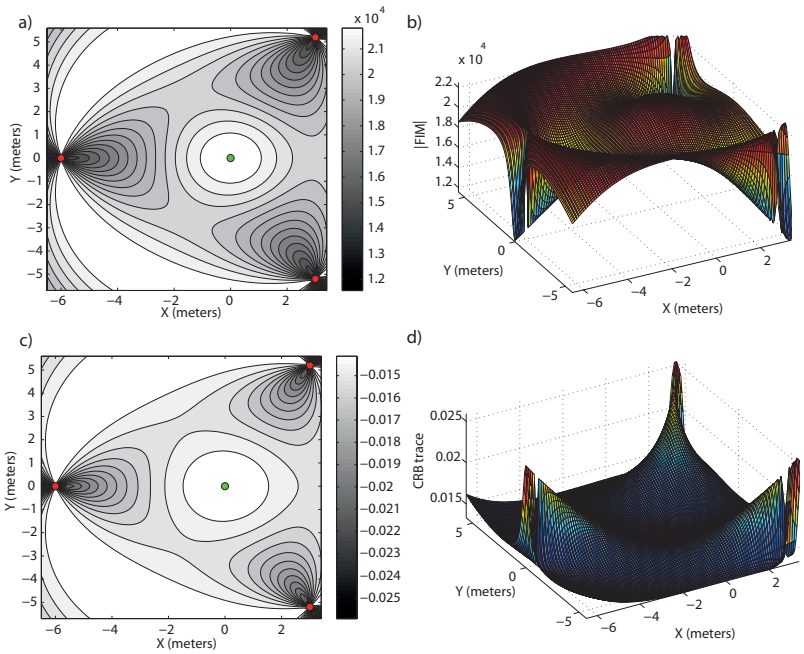

Figure 2.3: Optimal sensor placement for 3 sensors. In (a) $|FIM|_{\mathcal{D}}$ is shown (lighter regions, larger accuracy) and in (b) the FIM determinant value in $\mathcal{D}$. In (c) $tr(CRB)_{\mathcal{D}}$ is shown (lighter regions, larger accuracy) and in (d) the value of the trace of the CRB in $\mathcal{D}$.

It is interesting enough to notice in Figure 2.3 (a) and (c) that there exist three more points where the design conditions (2.27), and then the maximum FIM determinant and minimum CRB trace, are achieved. These points are located outside the equilateral triangle formed by the sensors and placed in symmetric positions. Therefore, if another target would be placed in any of these points, it will be positioned with the maximum accuracy. This fact is very important to define alternative optimal formations, and in forthcoming chapters, to define optimal formations for multiple target positioning. It is also important to notice that these alternative points with maximum FIM determinant only exist in the constant covariance scenario. If we consider the same example for distance-dependent covariance error in which the sensors are limited to be placed at the positions shown in Figure 2.3 then there exists only one point with maximum determinant and it is placed at the centre of the formation (the target position). This issue is studied in the next section. ■

Example 2.3

It is important to remark on one important feature of the optimal solutions that can be computed based on the analysis explained above. As aforementioned, if two disjoint sets of n and m sensors each are optimally placed, the resulting formation of $n + m$ sensors is also optimal. Therefore, new higher order optimal solutions can be obtained by combining reduced order optimal configurations. It is a consequence of considering the measurements to be independent. It can be seen in Figure 2.4 how the combination of the 5 sensor regular formation of Example 2.1. with the 3 sensor regular formation of Example 2.2. provides another optimal formation in which the theoretical maximum accuracy for 8 sensors is obtained at the target location, it is, $|FIM| = 16 \cdot 10^4\ m^{-4}$. ■

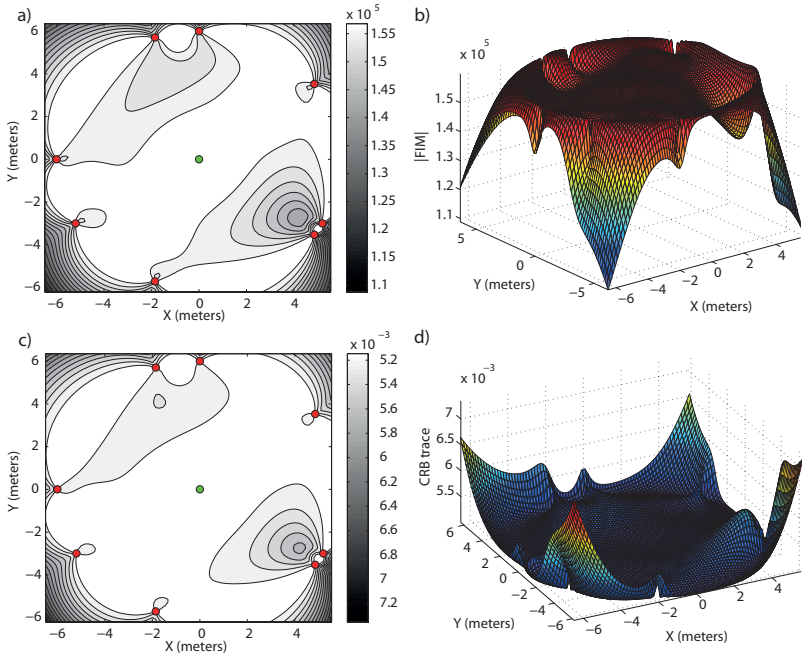

Figure 2.4: Optimal sensor configurations with the combination of a 5 sensor regular formation and a 3 sensor regular formation. In (a) $|FIM|_{\mathcal{D}}$ is shown (lighter regions, larger accuracy) and in (b) the FIM determinant value in $\mathcal{D}$.

As abovementioned, if we consider these same examples for distance-dependent covariance error in which the sensors are constrained to not lie closer to the target than the positions shown in the above figures, then the optimal solutions are the same formations. Moreover, with distance-dependent covariance error, there exists only one point with maximum determinant (or minimum CRB trace) and it is placed at the centre of the regular formation (the target position).

2.4 Gaussian error with distance-dependent covariance

In this scenario the dependence of the measurement error in the distance affects dramatically the optimal sensor configurations that may be defined. It can be seen that (2.10) depends explicitly on the distance between target and sensors, and then to maximize the determinant of (2.10) the sensors tend to collapse over the target position to reduce the distance-dependent measurement error as much as possible. Therefore, some constraints must be imposed to the sensors and the solution must be searched by some optimization algorithm.

There is a particular scenario in which an analytical solution can be derived following the same procedure explained in Section 2.3.1. This scenario corresponds to the case in which the sensors are placed at the same distance from the target, i.e., they are placed over a circumference centred at the target position and then the optimal solution only depends on the angles that the range vectors form between them, as defined in the constant covariance case. This problem is studied next.

2.4.1 Sensors placed at the same distance from the target

Following the same procedure of Section 2.3.1, let $q = [q_x, q_y]^T$ be the position of an arbitrary target, $p_i = [p_{i,x}, p_{i,y}]^T$; $i = 1, 2, .., n$, the position of the *i-th* acoustic ranging sensor, ω_i the corresponding measurement noise defined in (2.2) with $\eta \neq 0$, and r_i the distance between target q and the *i-th* sensor. Therefore, expanding (2.10) we find

$$FIM = \frac{1}{\sigma^2} \sum_{i=1}^{n} \begin{pmatrix} \cos^2(\alpha_i)\,\Gamma_i^2 & \cos(\alpha_i)\sin(\alpha_i)\,\Gamma_i^2 \\ \cos(\alpha_i)\sin(\alpha_i)\,\Gamma_i^2 & \sin^2(\alpha_i)\,\Gamma_i^2 \end{pmatrix} \tag{2.29}$$

where α_i is the angle that the *i-th* range vector forms with the $\{x_I\}$ axis of the inertial coordinate frame. It must be noticed at this point that the sensors are constrained to be placed at the same distance from the target and then $r_i = r$ for $i = 1, \cdots, n$. Moreover, Γ_i is constant and has the same value for all sensors, so $\Gamma_i = \Gamma_0$ for $i = 1, \cdots, n$. Thus, (2.29) can be rewritten as,

$$FIM = \frac{\Gamma_0^2}{\sigma^2} \sum_{i=1}^{n} \begin{pmatrix} \cos^2(\alpha_i) & \cos(\alpha_i)\sin(\alpha_i) \\ \cos(\alpha_i)\sin(\alpha_i) & \sin^2(\alpha_i) \end{pmatrix} \tag{2.30}$$

that is very similar to (2.12), but multiplied by Γ_0^2. Therefore, at this point, the vectors X, and Υ in $\Re^n$ (where n is the number of sensors involved in the target positioning task) are introduced again and the same theoretical analysis of Section 2.3.1 is performed, where it is found that vectors X, and Υ must be both equal to $n/2$.

If we define now the vector S as,

$$S = \begin{bmatrix} \Gamma_1 & \cdots & \Gamma_n \end{bmatrix} = \begin{bmatrix} \Gamma_0 & \cdots & \Gamma_0 \end{bmatrix}$$

then the expression of the Fisher Information Matrix that provides the maximum (logarithm of the) determinant possible yields,

$$FIM = \frac{1}{\sigma^2} \begin{pmatrix} \frac{|S|^2}{2} & 0 \\ 0 & \frac{|S|^2}{2} \end{pmatrix} = \frac{1}{\sigma^2} \begin{pmatrix} \frac{n}{2} \cdot \Gamma_0^2 & 0 \\ 0 & \frac{n}{2} \cdot \Gamma_0^2 \end{pmatrix} \tag{2.31}$$

And the value of the determinant of (2.31) is

$$|FIM| = \frac{|S|^4}{4\sigma^2} = \frac{n^2}{4\sigma^2} \cdot \Gamma_0^2 \tag{2.32}$$

It is interesting enough to comment at this point, that the determinant (2.32) defines the maximum FIM determinant when the covariance noise is distance-dependent and the sensors are placed over a circumference centred at the target position. If we consider a constant covariance measurement noise, it is, $\eta = 0$ and then $\Gamma_0 = 1$, (2.32) provides the optimal determinant defined in [11] and [55], and computed in (2.24).

Comparison of the optimal FIM in (2.31) with the generic one in (2.10) gives an implicit characterization of the conditions that must be satisfied by the sensor network in order for it to

be optimal, that yield:

$$\begin{aligned}
\sum_{i=1}^{n} \frac{p_{ix}^2}{r_i^2}\Gamma_i^2 &= \sum_{i=1}^{n} \frac{\Gamma_i^2}{2} \\
\sum_{i=1}^{n} \frac{p_{iy}^2}{r_i^2}\Gamma_i^2 &= \sum_{i=1}^{n} \frac{\Gamma_i^2}{2} \\
\sum_{i=1}^{n} \frac{p_{ix}p_{iy}}{r_i^2}\Gamma_i^2 &= 0
\end{aligned} \tag{2.33}$$

Equations (2.33), with $\Gamma_i = \Gamma_0$ and $r_i = r$, become the optimality conditions defined in (2.25):

$$\begin{aligned}
\sum_{i=1}^{n} \frac{p_{ix}^2}{r_i^2} \cdot \Gamma_i^2 = \sum_{i=1}^{n} \frac{\Gamma_i^2}{2} \rightarrow \sum_{i=1}^{n} \frac{p_{ix}^2}{r_i^2} &= \sum_{i=1}^{n} \cos^2(\alpha_i) = \frac{n}{2} \\
\sum_{i=1}^{n} \frac{p_{iy}^2}{r_i^2} \cdot \Gamma_i^2 = \sum_{i=1}^{n} \frac{\Gamma_i^2}{2} \rightarrow \sum_{i=1}^{n} \frac{p_{iy}^2}{r_i^2} &= \sum_{i=1}^{n} \sin^2(\alpha_i) = \frac{n}{2} \\
\sum_{i=1}^{n} \frac{p_{ix}p_{iy}}{r_i^2} \cdot \Gamma_i^2 = \sum_{i=1}^{n} \frac{\Gamma_i^2}{2} \rightarrow \sum_{i=1}^{n} \frac{p_{ix}p_{iy}}{r_i^2} &= \sum_{i=1}^{n} \sin(\alpha_i)\cos(\alpha_i) = 0
\end{aligned} \tag{2.34}$$

It is important to remark that this analytical solution is only feasible when the sensor are placed at the same distant from the target. For more complex constraints it is necessary to resort to optimization tools, as it will be seen in the following examples.

2.4.2 Optimal sensor configurations with arbitrary constraints

From (2.18) it is clear that the FIM is inversely proportional to the range distance between target and sensors. Therefore, it is necessary to reduce that distance as much as possible to increase the determinant, something not possible to do at will, due to physical constraints and to avoid singular configurations that are clearly non-optimal, for example the one in which the sensors lie over the target position. In this scenario it is imperative to impose constraints for the design of optimal sensor configurations to avoid the sensor to collapse over the target position (to reduce the distance-dependent error). The existence of constraints in the solution space limits the search space and makes it more difficult to define the solution since the optimality criterion defined by (2.27) may be impossible to achieve, i.e., some of the positions that define the theoretical optimal configuration may be unreachable.

On the one hand, if the problem has equality constraints it may be possible to use gradient optimization methods. The Lagrange method, in which a new cost function is constructed including these equality constraints, allows to find the optimal configuration. An example of this kind of problems is the one studied in the previous subsection, in which the sensors must be placed at a given distance from the target. In this particular case it is possible to resort to the analytic solution defined above or to optimization methods to obtain the feasible optimal sensor configurations. The

problem formulation can be cast in the following form:

$$\begin{aligned} &\bar{p}^{*} = arg\max_{\bar{p}} \log\left(|FIM|\right) \\ &s.t. \\ &g_k\left(x_i, y_i\right) - b_i = 0 \end{aligned} \tag{2.35}$$

where $g_i(x_i, y_i)$ can be any kind of function and b_i is a constant. The cost function now becomes:

$$L = \log\left(|FIM|\right) + \sum_{i=1}^{n} \bar{\lambda_i}\left(g_i\left(x_i, y_i\right) - b_i\right) \tag{2.36}$$

Equation (2.36) is now the function to maximize, where $\bar{\lambda_i}$, $i = 1, \cdots, n$, are the Lagrange Multipliers that must be determined (considering a constraint per sensor). The optimal solution is obtained from the system:

$$\frac{\partial L}{\partial x_i} = 0 \qquad \frac{\partial L}{\partial y_i} = 0 \qquad \frac{\partial L}{\partial \lambda_i} = 0 \tag{2.37}$$

Therefore, by using the gradient (or Newton) optimization method it is easy to define the optimal sensor formation that provides the maximum logarithm of the FIM determinant. In the following examples it is assumed that $\sigma = 0.1\ m$, $\eta = 0.05$, and $\gamma = 1$.

Example 2.4

In Figure 2.5 an optimal formation of 4 sensors for a distance-dependent measurement error is shown. The only constraint imposed to the design is that the sensors cannot be placed closer than 3 meters with respect to the target position. The maximum accuracy, given by a maximum FIM determinant or a minimum CRB trace, is obtained at the target position. It can be seen in detail in Figure 2.5 (b) and (d), respectively. It is easy to check that the sensors are placed at the limit distance, because, as abovementioned, the accuracy is inversely proportional to the distances between sensors and target, and thus, the sensors are placed as close as possible to reduce this error. In this particular example, the same solution is obtained both with the analytical procedure and the above optimization algorithm.

Table 2.1: Optimal sensor positions for $\sigma = 0.1\ m$, $\eta = 0.05$, and $\gamma = 1$.

	p_1	p_2	p_3	p_4
$\{x_I\} - coordinate\ (m)$	−2.1213	−2.1213	2.1213	2.1213
$\{y_I\} - coordinate\ (m)$	2.1213	−2.1213	−2.1213	2.1213

In Figure (2.5) (a) and (c) the target and sensor positions are shown, the latter are listed in Table 2.1. ■

On the other hand, if we have equality and inequality constraints, then we have to resort to non-lineal programming techniques to solve the problem, and the Karush-Kunt-Tucker conditions must be achieved to find the optimal solution. The problem formulation becomes:

$$\begin{aligned} &\bar{p}^{*} = arg\max_{\bar{p}} \log\left(|FIM|\right) \\ &s.t. \\ &g_i\left(x_i, y_i\right) - b_i \geq 0 \end{aligned} \tag{2.38}$$

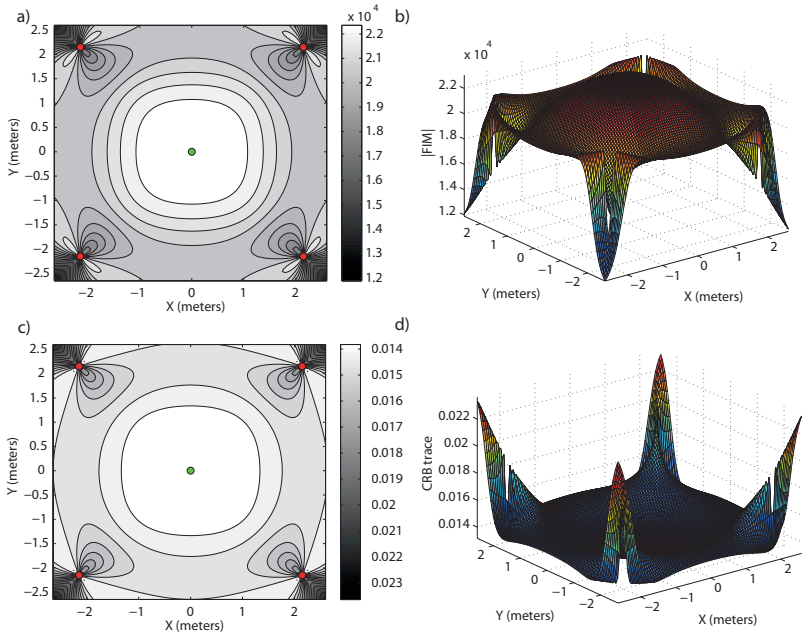

Figure 2.5: Optimal sensor placement for a 4 sensor formation with distance-dependent measurment noise. In (a) $|FIM|_{\mathcal{D}}$ is shown (lighter regions, larger accuracy) and in (b) the FIM determinant value in $\mathcal{D}$. In (c) $tr(CRB)_{\mathcal{D}}$ is shown (lighter, regions larger accuracy) and in (d) the value of the trace of the CRB in $\mathcal{D}$.

The residual variables s_i must be introduced to convert the inequality constraints into equality constraints.

$$g_i(x_i, y_i) + s_i - b_i = 0$$

Then, the optimization problem and the cost function associated yields

$$L = \log(|FIM|) + \sum_{i=1}^{n} \bar{\lambda_i}(g_i(x_i, y_i) + s_i - b_i) \tag{2.39}$$

And the optimality conditions are,

$$\frac{\partial L}{\partial x_i} = 0 \qquad \frac{\partial L}{\partial y_i} = 0 \qquad \frac{\partial L}{\partial \lambda_i} = 0 \qquad \frac{\partial L}{\partial s_i} = 2 s_i \bar{\lambda_i} \tag{2.40}$$

where the last equation implies either $s_i = 0$ and $\bar{\lambda_i} \neq 0$, or $s_i \neq 0$ and $\bar{\lambda_i} = 0$. This last condition is the complementary slackness. Thus, again, by using the gradient or Newton optimization method it is easy to find the optimal sensor formation that provides the maximum FIM determinant.

Example 2.5

In this example, 3 sensors are forced to lie in the upper semiplane limited by the line $y = 3\ m$, with the target placed at the origin of the inertial coordinate frame. It is possible to check from Figure (2.6) how this scenario could be studied as a problem with equality constraints because the

optimal positions for the sensors are over the line $y = 3\ m$. However, the optimization procedure run is the one described in (2.40). The optimal sensor positions are stated in Table 2.2.

Table 2.2: Optimal sensor positions for $\sigma = 0.1\ m$, $\eta = 0.05$, and $\gamma = 1$.

	p_1	p_2	p_3
$\{x_I\} - coordinate\ (m)$	3.69	0	−3.69
$\{y_I\} - coordinate\ (m)$	3	3	3

In Figure (2.6) it is shown how the optimal formation for the problem at hand does not provide the best accuracy possible because the accuracy that can be obtained is limited by the additional constraint and the measurement error.

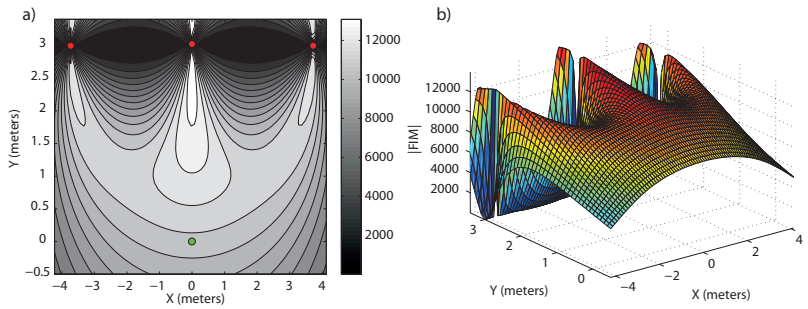

Figure 2.6: Optimal sensor placement for a 3 sensor formation that is restricted to lie in the upper semiplane limited by the line $y = 3\ m$. In (a) $|FIM|_{\mathcal{D}}$ is shown (lighter regions, larger accuracy) and in (b) the FIM determinant value in $\mathcal{D}$. In (c) $tr(CRB)_{\mathcal{D}}$ is shown (lighter regions, larger accuracy) and in (d) the value of the trace of the CRB in $\mathcal{D}$.

Figure 2.6 (a) and (c) show the positions that the sensors take so as to maximize the logarithm of the FIM determinant. In Figure 2.6(b) it is shown the value taken by the FIM determinant at each point in $\mathcal{D}$ and in (d) the value taken by the CRB trace at each point in $\mathcal{D}$. ■

2.5 Uncertainty in the target location

Now it is addressed the situation where the target to be positioned is known to lie in a well defined uncertainty region. The objective is to obtain an expedite numerical solution for the problem at hand. Inspired by the work in [39], it is assumed that the uncertainty in the target position is described by a given probability distribution function and we seek to maximize, by proper sensor placement, the average value of the determinant of the FIM for the target.

In what follows, $p_{i\xi}\ ;\ i = 1, 2, ..., n;\ \xi = x, y$ denotes the ξ-th coordinate of sensor i located at position p_i and $\overline{p} = [p_1^T, ..., p_n^T]^T$. We further denote by $\varphi(q)\ ;\ q \in \Re^2$ a probability density function with support $D \in \Re^2$ that describes the uncertainty in the position of the target in region D. With this notation, the problem of optimal sensor placement can be cast in the form of finding a vector $\overline{p}^*$ such that

$$\overline{p}^* = arg \max_{\overline{p}} \int_D \log|FIM(\overline{p}, q)| \cdot \varphi(q)\, dq \tag{2.41}$$

where we used the notation $|FIM(\bar{p}, q)|$ to clearly show the dependence of the FIM on the target and sensor locations. However, in the following $|FIM(\bar{p}, q)|$ will often be denoted simply as $|FIM|$. In a real situation, $\varphi(q)$ will depend on the type of mission carried out by the target. If the target operates mostly in the centre of the working area, $\varphi(q)$ can for example assume the form of a truncated, radially-symmetric probabilistic Gaussian distribution centred at an appropriate point. On the other hand, if only the work area is known and the target can operate anywhere inside it, $\varphi(q)$ can be taken as the unity function inside that area.

To proceed, one must compute $|FIM(\bar{p}, q)|$ in the equation above. At this point it is important to remark that, given the complexity of the optimal sensor placement problem at hand, the only viable solution is a numerical one. It now remains to solve the optimization problem defined above. As explained later, we opted to use a gradient-based method to do so. To this effect, it is important to compute the derivatives of the integral in (2.41) with respect to the sensor coordinates, that is,

$$\frac{\partial}{\partial p_{i\xi}} \int_D \log\left(|FIM(\bar{p}, q)|\right) \varphi(q) dq \tag{2.42}$$

for $i = 1, 2, ..., n$ and $\xi = x, y$. To proceed with the computations, the integral and derivative operations are interchanged: the derivatives are explicitly determined first and the integration over region D is performed afterwards. The derivatives finally look like,

$$\frac{\partial \log\left(|FIM|\right)}{\partial p_{i\xi}} = \frac{\partial |FIM|}{\partial p_{i\xi}} \cdot \frac{1}{|FIM|} \tag{2.43}$$

where $\xi = x, y$ and

$$\begin{aligned}
\frac{\partial |FIM|}{\partial p_{ix}} = &- \frac{2\cos(\alpha_i)\sin^2(\alpha_i)}{r_i}\Gamma_i^2 \sum_{s=1}^{n}\left(\sin^2(\alpha_s) - \cos^2(\alpha_s)\right)\Gamma_s^2 + \\
&+ \frac{\partial \Gamma_i^2}{\partial p_{ix}}\left(\cos^2(\alpha_i)\sum_{s=1}^{n}\sin^2(\alpha_s)\Gamma_s^2 + \sin^2(\alpha_i)\sum_{s=1}^{n}\cos^2(\alpha_s)\Gamma_s^2\right) - \\
&- 2\frac{\partial \Gamma_i^2}{\partial p_{ix}}\cos(\alpha_i)\sin(\alpha_i)\sum_{s=1}^{n}\cos(\alpha_s)\sin(\alpha_s)\Gamma_s^2 + \\
&+ 2\Gamma_i^2\left(\frac{\sin^3(\alpha_i)}{r_i} - \frac{\cos^2(\alpha_i)\sin(\alpha_i)}{r_i}\right)\sum_{s=1}^{n}\cos(\alpha_s)\sin(\alpha_s)\Gamma_s^2
\end{aligned} \tag{2.44}$$

$$\begin{aligned}
\frac{\partial |FIM|}{\partial p_{iy}} = &\frac{2\sin(\alpha_i)\cos^2(\alpha_i)}{r_i}\Gamma_i^2 \sum_{s=1}^{n}\left(\sin^2(\alpha_s) - \cos^2(\alpha_s)\right)\Gamma_s^2 + \\
&+ \frac{\partial \Gamma_i^2}{\partial p_{iy}}\left(\cos^2(\alpha_i)\sum_{s=1}^{n}\sin^2(\alpha_s)\Gamma_s^2 + \sin^2(\alpha_i)\sum_{s=1}^{n}\cos^2(\alpha_s)\Gamma_s^2\right) - \\
&- 2d\frac{\partial \Gamma_i^2}{\partial p_{iy}}\cos(\alpha_i)\sin(\alpha_i)\sum_{s=1}^{n}\cos(\alpha_s)\sin(\alpha_s)\Gamma_s^2 + \\
&+ 2\Gamma_i^2\left(\frac{\cos^3(\alpha_i)}{r_i} - \frac{\sin^2(\alpha_i)\cos(\alpha_i)}{r_i}\right)\sum_{s=1}^{n}\cos(\alpha_{sk})\sin(\alpha_s)\Gamma_s^2
\end{aligned} \tag{2.45}$$

with

$$\frac{\partial \Gamma_i^2}{\partial p_{ix}} = \cos(\alpha_i) \frac{2\eta\gamma r_i^{\gamma-1}}{\left(1+\eta r_i^{\gamma}\right)^3}$$

$$\frac{\partial \Gamma_i^2}{\partial p_{iy}} = \sin(\alpha_i) \frac{2\eta\gamma r_i^{\gamma-1}}{\left(1+\eta r_i^{\gamma}\right)^3}$$

These derivatives will be studied in depth in the next chapter for multiple target positioning. Regarding the computation of the double integral over the region D of interest, it is impossible to do it analytically. For this reason, the integral is computed numerically with the Monte Carlo method. Finally, the solution is obtained using a gradient optimization method with the Armijo rule, details are omitted. To overcome the possible occurrence of local maxima or the divergence of the algorithm, the initial guess in the iterative algorithm must be chosen with care. In the examples that we studied we found it useful and expedite to adopt as an initial guess the solution for the single target positioning problem described in previous sections, with the hypothetical single target placed at the centre of the work area. It is important to stress that the solution to (2.41) depends strongly on the probability density function adopted for the target position q (e.g., a truncated, radially-symmetric probabilistic Gaussian distribution or a radially-symmetric step distribution, [39]).

2.5.1 Simulation examples with unknown source position

Different situations and possible optimal sensor configurations when the target position is known with uncertainty are shown next. For the examples a step-like distribution is used as probability distribution function to define the target position. The only knowledge about the target is that it is placed inside a square area of $2 \times 2\ m^2$ centred at the origin of the inertial coordinate frame. Three simple examples corresponding to the three main problems for single target localization are shown for the case of uncertain target location. In the first problem, the scenario in which the covariance error is constant, with $\sigma = 0.1\ m$, is studied. In the second example, it is considered a distance-dependent measurement error with $\sigma = 0.1\ m$, $\gamma = 1$ and $\eta = 0.05$ and no constraints. Finally in the third example, it is studied a distance-dependent measurement error with $\sigma = 0.1\ m$, $\gamma = 1$ and $\eta = 0.05$ with the sensors constrained to lie in the region defined by $y < 3\ m$ and $y < -3\ m$.

Example 2.6: Constant covariance error and no constraints.

In the problem at hand it is possible to design sensor configurations that provide large accuracy over well defined regions, close to the optimal one that would be obtained for a single target working in isolation at a known position because distance does not affect the measurement error. The practical interest of this problem is the design of the smallest network possible that provides an accuracy close to the maximum for all the points inside the work area, that for the problem at hand will be of $2{\times}2\ m^2$. The formation size will be, of course, mission-dependent.

The probability distribution function that defines the target position in the work area is a step-like distribution, it is, the only *a priori* knowledge is that the target operates inside a certain area. In Figure 2.7 (a) it is possible to check that the FIM determinants obtained inside the work area are very close to theoretical maximum, with the 4 sensors placed at the points listed in Table 2.3.

In Figure 2.7 (c) the trace of the CRB is shown. Its minimum values fall over the area of interest and are close to the theoretical minimum, $tr(CRB) = \sigma^2 \cdot 4/n\ m^2$. Figure 2.7 (b) shows the level curves of $|FIM|_{\mathcal{D}}$, and (d) the level curves of the CRB trace. It is possible to appreciate how the

Table 2.3: Optimal sensor positions for constant covariance.

	p_1	p_2	p_3	p_4
$\{x_I\} - coordinate\ (m)$	−5.1066	−5.1066	5.1066	5.1066
$\{y_I\} - coordinate\ (m)$	5.1066	−5.1066	−5.1066	5.1066

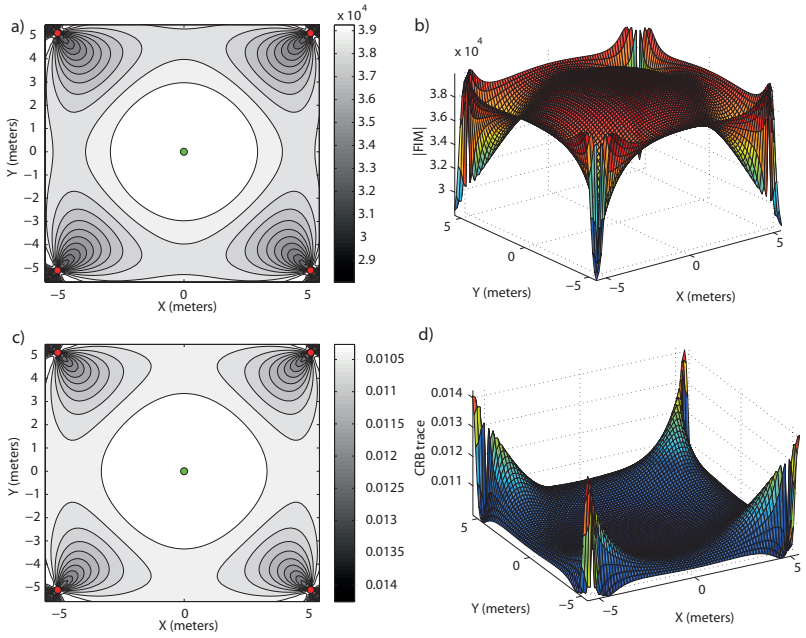

Figure 2.7: Optimal sensor formation to obtain the maximum average logarithm of the FIM determinant inside the work area of $2 \times 2\ m^2$ with a step-like distribution, constant covariance error and no constraints. On the left (a) $|FIM|_{\mathcal{D}}$ is shown (lighter regions, larger accuracy) and on the right (b) the FIM determinant values in $\mathcal{D}$. In (c) $tr(CRB)_{\mathcal{D}}$ is shown (lighter regions, larger accuracy) and in (d) the values of the trace of the CRB in $\mathcal{D}$.

determinant (and the CRB trace) over all the region is almost the theoretical maximum, providing a very large accuracy inside the work area.

One important feature to remark about this example, is that if we consider a very large region and there is no constraints for the sensor placement, then it is possible to design sensor configurations that provide a very large accuracy inside the area of interest because the distance does not affect the measurements. ■

Example 2.7: Distance-dependent covariance error and no constraints.

In this example, shown in Figure 2.8, the optimal formation is quite smaller than the one of the previous example because the distance between target and sensors dramatically affects the measurement error and the formation becomes smaller to reduce this distance-dependent added error. In 2.4.2 it was commented that some constraints must be imposed to the design of the optimal formation so that the sensor formation does not collapse over the target position in an attempt to reduce this distance-dependent added error as much as possible. This problem does not arise in the

Table 2.4: Optimal sensor positions for $\sigma = 0.1\ m$, $\gamma = 1$ and $\eta = 0.05$.

	p_1	p_2	p_3	p_4
$\{x_I\} - coordinate\ (m)$	0.69	−0.69	0.69	−0.69
$\{y_I\} - coordinate\ (m)$	0.69	0.69	−0.69	−0.69

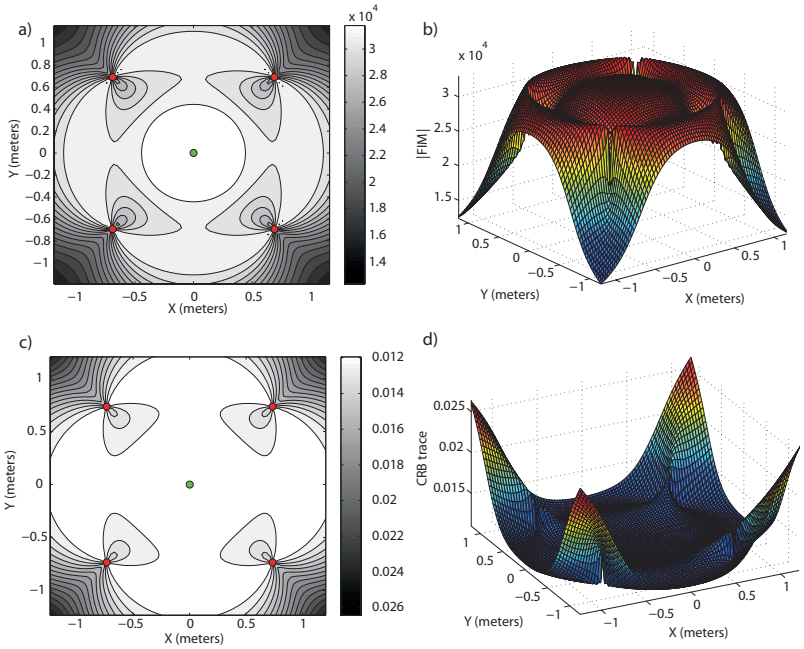

Figure 2.8: Optimal sensor formation for a 4 sensor network, distance-dependent covariance error and uncertainty in the target location defined by a step-like distribution over a region of $2 \times 2\ m^2$. On the left (a) $|FIM|_{\mathcal{D}}$ is shown and on the right (b) the FIM determinant value in $\mathcal{D}$. In (c) $tr(CRB)_{\mathcal{D}}$ is shown and in (d) the value of the trace of the CRB in $\mathcal{D}$.

problem at hand because the measurement accuracy must be maximized over a region, not for an isolate point, so the distance cannot be reduced to the minimum for all the points of the work area and a tradeoff solution must be adopted. The uncertainty in the target position is itself the necessary constraint for a correct design. The optimal sensor positions are shown in Table 2.4.

In Figure 2.8 (a) the average FIM determinant is maximized over the area of interest; and the magnitude of the determinants can be checked in 2.8 (b). In Figure 2.8 (c) the CRB trace corresponding to this sensor network is shown, and in Figure 2.8 (d) its value over the area of interest can be checked. It can be noticed how the maximization of the determinant over the work area provides a minimum CRB trace as well.

In this example a small area of interest has been considered just to illustrate the methodology developed to determine optimal sensor configurations. For larger areas, the formation will be conditioned by the distance-dependent added error and for very large areas the measurement accuracy will be drastically reduced. In a practical scenario, the accuracy will be mission-dependent so this accuracy will determine the number of sensors to be used and their configuration. The problem of a large area of interest shows clearly its practical interest for the multiple target

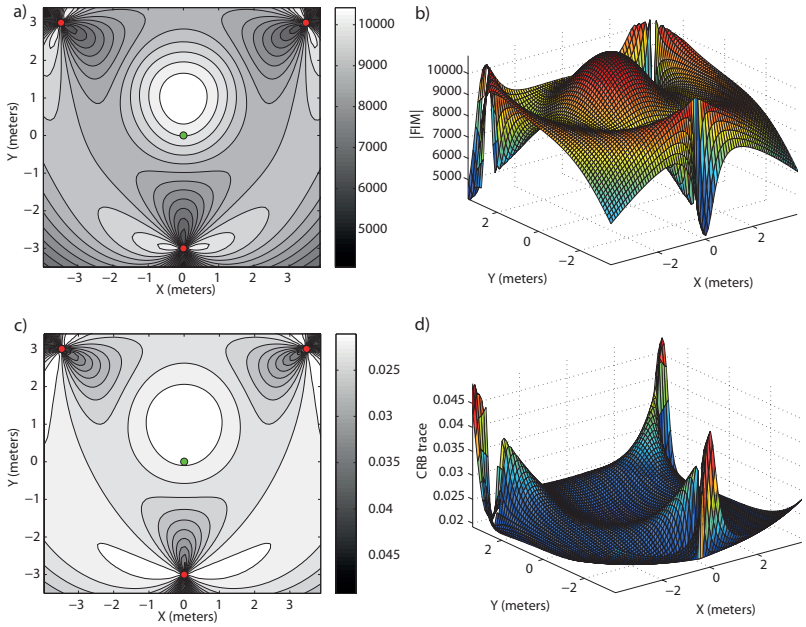

Figure 2.9: Optimal sensor formation for a 3 sensor network with distance-dependent measurement noise. The sensors must be placed in the region $\{y > 3\} U \{y < -3\}$ m. On the left (a) $|FIM|_{\mathcal{D}}$ is shown and on the right (b) the FIM determinant value in $\mathcal{D}$. In (c) $tr(CRB)_{\mathcal{D}}$ is shown and in (d) the value of the trace of the CRB in $\mathcal{D}$.

Table 2.5: Optimal sensor positions for $\sigma = 0.1$ m, $\gamma = 1$ and $\eta = 0.05$.

	p_1	p_2	p_3
$\{x_I\} - coordinate\ (m)$	-3.4749	0	3.4749
$\{y_I\} - coordinate\ (m)$	3	-3	3

positioning problem, that will be studied in detail in Chapter 3 and Chapter 5. ■

Example 2.8: Distance-dependent error with constraints

This last example tackles with the more complex problem of determining the optimal sensor configuration when the sensor network is subject to constraints and the measurement error is distance-dependent. A 3 sensor network that must be placed in the region defined by $\{y > 3\} U \{y < -3\}$ m is considered. We can notice in Figure 2.9 (a) how the sensors are placed at the limit of the design area to increase the average FIM determinant inside the work area by reducing as much as possible the distance-dependent measurement error, and in Figure 2.9 (b) we can check the magnitude of these FIM determinants inside the work area. In Figure 2.9 (c) and (d) similar plots to (a) and (b), respectively, are shown but considering the CRB trace. It can be noticed how the minimum values of the CRB trace belong to the work area. The optimal sensor positions are stated in Table 2.5. This is only a simple example on optimal sensor formation with constraints, because any constraint may be imposed to the design, and its corresponding optimal sensor network must be obtained via optimization tools. ■

2.6 Conclusions

The problem of optimal sensor placement for single target positioning in 2D scenarios has been studied in this chapter. Previous to the study of this problem, the optimal Fisher Information Matrix, with distance-dependent covariance error, that maximizes the logarithm of the FIM determinant was well defined. This optimal FIM defines the design conditions that the optimal sensor formation must achieve so that the maximum logarithm of the FIM determinant be obtained at the target position. The optimality conditions were defined by (2.25).

The first problem studied was the one in which the measurement error is Gaussian with its covariance being constant. This situation has been widely studied in the ground robotics field, where the distances are not so large and the covariance can be considered constant. From the study of the optimality conditions (2.25) the analytical solution in which the sensors must be first and second moment balanced to obtain the maximum FIM determinant was defined.

This study was extended to a second and more complex problem, when the distance affects to the measurement error and then the covariance of the measurement error is distance-dependent. In this kind of problems it is necessary to impose constraints to the sensor formation, because the sensors tend to converge at the target position to reduce the distance-dependent measurement error. The most simple constraint, that corresponds to the case in which the sensors lie in a circumference centred at the target position, was initially studied. The solution for this problem was the same analytical solution defined for the constant covariance error problem. After this simplest case, the more general problem with any number and any kind of constraints was studied. The impossibility to define an analytical solution drove to employ optimization methods to define the optimal sensor configurations, and it was shown that a simple method like the gradient or the Newton method are much more than satisfactory tools to find the optimal sensor configurations.

Finally, the above results were extended to the more realistic problem where the target position is known with uncertainty. This uncertainty can be defined by any probabilistic distribution function, and the kind of function used determines in high degree the optimal sensor formation. An optimization method similar to the one previously defined was used to determine the optimal sensor configurations. The main problem to overcome was the resolution of the integrals of the gradient equations, to determine the necessary gradients to increase the average FIM determinant over the work area. These integrals were solved numerically by the Monte Carlo method because of the impossibility to solve them analytically. Different design scenarios and their corresponding optimal solutions were studied.

Chapter 3

MULTIPLE TARGET POSITIONING IN 2D SCENARIOS WITH RANGE MEASUREMENTS

3.1 Introduction

In the present chapter, inspired by developments in ground robotics for single target positioning, we tackle the *multiple target positioning problem*. Clearly, there will be tradeoffs involved in the precision with which each of the targets can be localized; to study them, we resort to techniques that borrow from estimation theory and Pareto optimization. For the latter, the reader is referred to [45], [22], [90]. See also Appendix A for a very short review of some key concepts and results. Stated briefly, we avail ourselves of concepts on Pareto-optimality and maximize convex combinations of the logarithms of the determinants of the FIMs for each of the targets in order to compute the Pareto-optimal surface that gives a clear image of the tradeoffs involved in the multiobjective optimization problem. We thus obtain a powerful tool to determine the sensor configuration that yields, if possible, a proper tradeoff for the accuracy with which the position of the different targets can be computed. In what follows, and with an obvious abuse of notation, we often refer to Pareto-optimal solutions simply as optimal.

It is important to remark that for the multiobjective optimization problem, the logarithms of the determinants of the FIMs must be used. This makes the functions to be maximized jointly convex in the search parameter space, thus justifying the use of scalarization techniques in the computation of the Pareto-optimal surface, as described in Appendix A. For a discussion of the convexity of the functions adopted, see for example [12], Chapter 3 and the work in [85] on the D-optimality criterion.

For a multi-target localization problem, the optimal geometry of the sensor configuration depends strongly on the constraints imposed by the task itself (e.g. maximum number and type of sensors that can be used), the environment (e.g. ambient noise), the number of targets and their configuration, and the possibly different degrees of precision with which their positions should be

estimated. An inadequate sensor configuration may yield large localization errors for some of the targets. Even though the problem of optimal sensor placement for range based localization is of great importance, not many results are available on this topic yet, even more, the results are only for single target positioning. Some exceptions include the work of [91], that although it deals with the problem of single target positioning, the problem framework is the design of sensor networks for the maximization of the accuracy for a preplanned trajectory to be followed by the target, moreover, uncertainty in the target position along the trajectory is considered. This problem can be seen as a multiple target positioning problem in which the accuracy of some fixed points must be maximized, where these points belong to the desired preplanned trajectory. An incremental optimization algorithm is defined to increase the likelihood of the vehicle following its intended trajectory. Another interesting work is [2], in which the problem of detecting and locating subsurface objects by using a manoeuvring array that receives scattered seismic surface waves is considered. The goal is to minimize the number of distinct measurements (array movements) needed to localize objects, such as buried landmines, while maximizing the determinant of the FIM. The scenario in which two targets must be localized is studied too.

The key contributions of the present chapter are twofold: i) we fully exploit concepts and techniques from estimation theory and multiobjective optimization to obtain a numerical solution to the optimal sensor configuration problem for multiple targets, and ii) in striking contrast to what is customary in the literature, where zero mean Gaussian processes with fixed variances are assumed for the range measurements, the variances are now allowed to depend explicitly on the ranges themselves. This allows us to capture the fact that measurement noise increases in a non-linear manner with the distances measured.

The chapter is organized as follows. Section 3.2 defines the problem formulation and the set-up for multiple target positioning. In Section 3.3 this problem is studied when the measurement error is Gaussian with constant covariance. The extension of this problem to tackle with Gaussian error with distance-dependent covariance is explained in Section 3.4, in which the optimal sensor configurations are defined from concepts on Pareto optimization. In Section 3.5 the maximization of the average value of the logarithms of the FIM determinants is studied when a static fixed sensor network surveys a certain working area or when there is uncertainty in the *a priori* knowledge about the target positions. Finally, in Section 3.6 the conclusions are commented.

3.2 Problem formulation: multiple target in a 2D scenario

The problem of multiple target positioning in 2D scenarios is tackled as an introductory step for the multiple target positioning problem in 3D scenarios, which will be studied in Chapter 5. For the problem at hand the FIM is characterized for a two-dimensional (2D) scenario, following the same procedure shown in Chapter 2.

Thus let $\{I\}$ be an inertial reference frame with unit axis $\{x_I\}, \{y_I\}$, and let $q = [q_{kx}, q_{ky}]^T$; $k = 1, 2, .., m$, be the position of the $k-th$ target to be positioned in $\{I\}$. Further denote by $p_i = [p_{ix}, p_{iy}]^T$; $i = 1, 2, .., n$, the position of the $i-th$ acoustic ranging sensor, also in $\{I\}$. Let $r_{ki}(q) = |q_k - p_i|$ (abbv. r_{ki}) be the distance (range) between the target q_k and the $i-th$ sensor, where $|\cdot|$ denotes the Euclidean norm, and ω_i the corresponding measurement noise as explained in Chapter 2. The variables and the set-up that will be used are illustrated in Figure 3.1 for the case of one target and three sensors.

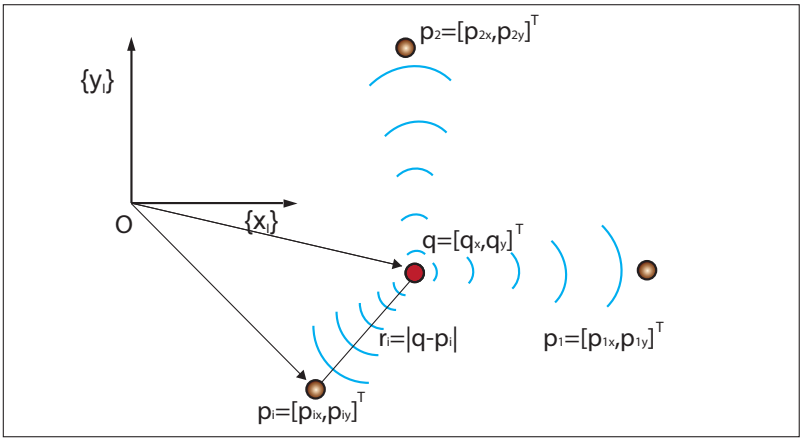

Figure 3.1: Target localization problem set-up.

With this notation, the FIM for the $k-th$ target becomes

$$FIM_k = \sum_{i=1}^{n} \begin{pmatrix} (u_{ix})^2 & (u_{iy})(u_{ix}) \\ (u_{ix})(u_{iy}) & (u_{iy})^2 \end{pmatrix} \tag{3.1}$$

where

$$u_i = [u_{ix}, u_{iy}]^T = \left[\frac{\partial |q_k - p_i|}{\partial q_x} \Gamma_i, \quad \frac{\partial |q_k - p_i|}{\partial q_y} \Gamma_i \right]^T; \tag{3.2}$$

and $\Gamma_i = 1/\left(1 + \eta r_{ki}^{\gamma}\right)$ for $i \in \{1, ..., n\}$ and $k \in \{1, ..., m\}$.

As explained, the determinants of the FIMs for each of the targets are used in the computation of an indicator of the performance that is achievable with a given sensor configuration. Maximizing this indicator (which, as a consequence of the Pareto-optimality conditions described in Appendix B, is a convex combination of the logarithms of the determinants of the different FIMs) yields the most appropriate sensor formation geometry for the multiple target positioning problem:

$$\bar{p}^* = arg \max_{\bar{p}} \sum_{k=1}^{m} \log |FIM_k| \tag{3.3}$$

where m is the number of targets involved in the multiple target positioning task, and $\bar{p}$ is the vector of sensor positions.

In the ground robotics field it is widely assumed that the measurement noise belongs to a Gaussian distribution with constant covariance. This kind of noise is considered for a first analysis of the multiple target positioning problem. Starting from this initial analysis, a deeper study is carried out next considering that the covariance can vary in a non-linear manner with the distance between sensors and targets, to overcome all the possible situations and application problems in a 2D scenario.

The optimal sensor configuration that maximizes the FIM determinant of each of the targets is searched from Pareto-optimality conditions and convex optimization tools, so the convexity for the problem at hand should be demonstrated. It is important to point out at this moment that although

we speak of convexity, we actually search for the concavity of the log determinant of the FIM since we deal with a maximization problem. In this sense, the simplest problem of a 2 sensor network is studied because it is possible to demonstrate analytically the convexity (concavity) of the optimality criterion, and thus that a global unique solution may be obtained with numerical methods. For a larger number of sensors the complexity of the functions does not allow to demonstrate the convexity (concavity) of the criterion. For a discussion of the convexity of the functions adopted, see for example [12], Chapter 3 and the work in [85] on the D-optimality criterion. For this purpose the notation introduced in [6] for the FIM determinant is used, that for a distance-dependent covariance error becomes

$$|FIM| = \frac{1}{\sigma^4} \sum_{j \leq l}^{n} \frac{\left(\left(u_j \times u_l \right) \cdot [0,0,1] \right)^2}{\left(1 + \eta r_j^{\gamma} \right)^2 \left(1 + \eta r_l^{\gamma} \right)^2} = \frac{1}{\sigma^4} \sum_{j \leq l}^{n} \frac{\sin^2 \left(\alpha_{jl} \right)}{\left(1 + \eta r_j^{\gamma} \right)^2 \left(1 + \eta r_l^{\gamma} \right)^2} \tag{3.4}$$

where

$$u_j = [u_{jx}, u_{jy}, 0]^T = \left[\begin{array}{ccc} \frac{\partial |q - p_j|}{\partial q_x} & \frac{\partial |q - p_j|}{\partial q_y} & 0 \end{array} \right]^T; \tag{3.5}$$

$j \in \{1, ..., n\}$; identical definitions apply to the index l; and α_{jl} is the angle formed by the vectors u_j and u_l. The optimal sensor configuration will be defined as the one which maximizes the logarithm of (3.4).

For the sake of simplicity and clarity in the exposition, both scenarios with constant covariance and distance-dependent covariance are studied separately. The main reason is that for constant covariance the demonstration of concavity is easy and straightforward. Moreover, in this scenario it is possible to achieve an accuracy close to the optimal one that would be obtained for one single target working in isolation for each of the targets involved in the positioning task. Thus, this simpler problem is dealt with first.

Equation (3.4) for $\eta = 0$ and n=2 becomes

$$|FIM| = \frac{1}{\sigma^4} \sin^2 (\alpha_{12}) \tag{3.6}$$

It is important to remark that the concavity of the logarithm of the FIM determinant is restricted to positive definite matrices, therefore the domain of the logarithm of (3.6) cannot contain FIM determinants equal to zero, i.e., the sensors and targets cannot be collinear and thus $\alpha_{12} \in]0, \pi[$. For the domain $\alpha_{12} \in]\pi, 2\pi[$ the solutions are equivalent and define the same formations only by rotating them the adequate angle. We compute the first derivative of the logarithm of (3.6) with respect to the angle α_{12}, that yields

$$\frac{\partial \log |FIM|}{\partial \alpha_{12}} = \frac{2 \sin (\alpha_{12}) \cos (\alpha_{12})}{\sigma^4 \cdot \sin^2 (\alpha_{12})} \tag{3.7}$$

The second derivative yields

$$\frac{\partial^2 \log |FIM|}{\partial \alpha_{12}^2} = \frac{-2 \sin^4 (\alpha_{12}) - 2 \sin^2 (\alpha_{12}) \cos^2 (\alpha_{12})}{\sigma^4 \cdot \sin^4 (\alpha_{12})} = \frac{-2}{\sigma^4 \cdot \sin^2 (\alpha_{12})} \tag{3.8}$$

that is negative for all the domain, therefore (3.6) is a concave function and we can employ Pareto optimization tools to determine the optimal sensor configurations. The analysis for a larger number of sensors is not undertaken due to the complexity of the functions, but we assume that we can employ these optimization tools to determine the optimal solutions in the scenarios in which an

analytical solution is not feasible.

For the distance-dependent covariance case the demonstration is not straightforward because it depends on the constraints imposed to the sensor network. For example, if the sensors are placed at a fixed distance from the target, the previous demonstration holds. For each different constraint, it is necessary to test if the criterion is concave or not, but the previous analysis, and the results commented in [12], Chapter 3 and the work in [85] on the D-optimality criterion, give us reasons to employ convex optimization tools. For this latter case, the initial guess will be chosen with care to avoid possible local maxima due to the concavity of the criterion for distance-dependent covariance has not been demonstrated analytically.

3.3 Gaussian error with constant covariance

In this scenario, as seen in Chapter 2, the distances between sensors and targets do not condition the optimal solutions. Only the angles that the range vectors form between them characterize the optimal solutions. If the covariance error is constant, $\eta = 0$, then (3.1) becomes

$$FIM_k = \frac{1}{\sigma^2}\sum_{s=1}^{n}\begin{pmatrix} (u_{sx})^2 & \left(u_{sy}\right)(u_{sx}) \\ (u_{sx})\left(u_{sy}\right) & \left(u_{sy}\right)^2 \end{pmatrix} \tag{3.9}$$

where $u_s = [u_{sx}, u_{sy}]^T = \left[\ \frac{\partial|q_k - p_s|}{\partial q_x},\ \ \frac{\partial|q_k - p_s|}{\partial q_y}\ \right]^T$, for $s \in \{1, ..., n\}$ and $k \in \{1, ..., m\}$. For the sake of clarity in the notations and demonstrations of the forthcoming analysis the index s is used instead the index i in the summations.

As abovementioned, the summation of the logarithms of the FIM determinants is used as an indicator of the performance that is achievable with a given sensor formation. Therefore, the solution for (3.3) defines the optimal sensor configuration. To shed light on this problem the simplest case of two targets and an arbitrary number of sensors (but at least 2 sensors) is studied first. Then this solution is extended to an arbitrary number of targets.

3.3.1 Two targets positioning

In Section 3.2 we have seen that the problem at hand is concave and the optimal solution can be searched with convex optimization techniques. However, in the special scenario of localizing only two targets in 2D it is possible to define an analytical solution. Equation (3.3) becomes

$$\bar{p}^* = arg\max_{\bar{p}} \left(\log|FIM_1| + \log|FIM_2|\right) \tag{3.10}$$

The summation of logarithms in (3.10) is equivalent to:

$$\log|FIM_1| + \log|FIM_2| = \log\left(|FIM_1| \cdot |FIM_2|\right) = \log\left(|FIM_T|\right) \tag{3.11}$$

where the meaning of FIM_T is clear from the context. Moreover, the determinant of (3.9) may be written as

$$|FIM| = \frac{1}{\sigma^4}\left(\sum_{s=1}^{n}\cos^2(\alpha_s),\ -\sum_{s=1}^{n}\cos(\alpha_s)\sin(\alpha_s)\right)\cdot\begin{pmatrix} \sum_{s=1}^{n}\sin^2(\alpha_s) \\ \sum_{s=1}^{n}\cos(\alpha_s)\sin(\alpha_s) \end{pmatrix} \tag{3.12}$$

Thus, from (3.11) and (3.12), (3.10) yields

$$\overline{p}^{*} = arg \max_{\overline{p}} \log \frac{1}{\sigma^{4m}} \prod_{k=1}^{m} \left(\left(\sum_{s=1}^{n} \cos^2(\alpha_{sk}), - \sum_{s=1}^{n} \cos(\alpha_{sk}) \sin(\alpha_{sk}) \right) \cdot \begin{pmatrix} \sum_{s=1}^{n} \sin^2(\alpha_{sk}) \\ \sum_{s=1}^{n} \cos(\alpha_{sk}) \sin(\alpha_{sk}) \end{pmatrix} \right) \tag{3.13}$$

where $k = 1, \cdots, m$ are the number of targets involved in the task. In this particular case $m = 2$.

Equation (3.13) can be written in the following compact form:

$$|FIM_T| = \log \left(\frac{1}{\sigma^{4m}} \prod_{k=1}^{m} \vec{P}_k \cdot \vec{Q}_k \right) \tag{3.14}$$

with

$$\vec{P}_k = \begin{pmatrix} \sum_{s=1}^{n} \cos^2(\alpha_{sk}) \\ - \sum_{s=1}^{n} \cos(\alpha_{sk}) \sin(\alpha_{sk}) \end{pmatrix}^T$$

$$\vec{Q}_k = \begin{pmatrix} \sum_{s=1}^{n} \sin^2(\alpha_{sk}) \\ \sum_{s=1}^{n} \cos(\alpha_{sk}) \sin(\alpha_{sk}) \end{pmatrix}$$

The optimal solution must be computed from the derivatives of (3.14) with respect to each sensor position coordinate, p_{ix} and p_{iy}, with $i = 1, \cdots, n$. The derivative of a dot product is defined by $\partial(\vec{P} \cdot \vec{Q}) = \partial\vec{P} \cdot \vec{Q} + \vec{P} \cdot \partial\vec{Q}$, and the derivative of a vector is defined by the derivatives of each of its elements, $\partial\vec{P} = \begin{bmatrix} \partial\vec{P}_1 & \cdots & \partial\vec{P}_n \end{bmatrix}$, so the derivatives of each vector element with respect to each sensor position coordinate must be defined.

Therefore, it is necessary to compute these derivatives before the complete derivatives of (3.14) with respect to the sensors position coordinates may be defined. The vector element derivatives with respect to the $\{x_I\}$ coordinate of sensor i are (for the $k - th$ target):

$$\frac{\partial \sum_{s=1}^{n} \cos^2(\alpha_{sk})}{\partial p_{ix}} = \frac{\partial \cos^2(\alpha_{ik})}{\partial p_{ix}} = -\frac{2 \cos(\alpha_{ik}) \sin^2(\alpha_{ik})}{r_{ik}} \tag{3.15}$$

$$\frac{\partial \sum_{s=1}^{n} \sin^2(\alpha_{sk})}{\partial p_{ix}} = \frac{\partial \sin^2(\alpha_{ik})}{\partial p_{ix}} = \frac{2 \cos(\alpha_{ik}) \sin^2(\alpha_{ik})}{r_{ik}} \tag{3.16}$$

$$\frac{\partial \sum_{s=1}^{n} \cos(\alpha_{sk}) \sin(\alpha_{sk})}{\partial p_{ix}} = \frac{\partial (\cos(\alpha_{ik}) \sin(\alpha_{ik}))}{\partial p_{ix}} = -\frac{\sin^3(\alpha_{ik})}{r_{ik}} + \frac{\cos^2(\alpha_{ik}) \sin(\alpha_{ik})}{r_{ik}} \tag{3.17}$$

The vector element derivatives with respect to the $\{y_I\}$ coordinate of sensor i are now computed, (for the $k-th$ target):

$$\frac{\partial \sum_{s=1}^{n} \cos^2(\alpha_{sk})}{\partial p_{iy}} = \frac{\partial \cos^2(\alpha_{ik})}{\partial p_{ix}} = \frac{2\cos^2(\alpha_{ik})\sin(\alpha_{ik})}{r_{ik}} \tag{3.18}$$

$$\frac{\partial \sum_{s=1}^{n} \sin^2(\alpha_{sk})}{\partial p_{iy}} = \frac{\partial \sin^2(\alpha_{ik})}{\partial p_{ix}} = -\frac{2\cos^2(\alpha_{ik})\sin(\alpha_{ik})}{r_{ik}} \tag{3.19}$$

$$\frac{\partial \sum_{s=1}^{n} \cos(\alpha_{sk})\sin(\alpha_{sk})}{\partial p_{iy}} = \frac{\partial (\cos(\alpha_{ik})\sin(\alpha_{ik}))}{\partial p_{iy}} = \frac{\cos(\alpha_{ik})\sin^2(\alpha_{ik})}{r_{ik}} - \frac{\cos^3(\alpha_{ik})}{r_{ik}} \tag{3.20}$$

From the above equations we can compute the derivative of (3.14) with respect to the $\{x_I\}$ coordinate of sensor i, that yields

$$\frac{\partial \log|FIM_T|}{\partial p_{ix}} = \begin{pmatrix} -\frac{2\cos(\alpha_{i1})\sin^2(\alpha_{i1})}{r_{i1}} \\ \frac{\sin^3(\alpha_{i1})}{r_{i1}} - \frac{\cos^2(\alpha_{i1})\sin(\alpha_{i1})}{r_{i1}} \end{pmatrix}^T \begin{pmatrix} \sum_{s=1}^{n} \sin^2(\alpha_{s1}) \\ \sum_{s=1}^{n} \cos(\alpha_{s1})\sin(\alpha_{s1}) \end{pmatrix} |FIM_1|^{-1} +$$

$$\begin{pmatrix} \sum_{s=1}^{n} \cos^2(\alpha_{s1}) \\ -\sum_{s=1}^{n} \cos(\alpha_{s1})\sin(\alpha_{s1}) \end{pmatrix}^T \begin{pmatrix} \frac{2\cos(\alpha_{i1})\sin^2(\alpha_{i1})}{r_{i1}} \\ -\frac{\sin^3(\alpha_{i1})}{r_{i1}} + \frac{\cos^2(\alpha_{i1})\sin(\alpha_{i1})}{r_{i1}} \end{pmatrix} |FIM_1|^{-1} +$$

$$\begin{pmatrix} -\frac{2\cos(\alpha_{i2})\sin^2(\alpha_{i2})}{r_{i2}} \\ \frac{\sin^3(\alpha_{i2})}{r_{i2}} - \frac{\cos^2(\alpha_{i2})\sin(\alpha_{i2})}{r_{i2}} \end{pmatrix}^T \begin{pmatrix} \sum_{s=1}^{n} \sin^2(\alpha_{s2}) \\ \sum_{s=1}^{n} \cos(\alpha_{s2})\sin(\alpha_{s2}) \end{pmatrix} |FIM_2|^{-1} +$$

$$\begin{pmatrix} \sum_{s=1}^{n} \cos^2(\alpha_{s2}) \\ -\sum_{s=1}^{n} \cos(\alpha_{s2})\sin(\alpha_{s2}) \end{pmatrix}^T \begin{pmatrix} \frac{2\cos(\alpha_{i2})\sin^2(\alpha_{i2})}{r_{i2}} \\ -\frac{\sin^3(\alpha_{i2})}{r_{i2}} + \frac{\cos^2(\alpha_{i2})\sin(\alpha_{i2})}{r_{i2}} \end{pmatrix} |FIM_2|^{-1}$$

Similarly, the derivative of (3.14) with respect to the $\{y_I\}$ coordinate of sensor i yields

$$\frac{\partial \log|FIM_T|}{\partial p_{iy}} = \begin{pmatrix} \frac{2\cos^2(\alpha_{i1})\sin(\alpha_{i1})}{r_{i1}} \\ -\frac{\cos(\alpha_{i1})\sin^2(\alpha_{i1})}{r_{i1}} + \frac{\cos^3(\alpha_{i1})}{r_{i1}} \end{pmatrix}^T \begin{pmatrix} \sum_{s=1}^{n} \sin^2(\alpha_{s1}) \\ \sum_{s=1}^{n} \cos(\alpha_{s1})\sin(\alpha_{s1}) \end{pmatrix} |FIM_1|^{-1} +$$

$$+\begin{pmatrix} \sum_{s=1}^{n}\cos^2(\alpha_{s1}) \\ -\sum_{s=1}^{n}\cos(\alpha_{s1})\sin(\alpha_{s1}) \end{pmatrix}^T \begin{pmatrix} -\frac{2\cos^2(\alpha_{i1})\sin(\alpha_{i1})}{r_{i1}} \\ +\frac{\cos(\alpha_{i1})\sin^2(\alpha_{i1})}{r_{i1}} - \frac{\cos^3(\alpha_{i1})}{r_{i1}} \end{pmatrix} |FIM_1|^{-1} +$$

$$\begin{pmatrix} \frac{2\cos^2(\alpha_{i2})\sin(\alpha_{i2})}{r_{i2}} \\ -\frac{\cos(\alpha_{i2})\sin^2(\alpha_{i2})}{r_{i2}} + \frac{\cos^3(\alpha_{i2})}{r_{i2}} \end{pmatrix}^T \begin{pmatrix} \sum_{s=1}^{n}\sin^2(\alpha_{s2}) \\ \sum_{s=1}^{n}\cos(\alpha_{s2})\sin(\alpha_{s2}) \end{pmatrix} |FIM_2|^{-1} +$$

$$\begin{pmatrix} \sum_{s=1}^{n}\cos^2(\alpha_{s2}) \\ -\sum_{s=1}^{n}\cos(\alpha_{s2})\sin(\alpha_{s2}) \end{pmatrix}^T \begin{pmatrix} -\frac{2\cos^2(\alpha_{i2})\sin(\alpha_{i2})}{r_{i2}} \\ \frac{\cos(\alpha_{i2})\sin^2(\alpha_{i2})}{r_{i2}} - \frac{\cos^3(\alpha_{i2})}{r_{i2}} \end{pmatrix} |FIM_2|^{-1}$$

Straightforward computations allow to rewrite the above derivatives as

$$\begin{aligned} \frac{\partial \log|FIM_T|}{\partial p_{ix}} = &-\frac{2\cos(\alpha_{i1})\sin^2(\alpha_{i1})}{r_{i1}}\sum_{s=1}^{n}\left(\sin^2(\alpha_{s1})-\cos^2(\alpha_{s1})\right)|FIM_1|^{-1}+ \\ &2\left(\frac{\sin^3(\alpha_{i1})}{r_{i1}}-\frac{\cos^2(\alpha_{i1})\sin(\alpha_{i1})}{r_{i1}}\right)\sum_{s=1}^{n}\cos(\alpha_{s1})\sin(\alpha_{s1})|FIM_1|^{-1}- \\ &\frac{2\cos(\alpha_{i2})\sin^2(\alpha_{i2})}{r_{i2}}\sum_{s=1}^{n}\left(\sin^2(\alpha_{s2})-\cos^2(\alpha_{s2})\right)|FIM_2|^{-1}+ \\ &2\left(\frac{\sin^3(\alpha_{i2})}{r_{i2}}-\frac{\cos^2(\alpha_{i2})\sin(\alpha_{i2})}{r_{i2}}\right)\sum_{s=1}^{n}\cos(\alpha_{s2})\sin(\alpha_{s2})|FIM_2|^{-1} \end{aligned} \tag{3.21}$$

$$\begin{aligned} \frac{\partial \log|FIM_T|}{\partial p_{iy}} = &\frac{2\cos(\alpha_{i1})\sin^2(\alpha_{i1})}{r_{i1}}\sum_{s=1}^{n}\left(\sin^2(\alpha_{s1})-\cos^2(\alpha_{s1})\right)|FIM_1|^{-1}+ \\ &2\left(\frac{\cos^3(\alpha_{i1})}{r_{i1}}-\frac{\cos(\alpha_{i1})\sin^2(\alpha_{i1})}{r_{i1}}\right)\sum_{s=1}^{n}\cos(\alpha_{s1})\sin(\alpha_{s1})|FIM_1|^{-1}+ \\ &\frac{2\cos(\alpha_{i2})\sin^2(\alpha_{i2})}{r_{i2}}\sum_{s=1}^{n}\left(\sin^2(\alpha_{s2})-\cos^2(\alpha_{s2})\right)|FIM_2|^{-1}+ \\ &2\left(\frac{\cos^3(\alpha_{i2})}{r_{i2}}-\frac{\cos(\alpha_{i2})\sin^2(\alpha_{i2})}{r_{i2}}\right)\sum_{s=1}^{n}\cos(\alpha_{s2})\sin(\alpha_{s2})|FIM_2|^{-1} \end{aligned} \tag{3.22}$$

Making these equations be equal to 0 the optimal sensor configuration may be defined. Equations (3.21) and (3.22) can be rewritten again as

$$\frac{\partial \log |FIM_T|}{\partial p_{ix}} = \frac{\sin(\alpha_{i1})}{r_{i1}}\left[\sin(2\alpha_{i1})\sum_{s=1}^{n}\cos(2\alpha_{s1}) - \cos(2\alpha_{i1})\sum_{s=1}^{n}\sin(2\alpha_{s1})\right]|FIM_2| + \frac{\sin(\alpha_{i2})}{r_{i2}}\left[\sin(2\alpha_{i2})\sum_{s=1}^{n}\cos(2\alpha_{s2}) - \cos(2\alpha_{i2})\sum_{s=1}^{n}\sin(2\alpha_{s2})\right]|FIM_1| = 0 \tag{3.23}$$

$$\frac{\partial \log |FIM_T|}{\partial p_{iy}} = \frac{\cos(\alpha_{i1})}{r_{i1}}\left[-\sin(2\alpha_{i1})\sum_{s=1}^{n}\cos(2\alpha_{s1}) + \cos(2\alpha_{i1})\sum_{s=1}^{n}\sin(2\alpha_{s1})\right]|FIM_2| + \frac{\cos(\alpha_{i2})}{r_{i2}}\left[-\sin(2\alpha_{i2})\sum_{s=1}^{n}\cos(2\alpha_{s2}) + \cos(2\alpha_{i2})\sum_{s=1}^{n}\sin(2\alpha_{s2})\right]|FIM_1| = 0 \tag{3.24}$$

Now (3.23) and (3.24) can be seen as dot products:

$$\frac{\partial \log |FIM_T|}{\partial p_{ix}} = \begin{pmatrix} \frac{\sin(\alpha_{i1})}{r_{i1}} \cdot v_{i1} & \frac{\sin(\alpha_{i2})}{r_{i2}} \cdot v_{i2} \end{pmatrix} \begin{pmatrix} \frac{1}{|FIM_1|} \\ \frac{1}{|FIM_2|} \end{pmatrix} = 0 \tag{3.25}$$

$$\frac{\partial \log |FIM_T|}{\partial p_{iy}} = \begin{pmatrix} -\frac{\cos(\alpha_{i1})}{r_{i1}} \cdot v_{i1} & -\frac{\cos(\alpha_{i2})}{r_{i2}} \cdot v_{i2} \end{pmatrix} \begin{pmatrix} \frac{1}{|FIM_1|} \\ \frac{1}{|FIM_2|} \end{pmatrix} = 0 \tag{3.26}$$

where $v_{ik} = \sin(2\alpha_{ik})\sum_{s=1}^{n}\cos(2\alpha_{sk}) - \cos(2\alpha_{ik})\sum_{s=1}^{n}\sin(2\alpha_{sk})$ for $k = 1, 2$. It is easy to check that if the dot products are equal to zero, then the vectors are orthogonal, and therefore the vectors

$$V_1 = \begin{pmatrix} \frac{\sin(\alpha_{i1})}{r_{i1}} \cdot v_{i1} & \frac{\sin(\alpha_{i2})}{r_{i2}} \cdot v_{i2} \end{pmatrix}$$

$$V_2 = \begin{pmatrix} -\frac{\cos(\alpha_{i1})}{r_{i1}} \cdot v_{i1} & -\frac{\cos(\alpha_{i2})}{r_{i2}} \cdot v_{i2} \end{pmatrix}$$

are equivalent, and then $V_1(1)/V_2(1) = V_1(2)/V_2(2)$, it is,

$$\frac{-\sin(\alpha_{i1}) \cdot r_{i1} \cdot v_{i1}}{\cos(\alpha_{i1}) \cdot r_{i1} \cdot v_{i1}} = \frac{-\sin(\alpha_{i2}) \cdot r_{i2} \cdot v_{i2}}{\cos(\alpha_{i2}) \cdot r_{i2} \cdot v_{i2}} \rightarrow \tan(\alpha_{i1}) = \tan(\alpha_{i2}) \tag{3.27}$$

Equation (3.27) holds when $\alpha_{i1} = \alpha_{i2} + t \cdot \pi$ with t being any natural number. This condition means that all the sensors must lie in the line joining the two targets since (3.27) must hold for all sensors; therefore this solution can be discarded because obviously it is not an optimal solution.

It is important to notice from (3.25) and (3.26) that the vector $\left[\ \frac{1}{|FIM_1|}, \ \frac{1}{|FIM_2|}\ \right]^T$ is always different from zero and positive, so the only possible solution is that vectors V_1 and V_2 be equal to zero. A closer look to these vectors shows that the condition for them to be zero is that v_{ik} be equal

to zero.

$$v_{ik} = \sin(2\alpha_{ik}) \sum_{s=1}^{n} \cos(2\alpha_{sk}) - \cos(2\alpha_{ik}) \sum_{s=1}^{n} \sin(2\alpha_{sk}) = 0 \tag{3.28}$$

with $k = 1, 2$. Now (3.28) can be seen again as a dot product between two vectors:

$$\left(\sum_{s=1}^{n} \cos(2\alpha_{sk}) \quad \sum_{s=1}^{n} \sin(2\alpha_{sk}) \right) \cdot \left(\sin(2\alpha_{ik}) \quad -\cos(2\alpha_{ik}) \right) = 0 \tag{3.29}$$

This equation must hold for each sensor and each target. It is clear that if both vectors are different from zero, (3.29) means that the vectors are orthogonal. In this case, the first array of the dot product of (3.29) is constant for each target and for a given sensor configuration, thus the second array of (3.29) that defines the orientation of the sensor i with respect to a given target k must be the same for all sensors, something that is not optimal for a single target and that is impossible to achieve for more than one target. Hence, this solution is discarded and the only valid solution is the one in which one of the vectors of (3.29) is the null vector. A simple look to (3.29) shows that

$$\left(\cos(2\alpha_{ik}) \quad \sin(2\alpha_{ik}) \right) \neq \left(0 \quad 0 \right)$$

and then, the optimality condition is

$$\left(\sum_{s=1}^{n} \cos(2\alpha_{sk}) \quad \sum_{s=1}^{n} \sin(2\alpha_{sk}) \right) = \left(0 \quad 0 \right) \tag{3.30}$$

Therefore, the sensor network must be second moment balanced with respect to both targets to obtain the maximum accuracy possible in the positioning of the two targets:

$$\begin{aligned} \sum_{s=1}^{n} \cos(2\alpha_{sk}) &= \sum_{s=1}^{n} \left(\cos^2(\alpha_{sk}) - \sin^2(\alpha_{sk}) \right) = 0 \\ \sum_{s=1}^{n} \sin(2\alpha_{sk}) &= \sum_{s=1}^{n} 2\cos(\alpha_{sk}) \sin(\alpha_{sk}) = 0 \end{aligned} \tag{3.31}$$

Conditions (3.30) are valid for any number of sensors. Moreover, the previous solution provides an optimal sensor formation that achieves the theoretical maximum accuracy for both targets at the same time and it is not necessary to define a trade-off solution. For more than two targets (3.30) is not the only valid solution, as it will be studied in the next section, moreover, it is possible that the maximum accuracy for all the targets cannot be obtained, and then a tradeoff solution must be adopted.

3.3.2 Multiple target positioning

Once the analytical solution for the two target positioning problem has been defined, the above analysis can be extended for an arbitrary number of targets. From (3.11) we can obtain again the equations (3.23) and (3.24) that define the optimal sensor configurations. In this scenario (3.23) and

(3.24) must be rewritten for the m targets:

$$\frac{\partial \log |FIM_T|}{\partial p_{ix}} = \frac{\sin(\alpha_{i1})}{r_{i1}\,|FIM_1|}\left[\sin(2\alpha_{i1})\sum_{s=1}^{n}\cos(2\alpha_{s1}) - \cos(2\alpha_{i1})\sum_{s=1}^{n}\sin(2\alpha_{s1})\right] + \cdots + \frac{\sin(\alpha_{im})}{r_{im}\,|FIM_m|}\left[\sin(2\alpha_{im})\sum_{s=1}^{n}\cos(2\alpha_{sm}) - \cos(2\alpha_{im})\sum_{s=1}^{n}\sin(2\alpha_{sm})\right] = 0 \tag{3.32}$$

$$\frac{\partial \log |FIM_T|}{\partial p_{iy}} = \frac{\cos(\alpha_{i1})}{r_{i1}\,|FIM_1|}\left[-\sin(2\alpha_{i1})\sum_{s=1}^{n}\cos(2\alpha_{s1}) + \cos(2\alpha_{i1})\sum_{s=1}^{n}\sin(2\alpha_{s1})\right] + \cdots + \frac{\cos(\alpha_{im})}{r_{im}\,|FIM_m|}\left[-\sin(2\alpha_{im})\sum_{s=1}^{n}\cos(2\alpha_{sm}) + \cos(2\alpha_{im})\sum_{s=1}^{n}\sin(2\alpha_{sm})\right] = 0 \tag{3.33}$$

Again (3.32) and (3.33) can be written as dot products between two vectors:

$$\frac{\partial \log |FIM_T|}{\partial p_{ix}} = \begin{pmatrix} \frac{\sin(\alpha_{i1})}{r_{i1}}\cdot v_{i1} & \cdots & \frac{\sin(\alpha_{im})}{r_{im}}\cdot v_{im} \end{pmatrix} \begin{pmatrix} \frac{1}{|FIM_1|} \\ \vdots \\ \frac{1}{|FIM_m|} \end{pmatrix} = 0 \tag{3.34}$$

$$\frac{\partial \log |FIM_T|}{\partial p_{iy}} = \begin{pmatrix} -\frac{\cos(\alpha_{i1})}{r_{i1}}\cdot v_{i1} & \cdots & -\frac{\cos(\alpha_{im})}{r_{im}}\cdot v_{im} \end{pmatrix} \begin{pmatrix} \frac{1}{|FIM_1|} \\ \vdots \\ \frac{1}{|FIM_m|} \end{pmatrix} = 0 \tag{3.35}$$

with $v_{ik} = \sin(2\alpha_{ik})\sum_{s=1}^{n}\cos(2\alpha_{sk}) - \cos(2\alpha_{ik})\sum_{s=1}^{n}\sin(2\alpha_{sk})$. Equations (3.34) and (3.35) must hold for all the sensors of the network. It should be noticed that the above system of equations could have multiple tradeoff solutions. Nevertheless, the solution (3.30) is one of the valid solutions for (3.34) and (3.35) that also provides the theoretical maximum FIM determinant for each target. Thus if it is possible to obtain a sensor configuration where (3.30) holds, then the minimum covariance error (or maximum FIM determinant) for each target is obtained. This optimal configuration will provide the maximum FIM determinant $n^2/\sigma^4 2^2$, as defined in [11] and [55].

However, (3.30) can be or not a solution for a given multiple target localization problem, depending on the configuration of the targets and the number of sensors. If it is not possible to define a sensor configuration with which (3.30) be true for all the targets, then a tradeoff solution must be adopted. The tradeoff solutions are obtained by resorting to an optimization algorithm that will be explained in detail in the following section for distance-dependent covariance error because for this latter case it is not possible to determine the optimal solution analytically. It is important to remark at this point that when the covariance is constant it is possible to obtain accuracies for each of the targets which are very close to the optimal one that would be obtained for a single target

working in isolation. For distance-dependent covariance, this situation changes drastically and the tradeoffs involved are clear. These tradeoffs are mission-dependent.

It can also be noticed that one possible optimal solution for the problem at hand is a regular distribution of sensors around the centre of mass of the targets, with the sensors placed at an infinite distance from the centre of mass. Mathematically, this solution is feasible because for constant covariance the distance does not affect the measurement error. In this unrealistic solution the sensor network would be regularly distributed around all the targets, and all the FIM determinants would be maximum. However, it is clear that it is not possible to reproduce this solution in a real environment due to physical constraints, moreover, this solution shows the unrealistic assumption of a constant covariance error for the measurements, so a more realistic error model must be defined and used.

3.3.3 Simulation examples

Some examples on optimal sensor placement for a multi-target scenario are studied to illustrate the methodology developed.

Clearly in order for the information about the optimal configurations to be useful, one must check if the determinants of the individual FIMs for each target meet desired specifications. To this effect, and for comparison purposes, the determinant of the FIMs obtained for a number of hypothetical target points (based on a fixed optimal sensor configuration corresponding to a well-defined multi-target scenario) will at times be computed by allowing these points to be on a grid in a finite spatial region $\mathcal{D}$. This will allow us to evaluate how good the sensor formation is in terms of yielding accurate localization of the real targets, in comparison with the performance localization accuracy that is possible for any hypothetical target (different from the real targets) positioned anywhere in $\mathcal{D}$. For the sake of clarity, and with an obvious abuse of notation, we will refer to that determinant, viewed as a function of its argument in $\mathcal{D}$, simply as $|FIM|_{\mathcal{D}}$. In this chapter, $\mathcal{D}$ will always be a rectangle in $\Re^2$. The same comments apply to $tr(CRB)_{\mathcal{D}}$.

Example 3.1: 4 sensor network, 2 targets.

This example tackles the case of a 4 sensor network for the positioning of two targets with no constraints in the sensor placement, with $\sigma = 0.1\ m$. The optimal solution for both targets can be designed through the design condition (3.30). The targets are considered to be placed at $q_1 = [2,\ 0]^T\ m$ and $q_2 = [-2,\ 0]^T\ m$. It must be noticed that the distance between targets is not really important and does not affect the sensor configuration. The same solution, in a geometric sense, would be obtained for any distance between targets by only applying the adequate scalarization to the sensor configuration, because the measurement error is distance-independent.

Table 3.1: Target positions and optimal sensor positions.

	q_1	q_2	p_1	p_2	p_3	p_4
$\{x_I\} - coordinate\ (m)$	2	−2	−3.8435	−3.8435	3.8435	3.8435
$\{y_I\} - coordinate\ (m)$	0	0	3.2861	−3.2861	−3.2861	3.2861

One of the feasible optimal sensor formations may be defined by the positions listed in Table 3.1 and shown in Figure 3.2 (a), which provides the maximum FIM determinant $|FIM| = n^2/(\sigma^4 \cdot 4)\ m^{-4}$ for each target. In Figure 3.2 (c), we can notice how the formation provides also the minimum CRB trace, $tr(CRB) = \sigma^2 \cdot 4/n\ m^2$. The solution shown in this example is not unique, it is possible to design several optimal sensor configurations.

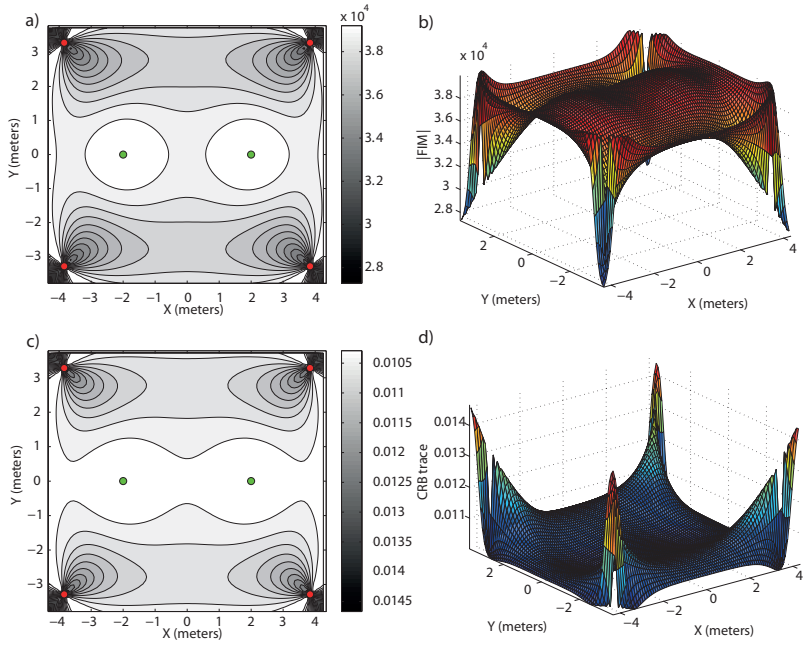

Figure 3.2: Optimal 4 sensor formation for 2 target positioning with constant covariance error. In (a) $|FIM|_{\mathcal{D}}$ in $\Re^2$ is shown and in (b) its magnitude in $\Re^2$. Similarly, in (c) $tr(CRB)_{\mathcal{D}}$ is shown and in (d) its magnitude for each point in $\Re^2$.

We can appreciate in Figure 3.2 (b) and (d) how the maximum value of the FIM determinant and the minimum value of the CRB trace, respectively, are over the target positions. We can notice how the design condition (3.30) is achieved by the present formation for both targets. For $q_1 = [2,\ 0]^T$ m we have:

$$\sum_{i=1}^{n}\left(\cos^2(\alpha_{i1}) - \sin^2(\alpha_{i1})\right) = \left(\frac{-3.8435-2}{6.7041}\right)^2 + \left(\frac{-3.8435-2}{6.7041}\right)^2 + \left(\frac{3.8435-2}{3.7679}\right)^2$$

$$+\left(\frac{3.8435-2}{3.7679}\right)^2 - \left(\frac{-3.8435}{6.7041}\right)^2 - \left(\frac{-3.8435}{6.7041}\right)^2$$

$$-\left(\frac{3.8435}{3.7679}\right)^2 - \left(\frac{3.8435}{3.7679}\right)^2 = 0$$

$$\sum_{i=1}^{n} 2\cos(\alpha_{i1})\sin(\alpha_{i1}) = \left(\frac{-3.8435-2}{6.7041}\right)\left(\frac{-3.8435}{6.7041}\right) + \left(\frac{-3.8435-2}{6.7041}\right)\left(\frac{-3.8435}{6.7041}\right)$$

$$\left(\frac{3.8435-2}{3.7679}\right)\left(\frac{3.8435}{3.7679}\right) + \left(\frac{3.8435-2}{3.7679}\right)\left(\frac{3.8435}{3.7679}\right) = 0$$

and for the target $q_2 = [-2,\ 0]^T\ m$:

$$\sum_{i=1}^{n}\left(\cos^2(\alpha_{i2}) - \sin^2(\alpha_{i2})\right) = \left(\frac{3.8435+2}{6.7041}\right)^2 + \left(\frac{3.8435+2}{6.7041}\right)^2 + \left(\frac{-3.8435+2}{3.7679}\right)^2$$

$$+\left(\frac{-3.8435+2}{3.7679}\right)^2 - \left(\frac{3.8435}{6.7041}\right)^2 - \left(\frac{3.8435}{6.7041}\right)^2$$

$$-\left(\frac{-3.8435}{3.7679}\right)^2 - \left(\frac{-3.8435}{3.7679}\right)^2 = 0$$

$$\sum_{i=1}^{n} 2\cos(\alpha_{i2})\sin(\alpha_{i2}) = \left(\frac{3.8435+2}{6.7041}\right)\left(\frac{3.8435}{6.7041}\right) + \left(\frac{3.8435+2}{6.7041}\right)\left(\frac{3.8435}{6.7041}\right)$$

$$\left(\frac{-3.8435+2}{3.7679}\right)\left(\frac{-3.8435}{3.7679}\right) + \left(\frac{-3.8435+2}{3.7679}\right)\left(\frac{-3.8435}{3.7679}\right) = 0$$

Therefore it is easy to check that an optimal formation that provides the theoretical maximum FIM determinant, and also the theoretical minimum CRB trace, is achieved when (3.30) holds for each target. ■

Example 3.2: 5 sensors, 3 targets.

A more complex example is now defined, with 5 sensors and 3 targets. Again with (3.30) it is possible to define an optimal configuration with which the maximum measurement accuracy is obtained for each target. The target and sensor positions are stated in Table 3.2, and in Figure 3.3 the optimal configuration is shown.

Table 3.2: Target positions and optimal sensor positions.

	q_1	q_2	q_3	p_1	p_2	p_3	p_4	p_5
$\{x_I\}$ – *coordinate* (m)	−2.5	−2.5	5	6.01	−3.12	−8	−2.35	6.91
$\{y_I\}$ – *coordinate* (m)	1.7	−3.5	0	3.11	6.31	1.37	−6.17	−3.76

In Figure 3.3 (a) and (b) it can be seen how the theoretical maximum FIM determinant is obtained at the target positions, $|FIM| = n^2/(4\sigma^4) = 6.25 \cdot 10^4\ m^{-4}$. In Figure 3.3 (c) and (d) we can see how the theoretical minimum CRB trace is obtained at the target positions too, $tr(CRB) = \sigma^2 \cdot 4/n = 0.08\ m^2$.

The optimality condition (3.30), that holds with this configuration, is not computed in this example to avoid tedious repetition of the same previous arguments, but it is easy for the reader to check, in a similar way as the previous example, that this design condition is kept for each target. ■

Example 3.3: 5 sensors and 3 targets in a wide area.

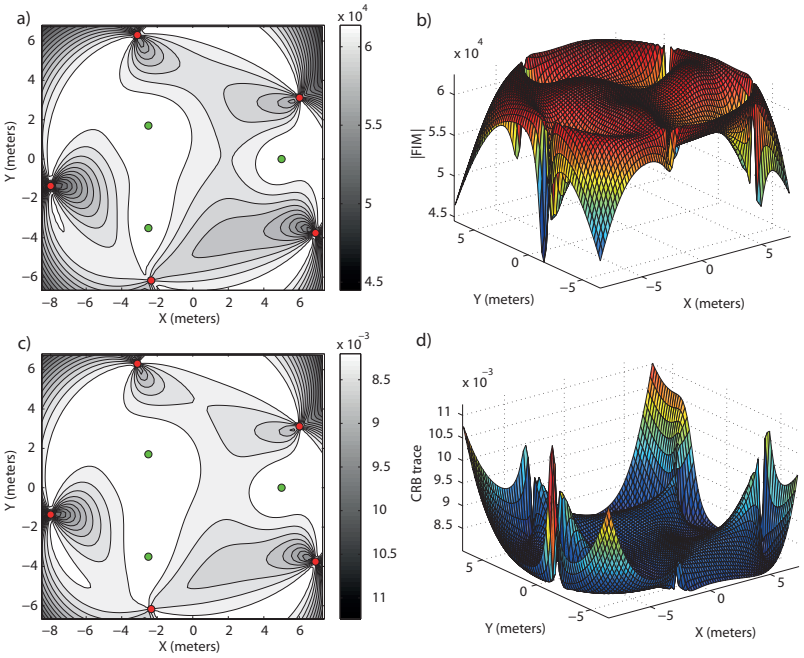

Figure 3.3: Optimal sensor formation for 5 sensors and 3 targets. In (a) $|FIM|_{\mathcal{D}}$ in $\Re^2$ is shown and in (b) its magnitude in $\Re^2$. Similarly, in (c) $tr(CRB)_{\mathcal{D}}$ is shown and in (d) its magnitude for each point in $\Re^2$.

The optimal positioning of 3 targets with a sensor network composed by 5 elements is now studied maintaining the relative positions of the targets shown in Example 3.2 but increasing the distances between them. The targets positions keep the same formation of Example 3.2 but their position coordinates are 50 times larger. The procedure to obtain the optimal formation consist in solving the design condition (3.30) for all the targets, see Table 3.3.

Table 3.3: Target positions and optimal sensor positions.

	q_1	q_2	q_3	p_1	p_2	p_3	p_4	p_5
$\{x_I\} - coord.\ (m)$	-125	-125	250	300.43	-156.17	-400	-117.28	-308.52
$\{y_I\} - coord.\ (m)$	85	-175	0	155.88	315.37	-68.48	-308.52	-187.81

In Figure 3.4 an optimal formation is shown. We can notice how the geometric configuration of the sensors is the same obtained in Example 3.2, but in the problem at hand the resultant sensor formation has a size 50 times larger than the above example, due to the new target formation. In Figure 3.4 (a) and (b) it can be seen how the maximum possible determinant is obtained over the target positions again, $|FIM| = n^2/(4\sigma^4) = 6.25 \cdot 10^4\ m^{-4}$, and in Figure 3.4 (c) and (d) we can see how the minimum CRB trace is obtained over the target positions too, $tr(CRB) = \sigma^2 \cdot 4/n = 0.008\ m^2$.

Hence it is possible to design optimal sensor networks to localize multiple targets where the distance between them is not significant, the geometric configuration of the target formation determines the optimal sensor placement. However there exist some complex configurations of targets for which the maximum $|FIM|$ cannot be achieved for all the targets and therefore a tradeoff

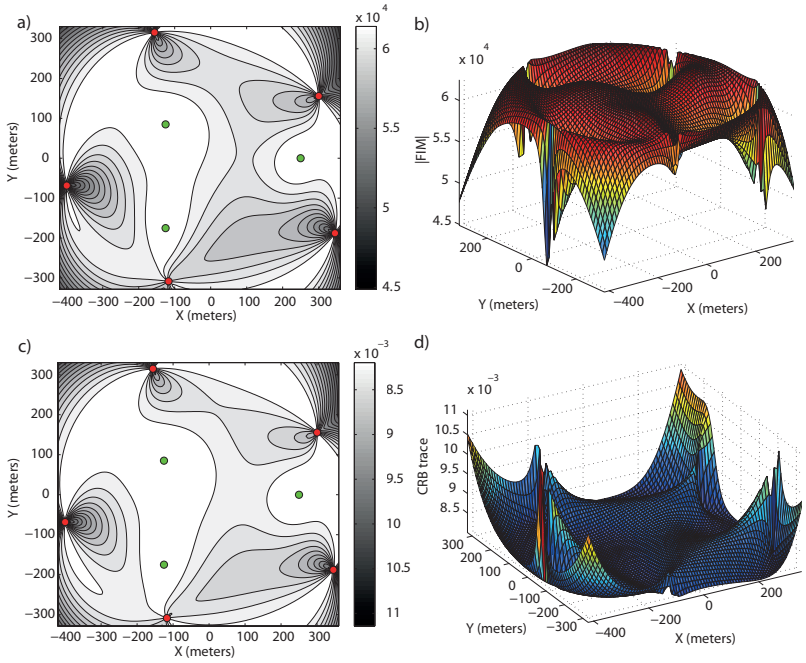

Figure 3.4: Optimal sensor network for 5 sensors and 3 targets for a wide area. In (a) $|FIM|_{\mathcal{D}}$ in $\Re^2$ is shown and in (b) its magnitude in $\Re^2$. Similarly, in (c) $tr(CRB)_{\mathcal{D}}$ is shown and in (d) its magnitude for each point in $\Re^2$.

solution must be adopted. ■

Example 3.4: 10 sensors and 7 targets.

In this example it is studied the problem in which there is a large number of targets whose configuration does not allow to obtain the maximum FIM determinant for each target. The optimal configuration, when an analytical solution is not possible to be defined with (3.30), is computed by resorting to optimization algorithms. We omit the details of these optimization algorithms, the reader is referred to the next section in which these algorithms are explained in depth.

The targets positions, that were generated with a pseudo-aleatory algorithm, and the optimal sensor formation are listed in Table 3.4.

Table 3.4: Target positions and optimal sensor positions.

	q_1	q_2	q_2	q_4	q_5	q_6	q_7	p_1
$\{x_I\} - coord.\ (m)$	15.3	−10.64	12.35	−15.06	−1.56	−2.61	3.92	17.75
$\{y_I\} - coord.\ (m)$	−2.49	16.03	−2.30	−4.45	2.76	4.43	−12.5	12.48
	p_2	p_3	p_4	p_5	p_6	p_7	p_8	p_9
$\{x_I\} - coord.\ (m)$	14.91	6.33	−15.17	−16.74	−13.85	−6.53	1.77	15.37
$\{y_I\} - coord.\ (m)$	18.67	24.21	11.99	10.53	−7.87	−14.11	−13.2	−12.9

In Figure 3.5 (a) and (b) it is shown how the maximum FIM determinants are defined at the targets positions, and in Figure 3.5 (c) and (d) how the same occurs with the minimum CRB trace.

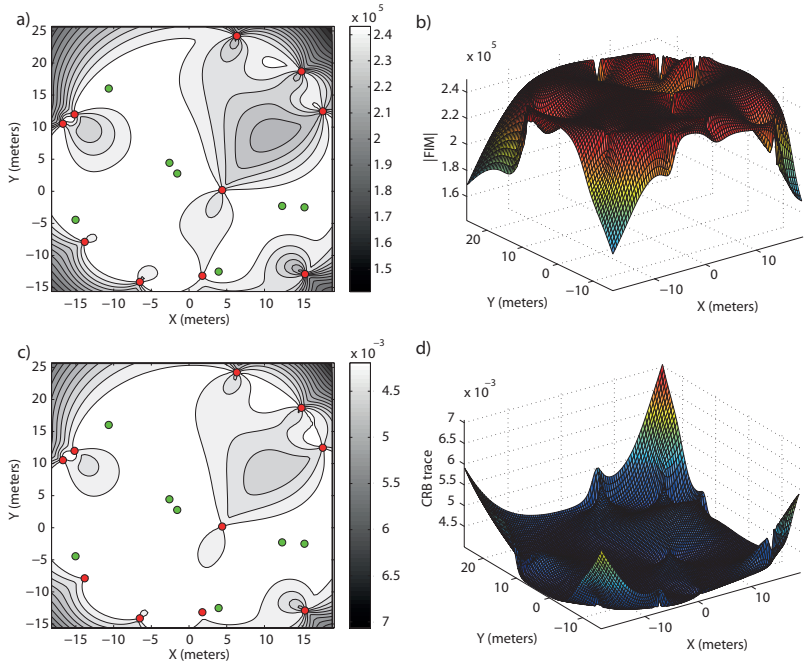

Figure 3.5: Optimal formation for 10 sensors and 7 targets. In (a) $|FIM|_{\mathcal{D}}$ in $\Re^2$ is shown and in (b) its magnitude in $\Re^2$. Similarly, in (c) $tr(CRB)_{\mathcal{D}}$ is shown and in (d) its magnitude for each point in $\Re^2$.

The FIM determinants obtained with this formation for each of the targets are stated in Table 3.5. It is easy to check that the FIM determinants are very close to the optimal one, $|FIM| = n^2/(\sigma^2 \cdot 4) = 10^2/(0.1^2 \cdot 4) = 2.5 \cdot 10^5\ m^{-4}$.

Table 3.5: FIM determinant for each of the targets.

	q_1	q_2	q_3	q_4	q_5	q_6	q_7
$\|FIM\|$	$2.498 \cdot 10^5$	$2.5 \cdot 10^5$	$2.499 \cdot 10^5$	$2.5 \cdot 10^5$	$2.499 \cdot 10^5$	$2.499 \cdot 10^5$	$2.5 \cdot 10^5$

Therefore, when the error measurement has its covariance constant, it is possible to design sensor configurations that provide the theoretical maximum FIM determinant for each target, or a value very close to the maximum one. ■

3.4 Gaussian error with distance-dependent covariance

For a wide range of robotics applications, for example an indoor environment, the error can be considered Gaussian with constant covariance since distance does not significantly affect the measurements. This approach may be erroneous for sensor networks that cover a wide area, because the distance between sensors and targets may affect dramatically the measurement error. For this

reason, the previous analysis is now extended for the scenario in which the covariance error is distance-dependent, and thus the FIM is defined by (3.3).

It is important to remark that for the problem at hand it is not possible to achieve the theoretical maximum accuracy for all the targets. This can be seen clearly by noticing that the accuracy increases when the distance between sensors and targets is reduced, something that cannot be achieved for all the targets at the same time. This fact is coupled with the constraint that the sensors cannot lie at the target positions, they must keep a safe or limit distance with respect to the targets. This limit distance between sensors and targets cannot be reduced due to physical constraints and/or limitations for a correct positioning and tracking strategy.

Therefore there will be tradeoffs involved in the precision with which each of the targets can be localized; to study them, as abovementioned, techniques that borrow from estimation theory and Pareto optimization are used. For the latter, the reader is referred to [45], [22], [90]. Therefore, concepts on Pareto-optimality are employed to maximize convex combinations of the logarithms of the determinants of the FIMs for each of the targets in order to compute the Pareto-optimal surface that gives an image of the tradeoffs involved in the multiobjective optimization problem. Thus, we seek to determine the sensor configuration that yields, if possible, a proper tradeoff for the accuracy with which the position of the different targets can be computed.

3.4.1 Gradient optimization algorithm for optimal sensor placement

The logarithms of the FIM determinants for each of the targets are used in the computation of the indicator of the performance that is achievable with a given sensor configuration,

$$\bar{p}^{*} = arg\max_{\bar{p}} \left(\log|FIM_1| + \cdots + \log|FIM_m|\right) = arg\max_{\bar{p}} \log|FIM_T| \tag{3.36}$$

One simple method to find the optimal formation is the gradient optimization method. Thus the derivative of the logarithm of the FIM determinant of each target with respect to all sensor coordinates must be computed. It is necessary to expand (3.36) to compute its derivatives, and similarly to the analysis of Section 3.3, from (3.11) and (3.12), $|FIM_T|$ yields

$$|FIM_T| = \frac{1}{\sigma^{4m}} \prod_{k=1}^{m} \left(\left(\sum_{s=1}^{n} \cos^2(\alpha_{sk}) \Gamma_{sk}^2, - \sum_{s=1}^{n} \cos(\alpha_{sk}) \sin(\alpha_{sk}) \Gamma_{sk}^2 \right) \cdot \begin{pmatrix} \sum_{s=1}^{n} \sin^2(\alpha_{sk}) \Gamma_{sk}^2 \\ \sum_{s=1}^{n} \cos(\alpha_{sk}) \sin(\alpha_{sk}) \Gamma_{sk}^2 \end{pmatrix} \right) \tag{3.37}$$

Therefore the cost function can be rewritten as a product of dot products:

$$\log|FIM_T| = \log\left(\frac{1}{\sigma^{4m}} \prod_{k=1}^{m} \vec{P}_k \cdot \vec{Q}_k \right) \tag{3.38}$$

where

$$\vec{P}_k = \begin{pmatrix} \sum_{s=1}^{n} \cos^2(\alpha_{sk}) \Gamma_{sk}^2 \\ -\sum_{s=1}^{n} \cos(\alpha_{sk}) \sin(\alpha_{sk}) \Gamma_{sk}^2 \end{pmatrix}^T \quad \vec{Q}_k = \begin{pmatrix} \sum_{s=1}^{n} \sin^2(\alpha_{sk}) \Gamma_{sk}^2 \\ \sum_{s=1}^{n} \cos(\alpha_{sk}) \sin(\alpha_{sk}) \Gamma_{sk}^2 \end{pmatrix}$$

The derivative of a vector is defined by the derivatives of each of its elements, $\partial\vec{P} = \left[\begin{array}{ccc} \partial\vec{P}_1 & \cdots & \partial\vec{P}_n \end{array}\right]$, so the derivatives of each vector element with respect to each sensor position coordinate must be defined. These derivatives were computed in the previous section in (3.15), (3.16), (3.17), with respect to the $\{x_I\}$ coordinate, and in (3.18), (3.19), (3.20), with respect to the $\{y_I\}$ coordinate. In the distance-dependent covariance scenario we must also compute the following additional derivatives:

$$\frac{\partial\Gamma_i^2}{\partial p_{ix}} = \cos(\alpha_i)\frac{2\eta\gamma r_i^{\gamma-1}}{\left(1+\eta r_i^{\gamma}\right)^3} \qquad \frac{\partial\Gamma_i^2}{\partial p_{iy}} = \sin(\alpha_i)\frac{2\eta\gamma r_i^{\gamma-1}}{\left(1+\eta r_i^{\gamma}\right)^3} \tag{3.39}$$

Thus the derivatives of (3.38) with respect to each sensor position coordinate yield

$$\frac{\partial\log|FIM_T|}{\partial p_{ix}} = \sum_{k=1}^{m}\left(\left[\begin{array}{c} -\dfrac{2\cos(\alpha_{ik})\sin^2(\alpha_{ik})}{r_{ik}}\Gamma_{ik}^2 + \cos^2(\alpha_{ik})\dfrac{\partial\Gamma_{ik}^2}{\partial p_{ix}} \\ \left(\dfrac{\sin^3(\alpha_{ik})}{r_{ik}} - \dfrac{\cos^2(\alpha_{ik})\sin(\alpha_{ik})}{r_{ik}}\right)\Gamma_{ik}^2 - \dfrac{\partial\Gamma_{ik}^2}{\partial p_{ix}}\cos(\alpha_{ik})\sin(\alpha_{ik}) \end{array}\right]^T \cdot \left[\begin{array}{c} \sum_{s=1}^{n}\sin^2(\alpha_{sk})\Gamma_{sk}^2 \\ \sum_{s=1}^{n}\cos(\alpha_{sk})\sin(\alpha_{sk})\Gamma_{sk}^2 \end{array}\right]\frac{1}{|FIM_k|}\right) + \sum_{k=1}^{m}\left(\left[\begin{array}{c} \sum_{s=1}^{n}\cos^2(\alpha_{sk})\Gamma_{sk}^2 \\ -\sum_{s=1}^{n}\cos(\alpha_{sk})\sin(\alpha_{sk})\Gamma_{sk}^2 \end{array}\right]^T \cdot \left[\begin{array}{c} \dfrac{2\cos(\alpha_{ik})\sin^2(\alpha_{ik})}{r_{ik}}\Gamma_{ik}^2 + \sin^2(\alpha_{ik})\dfrac{\partial\Gamma_{ik}^2}{\partial p_{ix}} \\ -\left(\dfrac{\sin^3(\alpha_{i1})}{r_{i1}} - \dfrac{\cos^2(\alpha_{i1})\sin(\alpha_{i1})}{r_{i1}}\right)\Gamma_{ik}^2 + \dfrac{\partial\Gamma_{ik}^2}{\partial p_{ix}}\cos(\alpha_{ik})\sin(\alpha_{ik}) \end{array}\right]\frac{1}{|FIM_k|}\right)$$

$$\frac{\partial\log|FIM_T|}{\partial p_{iy}} = \sum_{k=1}^{m}\left(\left[\begin{array}{c} \dfrac{2\cos^2(\alpha_{ik})\sin(\alpha_{ik})}{r_{ik}}\Gamma_{ik}^2 + \cos^2(\alpha_{ik})\dfrac{\partial\Gamma_{ik}^2}{\partial p_{iy}} \\ \left(\dfrac{\cos^3(\alpha_{ik})}{r_{ik}} - \dfrac{\sin^2(\alpha_{ik})\cos(\alpha_{ik})}{r_{ik}}\right)\Gamma_{ik}^2 - \dfrac{\partial\Gamma_{ik}^2}{\partial p_{iy}}\cos(\alpha_{ik})\sin(\alpha_{ik}) \end{array}\right]^T \cdot \left[\begin{array}{c} \sum_{s=1}^{n}\sin^2(\alpha_{sk})\Gamma_{sk}^2 \\ \sum_{s=1}^{n}\cos(\alpha_{sk})\sin(\alpha_{sk})\Gamma_{sk}^2 \end{array}\right]\frac{1}{|FIM_k|}\right) + \sum_{k=1}^{m}\left(\left[\begin{array}{c} \sum_{s=1}^{n}\cos^2(\alpha_{sk})\Gamma_{sk}^2 \\ -\sum_{s=1}^{n}\cos(\alpha_{sk})\sin(\alpha_{sk})\Gamma_{sk}^2 \end{array}\right]^T \cdot \left[\begin{array}{c} -\dfrac{2\cos^2(\alpha_{ik})\sin(\alpha_{ik})}{r_{ik}}\Gamma_{ik}^2 + \sin^2(\alpha_{ik})\dfrac{\partial\Gamma_{ik}^2}{\partial p_{iy}} \\ -\left(\dfrac{\cos^3(\alpha_{i1})}{r_{i1}} - \dfrac{\sin^2(\alpha_{ik})\cos(\alpha_{ik})}{r_{i1}}\right)\Gamma_{ik}^2 + \dfrac{\partial\Gamma_{ik}^2}{\partial p_{iy}}\cos(\alpha_{ik})\sin(\alpha_{ik}) \end{array}\right]\frac{1}{|FIM_k|}\right)$$

Some straightforward computations over the above derivatives yield

$$\frac{\partial \log |FIM_T|}{\partial p_{ix}} = \sum_{k=1}^{m} \frac{1}{|FIM_k|} \left(-\frac{2\cos(\alpha_{ik})\sin^2(\alpha_{ik})}{r_{ik}} \Gamma_{ik}^2 \sum_{s=1}^{n} \left(\sin^2(\alpha_{sk}) - \cos^2(\alpha_{sk}) \right) \Gamma_{sk}^2 + \right.$$

$$\frac{\partial \Gamma_{ik}^2}{\partial p_{ix}} \left(\cos^2(\alpha_{ik}) \sum_{s=1}^{n} \sin^2(\alpha_{sk}) \Gamma_{sk}^2 + \sin^2(\alpha_{ik}) \sum_{s=1}^{n} \cos^2(\alpha_{sk}) \Gamma_{sk}^2 \right) -$$

$$2\frac{\partial \Gamma_{ik}^2}{\partial p_{ix}} \cos(\alpha_{sk}) \sin(\alpha_{sk}) \sum_{s=1}^{n} \cos(\alpha_{sk}) \sin(\alpha_{sk}) \Gamma_{sk}^2 - \tag{3.40}$$

$$\left. 2\left(\frac{\sin^3(\alpha_{ik})}{r_{ik}} - \frac{\cos^2(\alpha_{ik})\sin(\alpha_{ik})}{r_{ik}} \right) \Gamma_{ik}^2 \sum_{s=1}^{n} \cos(\alpha_{sk}) \sin(\alpha_{sk}) \Gamma_{sk}^2 \right)$$

$$\frac{\partial \log |FIM_T|}{\partial p_{iy}} = \sum_{k=1}^{m} \frac{1}{|FIM_k|} \left(\frac{2\sin(\alpha_{ik})\cos^2(\alpha_{ik})}{r_{ik}} \Gamma_{ik}^2 \sum_{s=1}^{n} \left(\sin^2(\alpha_{sk}) - \cos^2(\alpha_{sk}) \right) \Gamma_{sk}^2 + \right.$$

$$\frac{\partial \Gamma_{ik}^2}{\partial p_{iy}} \left(\cos^2(\alpha_{ik}) \sum_{s=1}^{n} \sin^2(\alpha_{sk}) \Gamma_{sk}^2 + \sin^2(\alpha_{ik}) \sum_{s=1}^{n} \cos^2(\alpha_{sk}) \Gamma_{sk}^2 \right) -$$

$$2\frac{\partial \Gamma_{ik}^2}{\partial p_{iy}} \cos(\alpha_{sk}) \sin(\alpha_{sk}) \sum_{s=1}^{n} \cos(\alpha_{sk}) \sin(\alpha_{sk}) \Gamma_{sk}^2 - \tag{3.41}$$

$$\left. 2\left(\frac{\cos^3(\alpha_{ik})}{r_{ik}} - \frac{\sin^2(\alpha_{ik})\cos(\alpha_{ik})}{r_{ik}} \right) \Gamma_{ik}^2 \sum_{s=1}^{n} \cos(\alpha_{sk}) \sin(\alpha_{sk}) \Gamma_{sk}^2 \right)$$

Once the gradients have been computed for each target, they are combined to update the sensor configuration so as to yield an increase in the specified convex combination of the logarithms of the FIM determinants. This computation is recursive, until the optimal position is found. For the single target positioning problem, an adequate initial guess for the solution is for example any regular distribution around the target. Checking that this algorithm behaves well for single target positioning is easy, for an analytical solution to the optimal sensor positions is available in Chapter 2. For the multiple target localization problem, the initial guess may be a regular distribution around the mass centre of the target group, with all the targets inside the sensor formation, or the solution that would be obtained for the constant covariance case. Moreover, as abovementioned, tradeoff solutions must be adopted for the problem at hand so Pareto optimization tools are employed to determine the optimal sensor configurations depending on the mission constraints and requirements. Therefore, (3.4) is rewritten as

$$\bar{p}^* = arg \max_{\bar{p}} \sum_{k=1}^{m} \lambda_k \log |FIM_k| \tag{3.42}$$

where $k = 1, \cdots, m$ with m being the number of targets, and λ_k is the Pareto weight for target k

and $\lambda_1 + \cdots + \lambda_m = 1$. The Armijo rule is used for the sensor placement update phase, yielding the following iterative gradient optimization algorithm.

1. For each target, (3.42) is computed for the current sensor formation at iteration t, from which $|FIM_\lambda|$, the convex combination of the logarithms of the determinants, given by $|FIM_\lambda|[t] = \sum_{k=1}^{m} \lambda_k \log|FIM_k|[t]$, follows for a specific choice of $\lambda_k; k = 1, 2, ..m;\ \lambda_1 + ... + \lambda_m = 1$, where m is the number of targets.

2. Using (3.40) and (3.41) the gradient of $|FIM_\lambda|[t]$ is computed, yielding $\nabla_{i,\xi}|FIM_\lambda|[t]$ with $\xi = x, y$; and $i = 1, ..., n$.

3. The sensor positions are updated according to the gradients: $p_{i,\xi}[t+1] = p_{i,\xi}[t] + \mu^{\zeta[t]}\nabla_{i,\xi}|FIM_\lambda|[t]$, with $\mu \in 0, 1$, $\zeta[0] = 1$, and $\zeta[t] = \zeta[t-1] + 1$.

4. If $|FIM_\lambda|[t+1] > |FIM_\lambda|[t]$, then $p_i[t+1]$ becomes the new set of sensor positions, $\zeta[t] = \zeta[t] + 1$, and the iteration goes back to step 1, with $p_i[t+1] = \left[p_{i,x}[t+1], p_{i,y}[t+1]\right]$.

5. If $|FIM_\lambda|[t+1] < |FIM_\lambda|[t]$, then there is no improvement in the convex combination of the determinants, $\zeta[t] = 0$, the iterative algorithm stops, and $p_i[t]$ is considered to be the optimal configuration for the current target positions.

The above cycle is only run once if the targets are stationary. Notice the unrealistic assumption, also made in many of the publications available in this area, that the positions of the targets are known in advance. This is done to simplify the problem and to first fully understand its solution before the realistic scenario where the positions of the targets are known with error can be tackled. In this respect, see Section 3.5, which is largely inspired by the work in [39].

Clearly, in order for the information about the Pareto-optimal configurations to be useful, one must check if the determinants of the individual FIMs for each target meet desired specifications. To evaluate how good the sensor formation is in terms of yielding accurate localization of the real targets the determinant $|FIM_\mathcal{D}|$ previously introduced is used.

In a practical situation where the targets are in motion, the sensor network must adapt its optimal configuration as the mission unfolds in three different intertwined processes:

i) *multiple target position estimation*, albeit with a possibly large error, using the current sensor configuration and resorting to a dedicated nonlinear filter (e.g. Extended Kalman filter);

ii) *optimal sensor configuration computation*, based on the data provided by the previous process and the algorithm described above or its modification in Section 3.5;

iii) *coordinated motion control* to actually drive the moving sensors to the optimal positions determined in ii).

We thus envision the situation where the algorithm described is run during each cycle of the positioning system in ii). Interestingly enough, we can also think of a situation where the different iterates of process ii) can be used to yield set points for the autonomous sensor network to move to, effectively guiding them collectively to the optimal configuration that is being computed.

The advantage of using a gradient optimization method is its simplicity. As it will be seen later, based on the simulations done so far, the method has proven to be quite satisfactory. However, should there be a need for a more refined method, the sensor network positions given by the gradient algorithm can be used as initial estimates in the new method.

The rest of this section contains the results of simulations that illustrate the potential of the method developed for optimal sensor placement when multiple targets are involved. As an introductory step, only the case where the targets have equal Pareto weights, that is, $\lambda_1 = \lambda_2 = ... = \lambda_m$ is considered. The case where the targets have different weights is addressed after the following examples.

Example 3.5: 4 sensors and 2 targets.

This example deals with the problem of 2 targets positioning with a 4 sensor network and distance-dependent error defined by $\sigma = 0.1\ m$, $\gamma = 1$, and $\eta = 0.05$. The optimization method described above is used to determine the optimal sensor configuration. The targets are placed at $q_1 = [-5,\ 0]^T\ m$ and $q_2 = [5,\ 0]^T\ m$. The additional constraint that the sensors cannot be placed closer than 2 meters from the targets has been imposed to the design because if no constraints are taken into account then the sensor would be too close to the targets and would provide an unrealistic solution. In this sense, we can notice in Figure 3.6 and in Table 3.6 how the sensors are placed over this constraint to reduce as much as possible the distance-dependent added error.

Table 3.6: Target positions and optimal sensor positions for $\sigma = 0.1\ m$, $\gamma = 1$, and $\eta = 0.05$.

	q_1	q_2	p_1	p_2	p_3	p_4
$\{x_I\} - coord.\ (m)$	−5	5	−3.97	−3.973	3.973	3.973
$\{y_I\} - coord.\ (m)$	0	0	1.73	−1.73	−1.73	−1.73

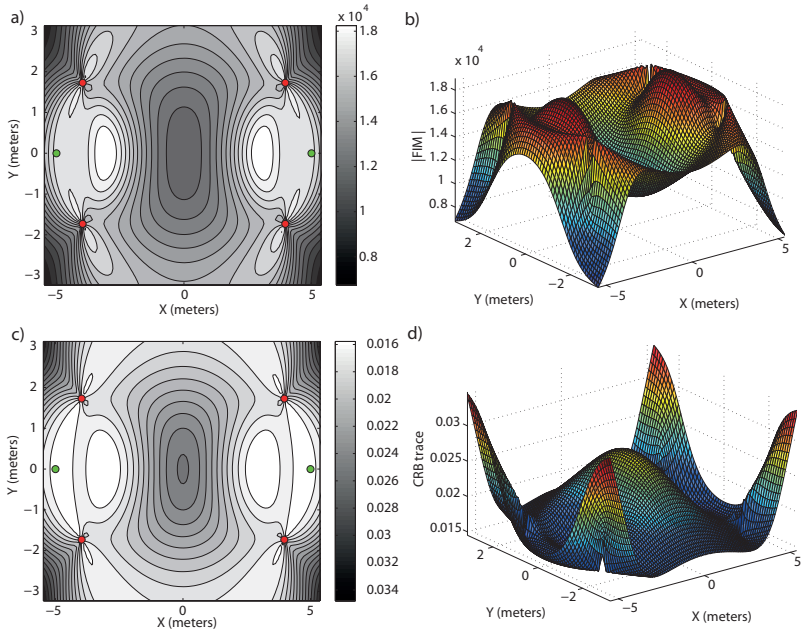

Figure 3.6: Optimal sensor placement for 2 targets with 4 sensors, with $\eta = 0.05$ and $\sigma = 0.1\ m$. In (a) $|FIM|_{\mathcal{D}}$ in $\Re^2$ is shown and in (b) its magnitude in $\Re^2$. Similarly, in (c) $tr(CRB)_{\mathcal{D}}$ is shown and in (d) its magnitude for each point in $\Re^2$.

The optimal formation is the one shown in Figure 3.6 (a) and (c), where we can see how the maximum FIM determinant and minimum CRB trace are obtained at the target positions. The sensors lie just at the limit distance of 2 meters. The FIM determinants for this example are $|FIM|_1 = 1.6823 \cdot 10^4\ m^{-4}$ and $|FIM|_2 = 1.6823 \cdot 10^4\ m^{-4}$. It can be noticed that the FIM determinant for each target is lower than in the previous situation, because now the solution space is limited by the design constraints, and the distance-dependent added error. Thus a tradeoff solution is adopted so that the largest accuracy possible is achieved for both targets. ■

Example 3.6: 6 sensors and 3 targets.

In this second example with equal Pareto weights the problem of 3 targets positioning by a 6 sensor network is studied, with the constraint that the sensors cannot lie closer than 2 meters from the targets and a distance-dependent error modelled by $\sigma = 0.1\ m$, $\gamma = 1$, and $\eta = 0.05$. In Table 3.7 the positions of the targets and the sensors are shown, the latter providing the maximum possible accuracy for the problem at hand.

Table 3.7: Target positions and optimal sensor positions for $\sigma = 0.1\ m$, $\gamma = 1$, and $\eta = 0.05$.

	q_1	q_2	q_3	p_1	p_2	p_3	p_4	p_5	p_6
$\{x_I\} - coord.\ (m)$	−2.5	−2.5	5	4.12	−0.57	−2.22	−3.46	−0.53	4.46
$\{y_I\} - coord.\ (m)$	1.7	−3.5	0	1.75	2.13	−0.23	−1.76	−3.73	−1.90

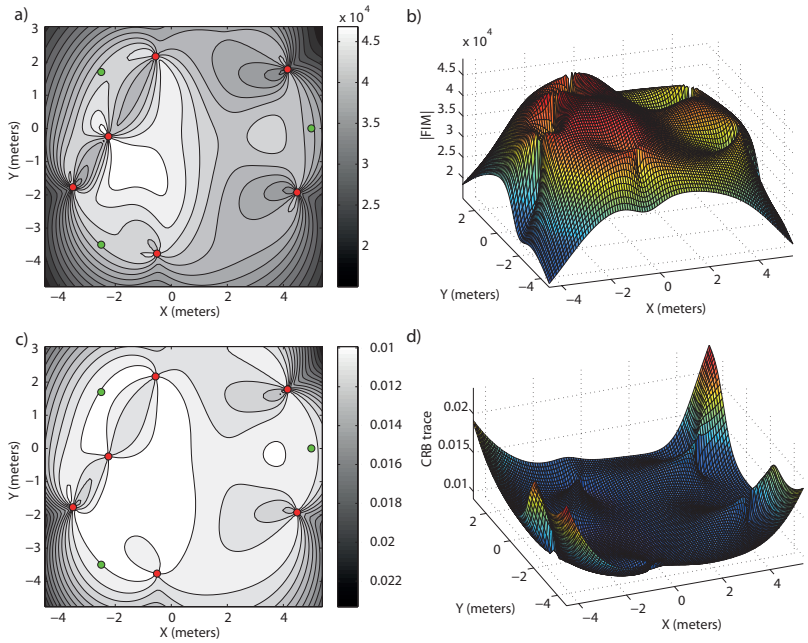

Figure 3.7: Tradeoff solution for a 6 sensor network and 3 targets with $\eta = 0.05$. In (a) $|FIM|_{\mathcal{D}}$ in $\Re^2$ is shown and in (b) its magnitude in $\Re^2$. Similarly, in (c) $tr(CRB)_{\mathcal{D}}$ is shown and in (d) its magnitude for each point in $\Re^2$.

In Figure 3.7 (a) and (b) it can be seen how the maximum FIM determinants in the region $\mathcal{D}$ are over points that differ from the target positions. This is due to the constraints imposed to the problem at hand that make that a tradeoff solution must be adopted. For the tradeoff solution defined an equivalent accuracy, as large as possible, is obtained for each target. The FIM determinants obtained for each of the targets are $|FIM|_1 = 4.0799 \cdot 10^4\ m^{-4}$, $|FIM|_2 = 4.01 \cdot 10^4\ m^{-4}$, and $|FIM|_3 = 3.6359 \cdot 10^4\ m^{-4}$. The three determinants are as large as the constraints allow. It can be also seen in Figure 3.7 (c) and (d) how an equivalent accuracy is obtained for the targets in terms of the CRB trace. ■

Example 3.7: 6 sensors and 3 targets in a wide area.

In this third example the problem of 3 targets positioning by a 6 sensor network is studied when the targets are placed in a wide area, with the constraint that the sensors cannot lie closer than 20 meters from the targets and with a distance-dependent error modelled by $\sigma = 0.1\ m$, $\gamma = 1$, and $\eta = 0.05$. The targets are placed such that the geometric configuration of Example 3.6 is kept but the distances between targets are larger, in fact the target coordinates are 50 times larger, as it can be seen in Table 3.8, where the optimal sensor positions are also shown.

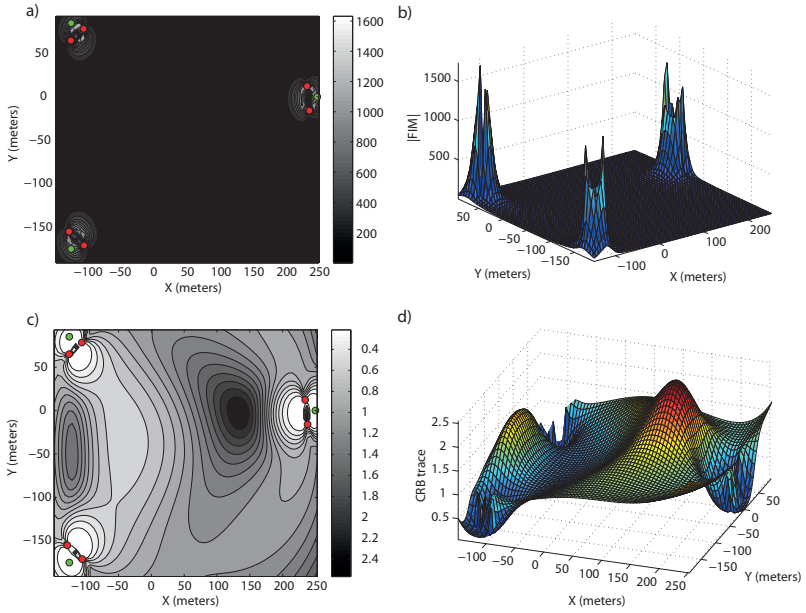

Figure 3.8: Tradeoff solution for a 6 sensor network and 3 targets with $\eta = 0.05$. In (a) $|FIM|_{\mathcal{D}}$ in $\Re^2$ is shown and in (b) its magnitude in $\Re^2$. Similarly, in (c) $tr(CRB)_{\mathcal{D}}$ is shown and in (d) its magnitude for each point in $\Re^2$.

In Figure 3.8 (a) and (b) it can be seen how the maximum FIM determinants in region $\mathcal{D}$ are at the target positions and how the sensors are close to them to reduce the distance-dependent added error. The FIM determinants obtained for each of the targets are $|FIM|_1 = 603.6742\ m^{-4}$, $|FIM|_2 = 663.5002\ m^{-4}$, and $|FIM|_3 = 653.0239\ m^{-4}$. These small values compared with those obtained in Example 3.6 are due to the constraints imposed to the problem at hand, and the wide area considered, that make more evident the importance of considering a distance-dependant measurement error. It

Table 3.8: Target positions and optimal sensor positions for $\sigma = 0.1\ m$, $\gamma = 1$, and $\eta = 0.05$.

	q_1	q_2	q_3	p_1	p_2	p_3	p_4	p_5	p_6
$\{x_I\} - coord.\ (m)$	−125	−125	25	234.3	−106.2	−125.2	−105.4	237.9	4.5
$\{y_I\} - coord.\ (m)$	85	−175	0	12.3	78.5	65	−171.1	−15.8	−1.9

can be seen in Figure 3.8 (c) and (d) the accuracy that is obtained in $\mathcal{D}$ in terms of the CRB trace.

This example shows clearly the importance of the size of the work area because the distance dramatically affects the measurement accuracy and consequently the optimal sensor configurations that can be defined. ■

It is not hard to envision situations where different "levels of importance" and therefore different localization accuracies are required for the elements in a group of targets. For example, in a 2 target scenario one of the targets may be executing a very demanding and risky task, while the other is carrying out an easy, routine task. In this situation, the sensor network should "focus its attention" on the first target, effectively imposing strict requirements on the accuracy with which its position must be estimated, while relaxing the level of localization accuracy required for the second target. This situation may be inverted during the mission, so the formation should be able to accordingly reconfigure itself.

It is obvious that the geometry of the sensor network will impact on the accuracy with which the position of each target can be computed. In the case of multiple targets, improving the accuracy in the estimate of one target may at times be done only in detriment of the accuracy of the other estimates. There are therefore tradeoffs that must be examined carefully. An example of a multi-target localization problem can be briefly described as follows: "given m targets and n sensors, determine, if possible, a geometric configuration for the sensors that will maximize the accuracy with which the position of target i can be estimated, while keeping the accuracy of the other target estimates above a desired threshold level". It is at this stage that the power of multi-objective Pareto optimization must be brought into the picture. Clearly, in order to fully understand the problem, the corresponding set of Pareto-optimal points must be computed and make decisions accordingly. See the presentation in Appendix B. As explained before, this can be done by computing

$$\bar{p}^* = arg \max_{\bar{p}} |FIM_\lambda| = arg \max_{\bar{p}} \log |FIM_T| \tag{3.43}$$

over all possible sensor positions, and for all $\lambda = [\lambda_1, \lambda_2, ..., \lambda_m]$ such that $\lambda_1 + ... + \lambda_m = 1$. In practice a grid of points is adopted for vector λ. The maximization above is done by resorting to the gradient optimization algorithm previously introduced.

For simplicity of explanation, a 2-target positioning problem with 6 sensors is studied although the procedure would be the same for more targets and a different number of sensors. This particular problem is studied in detail in Example 3.8, here we simply give a brief overview of the problem of Pareto optimization. Since only two targets are involved, the Pareto-optimal curve is parametrized by a single parameter $\lambda \in [0, 1]$. For simplicity of notation, we use the same symbol for this scalar as well as for vector λ. The meaning will be clear from the context. We assume that $\lambda_1 = \lambda$ and $\lambda_2 = 1 - \lambda$. When λ varies from 0 to 1, the weight on one of the targets changes accordingly. Thus, in the extreme cases of 0 and 1 the solutions degenerate into those two of the single target localization problems for target 2 and 1, respectively. Two different curves that show the tradeoffs in the determinants of the Fisher Information Matrices for each of the targets (with the sensor geometry

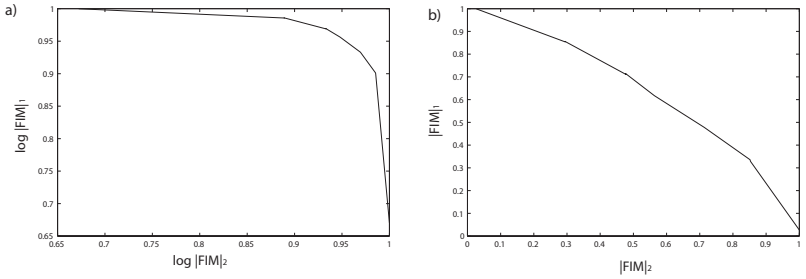

Figure 3.9: Pareto curve (solid line) for a 2 target localization problem, using 6 sensors for $\eta = 0.2$, and the corresponding FIM determinants (dotted line) for different values of the Pareto scalarization weights in λ.

obtained by running the gradient optimization algorithm) are plotted in Fig. 3.9. The left plot corresponds to the Pareto curve for the maximization of $|FIM_\lambda|$, whereas the right plot shows the corresponding FIM determinants. The two curves are normalized between 0 and 1.

Notice in Fig. 3.9 how the cost function $|FIM_\lambda| = \log|FIM_T|$ provides a concave Pareto curve (solid line), as expected for a maximization problem. As explained before, this is a consequence of the fact that in this case the criterion for each target is indeed concave. The right plot shows the corresponding evolution of the FIM determinants. Notice that the curve shown is concave for this particular example because the distance between targets is small, as will be detailed in Example 3.8, however in multitude of scenarios it will not be concave (depending on the targets configuration), thus supporting the statement that the determinants of the FIMs are not adequate criteria to be maximized jointly (in the Pareto-optimal sense).

Fig. 3.9 shows how the accuracy of the measurements changes for different values of λ. At this point it is important to remark that if the measurement error does not depend on the distance between targets and sensors, that is, $\eta = 0$, it is possible to obtain sensor locations for which the accuracies obtained for each of the targets simultaneously are close to the optimal ones that would be obtained if the targets were operating in isolation. This follows from the shape of the Pareto curve when $\eta = 0$, not shown here. For example, with $\lambda = 0.5$ the performance achievable in the localization of targets 1 and 2 simultaneously does not degrade when compared to the best performance achievable for the two targets isolated. Of course the acceptable level of degradation in performance is problem-dependent (for more than 2 targets). When the measurement error is distance-dependent, the situation changes drastically because of the "steepness" of the Pareto curve. For example, when $\lambda = 0.5$ the performance that can be simultaneously achieved for both targets degrades substantially. The tradeoffs involved are clear.

Now some examples of Pareto optimization are shown for different number of targets and sensors. For the sake of clarity in the exposition of the previous arguments, the distances between targets are considered small to show clearly the evolution of the optimal formation when the Pareto weights are modified. For larger distances the changes would be less evident, as it can be deduced from Example 3.7, and the problem understanding less clear. In all the examples the sensors cannot lie closer than 2 meters from the targets and the noise model is defined by $\sigma = 0.1$, $\gamma = 1$, and $\eta = 0.05$, therefore the error depends on the distance in a linear manner.

Example 3.8: 6 sensors and 2 targets.

In this example a 6 sensor formation is used to localize two targets with different values of the

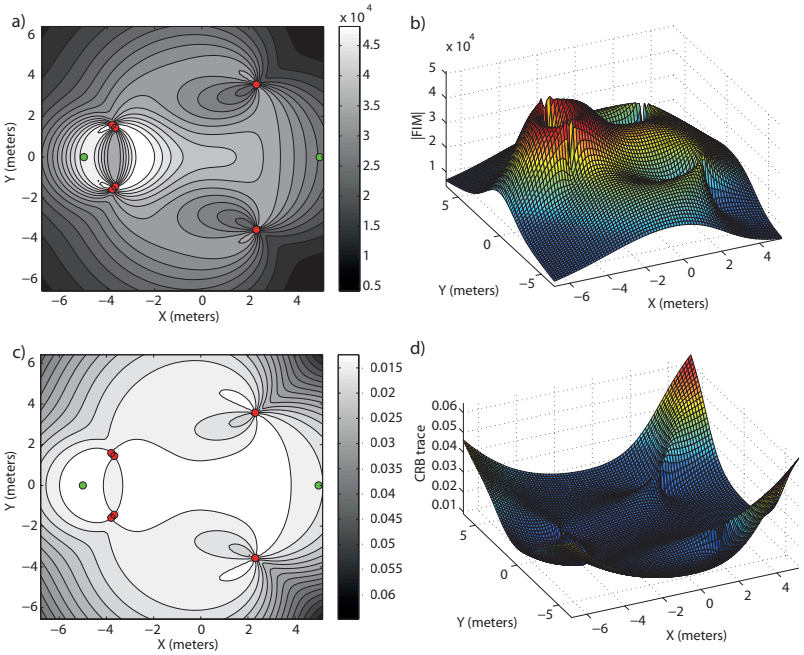

Figure 3.10: Optimal sensor formation for $\lambda = 0.2$. In (a) $|FIM|_{\mathcal{D}}$ in $\Re^2$ is shown and in (b) its magnitude in $\Re^2$. Similarly, in (c) $tr(CRB)_{\mathcal{D}}$ is shown and in (d) its magnitude for each point in $\Re^2$.

Pareto weights that illustrate how the sensors must change their configuration to achieve the accuracy requirements imposed to each target. The targets are placed at $q_1 = [-5,\ 0]^T\ m$ and $q_2 = [5,\ 0]^T\ m$. As mentioned above, as only two targets are involved, the Pareto-optimal curve is parametrized by a single parameter $\lambda \in [0, 1]$. We assume in this example that $\lambda_1 = \lambda$ and $\lambda_2 = 1 - \lambda$. When λ varies from 0 to 1, the weight on one of the targets changes accordingly. The Pareto curve is shown in Figure 3.9.

Some optimal configurations for different Pareto weights are now shown to illustrate the above comments. For example in Figure 3.10 the optimal sensor network for $\lambda = 0.2$ is shown. The sensors are placed at the positions listed in Table 3.9. It is clear how the formation is focused on target 2, but maintaining a minimum accuracy for target 1.

Table 3.9: Target positions and optimal sensor positions for $\sigma = 0.1$, $\gamma = 1$, and $\eta = 0.05$.

$\lambda = 0.2$	q_1	q_2	p_1	p_2	p_3	p_4	p_5	p_6
$\{x_I\} - coord.\ (m)$	-5	5	2.31	-3.67	-3.79	-3.79	-3.67	2.31
$\{y_I\} - coord.\ (m)$	0	0	3.57	1.44	1.59	-1.59	-1.44	-3.57

In Figure 3.10 (a) and (b) the FIM determinants in $\mathcal{D}$ are shown, which are $|FIM|_1 = 4.6693 \cdot 10^4\ m^{-4}$ and $|FIM|_2 = 2.1355 \cdot 10^4\ m^{-4}$ at the target positions. In Figure 3.10 (c) and (d) the CRB traces for $\mathcal{D}$ are shown too, which in the target positions become $tr(CRB)_1 = 0.0093\ m^2$ and $tr(CRB)_2 = 0.0153\ m^2$.

In Figure 3.11 it can be seen that for $\lambda = 0.5$ the formation is symmetric and therefore both targets are localized with the same accuracy. The sensor positions are shown in Table 3.10.

Table 3.10: Target positions and optimal sensor positions for $\sigma = 0.1$, $\gamma = 1$, and $\eta = 0.05$.

$\lambda = 0.5$	q_1	q_2	p_1	p_2	p_3	p_4	p_5	p_6
$\{x_I\} - coord.\ (m)$	-5	5	4.20	0	-4.20	-4.20	0	4.20
$\{y_I\} - coord.\ (m)$	0	0	1.79	3.22	1.79	-1.79	-3.21	-1.79

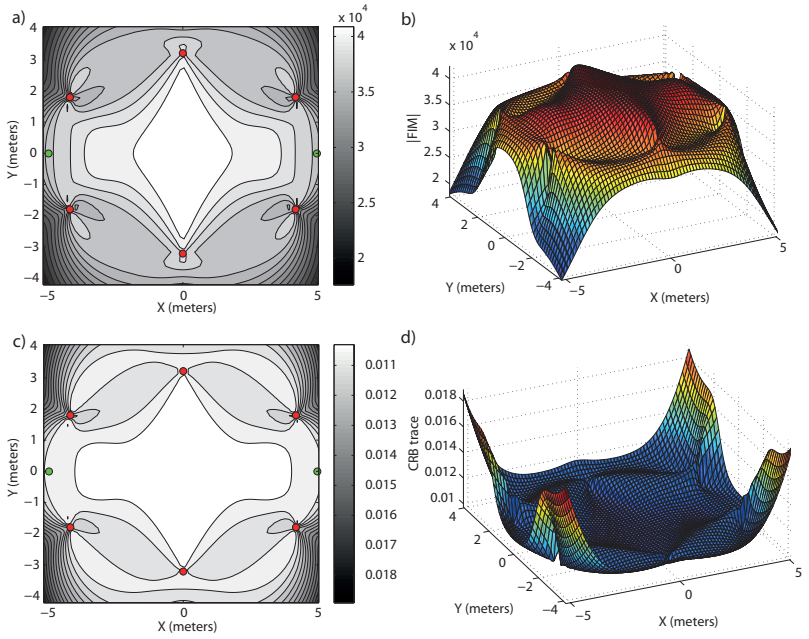

Figure 3.11: Optimal sensor formation for $\lambda = 0.5$. In (a) $|FIM|_{\mathcal{D}}$ in $\Re^2$ is shown and in (b) its magnitude in $\Re^2$. Similarly, in (c) $tr(CRB)_{\mathcal{D}}$ is shown and in (d) its magnitude for each point in $\Re^2$.

In Figure 3.11 (a) and (b) the FIM determinants are shown over $\mathcal{D}$, which in the target positions are $|FIM|_1 = 3.5458 \cdot 10^4\ m^{-4}$ and $|FIM|_2 = 3.5458 \cdot 10^4\ m^{-4}$, that imply the same accuracy for both targets. In Figure 3.11 (c) and (d) the CRB traces in $\mathcal{D}$ are plotted, which at the target positions are $tr(CRB)_1 = 0.0106\ m^2$ and $tr(CRB)_2 = 0.0106\ m^2$. It can be noticed from these results, with respect to the previous case with $\lambda = 0.2$, how the accuracy of one target increases while the other target accuracy decreases to provide an equivalent accuracy for both targets. It is important to remark at this point that if the distance between targets was to be larger, the optimal configuration would be such that the 6 sensors are split into two formations of 3 sensors, each of these formations focused on one of the targets.

Another interesting situation is when the sensor network is focused on target 1 but the importance of target 2 is large too, it is, when $\lambda = 0.7$. Figure 3.12 shows how the formation is split into a 4 sensor network close to target 1 and a 2 sensor network close to target 2 (in fact the sensors are over the limit distance), see Table 3.11.

It is clear how the formation is focused on target 1, but maintaining a minimum accuracy for target 2, larger than the one obtained for target 1 when $\lambda = 0.2$. In Figure 3.12 (a) and (b) the FIM determinants are shown in $\mathcal{D}$, which at the target positions are $|FIM|_1 = 3.1202 \cdot 10^4\ m^{-4}$ and $|FIM|_2 = 4.4533 \cdot 10^4\ m^{-4}$. In Figure 3.12 (c) and (d) the CRB traces in $\mathcal{D}$ are shown, which at the

Table 3.11: Target positions and optimal sensor positions for $\sigma = 0.1$, $\gamma = 1$, and $\eta = 0.05$.

$\lambda = 0.7$	q_1	q_2	p_1	p_2	p_3	p_4	p_5	p_6
$\{x_I\} - coord.\ (m)$	−5	5	4.25	3.40	−4.37	−4.37	3.40	4.25
$\{y_I\} - coord.\ (m)$	0	0	1.85	1.20	1.88	−1.88	−1.20	−1.85

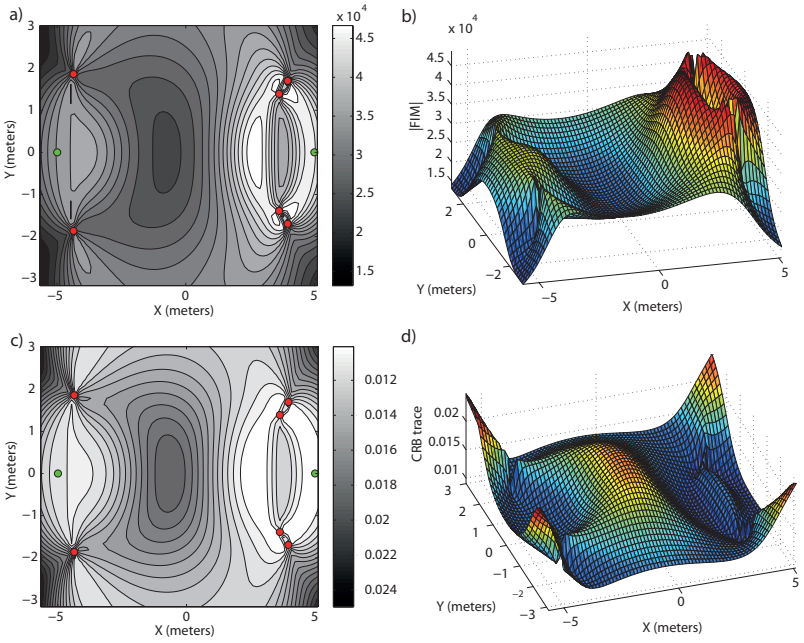

Figure 3.12: Optimal sensor network for $\lambda = 0.7$. In (a) $|FIM|_{\mathcal{D}}$ in $\Re^2$ is shown and in (b) its magnitude in $\Re^2$. Similarly, in (c) $tr(CRB)_{\mathcal{D}}$ is shown and in (d) its magnitude for each point in $\Re^2$.

target positions are $tr(CRB)_1 = 0.0114\ m^2$ and $tr(CRB)_2 = 0.0095\ m^2$.

Finally, Figure 3.13 shows the optimal formation when the sensors are focused on the localization of target 1 but a minimum accuracy must be maintained on target 2, it is, when $\lambda = 0.9$. The sensors positions are stated in Table 3.12.

Table 3.12: Target positions and optimal sensor positions for $\sigma = 0.1$, $\gamma = 1$, and $\eta = 0.05$.

$\lambda = 0.7$	q_1	q_2	p_1	p_2	p_3	p_4	p_5	p_6
$\{x_I\} - coord.\ (m)$	−5	5	4.25	3.40	−0.88	−0.88	3.40	4.25
$\{y_I\} - coord.\ (m)$	0	0	1.85	1.20	3.30	−3.30	−1.20	−1.85

In Figure 3.13 (a) and (b) the FIM determinants are shown in $\mathcal{D}$, which in the target positions are $|FIM|_1 = 1.4283 \cdot 10^4\ m^{-4}$ and $|FIM|_2 = 4.8898 \cdot 10^4\ m^{-4}$, showing a larger accuracy for the second target as it was expected. In Figure 3.13 (c) and (d) the CRB traces for all the points in $\mathcal{D}$ are shown, which in the target positions are $tr(CRB)_1 = 0.0221\ m^2$ and $tr(CRB)_2 = 0.0090\ m^2$. From the above figures we can notice how the formation adapts its shape accordingly to the required accuracy for each of the targets. ■

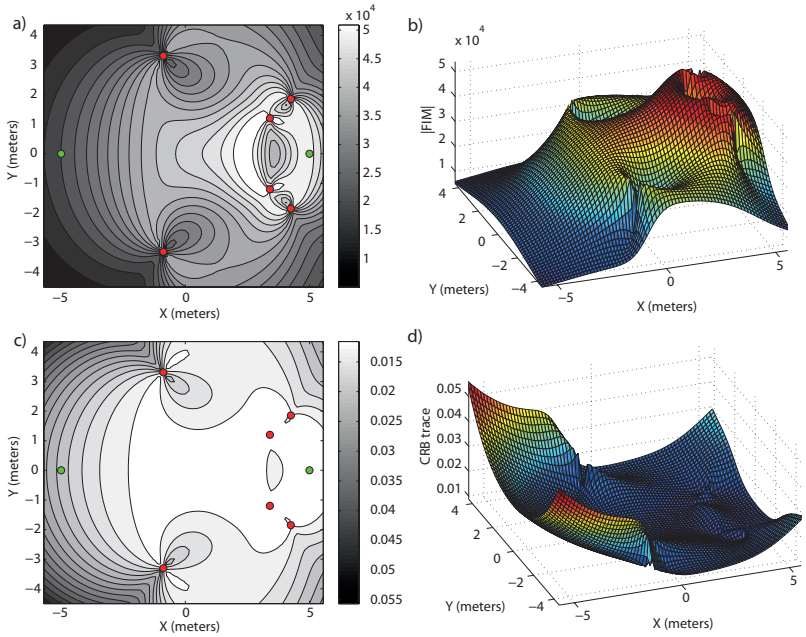

Figure 3.13: Optimal sensor network for $\lambda = 0.9$. In (a) $|FIM|_{\mathcal{D}}$ in $\Re^2$ is shown and in (b) its magnitude in $\Re^2$. Similarly, in (c) $tr(CRB)_{\mathcal{D}}$ is shown and in (d) its magnitude for each point in $\Re^2$.

Example 3.9: 6 sensors and 3 targets.

In this example the problem of 3 targets positioning with a network composed by 6 sensors is studied. The increasing in the problem complexity is clear because the 6 sensors must adapt their configuration to achieve the accuracy requirements and constraints while they must deal with an additional target compared with the previous example. The targets are placed at $q_1 = [4, -3]^T\ m$, $q_2 = [-4, -3]^T\ m$ and $q_3 = [5, 0]^T\ m$. These target positions have been chosen arbitrarily. Several scenarios for different values of the λs and their tradeoff solutions are shown next.

For example, in Figure 3.14 the tradeoff solution for $\lambda_1 = \lambda_2 = \lambda_3 = 0.333$ is shown. After the optimization process the sensors are in the positions shown in Table 3.13.

Table 3.13: Target positions and optimal sensor positions for $\sigma = 0.1$, $\gamma = 1$, and $\eta = 0.05$.

$\lambda_{1,2,3} = 0.33, 0.33, 0.33$	q_1	q_2	q_3	p_1	p_2	p_3	p_4	p_5	p_6
$\{x_I\} - coord.\ (m)$	4	−4	5	4.06	1.76	−1.76	−0.99	−2.18	2.20
$\{y_I\} - coord.\ (m)$	−3	−3	0	−1	4.05	4.05	−4.03	−3.84	−3.61

It is easy to check how the formation is placed adequately to provide similar accuracy for all targets and as large as possible. In Figure 3.14 (a) and (b) the $|FIM|_{\mathcal{D}}$ and its representation in 3D are shown, respectively. The FIM determinants obtained for the targets are $|FIM|_1 = 3.4681 \cdot 10^4\ m^{-4}$, $|FIM|_2 = 3.4635 \cdot 10^4\ m^{-4}$, and $|FIM|_3 = 3.3637 \cdot 10^4\ m^{-4}$. In a similar way in Figure 3.14 (c) and (d) the $tr(CRB)_{\mathcal{D}}$ and the representation of its magnitude in 3D are shown. The values of the CRB trace

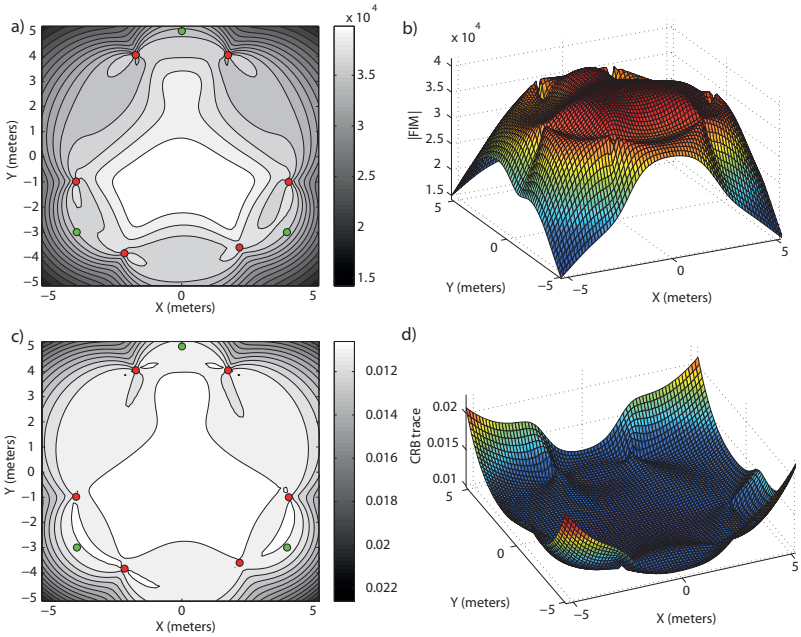

Figure 3.14: Tradeoff solution for $\lambda_1 = \lambda_2 = \lambda_3 = 0.333$. In (a) $|FIM|_{\mathcal{D}}$ in $\Re^2$ is shown and in (b) its magnitude in $\Re^2$. Similarly, in (c) $tr(CRB)_{\mathcal{D}}$ is shown and in (d) its magnitude for each point in $\Re^2$.

at the targets position are $tr(CRB)_1 = 0.0108\ m^2$ $tr(CRB)_2 = 0.0108\ m^2$, and $tr(CRB)_3 = 0.0110\ m^2$.

In Table 3.14 and in Figure 3.15 the optimal solution is shown for the Pareto weights given by $\lambda_1 = 0.4$, $\lambda_2 = 0.4$, and $\lambda_3 = 0.2$.

Table 3.14: Target positions and optimal sensor positions for $\sigma = 0.1$, $\gamma = 1$, and $\eta = 0.05$.

$\lambda_{1,2,3} = 0.4, 0.4, 0.2$	q_1	q_2	q_3	p_1	p_2	p_3	p_4	p_5	p_6
$\{x_I\} - coord.\ (m)$	4	−4	5	4	2.69	−2.69	−3.02	−2.24	2.24
$\{y_I\} - coord.\ (m)$	−3	−3	0	−1	2.92	2.92	−1	−3.96	−3.95

In Figure 3.15 (a) and (b) we can see how the formation is focused on targets 1 and 2, providing a larger accuracy (FIM determinant) than for target 3. These determinants are $|FIM|_1 = 3.5962 \cdot 10^4\ m^{-4}$, $|FIM|_2 = 3.6034 \cdot 10^4\ m^{-4}$, and $|FIM|_3 = 2.8334 \cdot 10^4\ m^{-4}$. In Figure 3.15 (c) and (d) the trace of the CRB matrix is shown in $\mathcal{D}$, taking at the target positions the following values, $tr(CRB)_1 = 0.0106\ m^2$, $tr(CRB)_2 = 0.0105\ m^2$, and $tr(CRB)_3 = 0.0123\ m^2$.

The situation shown in Figure 3.16 corresponds to the case in which the Pareto weights are $\lambda_1 = 0.2$, $\lambda_2 = 0.2$, and $\lambda_3 = 0.6$. The sensor positions for the corresponding tradeoff solution are listed in Table 3.15.

In Figure 3.16 (a) and (b) the FIM determinants in $\mathcal{D}$ are shown, which for the target positions are $|FIM|_1 = 2.9083 \cdot 10^4\ m^{-4}$, $|FIM|_2 = 2.8385 \cdot 10^4\ m^{-4}$, and $|FIM|_3 = 4.1533 \cdot 10^4\ m^{-4}$. In Figure 3.16 (c) and (d) the trace of the CRB matrix in $\mathcal{D}$ is also shown, which for the targets are $tr(CRB)_1 = 0.0121\ m^2$, $tr(CRB)_2 = 0.0124\ m^2$, and $tr(CRB)_3 = 0.0098\ m^2$.

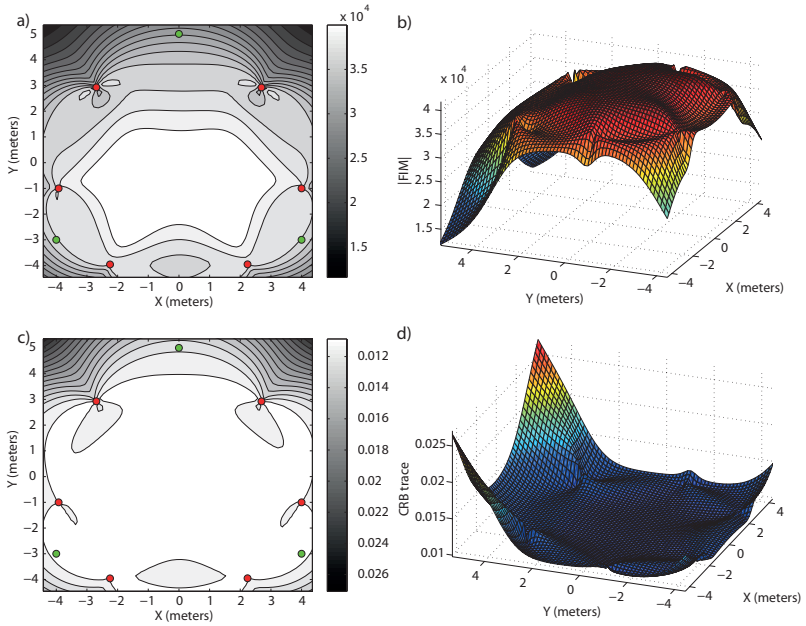

Figure 3.15: Tradeoff solution for $\lambda_1 = 0.4$, $\lambda_2 = 0.4$, $\lambda_3 = 0.2$. In (a) $|FIM|_{\mathcal{D}}$ in $\Re^2$ is shown and in (b) its magnitude in $\Re^2$. Similarly, in (c) $tr(CRB)_{\mathcal{D}}$ is shown and in (d) its magnitude for each point in $\Re^2$.

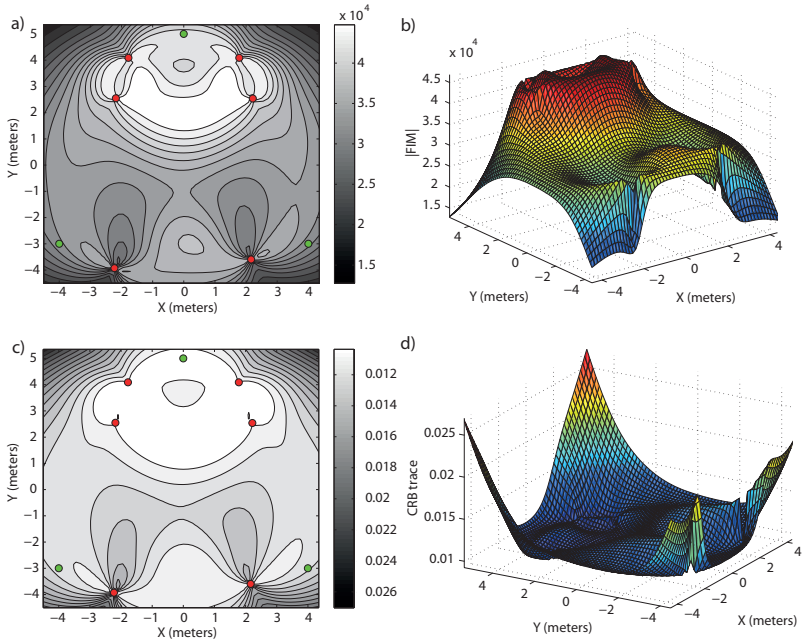

Figure 3.16: Tradeoff solution for $\lambda_1 = 0.2$, $\lambda_2 = 0.2$, $\lambda_3 = 0.6$. In (a) $|FIM|_{\mathcal{D}}$ in $\Re^2$ is shown and in (b) its magnitude in $\Re^2$. Similarly, in (c) $tr(CRB)_{\mathcal{D}}$ is shown and in (d) its magnitude for each point in $\Re^2$.

Table 3.15: Target positions and optimal sensor positions for $\sigma = 0.1$, $\gamma = 1$, and $\eta = 0.05$.

$\lambda_{1,2,3} = 0.2, 0.2, 0.6$	q_1	q_2	q_3	p_1	p_2	p_3	p_4	p_5	p_6
$\{x_I\} - coord.\ (m)$	4	−4	5	2.22	1.79	−1.79	−2.19	−2.23	2.16
$\{y_I\} - coord.\ (m)$	−3	−3	0	2.54	4.1	4.1	2.54	−3.93	−3.6

Finally the situation in which the targets must be positioned with a different accuracy each is studied. Therefore the Pareto weights are now $\lambda_1 = 0.1$, $\lambda_2 = 0.3$, and $\lambda_3 = 0.6$. The tradeoff solution provides a network with the sensors placed at the positions shown in Table 3.16.

Table 3.16: Target positions and optimal sensor positions for $\sigma = 0.1$, $\gamma = 1$, and $\eta = 0.05$.

$\lambda_{1,2,3} = 0.1, 0.3, 0.6$	q_1	q_2	q_3	p_1	p_2	p_3	p_4	p_5	p_6
$\{x_I\} - coord.\ (m)$	4	−4	5	4.25	1.80	−1.79	−1.30	0.27	2
$\{y_I\} - coord.\ (m)$	−3	−3	0	0.55	4.14	4.11	3.49	−4.30	−3

As in the previous situations, in Figure 3.17 (a) and (b) the FIM determinants are shown, which for the targets are $|FIM|_1 = 2.3052 \cdot 10^4\ m^{-4}$, $|FIM|_2 = 3.3721 \cdot 10^4\ m^{-4}$, and $|FIM|_3 = 4.0629 \cdot 10^4\ m^{-4}$. In Figure 3.17 (c) and (d) the traces of the CRB matrices are shown, which for the targets are $tr(CRB)_1 = 0.0142\ m^2$, $tr(CRB)_2 = 0.0111\ m^2$, and $tr(CRB)_3 = 0.0099\ m^2$. ■

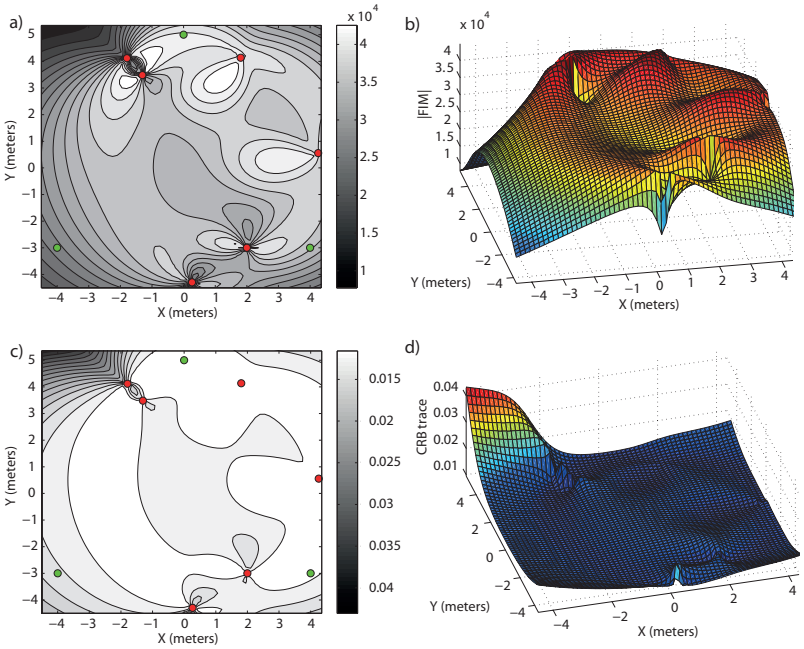

Figure 3.17: Tradeoff solution for $\lambda_1 = 0.1$, $\lambda_2 = 0.3$, $\lambda_3 = 0.6$. In (a) $|FIM|_{\mathcal{D}}$ in $\Re^2$ is shown and in (b) its magnitude in $\Re^2$. Similarly, in (c) $tr(CRB)_{\mathcal{D}}$ is shown and in (d) its magnitude for each point in $\Re^2$.

Therefore from the two examples above, and the different situations studied for different Pareto weights, it is clear that there exist tradeoffs in the design of optimal sensor configurations that must be kept. Depending on the accuracy with which each of the targets must be localized, and depending on the number of sensors, number of targets, and their own configuration, the sensors must adapt their configuration accordingly to the accuracy required at each moment for each target. Of course, these accuracies can change during a mission, so the formation must be able to adapt its configuration for the different possible situations in a similar way as in the different situations seen in the previous examples.

3.5 Uncertainty in the target location

Now it is addressed the situation where the targets to be positioned are known to lie in well defined uncertainty regions. Inspired by the work in [39] and similarly to Chapter 2, it is assumed that the uncertainty in the target positions is described by given probability distribution functions and we seek to maximize, by proper sensor placement, the average value of the log determinants of the FIMs for the targets.

In what follows, $p_{i\xi}$; $i = 1, 2, ..., n$; $\xi = x, y$ denotes the $\xi - th$ coordinate of sensor i located at position p_i, $\overline{p} = [p_1^T, ..., p_n^T]^T$, and $\overline{q} = [q_1^T, ..., q_m^T]^T$. We further denote by $\varphi(\overline{q})$; $\overline{q} \in \mathcal{R}^{m\times 2}$ the probability density functions with support $D \in R^2$ that describe the uncertainty in the position of the targets in region D, where $D = D_1 + \cdots + D_m$. With this notation, the problem of optimal sensor placement can be cast in the form of finding a vector $\overline{p}^*$ such that

$$\overline{p}^* = arg \max_{\overline{p}} \int_D |FIM(\overline{p}, \overline{q})_\lambda| \cdot \varphi(\overline{q})\, d\overline{q} \tag{3.44}$$

where we used the notation $|FIM(\overline{p}, \overline{q})_\lambda|$ to clearly show the dependence of the FIM on the target and sensor locations. However, in the following $|FIM(\overline{p}, \overline{q})_\lambda|$ will often be denoted simply as $|FIM_\lambda|$. In a real situation, $\varphi(\overline{q})$ will depend on the type of mission carried out by the targets. Therefore, different distributions can be taken for different targets and different scenarios.

To proceed, one must compute $|FIM(\overline{p}, \overline{q})_\lambda|$ in the equation above. At this point it is important to remark that, given the complexity of the optimal sensor placement problem at hand, the only viable solution is a numerical one.

It now remains to solve the optimization problem defined above. Conceptually, the procedure to determine the optimal sensor configuration is similar to that explained in the previous sections, that is, one must compute the derivatives of (3.44) with respect to the sensor coordinates

$$\frac{\partial}{\partial p_{i\xi}} \int_D \log\left(|FIM(\overline{p}, \overline{q})_T|\right) \varphi(\overline{q}) d\overline{q} = \frac{\partial}{\partial p_{i\xi}} \int_D |FIM(\overline{p}, \overline{q})_\lambda| \cdot \varphi(\overline{q})\, d\overline{q} \tag{3.45}$$

for $i = 1, 2, ..., n$ and $\xi = x, y$.

To proceed with the computations, the integral and derivative operations are interchanged: the derivatives are explicitly determined first, and the integration over region D is performed afterwards.

The derivatives can be computed in a recursive way using (3.40) and (3.41) for any number of targets. In what regards the computation of the double integral over the region D of interest, however, this is virtually impossible to do analytically. For this reason, the integral is computed numerically

with a Monte Carlo method. Finally, the solution of (3.44) is obtained using the gradient optimization method detailed in Section 3.4.1. Again, to overcome the possible occurrence of local maxima or the divergence of the algorithm, the initial guess in the iterative algorithm must be chosen with care. In the examples that we studied we found it useful and expedite to adopt as an initial guess the solution for the single target positioning problem described in Chapter 2, with the hypothetical single target placed at the centre of mass of the work area, or the solutions obtained in the previous sections of this chapter. It is important to stress that the solution to (3.44) depends strongly on the probability density function adopted for the target positions $\overline{q}$.

3.5.1 Simulation examples

Some examples for multiple target positioning when the target positions are known with uncertainty are studied now. In these examples we consider an error model defined by $\sigma = 0.1\ m$, $\beta = 1$ and $\eta = 0.1$ or $\eta = 0$. In these examples we only know the region in which the targets operate instead of the target positions themselves. We deal with equal Pareto weights for all the targets, but the procedure would be exactly the same for different Pareto weights.

Example 3.10: Constant covariance error, 2 targets and 6 sensors.

In this first example the scenario with 2 targets and 6 sensors is studied. The only knowledge about the target positions is that the targets operate inside a certain area, therefore the probability distribution functions are step-like distribution functions because the targets can be placed at any point inside their corresponding work areas. The areas in which the targets operate are squares of $2 \times 2\ m^2$ whose vertices are given by the points $D_1 = [-5\ 1;\ -5\ -1;\ -3\ 1;\ -3\ -1]^T\ m$ for target 1, and $D_2 = [5\ 1;\ 5\ -1;\ 3\ 1;\ 3\ -1]^T\ m$ for target 2. After the optimization process commented above the optimal formation is defined by the sensor formation described in Table 3.17 and shown in Figure 3.18.

Table 3.17: Optimal sensor positions for constant covariance.

	p_1	p_2	p_3	p_4	p_5	p_6
$\{x_I\} - coord.\ (m)$	4.13	0	−4.16	−4.15	0	4.13
$\{y_I\} - coord.\ (m)$	2.90	3.58	2.89	−2.89	−3.57	−2.89

We can check in Figure 3.18 (a) and (b) how a large average FIM determinant, close to the optimal one, is obtained over the work areas. In fact, the maximum and minimum determinant that this optimal formation provides inside the areas of interest are $|FIM|_{max} = 9 \cdot 10^4\ m^{-4}$ and $|FIM|_{min} = 8.8672 \cdot 10^4\ m^{-4}$. We can notice how the maximum determinant is the theoretical one, $|FIM|_{opt} = n^2/(4\sigma^4)\ m^{-4}$, and how the minimum determinant is very close to this optimal value too, given a large accuracy in all the points if the uncertainty regions. In a similar manner, in Figure 3.18 (c) and (d) the CRB trace in $\mathcal{D}$ is shown, and it can be seen how inside the work areas a small average CRB trace is obtained. The minimum and maximum CRB trace inside the areas of interest are $tr(CRB)_{min} = 0.0067\ m^2$ and $tr(CRB)_{max} = 0.0068\ m^2$. The minimum CRB trace is again the theoretical minimum for constant covariance, $tr(CRB)_{opt} = 4\sigma^2/n\ m^2$, and the maximum is very close to this minimum.

Thus, from this example it is clear that when a distance-independent measurement error is considered it is possible to define optimal sensor configurations for which the accuracy inside the work areas is very close to the maximum accuracy that would be obtained for a single target with

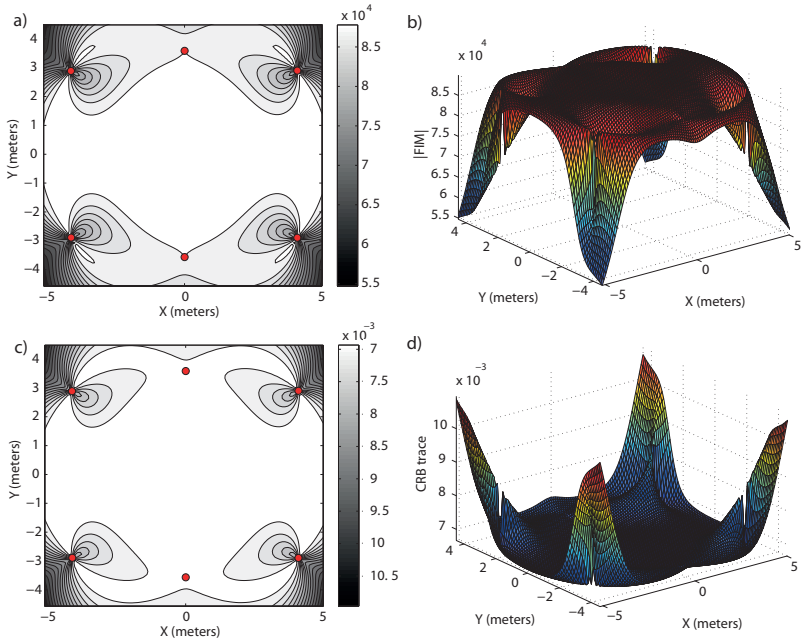

Figure 3.18: Optimal sensor placement for 2 target positioning with uncertainty and constant covariance error. In (a) $|FIM|_{\mathcal{D}}$ in $\Re^2$ is shown and in (b) its magnitude in $\Re^2$. Similarly, in (c) $tr(CRB)_{\mathcal{D}}$ is shown and in (d) its magnitude for each point in $\Re^2$.

known position working in isolation. ■

Example 3.11: Distance-dependent covariance error, 2 targets and 6 sensors.

The above example is now studied with distance-dependent measurement error, for which $\eta = 0.1$ and $\gamma = 1$. Again the targets operate inside two square areas of $2 \times 2\ m^2$ defined by the vertices $D_1 = [-5\ 1;\ -5\ -1;\ -3\ 1;\ -3\ -1]^T\ m$ for target 1, and $D_2 = [5\ 1;\ 5\ -1;\ 3\ 1;\ 3\ -1]^T\ m$ for target 2. The only knowledge about the target positions is that the targets operate inside a certain area, they can be placed at any point of their corresponding work area and therefore the probability distribution functions are step-like distribution functions. Once the optimization process is finished, the sensor positions that define the optimal formation are listed in Table 3.18.

Table 3.18: Optimal sensor positions for $\sigma = 0.1$, $\gamma = 1$, and $\eta = 0.1$.

	p_1	p_2	p_3	p_4	p_5	p_6
$\{x_I\} - coord.\ (m)$	3.91	−3.22	−4.41	−3.91	3.21	4.42
$\{y_I\} - coord.\ (m)$	0.97	1.13	1.15	−0.95	−1.11	−1.13

It is interesting enough to notice how in this example the 6 sensor formation is split into two formations of 3 sensors, which are focused on the work areas as two independent formations.

In Figure 3.19 (a) and (b) the FIM determinants for $\mathcal{D}$ are shown. The accuracy inside the work areas has been substantially reduced with respect to the previous example, due to the distance-

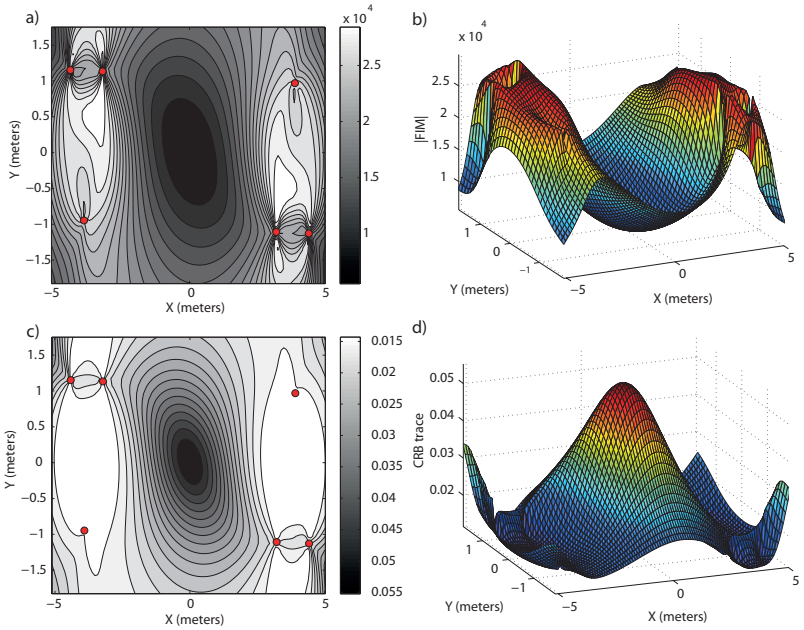

Figure 3.19: Optimal sensor placement for 2 target positioning with uncertainty and distance-dependent covariance error. In (a) $|FIM|_{\mathcal{D}}$ in $\Re^2$ is shown and in (b) its magnitude in $\Re^2$. Similarly, in (c) $tr(CRB)_{\mathcal{D}}$ is shown and in (d) its magnitude for each point in $\Re^2$.

dependent added error, and we can see how the sensor formation takes a configuration in which this added error is reduced as much as possible to keep a large accuracy over the regions of interest. This fact can be seen as well in Figure 3.19 (c) and (d) in terms of the trace of the CRB for $\mathcal{D}$. The maximum and minimum FIM determinants obtained inside the work areas are $|FIM|_{max} = 2.9941 \cdot 10^4\ m^{-4}$ and $|FIM|_{min} = 1.5577 \cdot 10^4\ m^{-4}$, respectively, and the minimum and maximum CRB trace are, $tr(CRB)_{min} = 0.0116\ m^2$ and $tr(CRB)_{max} = 0.0208\ m^2$, respectively. Although the global accuracy is reduced, we can observe how an adequate design can optimize the accuracy over the areas of interest. ■

Example 3.12: Constant covariance error, 3 targets and 6 sensors.

The problem of 3 target positioning with a 6 sensor network with constant covariance is tackled. In this example the sensors can be placed in a wide area and the uncertainty regions are larger. The uncertainty regions where the targets operate are square areas of $40 \times 40\ m^2$ defined by the vertices $D_1 = [-100\ -20;\ -100\ 20;\ -60\ -20;\ -60\ 20]^T\ m$ for target 1, $D_2 = [100\ -20;\ 100\ 20;\ 60\ -20;\ 60\ 20]^T\ m$ for target 2, and $D_3 = [-20\ 100;\ -20\ 140;\ 20\ 100;\ 20\ 140]^T\ m$ for target 3. The only knowledge about the target positions is again that the targets are inside these areas, thus the probability distributions are step-like distributions. The sensor formation that maximizes the average logarithm of the FIM determinant is defined by the sensor positions in Table 3.19.

Again it is possible to notice in Figure 3.20 how a large accuracy is obtained inside the areas of interest when a constant covariance error is considered.

In Figure 3.20 (a) and (b) the FIM determinants over $\mathcal{D}$ are shown. The maximum and

Table 3.19: Optimal sensor positions for constant covariance.

	p_1	p_2	p_3	p_4	p_5	p_6
$\{x_I\} - coord.\ (m)$	153.36	−43.31	−190.92	−166.80	31.02	138.09
$\{y_I\} - coord.\ (m)$	123.36	75.43	176.83	−194.48	−86.92	−60.13

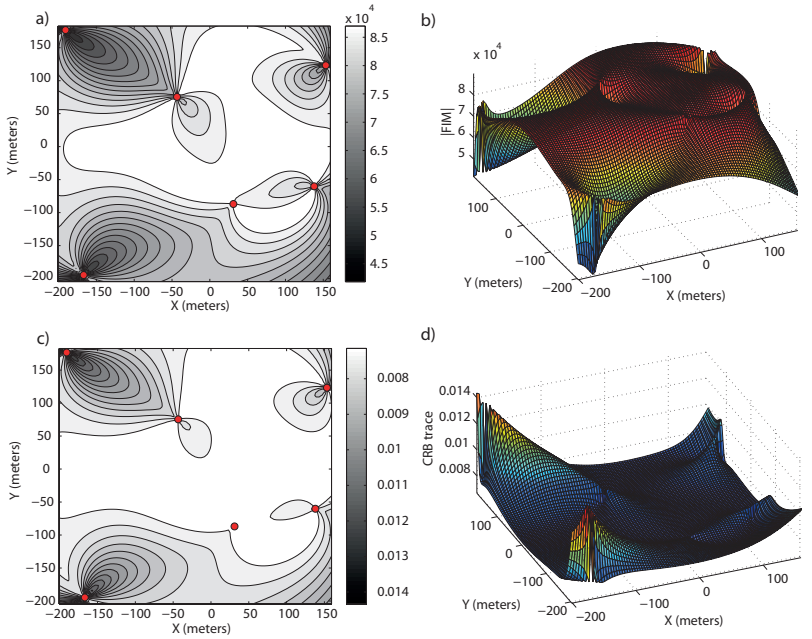

Figure 3.20: Optimal sensor placement for 3 target positioning with uncertainty and constant covariance error. In (a) $|FIM|_{\mathcal{D}}$ in $\Re^2$ is shown and in (b) its magnitude in $\Re^2$. Similarly, in (c) $tr(CRB)_{\mathcal{D}}$ is shown and in (d) its magnitude for each point in $\Re^2$.

minimum FIM determinants obtained inside the work areas are $|FIM|_{max} = 9 \cdot 10^4\ m^{-4}$ and $|FIM|_{min} = 8.7849 \cdot 10^4\ m^{-4}$, respectively. The average value inside the regions of interest is $|FIM|_{av} = 8.9760 \cdot 10^4\ m^{-4}$. We can notice how the maximum FIM determinant corresponds to the theoretical maximum FIM determinant that can be obtained for a single target working in isolation, $|FIM|_{opt} = n^2/(4\sigma^4)\ m^{-4}$, and that the minimum FIM determinant is very close to this theoretical optimal value, so that the accuracy inside the regions of interest is very close to the optimal one. Similarly, in Figure 3.20 (c) and (d) the trace of the CRB for each point in $\mathcal{D}$ is shown. The minimum and maximum CRB trace are, $tr(CRB)_{min} = 0.0067\ m^2$ and $tr(CRB)_{max} = 0.0068\ m^2$, respectively, with the minimum value equal to the theoretical one, $tr(CRB)_{opt} = 4\sigma^2/n\ m^2$, and the maximum very close to it, as commented for the FIM determinant plots. ■

Example 3.13: Distance-dependent covariance error, 3 targets and 6 sensors.

The above problem is studied now considering a distance-dependent error modelled with $\eta = 0.1$ and $\gamma = 1$. The uncertainty regions are the same square areas of $40 \times 40\ m^2$ defined by the vertices $D_1 = [-100\ \ -20;\ -100\ 20;\ -60\ \ -20;\ -60\ 20]^T\ m$ for target 1, $D_2 = [100\ \ -20;\ 100\ 20;\ 60\ -$

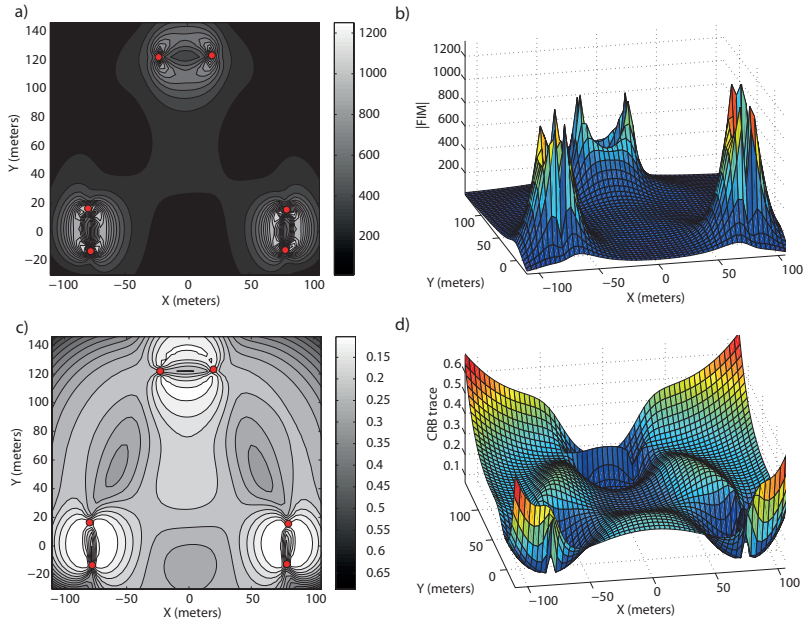

Figure 3.21: Optimal sensor placement for 3 target positioning with uncertainty and distance-dependent covariance error. In (a) $|FIM|_{\mathcal{D}}$ in $\Re^2$ is shown and in (b) its magnitude in $\Re^2$. Similarly, in (c) $tr(CRB)_{\mathcal{D}}$ is shown and in (d) its magnitude for each point in $\Re^2$.

$20;\ 60\ 20]^T\ m$ for target 2, and $D_3 = [-20\ 100;\ -20\ 140;\ 20\ 100;\ 20\ 140]^T\ m$ for target 3. The probability distributions for the uncertainty areas are step-like distributions, as in the previous examples. The sensor formation that maximizes the average logarithm of the FIM determinant is defined by the sensor positions in Table 3.20.

Table 3.20: Optimal sensor positions for $\sigma = 0.1$, $\gamma = 1$, and $\eta = 0.1$.

	p_1	p_2	p_3	p_4	p_5	p_6
$\{x_I\} - coord.\ (m)$	79.61	−23.10	−79.77	−77.65	19.64	78.59
$\{y_I\} - coord.\ (m)$	15.52	121.96	16.44	−13.41	123.10	−12.62

In Figure 3.21 (a) and (b) the FIM determinants in $\mathcal{D}$ are shown. In this case the accuracy with which each of the targets (actually its associated area) can be localized is reduced with respect to Example 3.12 due to the distance-dependent added error. However the accuracy obtained inside the work areas is large and homogeneous for all the areas, providing a similar accuracy for the three uncertainty areas. This fact can be seen too in Figure 3.21 (c) and (d) in terms of the trace of the CRB in $\mathcal{D}$. The maximum and minimum FIM determinants obtained inside the work areas are $|FIM|_{max} = 1.8616 \cdot 10^3\ m^{-4}$ and $|FIM|_{min} = 146.0117\ m^{-4}$, respectively, with an average value of $|FIM|_{avg} = 588.9221\ m^{-4}$. The minimum and maximum CRB trace are, $tr(CRB)_{min} = 0.0648\ m^2$ and $tr(CRB)_{max} = 0.2553\ m^2$, respectively.

Comparing these results with the results obtained in Example 3.11, we can see that the accuracies are smaller in the problem at hand because the formation has to maximize the FIM determinant over three wide regions that are separated by a larger distance than the two areas of Example 3.11.

Although the accuracy is reduced for this case, we can observe how with an adequate design it is possible to optimize the accuracy over the areas of interest. ■

3.6 Conclusions

The problem of optimal sensor placement for multiple target positioning in 2D scenarios has been studied in this chapter. Clearly, there exist tradeoffs involved in the precision with which each of the targets can be localized; to study them, we resorted to techniques that borrow from estimation theory and Pareto optimization. Stated briefly, we availed ourselves of concepts on Pareto-optimality and maximized convex combinations of the logarithms of the determinants of the FIMs for each of the targets in order to compute the Pareto-optimal surface that gives a clear image of the tradeoffs involved in the multiobjective optimization problem.

The first problem studied was the one in which the measurement error was Gaussian with its covariance being constant. This situation has been widely studied in the ground robotics field, where the distances are not large and the covariance can be considered constant. Despite this, most works in the literature deal with single target positioning, so the extension to multiple target positioning has been done in this chapter. It has been studied that under some conditions, an analytical solution can be defined and that this solution provides the maximum FIM determinant for each target. In other situations with complex target configurations, this analytical solution cannot be achieved, and then the optimal sensor configurations have been defined with a gradient optimization method. The examples shown in this chapter with constant covariance illustrated that this approach is correct and that the accuracy obtained for each target is very close to the theoretical maximum that would be obtained for a single target working in isolation.

Then this study was extended to a second and more complex problem, when the distance affects the measurement error and then the covariance of the measurement error is distance-dependent. In this problem it is necessary to resort to optimization techniques to define an optimal formation because it is not possible to define an analytical solution. In this sense Pareto optimization is used for the maximization of convex combinations of the logarithms of the determinants of the FIMs for each of the targets. The optimal solution has been obtained again via a gradient optimization method. It has been reported that depending on the error model, on the targets configuration, and on the Pareto weights assigned to each of the targets, several optimal configurations may be defined. These optimal configurations are clearly mission-dependent.

Finally, the previous results were extended to the more realistic problem where the target positions are known with uncertainty. This uncertainty can be defined by any probabilistic distribution function, and the kind of function used determines in high degree the optimal sensor formation. An optimization method similar to the previously defined was used to determine the optimal sensor configurations. The main problem to overcome was the resolution of the integrals of the gradient equations, to determine the necessary gradients to increase the average FIM determinant over the work area in the optimization algorithm. These integrals were solved numerically by a Monte Carlo method because of the impossibility of solving them analytically. Different design scenarios were studied.

Therefore, in this chapter, a methodology to define optimal sensor configurations for multiple target positioning in 2D considering constant and distance-dependent covariance error has been defined and the well behaviour of this methodology has been proved through several illustrative examples.

Chapter 4

SINGLE TARGET POSITIONING IN 3D SCENARIOS WITH RANGE MEASUREMENTS

4.1 Introduction

The use of autonomous underwater vehicles (AUVs) in different research and commercial areas has been increasing in the last few years. For reasons that have to do with autonomy, flexibility, and the new trend in miniaturization, AUVs are steadily emerging as tools par excellence to replace ROVs and also humans in the execution of many demanding tasks at sea that include pipeline inspection, seabed surveying, and archaeological research, to name but a few. Furthermore, their use in collaborative tasks allows for the realization of complex missions, often with relatively simple systems; see [32].

Central to the operation of some classes of AUVs is the availability of good underwater positioning systems to localize one or more vehicles simultaneously based on information received on-board a support ship or an autonomous surface system. The info thus obtained is at times used to follow the state of progress of a particular mission or, if reliable acoustic modems are available, to relay it as a navigation aid to the navigation systems existent on-board the AUV. Identical comments apply to a new generation of positioning systems to aid in the tracking of one or more human divers, as proposed in the context of the EC CO3AUVs project [9].

Inspired by similar developments in ground robotics, in this chapter we address the problem of single target positioning in 3D scenarios based on measurements of the ranges between the target and a set of sensors, obtained via acoustic ranging devices. In particular, and speaking in loose terms, we are interested in determining the optimal configuration (formation) of a sensor network that will, in a well defined sense, maximize the range-related information available for underwater target positioning. To this effect, we assume that the range measurements are corrupted by white Gaussian noise the variance of which is distance-dependent. The actual computation of the target position may be done by resorting to trilateration algorithms. See for example [4], [3], [7], and the

references therein for an introduction to this circle of ideas, covering both theoretical and practical aspects.

Given a target positioning problem, the optimal sensor configuration can be ascertained by examining the corresponding Cramer-Rao Bound (CRB) or Fisher Information Matrix (FIM). See [87] for a lucid presentation of this subject in the context of estimation theory. To this effect, the determinant of the FIM is used as an indicator of the performance that is achievable with a given sensor configuratin. Maximizing this quantity yields the most appropriate sensor formation geometry. Thus, the FIM corresponding to a 3D scenario is computed to derive the sensor configuration that yields the best precision with which the position of a target can possibly be estimated considering a distance-dependent variance of the noise model. In this sense, in [84] the Cramer-Rao Bound is derived for a distance-dependent error model for Time-Of-Arrival based localization in the two-dimensional (2D) space, showing that an error model with distance-dependent covariance has an important impact on the geometric configuration of nodes on the localization accuracy. The underwater target positioning problem was addressed by the authors previously in [61] and [62].

For a given target positioning problem, the optimal geometry of the sensor configuration depends strongly on the constraints imposed by the task itself (e.g. maximum number and type of sensors that can be used) and the environment (e.g. ambient noise). In fact, an inadequate sensor configuration may yield large positioning errors. It is interesting to remark that in spite of the importance and relevance of the optimal sensor placement problem, the topic is far from being studied exhaustively.

Interesting results in the area go back to the works commented on the introduction of Chapter 2. Some interesting works that deal with the problem of target positioning in 3D can be found in [94] and [95], where the authors derive some properties of the CRB and state conditions that the optimal formations must satisfy. In addition, several solutions to the 2D and 3D positioning problems are proposed. In [66] a method for optimal sensor placement that minimizes the condition number of a matrix involved in a linear least squares (LLS) solution is proposed and it exploits the use of an iterative linearized model (LM) estimator. The authors further derive the analytical form of some optimal sensor configurations. In [61] and [62] an initial solution for the problem of underwater target positioning with a surface sensor network was introduced for the scenarios where the target position is known *a priori* and when it is known with uncertainty, respectively.

Motivated by previous work, in this chapter we address the problem of finding the optimal geometric configuration of a sensor formation for the positioning of a target, based on target-to-sensor range measurements only. In contrast to what has so far been published in the literature, we address explicitly the positioning problem in 3D with the sensor array in 3D. The special scenario where the sensor array is located in a plane (2D) is studied as a particular example of the methodology developed; this application scenario arises for example in the case where an underwater target is positioned by an ocean surface sensor network. A problem of this type was previously studied in [99], where a method to determine the optimal two-dimensional spatial placement of multiple sensors participating in a robot perception task was derived. One of the scenarios considered was that of localizing an underwater vehicle, the acoustic receivers being constrained to lie on a horizontal plane.

The key contributions of the present chapter are fivefold: i) a general solution is obtained analytically for the problem of optimal sensor placement when the sensors are allowed to be placed freely in 3D space. Thus, depending on the mission at hand, for example for underwater target positioning, the sensor network may be completely underwater or at the surface, or even configured such that a sub-group of sensors is at the surface and the remaining sub-group close to the sea-bottom, ii) it is shown that the optimal configuration lends itself to an interesting intuitive geometric

characterization of all possible (optimal sensor placement) solutions that can be obtained in 3D, iii) a solution is also offered for the important case where the depth of the target is computed directly, thus dispensing with the need to estimate it using acoustic range measurements; with the solution obtained, the relationship between 3D and 2D scenarios (commonly exploited in land robotics) where the target and the sensor network lie in the same plane, becomes clear; iv) the solutions derived are extended to the case where *a priori* knowledge about the target in 3D is given in terms of a probability density function, and finally, v) the variances are allowed to depend explicitly on the ranges themselves. This allows us to capture the fact that measurement noise increases in a non-linear manner with the distances measured.

It is important to point out that, as commented in previous chapters, it may be argued that considering an assumed position for the target defeats the purpose of devising a method to compute it, for the latter is known in advance. The rationale for the problem at hand stems from the need to first fully understand the simpler situation where the position of the target is known and to characterize, in a rigorous manner, the types of solutions obtained for the optimal sensor placement problem. In a practical situation, the position of the target is only known with uncertainty and this problem must be tackled directly. However, in this case it is virtually impossible to a general analytical characterization of the optimal solutions, and one must resort to numerical search methods. At this stage, an in-depth understanding of the types of solutions obtained for the ideal case is of key importance to compute an initial guess for the optimal sensor placement algorithm adopted. These issues are rarely discussed in the literature, a notable exception being [39]. Thus, this chapter establishes the core theoretical tools to address and solve the case when there is uncertainty in the position of the underwater target

For the sake of completeness similar definitions and demonstrations to those given in Chapter 2, i.e., the problem formulation, information inequality and optimal FIM, are stated again for three-dimensional scenarios. This repetition of arguments seeks to make the present chapter self-contained and more readable, since the optimal solutions are far more rich and complex.

The chapter is organized as follows. Section 4.2 derives the FIM for the optimal sensor placement problem when the measurement noise is Gaussian, with distance-dependent variance. The optimal FIM that provides the maximum determinant at the target position is analytically defined in Section 4.3. Section 4.4 characterizes all the possible optimal sensor configurations in 3D space when the error covariance is constant. Moreover the application scenario in which the sensors are placed in a plane is tackled. Both situations where the target depth is known and unknown are also studied. Section 4.5 contains the derivation of optimal sensor configurations with distance-dependent covariance error. The particular case where the sensors can be placed on a sphere centred at the target position in 3D space is tackled, and the results are then re-examined for the application scenario where a n sensor formation is located on a plane. For the latter case, both situations where the target depth is known and unknown are studied again. In Section 4.6 the optimal sensor placement problem is solved for the case where the prior knowledge about the target is given in terms of a probability density function, and several simulation examples are included. Finally, Section 4.7 contains the conclusions and a brief discussion of topics.

4.2 Information Inequality with distance-dependent measurement noise

Let $\{I\}$ be an inertial reference frame with unit axis $\{x_I\}, \{y_I\}, \{z_I\}$ and let $q = [q_x, q_y, q_z]^T$ be the position of the target to be positioned in $\{I\}$. Further denote by $p_i = [p_{ix}, p_{iy}, p_{iz}]^T$; $i = 1, 2, .., n$,

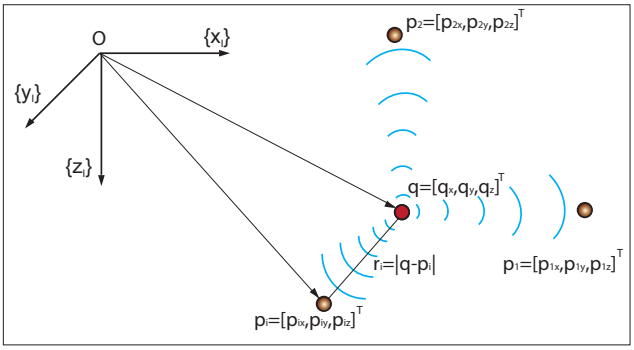

Figure 4.1: Target localization problem set-up.

the position of the $i-th$ acoustic ranging sensor, also in $\{I\}$. Let $r_i(q) = |q - p_i|$ (abbv. r_i) be the distance (range) between the target q and the $i-th$ sensor, where $|\cdot|$ denotes the Euclidean norm. The variables and the set-up that will be used are illustrated in Figure 4.1 for the case of one target and three sensors. We denote by z_i the measurements of the actual range $r_i(q)$, corrupted by additive noise ω_i. With the above notation, the measurement model adopted is given by

$$z_i = |q - p_i| + \omega_i = r_i(q) + \omega_i \tag{4.1}$$

Range measurements between two objects are plagued with errors that depend on a multitude of effects: depth-dependent speed of propagation of sound in water, physical propagation barriers, ambient noise, and degrading signal-to-noise ratio as the distance between the two objects increases, to name but a few. For analytical tractability, it is commonly assumed that the measurement errors can be captured by Gaussian, zero mean, additive noise with constant covariance. Clearly, this assumption is artificial in view of the simple fact that the "level of noise" is distance-dependent. In this chapter we assume again that the measurement noise can be modelled by a zero-mean Gaussian process where the covariance depends on the distance between the two objects that exchange range data. Stated mathematically,

$$\omega = (I + \eta\delta(r(q)^\gamma)) \cdot \omega_0 \tag{4.2}$$

where $r(q)$ is the vector of actual ranges, η and γ are the modelling parameters for the distance-dependent noise component, and $\omega = [\omega_1 \cdots \omega_n]^T$ is measurement noise assuming that all noise sources ω_i are independent, and the vector ω_0 is a zero mean Gaussian process $N(0, \Sigma_0)$ with $\Sigma_0 = \sigma^2 \cdot I$, where I is the identity matrix. In the above, δ is the operator *diag*, that either converts a square matrix into a vector consisting of its diagonal elements, or converts a vector into a square diagonal matrix whose diagonal components are the array elements. With these assumptions, the measurement noise covariance matrix is given by

$$\Sigma = \sigma^2 (I + \eta\delta(r(q)^\gamma))^2 = \delta\left(\sigma^2 \cdot \left(1 + \eta r_1^\gamma\right)^2, \cdots, \sigma^2 \cdot \left(1 + \eta r_n^\gamma\right)^2\right) \tag{4.3}$$

Stated in simple terms, the FIM captures the amount of information that measured data provide about an unknown parameter (or vector of parameters) to be estimated. Under known assumptions, the FIM is the inverse of the Cramer-Rao Bound matrix (abbv. CRB), which lower bounds the covariance of the estimation error that can possibly be obtained with any unbiased estimator. Thus,

"minimizing the CRB" may yield (by proper estimator selection) a decrease of uncertainty in the parameter estimation.

Formally, let $\hat{q}(z)$ be any unbiased estimator of q, that is, a mapping $\hat{q} : \Re^n \rightarrow \Re^3$ between the observations z and the target position space such that $E\{\hat{q}\} = q$ for all $q \in \Re^3$, where $E\{\cdot\}$ denotes the average operator. Let $p_q(z)$ be the likelihood function that defines the probability of obtaining the observation z given that the true target position is q. It is well known that under some regularity conditions on $p_q(z)$ the following inequality holds:

$$Cov\{\hat{q}\} \geq FIM(q)^{-1} = CRB(q) \tag{4.4}$$

where

$$Cov\{\hat{q}\} = E\{(\hat{q} - q)(\hat{q} - q)^T\}, \tag{4.5}$$

FIM (q) (often abbreviated simply as FIM) is the Fisher Information Matrix defined as

$$FIM(q) = E\left\{(\nabla_q \log p_q(z))(\nabla_q \log p_q(z))^T\right\}, \tag{4.6}$$

and $CRB(q)$ is the Cramer-Rao Bound matrix. In the above, $\nabla_q \log p_q$ denotes the gradient of the log of the likelihood function with respect to the unknown parameter q. Taking the trace of both sides of the covariance inequality yields

$$var\{\hat{q}\} := tr(Cov\{\hat{q}\}) = tr(E\{(\hat{q} - q)(\hat{q} - q)^T\}) \geq tr(FIM(q))^{-1} \tag{4.7}$$

that sets a lower bound on the mean-square error of any unbiased estimator.

Equipped with the above notation and tools of estimation theory we now address the optimal sensor placement problem by solving a related equivalent optimization one: given the FIM for the problem at hand, maximize its determinant by proper choice of the acoustic sensor coordinates. This strategy for sensor placement underlies much of the previous work available in the literature; see for example [55] , [39] and the references therein. Following standard procedures, the FIM corresponding to the problem of range-based single target positioning in 3D can be computed from the likelihood function $p_q(z)$ given by

$$p_q(z) = \frac{1}{(2\pi)^{\frac{n}{2}}|\Sigma|^{\frac{1}{2}}} \exp\left\{-\frac{1}{2}(z - r(q))^T \Sigma^{-1}(z - r(q))\right\} \tag{4.8}$$

where n is the number of receivers, $z = [z_1, z_2, ..., z_n]^T$ consists of n measured ranges, and $r(q)$ are the actual ranges. Taking the logarithm of (4.8), computing its derivative with respect to q, and then its expected value, the FIM is defined as

$$FIM = C(\delta(r)\Sigma\delta(r))^{-1}C^T \tag{4.9}$$

where $C = (q1_n^T - p) \in \Re^{3xn}$, $1_n \in \Re^{nx1}$ is a vector of 1s, and p is the vector of sensor positions, the latter being defined in $\Re^{3xn}$. The FIM is constructed by allowing the measurement error to be distance-dependent. Note that Σ depends on the actual range distances, not the measured ones, so its derivative with respect to the estimation parameters of q must not be computed in (4.9). Once the FIM is computed, the Cramer Rao Bound matrix is defined as $CRB = FIM^{-1}$. In this context, the optimal sensor placement strategy for a single vehicle localization problem is obtained by maximizing the determinant of the FIM, which must be computed explicitly. To this effect, we

start by expanding (4.9) to obtain

$$FIM = \frac{1}{\sigma^2}\sum_{i=1}^{n}\begin{pmatrix} \frac{p_{ix}^2}{r_i^2}\Gamma_i^2 & \frac{p_{ix}p_{iy}}{r_i^2}\Gamma_i^2 & \frac{p_{ix}p_{iz}}{r_i^2}\Gamma_i^2 \\ \frac{p_{ix}p_{iy}}{r_i^2}\Gamma_i^2 & \frac{p_{iy}^2}{r_i^2}\Gamma_i^2 & \frac{p_{iy}p_{iz}}{r_i^2}\Gamma_i^2 \\ \frac{p_{ix}p_{iz}}{r_i^2}\Gamma_i^2 & \frac{p_{iy}p_{iz}}{r_i^2}\Gamma_i^2 & \frac{p_{iz}^2}{r_i^2}\Gamma_i^2 \end{pmatrix} \tag{4.10}$$

where $\Gamma_i = 1/\left(1+\eta r_i^{\gamma}\right)$ for $i \in \{1,...,n\}$, and without loss of generality, the target is considered to be placed at the origin of the inertial coordinate frame, $q = [0,0,0]^T$. Clearly, the expression of the FIM considering a distance-dependence covariance error is well defined.
As explained before, the determinant of the FIM is used for the computation of an indicator of the performance that can be achieved (by proper choice of an estimator) with a given sensor configuration. Maximizing this indicator, as proposed in the so-called the *D-optimum design* strategy [85], yields the most appropriate sensor formation geometry for the single target positioning problem.

It is important to remark that is crucial the imposition or existence of constraints in the design of an optimal sensor network when a variable error covariance is considered. It can be seen that the determinant of (4.10) is inversely proportional to the measurement error, so it depends explicitly on the distance between sensors and target. Hence if the sensors can be placed freely in the 3D space they will tend to concentrate over the target position to reduce as much as possible the distance-dependent added error. Therefore, different optimal formations may be defined depending on the constraints imposed by the environment, by the task, or by the sensor network itself. In the forthcoming sections we study some of the more usual practical scenarios, but the procedure would be similar for any alternative scenario.

4.3 Optimal Fisher Information Matrix

To compute the determinant of the FIM it is convenient to introduce the following three vectors in $\Re^n$:

$$\begin{aligned} \mathrm{X} &= \left[\begin{array}{ccc} \frac{p_{1x}}{r_1}\cdot\Gamma_1 & \ldots & \frac{p_{nx}}{r_n}\cdot\Gamma_n \end{array}\right] \\ \Upsilon &= \left[\begin{array}{ccc} \frac{p_{1y}}{r_1}\cdot\Gamma_1 & \ldots & \frac{p_{ny}}{r_n}\cdot\Gamma_n \end{array}\right] \\ \mathrm{Z} &= \left[\begin{array}{ccc} \frac{p_{1z}}{r_1}\cdot\Gamma_1 & \ldots & \frac{p_{nz}}{r_n}\cdot\Gamma_n \end{array}\right] \end{aligned} \tag{4.11}$$

The latter should be viewed as vectors of a Hilbert space with elements in $\Re^n$, endowed with an inner product structure $<,>$. This allows for the computation of the length of a vector and also for the angle between two vectors. Namely, given X and Υ in $\Re^n$, then $|\mathrm{X}|^2 =< \mathrm{X},\mathrm{X} >$ and $< \mathrm{X},\Upsilon >= |\mathrm{X}||\Upsilon|\cos(\theta_{\mathrm{X}\Upsilon})$, from which it follows that the angle $\theta_{\mathrm{X}\Upsilon}$ between vectors X and Υ is given by $\theta_{\mathrm{X}\Upsilon} = \cos^{-1}(< \mathrm{X},\Upsilon > /(|\mathrm{X}||\Upsilon|))$.

With this notation, the FIM for a distance-dependent covariance error becomes

$$FIM = \begin{pmatrix} \mathrm{X}\cdot\mathrm{X} & \mathrm{X}\cdot\Upsilon & \mathrm{X}\cdot\mathrm{Z} \\ \mathrm{X}\cdot\Upsilon & \Upsilon\cdot\Upsilon & \Upsilon\cdot\mathrm{Z} \\ \mathrm{X}\cdot\mathrm{Z} & \Upsilon\cdot\mathrm{Z} & \mathrm{Z}\cdot\mathrm{Z} \end{pmatrix} = \begin{pmatrix} |\mathrm{X}|^2 & |\mathrm{X}||\Upsilon|\cos(\theta_{\mathrm{X}\Upsilon}) & |\mathrm{X}||\mathrm{Z}|\cos(\theta_{\mathrm{X}\mathrm{Z}}) \\ |\mathrm{X}||\Upsilon|\cos(\theta_{\mathrm{X}\Upsilon}) & |\Upsilon|^2 & |\Upsilon||\mathrm{Z}|\cos(\theta_{\Upsilon\mathrm{Z}}) \\ |\mathrm{X}||\mathrm{Z}|\cos(\theta_{\mathrm{X}\mathrm{Z}}) & |\Upsilon||\mathrm{Z}|\cos(\theta_{\Upsilon\mathrm{Z}}) & |\mathrm{Z}|^2 \end{pmatrix}, \tag{4.12}$$

from which it follows that

$$|FIM| = |\mathrm{X}|^2 \cdot |\Upsilon|^2 \cdot |\mathrm{Z}|^2 \cdot \Theta, \tag{4.13}$$

where

$$\Theta = 1 + 2\cos(\theta_{\Upsilon\mathrm{Z}})\cos(\theta_{\mathrm{X}\mathrm{Z}})\cos(\theta_{\mathrm{X}\Upsilon}) - \cos^2(\theta_{\Upsilon\mathrm{Z}}) - \cos^2(\theta_{\mathrm{X}\mathrm{Z}}) - \cos^2(\theta_{\mathrm{X}\Upsilon}) \tag{4.14}$$

where $\theta_{\mathrm{X}\Upsilon}$, $\theta_{\mathrm{X}\mathrm{Z}}$ and $\theta_{\Upsilon\mathrm{Z}}$ are the angles defined by vectors X and Υ, X and Z, and Υ and Z, respectively, and $|FIM|$ denotes the determinant of the FIM.

Notice how $|FIM|$ has been expressed in terms of the norms of vectors X, Υ, and Z and the angles $\theta_{\mathrm{X}\Upsilon}$, $\theta_{\mathrm{X}\mathrm{Z}}$, and $\theta_{\Upsilon\mathrm{Z}}$ between them. The latter depend on $p_i = [p_{ix}, p_{iy}, p_{iz}]^T$; $i = 1, 2, ...n$, that define the positions of the sensors with respect to the target, with the target placed at the origin of the reference frame. Formally, in order to seek conditions that the optimal sensor configurations must satisfy in order to maximize $|FIM|$, one could compute the derivatives of $|FIM|$ with respect to p_{ix}, p_{iy}, and p_{iz}, and equate them to zero. This task is tedious and will not shed light on the form of the optimal sensor configurations. We therefore follow a different approach. From the expression of $|FIM|$ it is easy to check that the maximum value of Θ is 1. In fact, suppose that a larger value can be obtained, which clearly requires that

$$1 + 2\cos(\theta_{\Upsilon\mathrm{Z}})\cos(\theta_{\mathrm{X}\mathrm{Z}})\cos(\theta_{\mathrm{X}\Upsilon}) - \cos^2(\theta_{\Upsilon\mathrm{Z}}) - \cos^2(\theta_{\mathrm{X}\mathrm{Z}}) - \cos^2(\theta_{\mathrm{X}\Upsilon}) > 1 \tag{4.15}$$

The above inequality is equivalent to

$$0 < 2\cos(\theta_{\Upsilon\mathrm{Z}})\cos(\theta_{\mathrm{X}\mathrm{Z}})\cos(\theta_{\mathrm{X}\Upsilon}) - \cos^2(\theta_{\Upsilon\mathrm{Z}}) - \cos^2(\theta_{\mathrm{X}\mathrm{Z}}) - \cos^2(\theta_{\mathrm{X}\Upsilon}). \tag{4.16}$$

Notice, however that because $\cos^2(\theta_{\mathrm{X}\mathrm{Z}}) + \cos^2(\theta_{\mathrm{X}\Upsilon}) \geq 2\cos(\theta_{\mathrm{X}\mathrm{Z}})\cos(\theta_{\mathrm{X}\Upsilon})$ and $0 \leq |\cos(\theta_{\Upsilon\mathrm{Z}})| \leq 1$, it follows that

$$\cos^2(\theta_{\mathrm{X}\mathrm{Z}}) + \cos^2(\theta_{\mathrm{X}\Upsilon}) \geq 2\cos(\theta_{\Upsilon\mathrm{Z}})\cos(\theta_{\mathrm{X}\mathrm{Z}})\cos(\theta_{\mathrm{X}\Upsilon})$$

and then is clear that,

$$\cos^2(\theta_{\mathrm{X}\mathrm{Z}}) + \cos^2(\theta_{\mathrm{X}\Upsilon}) + \cos^2(\theta_{\Upsilon\mathrm{Z}}) \geq 2\cos(\theta_{\Upsilon\mathrm{Z}})\cos(\theta_{\mathrm{X}\mathrm{Z}})\cos(\theta_{\mathrm{X}\Upsilon})$$

which contradicts (4.16). Therefore,

$$1 + 2\cos(\theta_{\Upsilon\mathrm{Z}})\cos(\theta_{\mathrm{X}\mathrm{Z}})\cos(\theta_{\mathrm{X}\Upsilon}) - \cos^2(\theta_{\Upsilon\mathrm{Z}}) - \cos^2(\theta_{\mathrm{X}\mathrm{Z}}) - \cos^2(\theta_{\mathrm{X}\Upsilon}) \leq 1 \tag{4.17}$$

and its maximum value of 1 is obtained when all the angles are equal to $k \cdot \pi/2$, with k an odd natural number and then,

$$\cos(\theta_{\mathrm{X}\Upsilon}) = \cos(\theta_{\mathrm{X}\mathrm{Z}}) = \cos(\theta_{\Upsilon\mathrm{Z}}) = 0. \tag{4.18}$$

We now define the auxiliary cost function

$$f^*(FIM) = |\mathrm{X}|^2 \cdot |\Upsilon|^2 \cdot |\mathrm{Z}|^2 \tag{4.19}$$

Consider now the problem of maximizing $f^*(FIM)$ by proper choice of $\bar{p} = [p_1, \cdots, p_n]^T$, and let $\bar{p}^*$; $i = 1, 2, ..., n$, be a maximizing solution. Let X^*, Υ^*, and Z^* be the corresponding vectors in $\Re^n$. Suppose also that the corresponding angles $\theta^*_{\mathrm{X}\Upsilon}$, $\theta^*_{\mathrm{X}\mathrm{Z}}$, and $\theta^*_{\Upsilon\mathrm{Z}}$ satisfy

$$\cos(\theta^*_{\mathrm{X}\Upsilon}) = \cos(\theta^*_{\mathrm{X}\mathrm{Z}}) = \cos(\theta^*_{\Upsilon\mathrm{Z}}) = 0. \tag{4.20}$$

Then $\overline{p}^*;\ i = 1, 2, ..., n$ maximize also (4.13), the FIM is a diagonal matrix and it implies that its determinant is the global maximum. Under the assumptions stated, the optimal FIM is a diagonal matrix, that is,

$$FIM = \begin{pmatrix} \mathrm{XX} & \mathrm{X\Upsilon} & \mathrm{XZ} \\ \mathrm{X\Upsilon} & \mathrm{\Upsilon\Upsilon} & \mathrm{\Upsilon Z} \\ \mathrm{XZ} & \mathrm{\Upsilon Z} & \mathrm{ZZ} \end{pmatrix} = \begin{bmatrix} |\mathrm{X}|^2 & 0 & 0 \\ 0 & |\Upsilon|^2 & 0 \\ 0 & 0 & |\mathrm{Z}|^2 \end{bmatrix} \tag{4.21}$$

With the above assumption on the general form that the simplified FIM matrix will take, we now introduce a simple general procedure to derive conditions for optimal sensor placement that lend themselves to clear geometric interpretations. The problem at hand can be converted into that of computing

$$\overline{p}^* = arg \max_{\overline{p}} |FIM| = |\mathrm{X}|^2 \cdot |\Upsilon|^2 \cdot |\mathrm{Z}|^2 \tag{4.22}$$

where $\overline{p} = [p_1^T, ..., p_n^T]^T$, and $\overline{p}^*$ are the optimal sensor positions. Notice that the sensor positions $\overline{p}^*$ must satisfy the additional constraint imposed by inequality (4.20), i.e., the angles $\theta_{\mathrm{X\Upsilon}}$, θ_{XZ}, and $\theta_{\mathrm{\Upsilon Z}}$ must be equal to $k \cdot \pi/2$ for some odd natural number k which, as explained, makes the off-diagonal elements of (4.21) equal to 0.

Formally, the conditions that an optimal sensor configuration must satisfy may now be obtained by computing the derivatives of (4.22) with respect to p_{ix}, p_{iy}, and p_{iz}; $i = 1, 2, ..., n$ and equating them to 0. The candidate solutions must also satisfy (4.20). This will naturally yield multiple optimal sensor configurations for single target positioning if no extra constraints are placed on the sensor configuration. To make the problem tractable, it is therefore important to impose configuration constraints rooted in operational considerations. In what follows, the methodology adopted is illustrated with two representative scenarios: i) for constant covariance error, as commonly reported in the literature of the area, to first fully understand the geometric configuration of the optimal sensor array, and ii) with distance-dependent covariance error, to illustrate how a different and more realistic measurement error model can modify and condition the optimal sensor configurations. The methodology adopted for both scenarios will be analysed through several simulation examples.

4.4 Gaussian error with constant covariance

In the existent literature it is commonly assumed that the range measurement error has constant covariance. Therefore it is important to study this problem before a distance-dependent covariance error may be considered. It is shown that the optimal configuration lends itself to an interesting intuitive geometric characterization of all possible (optimal sensor placement) solutions that can be obtained in 3D. This characterization yields a simple, geometrically based procedure to choose an optimal sensor placement strategy in situations of practical interest. In this sense the situation in which a surface sensor network computes the position of an underwater target is studied, and a solution is also offered for the important case where the depth of the target is computed directly, thus dispensing with the need to estimate it using acoustic range measurements. Thus, with the solution obtained for this latter scenario, the relationship between 3D and 2D scenarios (commonly exploited in land robotics) where the target and the sensor network lie in the same plane, becomes clear.

4.4.1 The optimal Fisher Information Matrix for constant covariance error

In this context, the optimal sensor placement strategy for a single vehicle localization problem is obtained by maximizing the determinant of (4.10), which must be computed explicitly for the case

in which the covariance error is constant. To this effect, making $\eta = 0$, (4.10) becomes

$$FIM = \frac{1}{\sigma^2} \sum_{i=1}^{n} \begin{pmatrix} (u_{ix})^2 & \left(u_{iy}\right)(u_{ix}) & (u_{iz})(u_{ix}) \\ (u_{ix})\left(u_{iy}\right) & \left(u_{iy}\right)^2 & (u_{iz})\left(u_{iy}\right) \\ (u_{ix})(u_{iz}) & \left(u_{iy}\right)(u_{iz}) & (u_{iz})^2 \end{pmatrix} \tag{4.23}$$

where

$$u_i = [u_{ix}, u_{iy}, u_{iz}]^T = \left[\begin{array}{ccc} \frac{\partial |q-p_i|}{\partial q_x}, & \frac{\partial |q-p_i|}{\partial q_y}, & \frac{\partial |q-p_i|}{\partial q_z} \end{array} \right]^T ; i \in \{1, ..., n\}. \tag{4.24}$$

As explained before, the optimal FIM is defined by (4.21), and its determinant is function of the vectors X, Υ, and Z in $\Re^n$ (where n is the number of sensors involved in the target positioning task) that for the constant covariance scenario become

$$\begin{aligned} \mathrm{X} &= \left[\begin{array}{ccc} u_{1x} & \ldots & u_{nx} \end{array} \right]^T = \left[\begin{array}{ccc} \frac{p_{1x}}{r_1} & \ldots & \frac{p_{nx}}{r_n} \end{array} \right]^T \\ \Upsilon &= \left[\begin{array}{ccc} u_{1y} & \ldots & u_{ny} \end{array} \right]^T = \left[\begin{array}{ccc} \frac{p_{1y}}{r_1} & \ldots & \frac{p_{ny}}{r_n} \end{array} \right]^T \\ \mathrm{Z} &= \left[\begin{array}{ccc} u_{1z} & \ldots & u_{nz} \end{array} \right]^T = \left[\begin{array}{ccc} \frac{p_{1z}}{r_1} & \ldots & \frac{p_{nz}}{r_n} \end{array} \right]^T \end{aligned} \tag{4.25}$$

Formally, the conditions that an optimal sensor configuration must satisfy may be obtained by computing the derivatives of (4.22) with respect to p_{ix}, p_{iy}, and p_{iz}; $i = 1, 2, ..., n$ and equating them to 0. The candidate solutions must also satisfy (4.20), as mentioned above.

It is interesting to notice that we can focus our attention on the computation of the derivatives of (4.22) with respect to the norms of the above vectors instead of computing these derivatives with respect to p_{ix}, p_{iy}, and p_{iz}; $i = 1, 2, ..., n$. Since

$$\frac{p_{ix}^2}{r_i^2} + \frac{p_{iy}^2}{r_i^2} + \frac{p_{iz}^2}{r_i^2} = 1, \tag{4.26}$$

it follows that

$$|\mathrm{X}|^2 = n - |\Upsilon|^2 - |\mathrm{Z}|^2 \tag{4.27}$$

Replacing (4.27) in the equation of the determinant of (4.22), the determinant of the FIM becomes

$$|FIM| = \frac{1}{\sigma^6} \left(n - |\Upsilon|^2 - |\mathrm{Z}|^2\right) |\Upsilon|^2 |\mathrm{Z}|^2$$

and therefore

$$\frac{\partial |FIM|}{\partial |\Upsilon|} = n - 2|\Upsilon|^2 - |\mathrm{Z}|^2 = 0, \tag{4.28}$$

$$\frac{\partial |FIM|}{\partial |\mathrm{Z}|} = n - |\Upsilon|^2 - 2|\mathrm{Z}|^2 = 0. \tag{4.29}$$

The last two equations yield $|\Upsilon|^2 = |\mathrm{Z}|^2$. Using (4.27) and (4.29) it now follows that $|\mathrm{X}|^2 = |\mathrm{Z}|^2$. As a consequence, $|\mathrm{X}|^2 = |\Upsilon|^2 = |\mathrm{Z}|^2$. Furthermore, from (4.27) it is easy to check that

$$|\mathrm{X}|^2 = |\Upsilon|^2 = |\mathrm{Z}|^2 = \frac{n}{3} \tag{4.30}$$

Therefore, the optimal Fisher Information Matrix is

$$FIM_{opt} = \frac{1}{\sigma^2}\begin{pmatrix} \frac{n}{3} & 0 & 0 \\ 0 & \frac{n}{3} & 0 \\ 0 & 0 & \frac{n}{3} \end{pmatrix} \tag{4.31}$$

Comparing the optimal FIM in (4.31) with the generic one in (4.10) gives an implicit characterization of the conditions that must be satisfied by the sensor network in order for it to be optimal:

$$\sum_{i=1}^{n} \frac{p_{ix}^2}{r_i^2} = \sum_{i=1}^{n} \frac{p_{iy}^2}{r_i^2} = \sum_{i=1}^{n} \frac{p_{iz}^2}{r_i^2} = \frac{n}{3}, \tag{4.32}$$

$$\sum_{i=1}^{n} \frac{p_{ix}p_{iy}}{r_i^2} = \sum_{i=1}^{n} \frac{p_{ix}p_{iz}}{r_i^2} = \sum_{i=1}^{n} \frac{p_{iz}p_{iy}}{r_i^2} = 0. \tag{4.33}$$

where (4.32) maximizes (4.22). Equation (4.33) satisfies the additional constraint imposed by inequality (4.20), i.e., the angles $\theta_{X\Upsilon}$, θ_{XZ}, and $\theta_{\Upsilon Z}$ must be equal to $k \cdot \pi/2$ for some odd natural number k which, as explained, makes the off-diagonal elements of (4.21) equal to 0. Therefore any sensor configuration that satisfies (4.32) and (4.33) is an optimal formation that implies the global maximum FIM determinant. It is also interesting how this solution defined by the optimality conditions (4.32) and (4.33) implies the orthogonality relations for sines and cosines from Fourier analysis [37].

From (4.31) it is obvious that the FIM is diagonal and its eigenvalues are equal. Therefore, the optimality conditions derived maximize not only the determinant of the FIM (D-optimum design) but also its minimum singular value (E-optimum design), and minimize the trace of its inverse too (A-optimim design).

4.4.2 Optimal sensor placement solutions

The contribution of this section is twofold: i) it offers a general characterization of the optimal sensor configurations for the problem of single target positioning in 3D and ii) it illustrates the computation of specific optimal configurations via three design examples.

4.4.2.1 A general characterization of optimal sensor configurations

Let σ_{ix}, σ_{iy}, and σ_{iz} be the direction angles that the *i-th* range vector forms with the vectors $\{x_I\}$, $\{y_I\}$, and $\{z_I\}$ of $\{I\}$ and let $\cos(\sigma_{ix}) = p_{ix}/r_i$, $\cos(\sigma_{iy}) = p_{iy}/r_i$, and $\cos(\sigma_{iz}) = p_{iz}/r_i$ be the corresponding direction cosines. Clearly, (4.32) and (4.33) can be written in terms of the direction cosines as

$$\sum_{i=1}^{n} \cos^2(\sigma_{ix}) = \sum_{i=1}^{n} \cos^2(\sigma_{iy}) = \sum_{i=1}^{n} \cos^2(\sigma_{iz}) = \frac{n}{3} \tag{4.34}$$

$$\sum_{i=1}^{n} \cos(\sigma_{ix})\cos(\sigma_{iy}) = \sum_{i=1}^{n} \cos(\sigma_{ix})\cos(\sigma_{iz}) = \sum_{i=1}^{n} \cos(\sigma_{iz})\cos(\sigma_{iy}) = 0 \tag{4.35}$$

The above equations show clearly that all optimal sensor configurations are characterized in terms of the angles that the range vectors form with the unit axis of the inertial frame. Therefore, there is no explicit dependence on the ranges themselves. This is because in the formulation adopted

it was tacitly assumed that the covariance of the range measurements is distance-invariant. For this reason we will henceforth assume, without any loss of generality, that the target is located at the origins of the inertial coordinate frame and that the optimal sensor formations are such that the sensors are placed on a sphere centred at the target. In this case, $\cos(\sigma_{ix}) = p_{ix}$, $\cos(\sigma_{iy}) = p_{iy}$, and $\cos(\sigma_{iz}) = p_{iz}$. Once an optimal solution on a sphere is found in terms of the direction cosines referred to above, an infinite number of optimal solutions can be generated by: i) multiplying the range of each sensor to the target by an arbitrary positive number (as will be explained later, the scaling of the ranges is dependent on the practical constraints imposed by physical considerations), and ii) rotating the sensor formation rigidly in terms of an arbitrary axis. The first statement is trivial to prove. To prove the second statement, let an initial sensor formation on the unit sphere be described by vectors $p_i; i = 1, 2, .., n$ and let $\tilde{p}_i = Rp_i; i = 1, 2, .., n$ be the formation that is obtained by applying the same rotation matrix R to all vectors. With $r_i = 1$, straightforward computations show that equations (4.32) and (4.33) can be written in compact form as

$$\sum_{i=1}^{n} p_i p_i^T = \frac{n}{3} I \tag{4.36}$$

where I is the identity matrix. It then follows that

$$\sum_{i=1}^{n} \tilde{p}_i \tilde{p}_i^T = \sum_{i=1}^{n} R p_i p_i^T R^T = \frac{n}{3} I \tag{4.37}$$

because $RR^T = I$; thus, the new sensor positions verify (4.36) and therefore (4.32) and (4.33).

Let $\sigma_q = p_1 + ... + p_n; n > 2$ denote the geometric centre of an optimal sensor formation and let r_q denote the vector directed from the origin to σ_q. Clearly, in view of the comments above, the formation that is obtained by moving the sensor rigidly with r_q until the latter vector is aligned with the $\{z_I\}$ axis of the inertial coordinate frame is also optimal. The centre of the resulting formation will be denoted by z_q. We will therefore assume, again without loss of generality, that the sensor positions satisfy the equations

$$\sum_{i=1}^{n} p_{ix} = 0 \quad \sum_{i=1}^{n} p_{iy} = 0 \quad \sum_{i=1}^{n} p_{iz} = n z_q \tag{4.38}$$

where $p_i = [p_{ix}, p_{iy}, p_{iz}]^T$ is the $i-th$ sensor position. At this point it is important to remark that even with the assumptions stated above it does not seem to be possible to classify all optimal solutions to the target localization problem in 3D in a simple manner. This is in striking contrast with the case of 2D, where all optimal solutions are obtained by distributing the sensors at equal angles along a circumference centred at the target, see [55] or Chapter 2. Once a solution is chosen, all solutions are simply generated by rotating the complete sensor formation rigidly about the target by an arbitrary angle $\alpha \in [0, \pi]$. The 3D case is far more complex, and therefore, in what follows, we restrict ourselves to presenting a method to generate a sufficiently rich set of solutions, which, as explained later, is appropriate to solve a number of problems of practical interest. To this effect, we start by restraining the types of solutions to lie not only on the unit sphere but also on a general quadratic surface (also called quadric) that intersects the sphere. As will be seen, the choice of the quadric affords the designer a very convenient "tuning knob" to "bias" the placement of the sensors towards regions of interest determined by practical considerations. We consider quadrics defined by

the equation

$$\begin{pmatrix} x & y & z & 1 \end{pmatrix}\begin{pmatrix} a_{11} & a_{12} & a_{13} & a_{14} \\ a_{12} & a_{22} & a_{23} & a_{24} \\ a_{13} & a_{23} & a_{33} & a_{34} \\ a_{14} & a_{24} & a_{34} & a_{44} \end{pmatrix}\begin{pmatrix} x \\ y \\ z \\ 1 \end{pmatrix} = a_{11}x^2 + a_{22}y^2 + a_{33}z^2 + a_{44} + 2a_{12}xy$$

$$+ 2a_{13}xz + 2a_{23}yz + 2a_{14}x + 2a_{24}y + 2a_{34}z = 0 \tag{4.39}$$

where $[x, y, z]^T$ are the coordinates of the points that belong to the quadric. The unit sphere, where all optimal sensor configurations lie, corresponds to the non-degenerate quadric surface given by

$$\begin{pmatrix} x & y & z & 1 \end{pmatrix}\begin{pmatrix} 1 & 0 & 0 & 0 \\ 0 & 1 & 0 & 0 \\ 0 & 0 & 1 & 0 \\ 0 & 0 & 0 & -1 \end{pmatrix}\begin{pmatrix} x \\ y \\ z \\ 1 \end{pmatrix} = x^2 + y^2 + z^2 - 1 = 0 \tag{4.40}$$

To determine the quadrics that are allowed we simply notice that for an optimal sensor formation that belongs to the intersection of a particular quadric and the unit sphere, the coordinates of each sensor must satisfy (4.39) and (4.40), together with (4.32), (4.33) , and (4.38). Adding n equations of the type (4.39), one for each sensor, yields the equality

$$a_{11}\sum_{i=1}^{n} p_{ix}^2 + a_{22}\sum_{i=1}^{n} p_{iy}^2 + a_{33}\sum_{i=1}^{n} p_{iz}^2 + na_{44} + 2a_{12}\sum_{i=1}^{n} p_{ix}p_{iy} + 2a_{13}\sum_{i=1}^{n} p_{ix}p_{iz}$$

$$+2a_{23}\sum_{i=1}^{n} p_{iy}p_{iz} + 2a_{14}\sum_{i=1}^{n} p_{ix} + 2a_{24}\sum_{i=1}^{n} p_{iy} + 2a_{34}\sum_{i=1}^{n} p_{iz} = 0$$

Using now (4.40) together with (4.32), (4.33) , and (4.38) with $r_i = 1$ gives the constraint

$$\frac{a_{11} + a_{22} + a_{33}}{3} + a_{44} + 2a_{34}z_q = 0 \tag{4.41}$$

This concludes the presentation of all the equations that allow for the computation of a solution to the optimal sensor placement problem. Granted, there is still an infinite number of degrees of freedom in the choice of a particular solution. The examples that follow show how this problem can be dealt with. Before we do so, however, it is important to remark on one important feature of the optimal solutions that can be computed based on the analysis explained above. If two disjoint sets of n and m sensors each are placed optimally, the resulting formation of $n + m$ sensors is also optimal. Therefore, new higher order optimal solutions can be obtained by combining reduced order optimal configurations.

4.4.2.2 Examples of optimal sensor placement

We now give three examples that illustrate the steps involved in the computation of optimal sensor configurations for the single target localization problem in 3D. We assume that all range measurements are corrupted by additive zero mean Gaussian noise with variance $\sigma^2 = 0.01\ m^2$. We impose the restriction that the maximum distance between the sensors and the target be 100 m. This

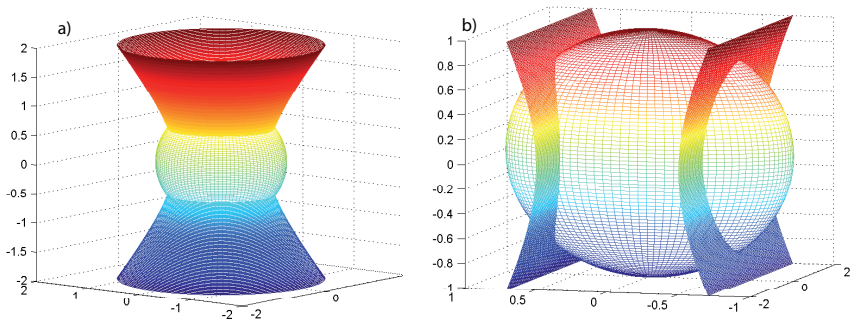

Figure 4.2: Intersection between the unit sphere and a hyperboloid of one sheet (a), and intersection between the unit sphere and a hyperbolic cylinder (b).

constraint can be easily accommodated by solving the optimal sensor placement problem with the assumption that the sensors lie on the unit sphere centred at the target and multiplying their distance to the origin by 100 at the end. As explained before, in order to make the problem tractable we consider that the sensors lie on the intersection of the unit sphere and a quadric, the coefficients of which must satisfy (4.41). In the examples, two quadrics are considered: an hyperboloid of one sheet defined by $2x^2 + 2y^2 - z^2 = 1$ and an hyperbolic cylinder defined by $4x^2 - y^2 = 1$. Their intersections with the unit sphere are shown in Fig. 4.2 (a) and Fig. 4.2 (b), respectively. In the first two examples, the number of sensors is $n = 4$. Example 4.1 refers to Fig. 4.2 (a), while Example 4.2 refers to Fig. 4.2 (b). Thus, the only difference between them are the loci where the sensors should be located. Without any loss of generality, the design procedure is explained by referring to Example 4.1.

Example 4.1: The system of equations used to compute the possible optimal configurations consists of the n equations

$$\cos^2(\sigma_{ix}) + \cos^2(\sigma_{iy}) + \cos^2(\sigma_{iz}) = 1; i = 1, 2, ..., n \tag{4.42}$$

that restrict each sensor to lie on the unit sphere, n additional equations

$$2\cos^2(\sigma_{ix}) + 2\cos^2(\sigma_{iy}) - \cos^2(\sigma_{iz}) = 1; i = 1, 2, ..., n \tag{4.43}$$

that express the fact that the sensors lie also on the quadric adopted, and an additional set of 6 equations derived directly from (4.34) and (4.35). The above equations were solved numerically using the Newton-Raphson method. As is well known, if F is the vector of equations to be solved, ∂F is the Jacobian of F with respect to the sensor coordinates, and $S^0 = \begin{bmatrix} p^0_{1x} & p^0_{1y} & p^0_{1z} & \cdots & p^0_{nx} & p^0_{ny} & p^0_{nz} \end{bmatrix}^T$ is an arbitrary initial vector that belongs to the intersection of the sphere and the quadric, a solution is obtained via the iteration

$$S^{(k+1)} = S^{(k)} - (\partial F^{(k)})^{-1} \cdot F^{(k)} \tag{4.44}$$

where $S^{(k)} = \begin{bmatrix} p^k_{1x} & p^k_{1y} & p^k_{1z} & \cdots & p^k_{nx} & p^k_{ny} & p^k_{nz} \end{bmatrix}^T$ is the vector of sensor coordinates at step k. The process finalizes when an appropriate stop criterion is met. See for example [24] for complete details.

In the case of Example 4.1, a solution was obtained that corresponds to placing the sensors at the positions stated in Table 4.1. It is easy to check that this configuration satisfies conditions (4.34) and (4.35), thus making the determinant of the FIM maximum at the target position. In this case $|FIM| = n^3/(\sigma^6 \cdot 3^3) = 2.3704 \cdot 10^6\ m^{-6}$.

Table 4.1: Optimal sensor positions.

Example 4.1	p_1	p_2	p_3	p_4
$\{x_I\} - coord.\ (m)$	81.497	−81.497	0	0
$\{y_I\} - coord.\ (m)$	0	0	−81.497	81.497
$\{z_I\} - coord.\ (m)$	−57.735	−57.735	57.735	57.735

For the sake of completeness, and to better understand the efficacy of the solution obtained, it was judged appropriate to evaluate how good the sensor formation is in terms of yielding accurate positioning of the real target, in comparison with the positioning accuracy that is possible for any hypothetical target (different from the real target) positioned anywhere in a finite spatial region $\mathcal{D}$ centred at the target. To this effect, the determinant of the FIM obtained for a number of hypothetical target points (based on the optimal sensor configuration obtained) was computed by allowing these points to be on a grid in $\mathcal{D}$. With an obvious abuse of notation, we refer to that determinant of the FIM, viewed as a function of its argument in $\mathcal{D}$, simply as $|FIM|_{\mathcal{D}}$. In the example, in order to enable a graphical representation, $\mathcal{D}$ consists of the three orthogonal planes in Fig. 4.3 (a) and the magnitude of $|FIM|_{\mathcal{D}}$ is indicated in a gray scale, lighter points corresponding to larger values of the $|FIM|$. The figure supports the fact that with the sensor placement adopted the position of the target can be determined with optimal accuracy. Should the target move to a different location, the precision with which it can be localized degrades. This raises the interesting practical problem of optimal sensor placement in the presence of target uncertainty, an issue that will be resolved later in the chapter. ■

Example 4.2: This second example is analogous to Example 4.1 but the quadric adopted is the hyperbolic cylinder depicted in Fig. 4.2 (b). The formation obtained with the above numerical procedure is the one in which the sensors are placed at the positions shown in Table 4.2. Equations (4.34) and (4.35) are achieved and the maximum FIM determinant is obtained with $|FIM| = n^3/(\sigma^6 \cdot 3^3) = 2.3704 \cdot 10^6\ m^{-6}$. Notice that the FIM determinant is the same of the previous example, as expected. This illustrates the fact that by choosing different quadrics one may generate a set of possible solutions to the single target localization problem. In Fig. 4.3 (b), $|FIM|_{\mathcal{D}}$ is mapped for the three orthogonal planes referred to above.

Table 4.2: Optimal sensor positions.

Example 4.2	p_1	p_2	p_3	p_4
$\{x_I\} - coord.\ (m)$	57.735	−57.735	−57.735	−57.735
$\{y_I\} - coord.\ (m)$	−57.735	57.735	−57.735	−57.735
$\{z_I\} - coord.\ (m)$	−57.735	−57.735	57.735	−57.735

■

Example 4.3: Finally, in this third example the number of sensors is reduced to $n = 3$. Using the quadric of Fig. 4.2 (b), a solution was found with the sensors placed at the positions listed in Table

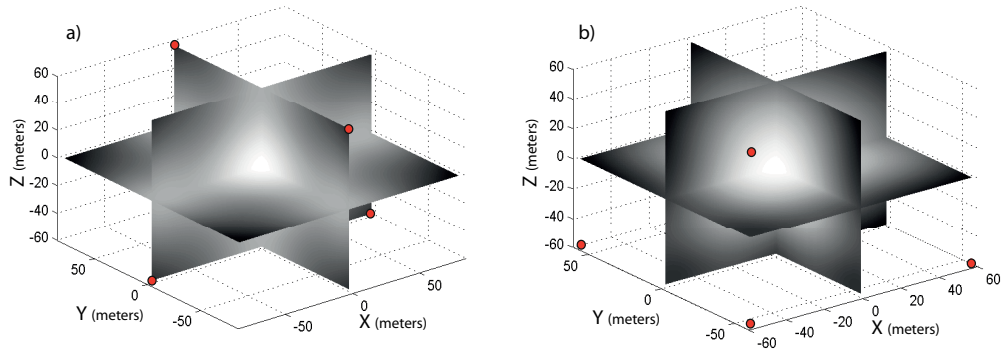

Figure 4.3: Plot of $|FIM|_{\mathcal{D}}$ in the three main planes, using 4 sensors. Lighter regions correspond to larger values of $|FIM|$; solutions obtained using a hyperboloid of one sheet (a) and a hyperbolic cylinder (b).

.

4.3. In this case, $|FIM| = n^3/(\sigma^6 \cdot 3^3) = 1 \cdot 10^6\ m^{-6}$. Note that the determinant of the FIM is smaller than that of Examples 4.1 and 4.2 due to the lower number of sensors. The sensor arrangement and the plot of $|FIM|_{\mathcal{D}}$; $\mathcal{D}$ for three orthogonal planes are shown in Fig. 4.4. ■

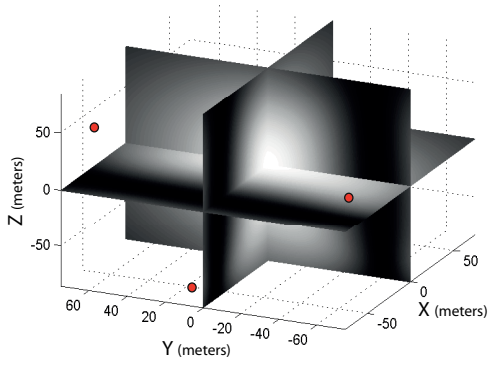

Figure 4.4: Plot of $|FIM|_{\mathcal{D}}$ in the three main planes, using 3 sensors; solution obtained using a hyperbolic cylinder.

The above examples illustrate the fact that a large number of solutions exists for the single target positioning problem in 3D and how a subset of them can be found by constraining the sensors to lie on the intersection of a quadric with a sphere. In this case, however, this constraint is purely artificial and is simply used as a "tuning knob" in the search for optimal solutions. In a great number of situations, however, there are practical issues that impose physically sound constraints on the possible sensor loci. One of these situations is studied next.

Table 4.3: Optimal sensor positions.

Example 4.3	p_1	p_2	p_3
$\{x_I\} - coord.\ (m)$	−59.45	−50.69	−62.42
$\{y_I\} - coord.\ (m)$	64.31	16.63	−74.75
$\{z_I\} - coord.\ (m)$	48.27	−84.58	22.71

4.4.3 Sensors lying in a plane: an application in underwater target positioning

This section addresses the problem of optimal sensor placement for underwater target positioning in 3D, subject to the condition that the sensors lie in a plane. This problem is of the utmost importance for underwater target positioning applications where the acoustic ranging devices are either located at the sea surface or on the seabed. A solution to this problem can be obtained using the results derived in the previous section and casting it in the following equivalent form: given a target at the origin of an inertial reference frame $\{I\}$, an unit sphere centred at the target, and a horizontal plane (a special case of a quadric), compute the distance z_q from the plane to the target such that a solution to the unconstrained single target localization problem lies on the intersection between the unit sphere and that plane. Once a solution to the latter problem is found, it is a simple matter to scale it while preserving the direction cosines of the range vectors (between the target and the sensors). Clearly, the scaling factor is d_t/z_q, where d_t is the target depth.

We start by characterizing the solutions for which the geometric centre of the sensors is located at $[0, 0, z_q]^T$. The computation of a solution unfolds in two steps: the z_q coordinate of the plane is computed; the geometric formation of the sensors on the plane is then derived. The first step is straightforward: because $z_1 = z_2 = ... = z_n = z_q$, it follows from (4.32) that

$$p_{1z} = ... = p_{nz} = z_q = \pm 1/\sqrt{3} \tag{4.45}$$

The above solutions correspond to two horizontal planes that intersect the unit sphere along two circumferences of radii r', as depicted in Fig. 4.5. Because $r'^2 + z_q^2 = 1$, it follows that the optimal radii are equal to $r' = \sqrt{1 - z_q^2} = \sqrt{\frac{2}{3}}$. These results yield straightforward solutions to the problem of underwater target positioning, as follows. Let d_t be the depth of the target, and assume that the array of n sensors to be used for target positioning is constrained to lie at the surface. An optimal solution to the problem of sensor placement corresponds to distributing the sensors along a circumference of radius $r_s = \sqrt{2}d_t$. In an analogous manner, if the target is at a distance (altitude) h_t above the seabed, and the array of n sensors to be used for target positioning is constrainted to lie at the seabottom, an optimal solution to the problem of sensor placement corresponds to distributing the sensors along a circumference of radius $r_s = \sqrt{2}h_t$. In the two cases, the centre of the circumferences is positioned either directly above or under the target.

It now remains to determine the geometric configuration of the sensors on the circumferences. To this effect, rewrite their positions in polar coordinates as $p_{ix} = r' \cos(\alpha_i)$, $p_{iy} = r' \sin(\alpha_i)$, and $p_{iz} = z_q$, where α_i is the angle that the projection of the $i - th$ range vector on the $\{x_I y_I\}$ plane forms

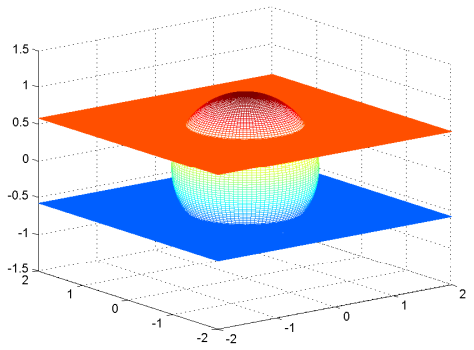

Figure 4.5: Intersection between two horizontal planes and the unit sphere.

with the $\{x_I\}$ axis, $r' = \sqrt{2}/\sqrt{3}$, and $z_q = 1/\sqrt{3}$. With this notation, (4.32) and (4.33) yield

$$\begin{aligned}
&\sum_{i=1}^{n} r'^2 \cos^2(\alpha_i) = \frac{n}{3} \rightarrow \frac{2}{3}\sum_{i=1}^{n} \cos^2(\alpha_i) = \frac{n}{3} \\
&\sum_{i=1}^{n} r'^2 \sin^2(\alpha_i) = \frac{n}{3} \rightarrow \frac{2}{3}\sum_{i=1}^{n} \sin^2(\alpha_i) = \frac{n}{3} \\
&\sum_{i=1}^{n} z_q^2 = \frac{n}{3} \rightarrow \sum_{i=1}^{n} \left(\frac{1}{\sqrt{3}}\right)^2 = \frac{n}{3} \\
&\sum_{i=1}^{n} r'^2 \cos(\alpha_i)\sin(\alpha_i) = 0 \rightarrow \sum_{i=1}^{n} \cos(\alpha_i)\sin(\alpha_i) = 0 \\
&z_q \sum_{i=1}^{n} r' \cos(\alpha_i) = 0 \rightarrow \sum_{i=1}^{n} \cos(\alpha_i) = 0 \\
&z_q \sum_{i=1}^{n} r' \sin(\alpha_i) = 0 \rightarrow \sum_{i=1}^{n} \sin(\alpha_i) = 0
\end{aligned} \tag{4.46}$$

Using by now classical terminology, the sensor formation must be first and second moment balanced. A simple and elegant solution is obtained by noticing the orthogonality relations for sines and cosines from Fourier analysis [37]

$$\begin{aligned}
&\sum_{i=0}^{n-1} \cos^2\left(\tfrac{2\pi}{n}\cdot i\right) = \sum_{i=0}^{n-1} \sin^2\left(\tfrac{2\pi}{n}\cdot i\right) = \frac{n}{2} \\
&\sum_{i=0}^{n-1} \cos\left(\tfrac{2\pi}{n}\cdot i\right)\sin\left(\tfrac{2\pi}{n}\cdot i\right) = \sum_{i=0}^{n-1} \cos\left(\tfrac{2\pi}{n}\cdot i\right) = \sum_{i=0}^{n-1} \sin\left(\tfrac{2\pi}{n}\cdot i\right) = 0
\end{aligned} \tag{4.47}$$

From (4.46) and (4.47) it follows that optimal solutions are obtained by distributing the n sensors uniformly along the circumferences, the vectors from the sensors to the centre of the circumferences making angles $2\pi i/n; i = 0, 1, ..., n-1$ with the $\{x_I\}$ axis. Obviously, an infinite number of solutions

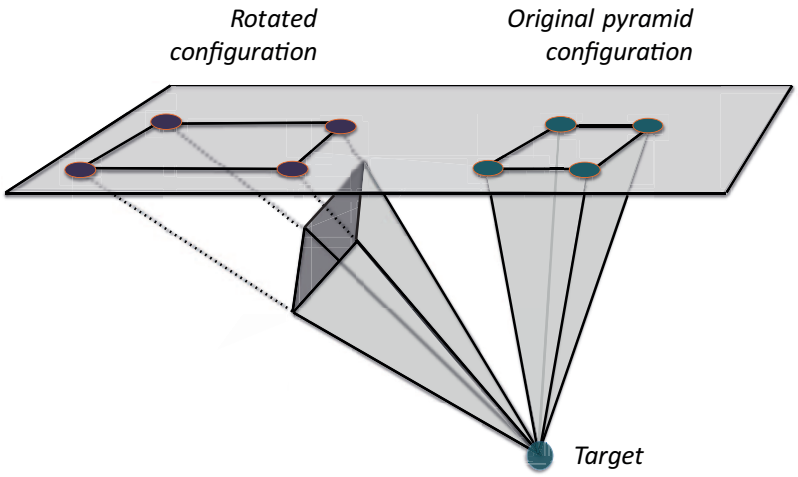

Figure 4.6: Target localization with sensors on a plane: two equivalent solutions obtained by rotation about one axis.

are obtained by rotating the sensors rigidly along the circumferences, that is, by allowing the above angles to become $2\pi i/n + \alpha_s; i = 0, 1, ..., n-1$, where α_s is a fixed but arbitrary angle in $[0, 2\pi]$

The results obtained in above sections imply that, once a solution to the above positioning problem is obtained, an infinite number of solutions can be generated in three steps: i) compute the vectors from the target to the sensor positions, ii) rotate them rigidly about a same axis, and iii) find (if they exist) the intersections of the extensions of the rotated vectors with the horizontal plane. This is illustrated in Fig. 4.6 where two equivalent solutions are presented for the special case of 4 sensors placed on a horizontal plane at the surface. In this case, the initial solution corresponds to the case where the 4 sensors are placed on the corners of the base of a regular pyramid with the apex at the target, the latter being directly under the geometric centre of the sensor formation. Another solution is obtained by rotating the pyramid about a selected axis while holding its apex fixed, and finding the new sensor locations at the intersection of the extended pyramid edges with the horizontal plane.

4.4.3.1 Example of target localization with sensors lying in a plane

The example in this section illustrates the methodology adopted for optimal sensor placement when the sensors are restricted to lie in a horizontal plane. In the example, for the sake of simplicity on the computation of the optimal solution, the origin of the inertial frame $\{I\}$ is considered to be placed at the target's projection on the horizontal plane, and the target placed at a depth of 100 m. A network of 5 sensors is considered.

Based on the theoretical analysis presented before, a simple optimal sensor configuration is derived that consists of placing the sensors regularly distributed on a circumference of radius $r' = 100 \cdot \sqrt{2}\ m$ centred at the target's projection on the horizontal plane. This formation yields the maximum value of the FIM determinant, $|FIM| = \frac{n^3}{\sigma^6 \cdot 3^3} = 4.6296 \cdot 10^6\ m^{-6}$. Figure 4.7 shows $|FIM|_{\mathcal{D}}$, that is, the evolution of $|FIM|$ as a function of the position of an hypothetical target placed arbitrarily in the region $\mathcal{D} := \{(x, y, z)^T : -150\ m \leq x \leq +150\ m, -150\ m \leq y \leq +150\ m, z = 100\ m\}$. Part (a) of the figure shows the level curves of $|FIM|$, with lighter colours corresponding

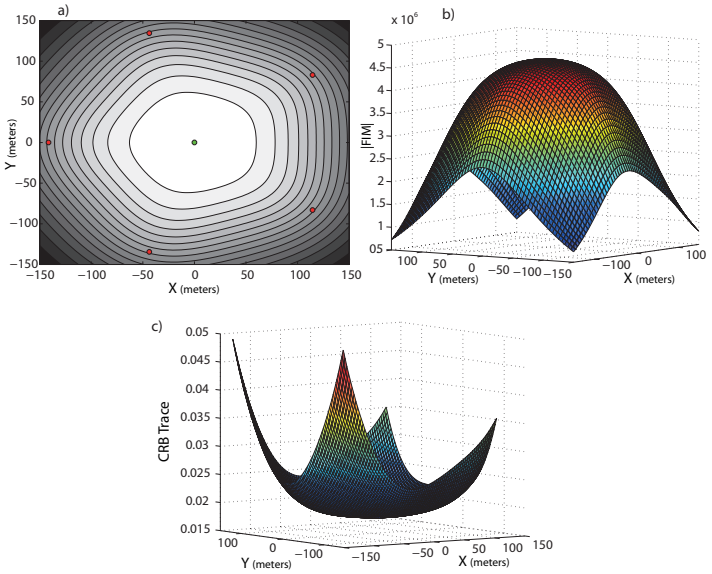

Figure 4.7: Optimal sensor formation for underwater target positioning in 3D with 5 sensors placed in a horizontal plane: (a) level curves of $|FIM|_{\mathcal{D}}$ in region $\mathcal{D}$; (b) $|FIM|_{\mathcal{D}}$; (c) CRB trace in $\mathcal{D}$.

to larger values of $|FIM|$. Part (b) shows the $|FIM|$ in 3D. Both figures show that $max|FIM|$ is attained when the target is placed at $q_x = q_y = 0\ m$, that is, directly under the geometric centre of the sensor network. The determinant of the FIM decreases as the hypothetical target moves away from $q_x = q_y = 0\ m, q_z = 100\ m$. Part (c) shows the evolution of the CRB trace. As expected, its minimum value is attained at the actual target position.

The plots in Fig. 4.8 are similar to those in Fig. 4.7 and correspond to a different optimal sensor placement problem solution that corresponds to rotating rigidly the pyramid (with apex at the target and a pentagonal base defined by the sensor positions in Fig. 4.7) about the $\{x_I\}$ axis of $\{I\}$ by an angle of $-20\ deg$. The figure illustrates the fact that the optimal value of $|FIM|$ is again obtained at $q_x = q_y = 0\ m, q_z = 100\ m$. However, the general evolution of $|FIM|_{\mathcal{D}}$ is substantially different from that in Fig. 4.7. This raises the interesting problem of robustness of the optimal solutions against uncertainty in the target position, a subject that will be dealt with later.

4.4.3.2 Underwater target positioning with known target depth

This section explores an interesting connection between target positioning in 2D and 3D. We start by observing that in the 3D solution studied so far, if the depth of the underwater target tends to 0, then an optimal sensor formation at the surface is such that the positions of all the sensors collapse on top of the target, that is, they tend to $[0,\ 0,\ 0]^T$. Clearly, this limit solution lacks realism and fails to degenerate into the solution that would be obtained had we assumed that the target and the sensors were exactly in the same horizontal plane. The reason for this discrepancy arises from the fact that in the pure 3D approach the depth of the target must be estimated explicitly. In many practical applications of interest, however, the target depth can be measured directly with small error, thus dispensing with the need to estimate it using acoustic range measurements. In this case, only the q_x and q_y target position coordinates should be determined, because q_z is known. This positioning

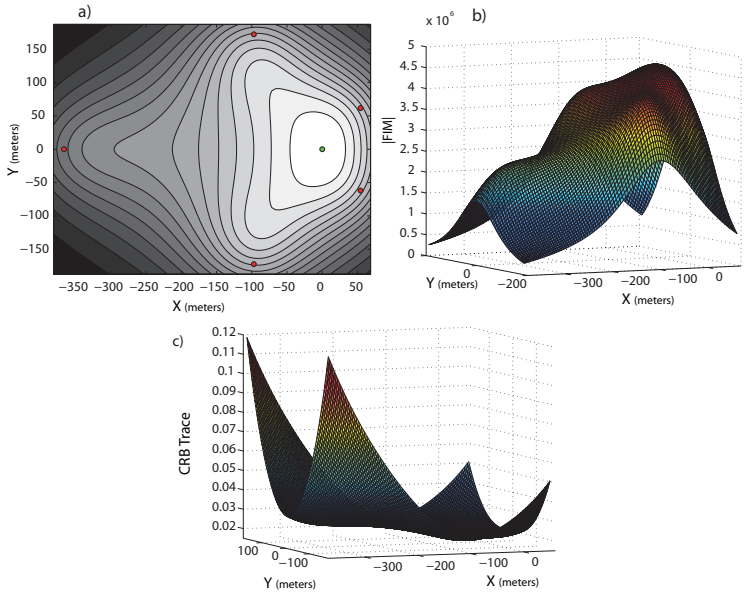

Figure 4.8: Optimal sensor formation for underwater target positioning in 3D with 5 sensors placed in a horizontal plane - an alternative solution obtained by rotation about one axis: (a) level curves of $|FIM|_{\mathcal{D}}$ in region $\mathcal{D}$; (b) $|FIM|_{\mathcal{D}}$; (c) CRB trace in $\mathcal{D}$.

problem is studied next.

We assume that all sensors lie on a horizontal plane. Following the procedure adopted to derive (4.10) yields the Fisher information matrix

$$FIM = \frac{1}{\sigma^2}\sum_{i=1}^{n}\begin{pmatrix} (u_{ix})^2 & (u_{iy})(u_{ix}) \\ (u_{ix})(u_{iy}) & (u_{iy})^2 \end{pmatrix} \tag{4.48}$$

where $u_i = \begin{bmatrix} \frac{\partial|q-p_i|}{\partial q_x}, & \frac{\partial|q-p_i|}{\partial q_y} \end{bmatrix}^T$, for $i \in \{1, ..., n\}$.

It is now necessary to find the sensor positions that maximize $|FIM|$. For the sake of conciseness and to avoid a tedious repetition of the arguments presented in the previous sections, the details of the computation are eschewed. For reasons that will become clear later, we restrict the maximum range of the target to the sensors to $r_{max} \geq 0\ m$. With this constraint, an optimal sensor geometry corresponds to placing all the sensors on a circumference centred on the projection of the target on the plane. The distribution of the sensors on the circumference exhibits the symmetry that is implied by conditions similar to those in (4.46). We assume, for clarity of exposition, that the reference frame adopted has its origin at the centre of the circumference. The resulting optimal FIM is

$$FIM_{opt} = \frac{1}{\sigma^2}\begin{pmatrix} \frac{n}{2}\left(1 - \frac{q_z^2}{r_{max}^2}\right) & 0 \\ 0 & \frac{n}{2}\left(1 - \frac{q_z^2}{r_{max}^2}\right) \end{pmatrix} \tag{4.49}$$

We now examine the relationship between the above 3D target positioning problem and the

purely 2D one. The latter, commonly studied in land robotics, corresponds to the case where the target and the sensor network lie in the same plane. From the analysis presented, it follows from (4.49) that when the target depth equals 0 then $|FIM| = n^2/(\sigma^4 \cdot 2^2)\ m^{-4}$. This is equal to the maximum possible FIM determinant in 2D, as explained in [11] and [55]. Furthermore, for any r_{max} the corresponding regular sensor formation satisfies the conditions obtained in [55] for the pure 2D case. Thus, if the target depth is known, then a 2D solution is easily obtained from the 3D one by simply letting the target depth equal 0.

It is interesting to notice that if the sensors and the target are not placed in the same plane, the optimal formation is the one in which the ranges (between the target and the sensors) are as large as possible. In fact, the larger the term r_{max} in (4.49), the closer the eigenvalues of the optimal FIM are to the optimal ones in 2D scenarios, that is, $n/2$. Finally, it is important to comment on and compare the best estimation accuracy that can be obtained in the purely 3D positioning case and in the case where the target depth is known. Notice that in the case studied the determinant of (4.31), computed as $n^3/(\sigma^6 \cdot 3^3)\ m^{-6}$, is larger than the determinant of (4.49), which at most is $n^2/(\sigma^4 \cdot 2^2)\ m^{-4}$. This may be misinterpreted as implying that the pure 3D solution yields better estimation accuracy, a conclusion that would be counter-intuitive.To clarify this issue, it is convenient to examine for both cases the inequality in (4.4) that sets a lower bound on the mean-square error of any unbiased estimator. The lower bound is $(9 \cdot \sigma^2)/n\ m^2$ for the purely 3D positioning case and has the minimum value of $(4 \cdot \sigma^2)/n\ m^2$ for the case where the depth is known. Thus, for sufficiently large r_{max} or, equivalently, for a sufficiently large radius of the circumference on which the sensors are placed, the solution that relies on knowledge about the target depth yields better estimation accuracy.

4.5 Gaussian error with distance-dependent covariance

It is important to remark that is crucial the imposition or existence of constraints in the design of an optimal sensor network when a variable error covariance is considered. It can be seen that the determinant of (4.10) is inversely proportional to the measurement error, so it depends explicitly on the distance between sensors and target. Thus, if sensors can be placed freely in the 3D space they will tend to concentrate over the target position to reduce as much as possible the distance-dependent added error. Therefore, different optimal formations may be defined depending on the constraints imposed by the environment, by the task, or by the sensor network itself. To make the problem tractable, it is therefore important to impose configuration constraints rooted in operational considerations. In what follows, the methodology adopted is illustrated with two representative design examples: i) first, by considering that the sensors are restricted to lie at the same distance from the target, that is, $r_i = r$ for all $i = 1, \cdots, n$, and ii) second, by considering that the sensors are restricted to lie in a horizontal plane, i. e., $q_z - p_{iz} = z_q$ is the target depth where $q_z = 0$ and $p_{iz} = -z_q$. The latter example captures the very important situation where the sensors are placed at the sea surface. The procedure adopted can of course be used to deal with other types of constraints on sensor placement.

4.5.1 Sensors placed on a sphere around the target

This section shows how the incorporation of physical or mission-related constraints on the positions of the sensors leads to a methodology to determine a solution to the optimal sensor placement problem that eschews tedious computations and lends itself to a simple geometric interpretation. To this effect, we consider the situation where all the sensors are placed on a sphere centred at the target position, that is, the distances from the sensors to the target are equal. With this assumption,

$r_i = r; i = 1, \cdots, n$, where r is the radius of the sphere. In this situation the distance does not condition the solution and the angles that the range vectors form with the axis of the inertial frame characterize the solution. The solution of this scenario is equivalent to find all the possible solutions for constant covariance measurement error because Γ_i is constant for all sensors and the FIM (4.10) can be rewritten as,

$$FIM = \frac{\Gamma_0^2}{\sigma^2} \sum_{i=1}^{n} \begin{pmatrix} \frac{p_{ix}^2}{r_i^2} & \frac{p_{ix}p_{iy}}{r_i^2} & \frac{p_{ix}p_{iz}}{r_i^2} \\ \frac{p_{ix}p_{iy}}{r_i^2} & \frac{p_{iy}^2}{r_i^2} & \frac{p_{iy}p_{iz}}{r_i^2} \\ \frac{p_{ix}p_{iz}}{r_i^2} & \frac{p_{iy}p_{iz}}{r_i^2} & \frac{p_{iz}^2}{r_i^2} \end{pmatrix} \tag{4.50}$$

where $\Gamma_i = \Gamma_0 = 1/(1 + \eta r^\gamma)$, and $r = r_i$, for all $i = 1, \cdots, n$. Thus the FIM (4.50) is the same matrix defined by (4.23) for the constant covariance error case but whose elements are scaled with a factor given by Γ_0.

In this case, the simplified optimal Fisher Information Matrix (4.21) can be written as

$$FIM = \frac{\Gamma_0^2}{\sigma^2} \cdot \delta\left(\begin{bmatrix} A; & B; & C \end{bmatrix}\right) \tag{4.51}$$

with $A = \sum_{i=1}^{n} \frac{p_{ix}^2}{r^2}$, $B = \sum_{i=1}^{n} \frac{p_{iy}^2}{r^2}$, and $C = \sum_{i=1}^{n} \frac{p_{iz}^2}{r^2}$. The above equations show clearly that all optimal sensor configurations are characterized in terms of the angles that the range vectors form with the unit axis of the inertial frame (division of each sensor coordinate by the range distance). Therefore, there is no explicit dependence on the ranges themselves. This is because in the formulation adopted it was tacitly assumed that the covariance of the range measurements is distance-invariant.

Following the same analytical procedure to that explained in Section 4.4.1 and that after simple computations, the relationship between A, B, and C yields

$$A = B = C = \frac{n}{3} \tag{4.52}$$

Therefore, the optimal Fisher Information Matrix is

$$FIM_{opt} = \frac{\Gamma_0^2}{\sigma^2} \begin{pmatrix} \frac{n}{3} & 0 & 0 \\ 0 & \frac{n}{3} & 0 \\ 0 & 0 & \frac{n}{3} \end{pmatrix} \tag{4.53}$$

Comparing the optimal FIM in (4.53) with the generic one in (4.50) gives an implicit characterization of the conditions that must be satisfied by the sensor network in order for it to be optimal:

$$\sum_{i=1}^{n} \frac{p_{ix}^2}{r^2} = \sum_{i=1}^{n} \frac{p_{iy}^2}{r^2} = \sum_{i=1}^{n} \frac{p_{iz}^2}{r^2} = \frac{n}{3} \tag{4.54}$$

$$\sum_{i=1}^{n} \frac{p_{ix}p_{iy}}{r^2} = \sum_{i=1}^{n} \frac{p_{ix}p_{iz}}{r^2} = \sum_{i=1}^{n} \frac{p_{iz}p_{iy}}{r^2} = 0 \tag{4.55}$$

Let now σ_{ix}, σ_{iy}, and σ_{iz} be the direction angles that the *i-th* range vector forms with the vectors $\{x_I\}, \{y_I\}$, and $\{z_I\}$ of $\{I\}$ and let $\cos(\sigma_{ix}) = p_{ix}/r_i$, $\cos(\sigma_{iy}) = p_{iy}/r_i$, and $\cos(\sigma_{iz}) = p_{iz}/r_i$ be the corresponding direction cosines. Clearly, (4.54) and (4.55) can be written in terms of the direction

cosines as

$$\sum_{i=1}^{n} \cos^2(\sigma_{ix}) = \sum_{i=1}^{n} \cos^2(\sigma_{iy}) = \sum_{i=1}^{n} \cos^2(\sigma_{iz}) = \frac{n}{3} \tag{4.56}$$

$$\sum_{i=1}^{n} \cos(\sigma_{ix})\cos(\sigma_{iy}) = \sum_{i=1}^{n} \cos(\sigma_{ix})\cos(\sigma_{iz}) = \sum_{i=1}^{n} \cos(\sigma_{iz})\cos(\sigma_{iy}) = 0 \tag{4.57}$$

The above equations show clearly that all optimal sensor configurations of this particular case are characterized in terms of the angles that the range vectors form with the unit axis of the inertial frame. Moreover, the optimal configurations of this particular case imply the same optimality conditions derived in Section 4.4.1 for constant covariance. It is because for the problem at hand, as commented above, it has been asummed a constant covariance error due to the sensors are all placed at the same distance from the target. Therefore, the same analysis made in Section 4.4.2 holds for this particular scenario, and once an optimal solution on the unit sphere is found in terms of the direction cosines referred to above, an infinite number of optimal solutions can be generated by: i) multiplying the range of each sensor to the target by an arbitrary positive number that will depend on the practical constraints imposed by physical considerations, and ii) rotating the sensor formation rigidly in terms of an arbitrary axis.

4.5.1.1 Example of optimal sensor configuration design

This example addresses the problem of optimal sensor placement for target positioning in 3D, subject to the condition that the sensors lie on the intersection of a sphere and a plane, i.e., the sensors are placed at a fixed distance from the target and in the same plane (the target cannot belong to that plane). Thus, the sensor configuration has to achieve two different constraints. The importance of this example resides in that this problem is equivalent to the case where the error covariance is constant and the sensors are placed in the same plane (the surface plane), as it will be seen next. The added interest lies in the comparison of the solution of this particular example with the solution obtained when the sensors are restricted to lie in a plane. Thus we can state their main differences, and the importance of the constraints imposed to the sensor formation and the noise model considered.

A solution to this problem can be obtained using the results derived previously and casting it in the following equivalent form: given a target at the origin of an inertial reference frame $\{I\}$, a unit sphere centred at the target, and a horizontal plane, compute the distance z_q from the plane to the target such that a solution to the unconstrained single target localization problem lies on the intersection between the unit sphere and that plane. Once a solution to the latter problem is found, it is scaled while preserving the direction cosines of the range vectors (between the target and the sensors). The scale factor is the radius of the sphere, r_s.

The same arguments commented in Section 4.4.3 holds for this case, and then the computation of a solution unfolds in two steps: the z_q coordinate of the plane is computed; the geometric formation of the sensors on the plane is then derived. The first step is straightforward: because $z_1 = z_2 = ... = z_n = z_q$, it follows from (4.56) that

$$p_{1z} = ... = p_{nz} = z_q = \pm 1/\sqrt{3} \tag{4.58}$$

Two horizontal planes that intersect the unit sphere along two circumferences of radii r' are defined from the above solutions. Because $r'^2 + z_q^2 = 1$, it follows that the optimal radii are equal

to $r' = \sqrt{1 - z_q^2} = \sqrt{\frac{2}{3}}$. An optimal solution to the problem of sensor placement corresponds to distributing the sensors along a circumference of radius $r' = \sqrt{\frac{2}{3}} r_s$, where r_s is the radius of the sphere, or similarly, a circumference of radius $r' = \sqrt{2} d_t$, where d_t is the distance of the target to the horizontal plane.

It now remains to determine the geometric configuration of the sensors on the circumferences. A simple and elegant solution is again obtained by noticing the orthogonality relations for sines and cosines from Fourier analysis [37]. It follows that optimal solutions are obtained by distributing the n sensors uniformly along the circumferences, the vectors from the sensors to the centre of the circumferences making angles $2\pi i/n; i = 0, 1, ..., n-1$ with the $\{x_I\}$ axis. Obviously, an infinite number of solutions are obtained by rotating the sensors rigidly along the circumferences, that is, by allowing the above angles to become $2\pi i/n + \alpha_s; i = 0, 1, ..., n-1$, where α_s is a fixed but arbitrary angle in $[0, 2\pi]$.

It is important to notice how the solution defined satisfies the optimality conditions of the simplified FIM (4.21), in particular (4.54) corresponds to the maximization of the norms of the vectors X, ϒ, and Z, i.e., it maximizes (4.19), and (4.55) makes the off-diagonal elements of the FIM equal to 0, i.e, it satisfies (4.20). Thus the solutions defined implies a global maximum on the FIM determinant for the case of study. The similarity with the constant covariance case is evident.

4.5.2 Underwater target positioning: sensors lying on a plane

This problem is of the utmost importance for underwater target positioning applications where the acoustic ranging devices are either located at the sea surface or on the seabed. The previous analysis is not valid for this scenario in which the sensors are constrained to lie on the sea surface and the covariance error is distance-dependent, i.e. for the problem at hand Γ_i, $i = 1, \cdots, n$ are not constant in the solution space, their values depend explicitly on the sensor positions, and thus the range distances are now a key element to define the optimal sensor formation.

The problem at hand will show the importance of considering a more complex error model to determine the optimal sensor configuration. The sensors are placed in the plane $z = z_q$, thus $p_{iz} = z_q$, and the target is at the origin of the inertial coordinate frame, $q = [0, 0, 0]^T$. The Fisher Information Matrix is the one defined in (4.10), and following the process explained in Section 4.3 we can define the simplified optimal FIM given by (4.21).

For the sake of simplicity the notation is changed to cylindric coordinates where α_i is the angle that the projection of the $i-th$ range vector in the surface plane forms with the $\{x_I\}$ axis; and β_i is the angle that the $i-th$ range vector forms with the surface plane $\{x_I y_I\}$. It must be noticed that $\beta_i \in [0, \pi/2]$ because the sensors are placed on the surface plane, above the target position. With this notation $p_{ix} = r_i \cos(\beta_i) \cos(\alpha_i)$, $p_{iy} = r_i \cos(\beta_i) \sin(\alpha_i)$, and $p_{iz} = z_q$, with $r_i = z_q / \sin(\beta_i)$, and (4.51) becomes,

$$FIM = \frac{1}{\sigma^2} \begin{pmatrix} A & 0 & 0 \\ 0 & B & 0 \\ 0 & 0 & C \end{pmatrix} \tag{4.59}$$

where

$$A = \sum_{i=1}^{n} \cos^2(\beta_i)\cos^2(\alpha_i)\Gamma_i^2$$

$$B = \sum_{i=1}^{n} \cos^2(\beta_i)\sin^2(\alpha_i)\Gamma_i^2$$

$$C = \sum_{i=1}^{n} \sin^2(\beta_i)\Gamma_i^2$$

with

$$\Gamma_i = \frac{1}{1 + \eta(z_q/\sin(\beta_i))^{\gamma}}$$

Then the determinant of (4.59) yields,

$$|FIM| = \frac{1}{\sigma^6} A \cdot B \cdot C \tag{4.60}$$

In this case A, B and C, depend on Γ_i and then, on the distance between target and sensors. Hence, we cannot proceed as in Section 4.4 and we cannot compute the derivatives of (4.60) with respect to A, B, and C explicitly. Therefore, we must compute the derivatives of (4.60) with respect to α_i and β_i. It is straightforward to compute the derivative of (4.60) with respect to α_i,

$$\frac{\partial |FIM|}{\partial \alpha_i} = 2\cos^2(\beta_i)\cos(\alpha_i)\sin(\alpha_i)\Gamma_i^2 C\,(A - B) = 0 \tag{4.61}$$

and the derivative of (4.60) with respect to β_i yields,

$$\begin{aligned}\frac{\partial |FIM|}{\partial \beta_i} =& \left(-2\cos(\beta_i)\sin(\beta_i)\cos^2(\alpha_i)\,\Gamma_i^2 + \cos^2(\beta_i)\cos^2(\alpha_i)\,\frac{\partial \Gamma_i^2}{\partial \beta_i}\right) BC \\ &+ \left(-2\cos(\beta_i)\sin(\beta_i)\sin^2(\alpha_i)\,\Gamma_i^2 + \cos^2(\beta_i)\sin^2(\alpha_i)\,\frac{\partial \Gamma_i^2}{\partial \beta_i}\right) AC \\ &+ \left(2\cos(\beta_i)\sin(\beta_i)\,\Gamma_i^2 + \sin^2(\beta_i)\,\frac{\partial \Gamma_i^2}{\partial \beta_i}\right) AB = 0\end{aligned} \tag{4.62}$$

with

$$\frac{\partial \Gamma_i^2}{\partial \beta_i} = \frac{2\gamma\eta(z_q/\sin(\beta_i))^{\gamma}\frac{\cos(\beta_i)}{\sin(\beta_i)}}{\left(1 + \eta(z_q/\sin(\beta_i))^{\gamma}\right)^3}$$

Clearly, (4.61) is satisfied if at least one of the following conditions holds: i) $\cos(\alpha_i) = 0$; ii) $\sin(\alpha_i) = 0$; iii) $A = B$. If $\cos(\alpha_i) = 0$ for each sensor in the formation then this means that all sensors are placed in the same vertical plane, $\{y_I z_I\}$, target and sensors are in the same plane and $|FIM| = 0$, therefore the solution is not optimal and it is discarded. The same occurs if $\sin(\alpha_i) = 0$ for each sensor in the formation but in this case the sensors are placed in the plane $\{x_I z_I\}$, $|FIM| = 0$ again and this solution is discarded too. If $\cos(\alpha_i) = 0$ or $\sin(\alpha_i) = 0$ for each sensor in the formation, (4.62) implies that the only feasible solution is that $A = B$. Therefore, $A = B$ is one of

the conditions that an optimal surface sensor network must satisfy. In what follows E can be A or B without any loss of generality due to $A = B$. Analysing the derivative (4.62) with $A = B = E$ yields,

$$\frac{\partial |FIM|}{\partial \beta_i} = E \cdot \frac{2\cos(\beta_i)}{\sin(\beta_i)} \Gamma_i^3 \cdot \left[-C \left(\sin^2(\beta_i) + \eta \left(\frac{z_q}{\sin(\beta_i)} \right)^{\gamma} (\sin^2(\beta_i) - \gamma \cos^2(\beta_i)) \right) + \right. \\ \left. + E \cdot \left(\sin^2(\beta_i) + \eta \left(\frac{z_q}{\sin(\beta_i)} \right)^{\gamma} \sin^2(\beta_i)(1+\gamma) \right) \right] = 0 \tag{4.63}$$

Straightforward computations give,

$$C = E \cdot \frac{\sin^2(\beta_i) + \eta \left(\frac{z_q}{\sin(\beta_i)} \right)^{\gamma} \sin^2(\beta_i)(1+\gamma)}{\sin^2(\beta_i) + \eta \left(\frac{z_q}{\sin(\beta_i)} \right)^{\gamma} (\sin^2(\beta_i) - \gamma \cos^2(\beta_i))} \tag{4.64}$$

Equation (4.64) must be satisfied for all the derivatives of (4.60) with respect to each β_i with $i = 1, \cdots, n$. Moreover, A, B, and C are constant for a given optimal configuration so it must be studied if (4.64) is hold for more than one value of β_i, i.e., if the sensors can have different angles β_i or all of them must be equal, it is $\beta_i = \beta$ for all i. Equation (4.64), after some computations, may be rewritten as,

$$C = E \cdot \frac{1}{1 - \Omega} \tag{4.65}$$

where

$$\Omega = \frac{\eta z_q^{\gamma} \gamma}{\sin^{\gamma+2}(\beta_i) + \eta z_q{}^{\gamma} \sin^2(\beta_i)(1+\gamma)} \tag{4.66}$$

with $\beta_i \in [0, \pi/2]$. The function Ω is strictly decreasing in the above domain of β_i, and we must focus on the positive values of $f(\beta_i) = 1/(1-\Omega)$, i.e, when $1 > \Omega$, since A, B, and C are always positive. Therefore the analysis of the possible solutions must take into account the variation of Ω from $\Omega = 1$ to Ω when $\beta_i = \pi/2$. In this domain Ω is always positive and smaller than 1, moreover, the function $f(\beta_i) = 1/(1-\Omega)$ is strictly decreasing. Thus (4.65) only holds for one value of β_i for a given optimal sensor configuration since (4.65) is strictly decreasing in the considered domain, and A, B, and C are constant for a given optimal formation. Therefore $\beta_i = \beta$ and $r_i = r$ for $i = 1, \cdots, n$.

From the previous analysis all the sensors must be placed over a circumference centred on the target projection on the surface plane and $A = \cos^2(\beta)\Gamma_0^2 \sum_{i=1}^{n} \cos^2(\alpha_i)$, $B = \cos^2(\beta)\Gamma_0^2 \sum_{i=1}^{n} \sin^2(\alpha_i)$, and $C = n \sin^2(\beta)\Gamma_0^2$, with $\Gamma_i = \Gamma_0$ for all $i = 1, \cdots, n$, because all sensors are at the same distance from the target.

To define β regardless of the sensor distribution over the resulting circumferences, we proceed by adding (4.64) with $E = A$ to (4.64) with $E = B$, it is $2C = (A+B)/(1-\Omega)$. When doing so, all the terms in α_i are cancelled and one obtains

$$2\left(\sin^{\gamma+2}(\beta) + \eta z_q^{\gamma} \sin^2(\beta)(1+\gamma) - \eta z_q^{\gamma} \gamma\right) = \cos^2(\beta)\left(\sin^{\gamma}(\beta) + \eta z_q^{\gamma}(1+\gamma)\right) \tag{4.67}$$

This expression can be rewritten to avoid the use of angles and to determine the range distance r of the optimal formation explicitly. It is clear that $\sin(\beta) = z_q/r$ and $\cos(\beta) = \sqrt{r^2 - z_q^2}/r$, so (4.67) yields,

$$3z_q^2 + 3(1+\gamma)\eta z_q^2 r^{\gamma} - 3\eta\gamma r^{\gamma+2} - r^2 - \eta r^{\gamma+2} = 0 \tag{4.68}$$

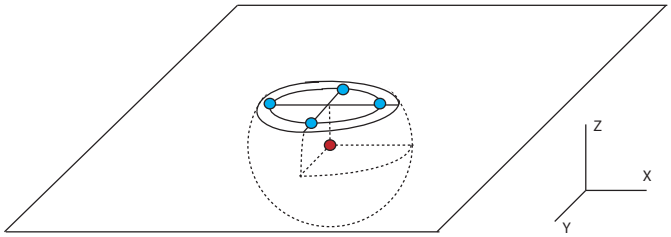

Figure 4.9: Optimal formation size for a 4 sensor network on a plane with distance dependent covariance. The intersection sphere-plane defines the optimal formation for constant covariance

The solution of (4.68) defines the optimal formation size, that depends on the error model and on the target depth. It is interesting to notice that if the covariance error is distance independent, i.e., $\eta = 0$, then (4.68) implies that $3z_q^2 - r^2 = 0$, that is the solution obtained in Section 4.5.1 when the sensors are restricted to lie on a horizontal plane and on a sphere, and also equivalent to the surface sensor placement problem with constant covariance.

It now remains to determine the geometric configuration of the sensors on the circumferences. Comparing the optimal FIM (4.59) with the generic one in (4.10) gives an implicit characterization of the conditions that must be satisfied by the sensor network in order for it to be optimal. From the condition $A = B$ and that all sensors have the same elevation angle, $\beta_i = \beta$, it is straightforward to obtain that the optimal formation must hold

$$\sum_{i=1}^{n} \left(\cos^2(\alpha_i) - \sin^2(\alpha_i)\right) = 0 \tag{4.69}$$

with $\sum_{i=1}^{n} \cos^2(\alpha_i)$ and $\sum_{i=1}^{n} \sin^2(\alpha_i)$ as large as possible. From the off diagonal elements we find that the optimal configuration must hold too

$$\begin{aligned}
&\sum_{i=1}^{n} \frac{p_{ix}p_{iy}}{r^2}\Gamma_0^2 = 0 \Longrightarrow \sum_{i=1}^{n} \cos(\alpha_i)\sin(\alpha_i) = 0 \\
&\sum_{i=1}^{n} \frac{p_{ix}z_q}{r^2}\Gamma_0^2 = 0 \Longrightarrow \sum_{i=1}^{n} \cos(\alpha_i) = 0 \\
&\sum_{i=1}^{n} \frac{p_{iy}z_q}{r^2}\Gamma_0^2 = 0 \Longrightarrow \sum_{i=1}^{n} \sin(\alpha_i) = 0
\end{aligned} \tag{4.70}$$

Thus the sensor formation must be first and second moment balanced, and a solution can be obtained by noticing the orthogonality relations for sines and cosines from Fourier analysis [37]. Therefore we can define an optimal sensor formation by distributing uniformly the sensors around the circumference where the sensors must stay. It can be noticed how the solution defined satisfies the optimality conditions of the simplified FIM (4.21); (4.68) and (4.69) correspond to the maximization of the product $A \cdot B \cdot C$ and thus to the maximization of (4.19), and (4.70) makes the off-diagonal elements of the FIM equal to 0, i.e, it satisfies (4.20). Thus, this solution implies a global maximum of the FIM determinant for the considered constraints.

In Figure 4.9 an optimal configuration for 4 sensors is shown. It can be seen how the ideal

formation considering a Gaussian noise with distance-dependent covariance has a smaller size than the optimal formation with constant covariance error. This smaller formation size searches to reduce the distance from sensors to target and therefore to minimize the distance-dependent measurement errors. Thus, a tradeoff solution may be defined analytically between the optimal angles and the optimal distances.

Notice the unrealistic assumption made until this point, also made in many of the publications available in this area, that the position of the target is known in advance. This is done to simplify the problem and to first fully understand its solution before the realistic scenario where the position of the target is known with error can be tackled. In this respect, see Section 4.6, which is largely inspired by the work in [39].

4.5.2.1 Underwater target positioning with known target depth

This section explores an interesting connection between target positioning in 2D and 3D similarly as it was done in Section 4.4.3.2. We start by observing that in the 3D solution studied so far, if the depth of the underwater target tends to 0, then an optimal sensor formation at the surface is such that the positions of all the sensors collapse on top of the target, that is, they tend to $[0,0,0]^T$. Moreover, the FIM determinant equals to 0 if the sensors and target are on the same plane, so an optimal solution cannot be derived. Clearly, this limit solution lacks realism and fails to degenerate into the solution and FIM determinant that would be obtained had we assumed that the target and the sensors were exactly in the same horizontal plane. This discrepancy arises from the fact that in the pure 3D approach the depth of the target must be estimated explicitly. Despite this, in many practical applications of interest, the target depth can be measured directly with small error, thus dispensing with the need to estimate it using acoustic range measurements. In this case, only the q_x and q_y target position coordinates should be determined, because q_z is known. This positioning problem is studied next.

We assume that all sensors lie on a horizontal plane. Following the procedure adopted in Section 4.2 to derive (4.10), it yields the Fisher Information Matrix

$$FIM = \frac{1}{\sigma^2}\sum_{i=1}^{n}\begin{pmatrix} \frac{p_{ix}^2}{r_i^2}\Gamma_i^2 & \frac{p_{ix}p_{iy}}{r_i^2}\Gamma_i^2 \\ \frac{p_{ix}p_{iy}}{r_i^2}\Gamma_i^2 & \frac{p_{iy}^2}{r_i^2}\Gamma_i^2 \end{pmatrix} \tag{4.71}$$

It is now necessary to find the sensor positions that maximize $|FIM|$. For the sake of conciseness and to avoid a tedious repetition of the arguments presented in the previous sections, the details of the computation are eschewed. Following the same procedure explained for (4.59), an optimal sensor geometry corresponds to placing all the sensors on a circumference centred on the projection of the target on the plane. The distribution of the sensors on the circumference exhibits the symmetry that is implied by conditions similar to those in (4.69) and (4.70). We assume, for clarity of exposition, that the reference frame adopted has its origin at the centre of the circumference. The resulting optimal FIM is

$$FIM_{opt} = \frac{1}{\sigma^2}\sum_{i=1}^{n}\begin{pmatrix} \left(1-\frac{z_q^2}{r_i^2}\right)\frac{\Gamma_i^2}{2} & 0 \\ 0 & \left(1-\frac{z_q^2}{r_i^2}\right)\frac{\Gamma_i^2}{2} \end{pmatrix} \tag{4.72}$$

We now examine the relationship between the above 3D target positioning problem and the purely 2D one. The latter, commonly studied in land robotics, corresponds to the case where the target and the sensor network lie in the same plane. From the analysis presented, it follows from

(4.72) that when the target depth is equal to 0 and we consider constant covariance ($\eta = 0$) then $|FIM| = n^2/\sigma^4 \cdot 2^2$. This makes the maximum FIM determinant possible in 2D, as explained in [11] and [55]. Furthermore, for any r the corresponding regular sensor formation satisfies the conditions obtained in [55] for the pure 2D case. Thus, if the target depth is known, then a 2D solution is easily obtained from the 3D one by simply letting the target depth equal 0.

If the covariance error is distance-dependent then it is possible to check, by an analysis similar to the previous one, that when the target depth becomes 0, the FIM is equivalent to the one of the pure 2D case and that we must impose constraints on the distance from sensors to target to avoid that the sensors collapse over the target position to reduce the distance-dependent covariance error as much as possible. It is interesting to notice that if the sensors and the target are not placed in the same plane, the optimal formation is placed on a circumference around the target projection on the horizontal plane and we can define again an optimal radius for the formation. The FIM computed this way yields

$$FIM = \frac{1}{\sigma^2}\delta\left(\left[\begin{array}{cc} \frac{n\cdot\Gamma_0^2\cdot\left(r^2-z_q^2\right)^2}{2\cdot r^2}; & \frac{n\cdot\Gamma_0^2\cdot\left(r^2-z_q^2\right)^2}{2\cdot r^2} \end{array}\right]\right) \tag{4.73}$$

Computing the determinant of (4.73) and its derivative with respect to r yields

$$r^2\left(1+\eta r^\gamma\right) - \left(r^2 - z_q^2\right)\left(1+\eta r^\gamma\left(1+\gamma\right)\right) = 0 \tag{4.74}$$

Thus solving (4.74) the optimal radius can be defined easily.

Finally, it is important to comment on and compare the best estimation accuracy that can be obtained in the purely 3D positioning case and in the case where the target depth is known. Notice that the determinant of (4.60) is larger than the determinant of (4.72). This may be misinterpreted as implying that the pure 3D solution yields better estimation accuracy, a conclusion that would be counter-intuitive. In fact, from the Cramer-Rao inequality the right comparison should be between the eigenvalues of the FIMs for the 2D and 3D cases, which are $n(1 - z_q^2/r^2)\Gamma_0/2$ and $n\Gamma_0/3$, respectively. Thus, for an adequate radius of the circumference on which the sensors are placed, the solution that relies on the knowledge about the target depth yields better estimation accuracy, as can be deduced from the larger eigenvalues of the FIM.

4.5.2.2 Examples of optimal sensor placement

Three examples of underwater target positioning with a network composed of 4 sensors are now studied to show the differences between optimal formations for both constant and distance-dependent covariance. The first example shows the optimal formation for $\sigma = 0.1$ and $\eta = 0$ (constant covariance); the second example studies the same problem but in this case with $\eta = 0.1$ and $\gamma = 1$ (distance-dependent covariance); both examples with the target at a depth of 50 meters. For the third example the same set-up of the latter scenario is studied but the target depth is known by additional sensors.

Clearly, in order for the information about the configuration to be useful in a practical situation, one must check if the determinant of the FIM meets desired specifications. To this effect, and for comparison purposes, the determinant of the FIM obtained for a number of hypothetical target points in $\mathcal{D}$ is again computed, $|FIM|_{\mathcal{D}}$. Similarly, the CRB trace will be computed for the same region $\mathcal{D}$ and named as $CRB_{\mathcal{D}}$.

Example 4.4: In Figure 4.10 we can see the optimal formation when the covariance is constant, $\eta = 0$. We can notice in Figure 4.10 (a) how the radius of the formation is the one defined in Section 4.4.3 and Section 4.5.1, $r' = \sqrt{2} \cdot z_q = 70.71\ m$, where $r^2 = r'^2 + z_q^2$. In Figure 4.10 (b) we can observe how this configuration implies the theoretical maximum determinant over the target position, $|FIM| = n^3/(\sigma^6 \cdot 3^3) = 2.3704 \cdot 10^6\ m^{-6}$. In Figure 4.10 (c) and (d) the CRB trace is shown, we can notice how the minimum value is also over the target position. ■

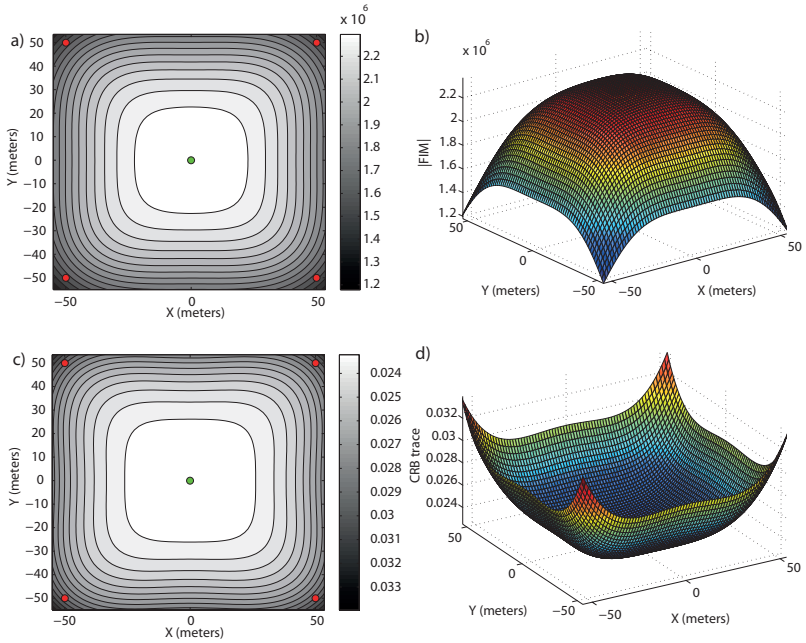

Figure 4.10: Constant covariance error. $|FIM|_{\mathcal{D}}$ around the target position (a). Value of the FIM determinant around the target position (b). $CRB_{\mathcal{D}}$ trace around the target position (c). Value of the CRB around around the target position (d)

Example 4.5: In the distance-dependent covariance case with unknown target depth, we can determine the optimal radius by means of (4.68) that, with $\gamma = 1$, becomes:

$$-4\eta r^3 - r^2 + 6\eta r z_q^2 + 3z_q^2 = 0 \tag{4.75}$$

Equation (4.75) provides the optimal radius for the formation depending on the target depth and on the noise parameter η. This equation can be rewritten as

$$1 + z_q^2 \frac{3 + 6\eta r}{-4\eta r^3 - r^2} = 0 \tag{4.76}$$

Notice that (4.76) has the form of a closed loop characteristic equation with the square of the depth as a gain; thus, the evolution of the roots can be analyzed using the root locus tool. The root locus plot is shown in Fig. 4.11.

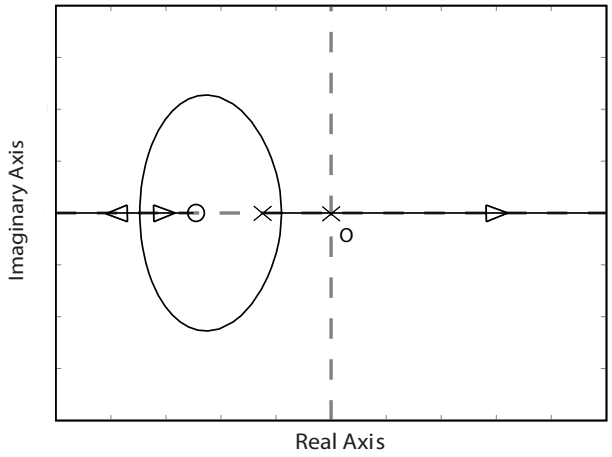

Figure 4.11: Graphical representation of the solutions of the third degree equation to determine the radius of the optimal surface sensor network with $\gamma = 1$ and $\eta \neq 0$.

Clearly, two roots have negative real part and can be discarded. The third root, however is positive and its magnitude increases with the gain. Hence, the plot shows clearly how the optimal radius varies with respect to the target depth; its value can be computed by solving (4.75). In Figure 4.12 (a) we can see the optimal formation and how its radius, $r' = 37.34$ *m*, becomes smaller (almost the half) than in the previous example to reduce as much as possible the added distance-dependent measurement error. In Figure 4.12 (b) the value of the determinant of the FIM is plotted around the target position. We can notice how the maximum value falls over the target position but how the accuracy is reduced dramatically due to the error model considered in this example. Similarly, in Figure 4.12 (c) and (d) the CRB trace is shown. It can be noticed how the CRB trace is larger than in the previous example due to the added measurement error, and how the minimum CRB trace is over the target position again. ■

Example 4.6: Finally if the target depth is known and $\gamma = 1$ we can determine the optimal radius from:

$$-\eta r^3 + 2\eta r q_z^2 + q_z^2 = 0 \tag{4.77}$$

Analyzing (4.77) the same way as (4.75) we find again that two solutions are always negative and the other one positive and depending on the square of the depth, so the optimal radius is again well defined and can be computed from (4.77). In Figure 4.13 (a) we can see the optimal formation and how its radius, $r' = 53.31$ *m*, becomes larger than in the previous example because the target depth is now known. In Figure 4.13 (b) the value of the determinant of the FIM is plotted around the target position. We can notice how the maximum value falls over the target position again. The value of the determinant is smaller than in the previous example because the FIM is now 2x2, however the value of the CRB trace is smaller, shown in Figure 4.13 (c) and (d), and therefore its covariance is smaller too providing a better estimation of the parameters of interest. ■

Therefore with this method and the adequate noise model we can design optimal sensor formations for underwater target positioning.

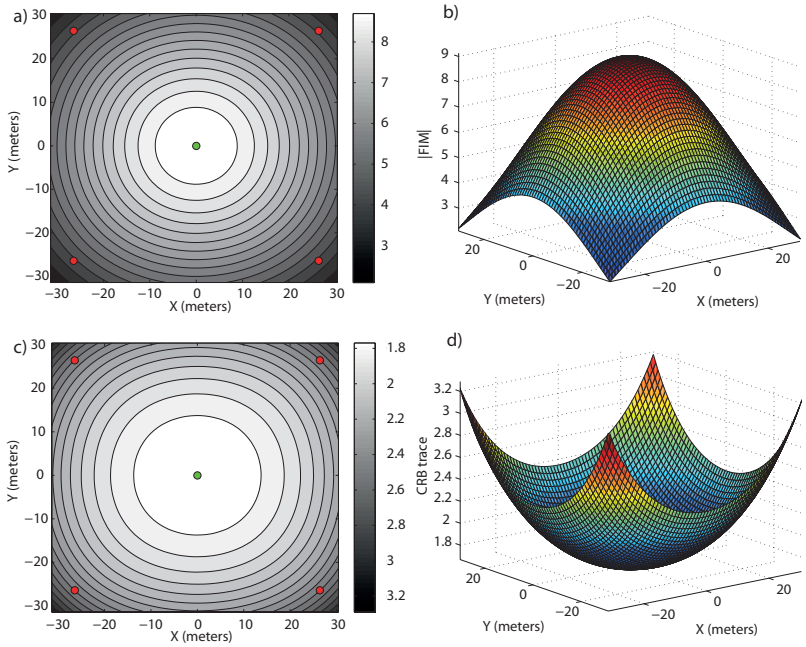

Figure 4.12: Distance-dependent covariance error. $|FIM|_{\mathcal{D}}$ around the target position (a). Value of the FIM determinant around the target position (b). $CRB_{\mathcal{D}}$ trace around the target position (c). Value of the CRB around around the target position (d)

4.6 Optimal sensor placement with uncertain target location

At this point, following what is commonly reported in the literature, we have started by addressing the problem of optimal sensor placement given an assumed position for the target. In a practical situation, the position of the target is only known with uncertainty and this problem must be tackled directly. However, in this case it is virtually impossible to make a general analytical characterization of the optimal solutions, and one must resort to numerical search methods. At this stage, an in-depth understanding of the types of solutions obtained for the ideal case is of the utmost importance to compute an initial guess for the optimal sensor placement algorithm adopted.

For the above reason, we now address the situation where the target to be positioned is known to lie in a well defined uncertainty region. The objective is to obtain an expedite numerical solution for the problem at hand. Inspired by the work in [39], we assume the uncertainty in the target position is described by a given probability distribution function and we seek to maximize, by proper sensor placement, the average value of the determinant of the FIM for the target.

In what follows, $p_{i\xi}$; $i = 1, 2, ..., n$; $\xi = x, y, z$ denotes the $\xi - th$ coordinate of sensor i located at position p_i and $\overline{p} = [p_1^T, ..., p_n^T]^T$. We further denote by $\varphi(q)\,; q \in \Re^3$ a probability density function with support $D \in \Re^3$ that describes the uncertainty in the position of the target in region D. With this notation, the problem of optimal sensor placement can be cast in the form of finding a vector $\overline{p}^*$ such that

$$\overline{p}^* = arg \max_{\overline{p}} \int_D |FIM(\overline{p}, q)| \cdot \varphi(q)\, dq \tag{4.78}$$

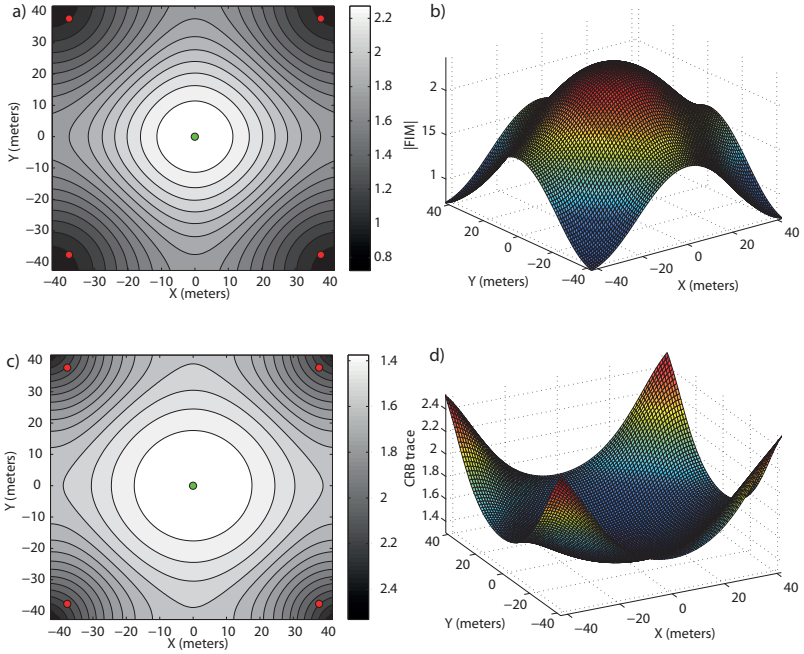

Figure 4.13: Distance-dependent covariance error with known target depth. $|FIM|_{\mathcal{D}}$ around the target position (a). Value of the FIM determinant around the target position (b). $CRB_{\mathcal{D}}$ trace around the target position (c). Value of the CRB around around the target position (d)

where we used the notation $|FIM(\bar{p}, q)|$ to clearly show the dependence of the FIM on the target and sensor locations. However, in the following $|FIM(\bar{p}, q)|$ will often be denoted simply as $|FIM|$. In a real situation, $\varphi(q)$ will depend on the type of mission carried out by the underwater target. If the target operates mostly in the centre of the working area, $\varphi(q)$ can for example assume the form of a truncated, radially-symmetric probabilistic Gaussian distribution centred at an appropriate point. On the other hand, if only the work area is known and the target can operate anywhere inside it, $\varphi(q)$ can be taken as the unity function inside that area.

To proceed, one must compute $|FIM(\bar{p}, q)|$ in the equation above. At this point it is important to remark that, given the complexity of the optimal sensor placement problem at hand, the only viable solution is a numerical one. For this reason, in contrast with the methodology adopted in the previous sections, the derivatives of the $|FIM|$ are computed explicitly with respect to the sensor position coordinates, i.e., $p_i = [p_{ix}, p_{iy}, p_{iz}]$. The computations are straightforward but lengthy, so details are omitted.

It now remains to solve the optimization problem defined above. As explained later, we opted to use a gradient-based method to do so. To this effect, it is important to compute the derivatives of the integral in (4.78) with respect to the sensor coordinates, that is,

$$\frac{\partial}{\partial p_{i\xi}} \int_D |FIM(\bar{p}, q)| \varphi(q) dq \tag{4.79}$$

for $i = 1, 2, ..., n$ and $\xi = x, y, z$. To proceed with the computations, the integral and the derivative

operations are interchanged: the derivatives are determined explicitly first, see Appendix C, and the integration over region D is performed afterwards.

In what concerns the computation of the triple integral over the region D of interest, we opted to do it numerically using a Monte Carlo method. Finally, a solution of (4.78) can be obtained using a gradient optimization method with the Armijo rule. However, the details are omitted (see [12] and the references therein). To overcome the occurrence of local maxima or the divergence of the algorithm, the initial guess in the iterative algorithm must be chosen with care. In the examples that we studied we found it useful and expedite to adopt as an initial guess the solution for the single target positioning problem described in previous sections, with an hypothetical single target placed at the centre of the work area. It is important to stress that the solution to (4.78) depends strongly on the probability density function adopted for the target position q (e.g. a truncated, radially-symmetric probabilistic Gaussian distribution or a radially-symmetric step distribution, [39]).

4.6.1 Simulation examples with unknown source location

The methodology developed is now illustrated with the help of two examples that address the problem of optimal surface sensor placement for uncertain underwater target positioning. In the design of both examples, 4 sensors are placed in the same horizontal plane at the sea surface. The target is known to operate at a constant depth $q_z = 50\ m$, in an area delimited by a circumference of 50 m radius. Therefore, the probabilistic distribution of the target position is a step-like function, taking the value 1 inside and on the circumference and the value 0 outside. Through a gradient optimization method with the Armijo rule, the ideal formation is searched, using as an initial guess the ideal configuration when the target position is known, as explained previously. Because the sensors lie on the same plane, the algorithm must be modified slightly. The relevant difference is in the computation of the derivatives of (4.78), because for the problem at hand only the derivatives with respect to the p_{ix} and p_{iy} coordinates of each sensor i must be computed. The computation of these derivatives is straightforward and details about their computation are in Appendix C.

Example 4.7: This example corresponds to the case where the covariance error is constant, $\eta = 0$. The optimization process results in a regular formation (shown in Fig. 4.14) of radius $r' = 82.2\ m$ similar to the one that would be obtained for the case where the target position has no uncertainty. However, the optimal formation radius $r' = 82.2\ m$ of the first is larger than that of the latter, given by $r' = q_z \cdot \sqrt{2} = 70.71\ m$. This has the effect of increasing the average FIM determinant inside the work area. As a consequence, the shape of the plot $|FIM|_{\mathcal{D}}$ in Fig. 4.14 (b) is flatter over a larger area. The obvious interpretation is that in the presence of uncertainty the sensors are placed in such a way as to tradeoff optimal performance at a point against slightly reduced performance, albeit uniformly over a large area around that point. The maximum FIM determinant is $2.3230 \cdot 10^6\ m^{-6}$ that is very close to the optimal value $2.37 \cdot 10^6\ m^{-6}$. Thus in in Fig. 4.14 (a) $|FIM|_{\mathcal{D}}$, $\mathcal{D} \in R^2$ shows that the largest accuracy is obtained inside the working area. In Fig. 4.14 (b) we can observe the magnitude of the FIM determinant for each point in the plane where the target lies. The average determinant inside the working area maintains a large value near to the theoretical maximum. Fig. 4.14 (c) and Fig. 4.14 (d) show similar plots to Fig. 4.14 (a) and Fig. 4.14 (b), respectively, but considering the CRB trace. We can notice how the CRB trace maintain a small value inside the working area and therefore a minimum global variance for the target positioning is obtained in the area of interest. ■

Example 4.8: In this second example the covariance error is distance-dependent, with $\eta = 0.1$

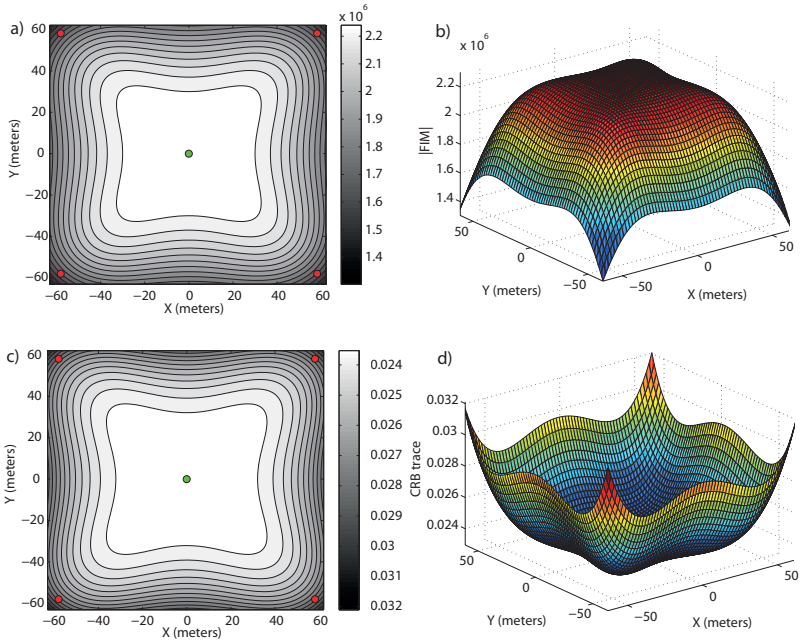

Figure 4.14: $|FIM|_{\mathcal{D}}$, $\mathcal{D} \in R^2$ (a), FIM determinant for each point in the plane where the target lies for the optimal sensor formation for an unknown source location (b). $CRB_{\mathcal{D}}$ trace around the target position (c). Value of the CRB around around the target position (d). ($\eta = 0$)

and $\gamma = 1$. The same optimization process as before results in a regular formation of radius $r' = 48.04\ m$. This formation shown in Fig. 4.15 is again larger than the optimal one that would be obtained when the target position has no uncertainty ($r' = 37.35\ m$). Fig. 4.15 (a) $|FIM|_{\mathcal{D}}$, $\mathcal{D} \in R^2$, shows how the largest accuracy is obtained inside the working area. In Fig. 4.15 (b) we can observe the magnitude of the FIM determinant for each point in the plane where the target lies. The average determinant inside the working area maintains a large value near to the maximum obtained when the target position has no uncertainty, but in this case the decrease of the determinant is faster due to the dependence on distance of the noise. In a similar way as in the previous example, Fig. 4.14 (c) and Fig. 4.14 (d) show equivalent plots to Fig. 4.14 (a) and Fig. 4.14 (b), respectively, but with the CRB trace. We can notice how the CRB trace maintains a small value inside the working area but larger than in the previous example due to the distance-dependent covariance error. Despite of this, the minimum global variance for the target positioning is obtained in the area of interest. ■

Similar results can also be obtained for other radially symmetric probability density functions. In fact, using the procedure proposed here, optimal sensor configurations can be obtained for arbitrary probability density functions. Depending on the knowledge about the target or the application, the optimal sensor configuration will change.

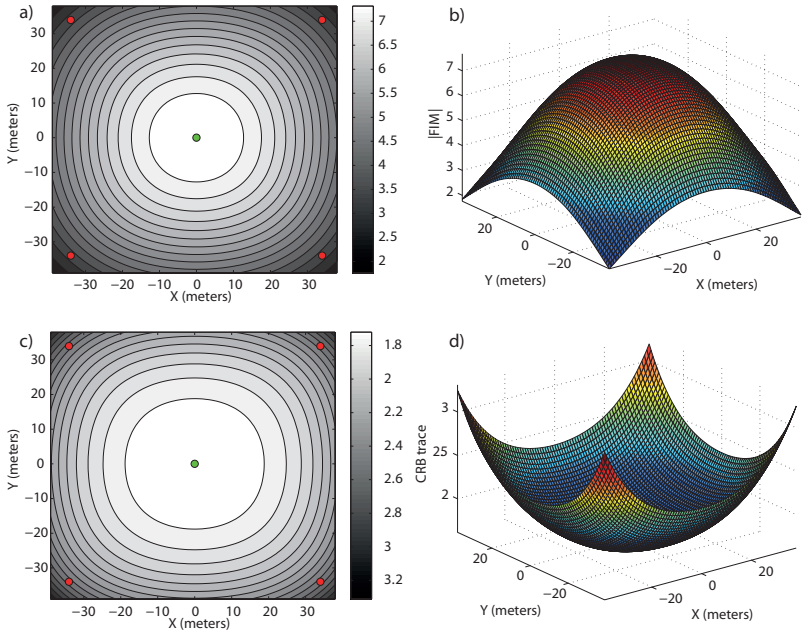

Figure 4.15: $|FIM|_{\mathcal{D}}$, $\mathcal{D} \in R^2$ (a), FIM determinant for each point in the plane where the target lies for the optimal sensor formation for an unknown source location (b). $CRB_{\mathcal{D}}$ trace around the target position (c). Value of the CRB around around the target position (d).($\eta = 0.1$)

4.6.2 Simulation examples when the sensors can be placed in two different planes

An interesting problem arises when the target is known to lie anywhere in a volume in the water column and one is free to distribute the sensors at the sea surface and on the sea-bottom. At this point, an interesting question arises: given the experimental conditions, should we place all the sensors in one plane (sea surface or sea-bottom), or distribute them between the two planes? In what follows we show, via a design example, how the circle of ideas exploited in the previous section can be used to solve this problem.

Suppose that the underwater target operates inside a rectangular parallelepiped with dimensions $60 \times 60 \times 40$ m^3 and geometrical centre at 50 m depth. The sea bottom is 100 m deep. We consider two possible arrangements for a 6 sensor network. In the first case, depicted in Figure 4.16 (a), all sensors are placed at the sea surface. In the second case, illustrated in Figure 4.16 (b), 3 of the sensors are placed at the surface, while the others are placed on the sea-bottom.

Example 4.9: Firstly we consider a constant covariance error, $\eta = 0$.

In the first scenario, Figure 4.16 (a), a solution was found whereby the sensors are distributed regularly on a circumference with radius $r' = 74.57$ m, centred at the projection of the parallelepiped's centroid on the sensor plane. The integral of the FIM determinant over the volume of interest was found to be $1.0483 \cdot 10^{12}$ m^{-6} and the maximum and minimum FIM determinants obtained inside this region were $8 \cdot 10^6$ m^{-6} and $5.5856 \cdot 10^6$ m^{-6} respectively. The maximum determinant is the theoretical maximum, $n^3/(\sigma^6 3^3)$ m^{-6}. Comparing the maximum and minimum

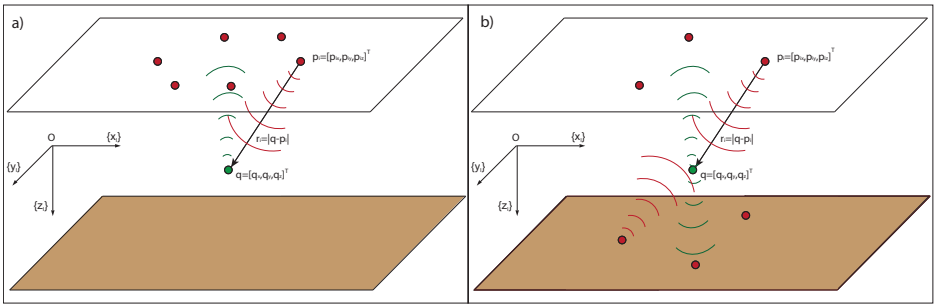

Figure 4.16: Maximization of the average FIM determinant inside a volume, with all the sensors placed in the same plane (a), or with the sensors distributed among two different parallel planes (b).

CRB trace, they were 0.0197 m^2 and 0.0150 m^2 respectively. Again, this last one is the theoretical minimum CRB trace.

In the second scenario, Figure 4.16 (b), 3 sensors were placed at the sea surface and the remaining ones on the sea-bottom. A solution was found in the form of two regular formations in circumferences with equal radii $r' = 71.62$ m, centred at the projection of the parallelepiped's centroid on the two sensor planes. The integral of $|FIM|$ is now $1.1379 \cdot 10^{12}$ m^{-6} and the maximum and minimum FIM determinants are $8 \cdot 10^6$ m^{-6} and $7.3103 \cdot 10^6$ m^{-6}, respectively. Notice how the integral is larger in the latter case. Furthermore, the minimum FIM determinant obtained inside the working area is larger, providing a more homogeneous estimation accuracy inside the volume of interest. In terms of the CRB trace, we found that the minimum and maximum values were 0.0150 m^2 and 0.0159 m^2, respectively. The minimum theoretical CRB trace is again achieved and the maximum CRB trace is lower than in the previous situation where the sensors are placed in only one plane. ■

Example 4.10: Secondly we consider a distance-dependent covariance error, $\eta = 0.1$ and $\gamma = 1$, and proceed as above.

In the first scenario, Figure 4.16 (a), the solution is again a regular formation around the origin but with radius $r' = 34.88$ m. The integral of the FIM determinant over the volume of interest is $5.7394 \cdot 10^6$ m^{-6} and the maximum and minimum FIM determinants are 228.7667 m^{-6} and 1.6311 m^{-6} respectively. These values are lower than in the previous case due to the effect of distance on the measurement noise.

In the second scenario, Figure 4.16 (b), 3 sensors were placed at the sea surface and the remaining ones on the sea-bottom. A solution was found in the form of two regular formations in circumferences with equal radii $r' = 32.08$ m, where the integral is now $4.5570 \cdot 10^6$ m^{-6}, and the maximum and minimum FIM determinants are 74.6648 m^{-6} and 16.6552 m^{-6}. We can notice how in the latter case the average FIM determinant is smaller and the maximum determinant is reduced too, so the largest accuracy in the volume is smaller. However the minimum FIM determinant is in this case larger providing a more homogeneous estimation accuracy. The adequate solution will be mission-dependent. ■

Therefore, for an unknown target location it is clear that the average accuracy inside the working area is improved if we can place the sensors in two different parallel planes.

4.7 Conclusions

This chapter offered a characterization of the solutions to the problem of optimal acoustic sensor placement for target positioning in 3D space, with special emphasis in the underwater target positioning by a surface sensor network. By assuming that the range measurements between the target and the acoustic sensors were corrupted by white Gaussian noise, the variance of which is distance-dependent, conditions were derived under which a sensor network maximizes the range-related information available for positioning. This was done by exploiting tools from estimation theory whereby the problem to be solved was converted into that of maximizing the determinant of a conveniently defined Fisher Information Matrix (FIM). The core result obtained was an analytic characterization of the conditions that must be met by a generic n sensor network in 3D in order for it to be optimal. This result was instrumental in deriving strategies to deal with practical situations where, depending on the mission at hand, the sensor network may be completely underwater or at the surface, or even configured such that a sub-group of sensors is at the surface and the remaining sub-group is close to the sea-bottom. The relationship between optimal solutions in 2D and 3D space was clarified. It was further shown that the optimal sensor configuration lends itself to an interesting geometrical interpretation and that the spreading of the sensor configuration depends explicitly on the intensity of the range measurement noise and on the probabilistic distribution that defines the prior uncertainty in the target position. Examples illustrated the application of the methodology in a number of applications-relevant scenarios.

Chapter 5

MULTIPLE TARGET POSITIONING IN 3D SCENARIOS WITH RANGE MEASUREMENTS

5.1 Introduction

It has been studied until this point that many AUV mission scenarios call for the availability of good underwater positioning systems to localize one or more vehicles simultaneously based on acoustic-related range information received on-board a support ship or an autonomous surface system (e.g. a number of autonomous surface vehicles equipped with acoustic receivers, moving in formation). The information obtained can be used to follow the state of progress of a particular mission or to relay it as a navigation aid to the navigation systems existent on-board the AUVs. Similar comments apply to a future envisioned generation of positioning systems to aid in the tracking of one or more human divers.

In this chapter, based on the results of the previous chapters, we address the problem of computing the optimal geometric configuration of a mobile sensor network that will maximize the range-related information available for *multiple target localization* in three-dimensional space. In contrast to what has so far been published in the literature, we address explicitly the localization problem in 3D using a sensor array located in a finite spatial region (3D). Furthermore, we incorporate directly into the problem formulation the fact that multiple targets must be localized simultaneously. The particular scenario in which the sensor array is located at the sea surface (2D) for multiple underwater target positioning (3D) will be studied in depth as an interesting application scenario, in a similar manner as in Chapter 4. We assume that the range measurements are again corrupted by white Gaussian noise, the variance of which is distance-dependent. The computation of the target positions may be done, as usual, by resorting to trilateration algorithms [3], [4], [7].

Clearly, there will be tradeoffs involved in the precision with which each of the targets can be localized; to study them, we resort to techniques that borrow from estimation theory and Pareto optimization. For the latter, the reader is referred to [45], [22], [90]. See also Appendix B for a

very short review of some key concepts and results. Stated briefly, we avail ourselves of concepts on Pareto-optimality and maximize convex combinations of the logarithms of the determinants of the FIMs for each of the targets in order to compute the Pareto-optimal surface that gives a clear image of the tradeoffs involved in the multiobjective optimization problem. We thus obtain a powerful tool to determine the sensor configuration that yields, if possible, a proper tradeoff for the accuracy with which the position of the different targets can be computed. In what follows, and with an obvious abuse of notation, we often refer to Pareto-optimal solutions simply as optimal.

It is important to remark that for the multiobjective optimization problem at hand, the logarithms of the determinants of the FIMs will be used instead of the determinants themselves. This makes the functions to be maximized jointly convex in the search parameter space, thus justifying the use of scalarization techniques in the computation of the Pareto-optimal surface, as described in Appendix B. For a discussion of the convexity of the functions adopted, see for example [12], Chapter 3 and the work in [85] on the D-optimality criterion.

For a multi-target localization problem, the optimal geometry of the sensor configuration depends strongly on the constraints imposed by the task itself (e.g. maximum number and type of sensors that can be used), the environment (e.g. ambient noise), the number of targets and their configuration, and the possibly different degrees of precision with which their positions should be estimated. An inadequate sensor configuration may yield large localization errors for some of the targets. It is interesting to remark that even though the problem of optimal sensor placement for range based localization is of great importance, not many results are available on this topic yet. Even more, the results are only for single target positioning. Exceptions include the works [63] and [74].

The key contributions of the present chapter are twofold: i) we fully exploit concepts and techniques from estimation theory and multiobjective optimization to obtain a numerical solution to the optimal sensor configuration problem for multiple targets in 3-dimensional space, and ii) in striking contrast to what is customary in the literature, where zero mean Gaussian processes with fixed variances are assumed for the range measurements, the variances are allowed to depend explicitly on the ranges themselves. This allows us to capture the fact that measurement noise increases in a non-linear manner with the distances measured.

The chapter is organized as follows. Section 5.2 summarizes the computation of the FIMs that are necessary to solve the optimal sensor placement problem under consideration. The demonstration of concavity of the logarithm of the FIM determinant for a global sensor placement in 3D with constant and distance-dependent covariance is shown in Section 5.3. The gradient optimization algorithm used to compute the optimal sensor configurations is summarized in Section 5.4; and the multiple localization problem for the case in which the targets have different importance weights during the mission, changing accordingly the sensor formation, is also studied. This same problem is studied in Section 5.5 for the application scenario of multiple underwater target positioning with surface sensor networks. Finally, in Section 5.6 the maximization of the average value of the logarithms of the FIM determinants is studied when a static fixed sensor network surveys a certain working area or when there is uncertainty in the *a priori* knowledge about the target positions. The conclusions are included in Section 5.7.

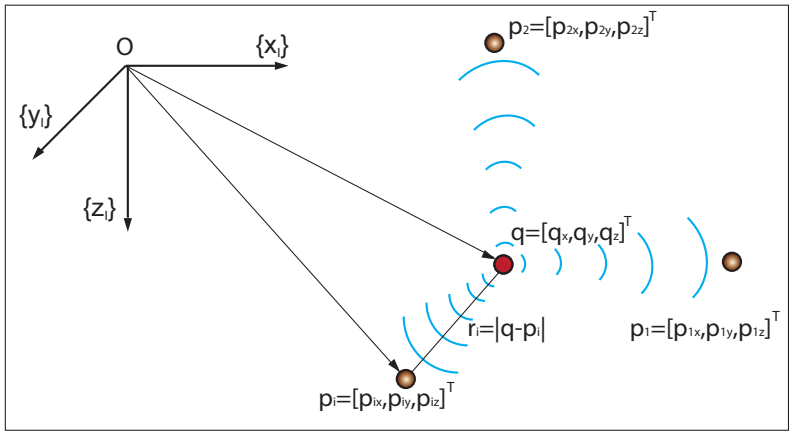

Figure 5.1: Target localization problem set-up.

5.2 Information Inequality with distance-dependent measurement noise

For the sake of completeness, we proceed to summarize the results obtained in Chapter 4 for the computation of the FIM for a 3-dimensional scenario. Let $\{I\}$ be an inertial reference frame with unit axis $\{x_I\}, \{y_I\}, \{z_I\}$ and let $q_k = [q_{kx}, q_{ky}, q_{kz}]^T$ be the position of the target k to be positioned in $\{I\}$, with $k = 1, \cdots, m$ where m is the number of targets. Further denote by $p_i = [p_{ix}, p_{iy}, p_{iz}]^T$; $i = 1, 2, .., n$, the position of the $i-th$ acoustic ranging sensor, also in $\{I\}$. Let $r_i(q_k) = |q_k - p_i|$ (abbv. r_{ki}) be the distance (range) between the target q_k and the $i-th$ sensor, where $|\cdot|$ denotes the Euclidean norm. The variables and the set-up that will be used are illustrated in Figure 5.1 for the case of one target and three sensors. We denote by z_{ki} the measurements of the actual range $r_i(q_k)$, corrupted by additive noise ω_{ki}. With the above notation, the measurement model adopted is given by

$$z_{ki} = |q_k - p_{ki}| + \omega_{ki} = r_i(q_k) + \omega_{ki} \tag{5.1}$$

We assume that the measurement noise ω_{ki} can be modelled by a zero-mean Gaussian process where the covariance depends on the distance between the two objects that exchange range data. Stated mathematically,

$$\omega_k = (I + \eta\delta(r(q_k)^\gamma)) \cdot \omega_0 \tag{5.2}$$

where $r(q_k)$ is the vector of actual ranges, η and γ are the modelling parameters for the distance-dependent noise component, and $\omega_k = [\omega_{k1} \cdots \omega_{kn}]^T$ is measurement noise assuming that all noise sources ω_{ki} are independent, and the vector ω_0 is a zero mean Gaussian process $N(0, \Sigma_0)$ with $\Sigma_0 = \sigma^2 \cdot I$, where I is the identity matrix. The measurement noise covariance matrix for target k is given by

$$\Sigma_k = \sigma^2 \left(I + \eta\delta(r(q_k)^\gamma)\right)^2 \tag{5.3}$$

Following standard procedures, the FIM corresponding to the problem of range-based single

target positioning can be computed from the likelihood function $p_q(z_k)$ given by

$$p_q(z_k) = \frac{1}{(2\pi)^{\frac{n}{2}}|\Sigma_k|^{\frac{1}{2}}} \exp\left\{-\frac{1}{2}\left(z_k - r(q_k)\right)^T \Sigma_k^{-1}\left(z_k - r(q_k)\right)\right\} \tag{5.4}$$

where n is the number of receivers, $z_k = [z_{k1}, z_{k2}, ..., z_{kn}]^T$ consists of n measured ranges for target k, and $r(q_k)$ are the actual ranges. Taking the logarithm of (5.4), computing its derivative with respect to q_k, and then its expected value, the FIM is defined as

$$FIM_k = C(\delta(r)\Sigma_k\delta(r))^{-1}C^T \tag{5.5}$$

where $C = (q_k 1_n^T - p) \in \Re^{3xn}$, $1_n \in \Re^{nx1}$ is a vector of 1s, and p is the vector of sensor positions, the latter being defined in $\Re^{3xn}$. This FIM was introduced in Chapter 4 for single target positioning in 3D scenarios, and for each of the targets its corresponding FIM will be computed to evaluate the accuracy with which the target is localized. Expanding (5.5) it is obtained:

$$FIM_k = \frac{1}{\sigma^2}\sum_{i=1}^{n}\begin{pmatrix} \frac{(q_{kx}-p_{ix})^2}{r_{ki}^2}\Gamma_{ki}^2 & \frac{(q_{kx}-p_{ix})(q_{ky}-p_{iy})}{r_{ki}^2}\Gamma_{ki}^2 & \frac{(q_{kx}-p_{ix})(q_{kz}-p_{iz})}{r_{ki}^2}\Gamma_{ki}^2 \\ \frac{(q_{kx}-p_{ix})(q_{ky}-p_{iy})}{r_{ki}^2}\Gamma_{ki}^2 & \frac{(q_{ky}-p_{iy})^2}{r_{ki}^2}\Gamma_{ki}^2 & \frac{(q_{ky}-p_{iy})(q_{kz}-p_{iz})}{r_{ki}^2}\Gamma_{ki}^2 \\ \frac{(q_{kx}-p_{ix})(q_{kz}-p_{iz})}{r_{ki}^2}\Gamma_{ki}^2 & \frac{(q_{ky}-p_{iy})(q_{kz}-p_{iz})}{r_{ki}^2}\Gamma_{ki}^2 & \frac{(q_{kz}-p_{iz})^2}{r_{ki}^2}\Gamma_{ki}^2 \end{pmatrix} \tag{5.6}$$

where $\Gamma_{ki} = 1/\left(1+\eta r_{ki}^{\gamma}\right)$ for $i \in \{1, ..., n\}$ and $k = 1, \cdots, m$. Clearly, the expression of the FIM considering a distance-dependence covariance error is well defined.

5.3 Convexity/concavity for a 3 sensor network

The optimal sensor configuration that maximizes the summation of the logarithms of the FIM determinants of the targets is searched from the Pareto-optimality conditions and convex optimization tools, so it is imperative to demonstrate the convexity, actually concavity as pointed out in Chapter 3, of the log determinant function. In this sense, the simplest problem of a 3 sensor network is studied because it is possible to analytically demonstrate the convexity (concavity) of the optimality criterion, and thus that a global unique solution may be obtained with numerical search methods. For this purpose the notation introduced in [6] for the FIM determinant is used, that for a distance-dependent covariance error becomes

$$|FIM| = \frac{1}{\sigma^6}\sum_{j\le k\le l}^{n}\frac{\left(\left(u_j \times u_k\right)\cdot u_l\right)^2}{\left(1+\eta r_j^{\gamma}\right)^2\left(1+\eta r_k^{\gamma}\right)^2\left(1+\eta r_l^{\gamma}\right)^2} = \frac{1}{\sigma^6}\sum_{j\le k\le l}^{n}\frac{\sin^2\left(\alpha_{jk}\right)\cos^2\left(\beta_{jk,l}\right)}{\left(1+\eta r_j^{\gamma}\right)^2\left(1+\eta r_k^{\gamma}\right)^2\left(1+\eta r_l^{\gamma}\right)^2} \tag{5.7}$$

where

$$u_j = [u_{jx}, u_{jy}, u_{jz}]^T = \left[\begin{array}{ccc} \frac{\partial|q-p_j|}{\partial q_x} & \frac{\partial|q-p_j|}{\partial q_y} & \frac{\partial|q-p_j|}{\partial q_z} \end{array}\right]^T; \tag{5.8}$$

$j \in \{1, ..., n\}$; identical definitions apply to the indices k, l; α_{jk} is the angle formed by the vectors u_j and u_k, and $\beta_{jk,l}$ is the angle that the vector u_k forms with the resultant vector of the cross product between u_j and u_k. The optimal sensor configuration is the one which maximizes the logarithm of

(5.7).

For the sake of simplicity and clarity in the exposition, both scenarios with constant covariance and distance-dependent covariance are studied separately. The main reason is because for constant covariance the demonstration of concavity is easy and straightforward. Moreover, it is possible to achieve an accuracy close to the optimal one that would be obtained for one single target working in isolation for each of the targets involved in the positioning task. Thus, this simpler problem is dealt with first.

5.3.1 Gaussian error with constant covariance

In this case, (5.7) becomes

$$|FIM| = \frac{1}{\sigma^6}\left((u_1 \times u_2)\cdot u_3\right)^2 = \frac{1}{\sigma^6}\sin^2(\alpha_{12})\cos^2(\beta_{12,3}) \tag{5.9}$$

It was demonstrated in Chapter 4 that, in 3D positioning problems with constant covariance error, the distance or orientation of the sensor network does not condition the optimal solution, only the angles that the range vectors form between them determine the optimal configuration. Therefore, without loss of generality, we can consider that vectors 1 and 2 are always in an arbitrary plane, so that angles α_{12} and $\beta_{12,3}$ are independent and we can compute their derivatives independently. This assumption is also valid for multiple targets.

We must compute the second derivatives of the logarithm of (5.9) with respect to angles α_{12} and $\beta_{12,3}$ to construct the Hessian matrix. It is important to remark that the concavity of the logarithm of the FIM determinant is restricted to positive definite matrices, therefore the domain of the logarithm of (5.9) cannot contain values of α_{12} and $\beta_{12,3}$ for which the determinant becomes equal to zero, it is, sensors and target cannot lie in the same plane. Therefore $\alpha_{12} \in]0,\pi[$ and $\beta_{12,3} \in]0,\pi[$. For the domains $\alpha_{12} \in]\pi,2\pi[$ and $\beta_{12,3} \in]\pi,2\pi[$, together or in combination with the domains commented above, the solutions are equivalent and define the same formations only by rotating them the adequate angle. We compute first the Jacobian of the logarithm of (5.9), that after some simplifications becomes:

$$\nabla \log|FIM| = \begin{bmatrix} \dfrac{\partial \log|FIM|}{\partial \alpha_{12}} \\ \dfrac{\partial \log|FIM|}{\partial \beta_{12,3}} \end{bmatrix} = \begin{bmatrix} \dfrac{2\cos(\alpha_{12})}{\sin(\alpha_{12})} \\ \dfrac{-2\sin(\beta_{12,3})}{\cos(\beta_{12,3})} \end{bmatrix} \tag{5.10}$$

The Hessian matrix yields

$$\mathcal{H}_{\log|FIM|} = \begin{bmatrix} \dfrac{\partial^2 \log|FIM|}{\partial \alpha_{12}^2} & \dfrac{\partial^2 \log|FIM|}{\partial \alpha_{12}\partial \beta_{12,3}} \\ \dfrac{\partial^2 \log|FIM|}{\partial \beta_{12,3}\partial \alpha_{12}} & \dfrac{\partial^2 \log|FIM|}{\partial \beta_{12,3}^2} \end{bmatrix} = \begin{bmatrix} \dfrac{-2}{\sin^2(\alpha_{12})} & 0 \\ 0 & \dfrac{-2}{\cos^2(\beta_{12,3})} \end{bmatrix} \tag{5.11}$$

Therefore it is clear that the Hessian matrix (5.11) is definite negative, and thus the logarithm of (5.9) is a concave function and we can employ Pareto optimization tools to define optimal sensor networks of 3 sensors for multiple target positioning.

As abovementioned, in the multiple target positioning problem the maximum log determinant

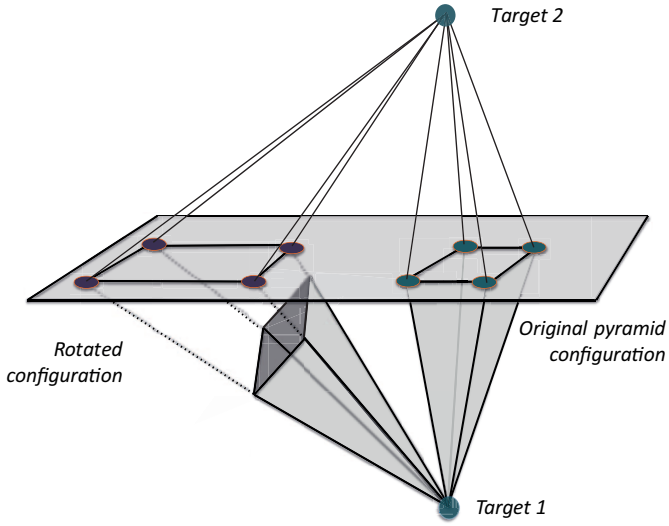

Figure 5.2: Example of optimal sensor networks for two targets and four sensors.

cannot be achieved for all targets at the same time, so a tradeoff solution must be adopted. This is true except for the special case of two targets and no constraints in the sensor placement. This case allows for optimal sensor configurations that provide the maximum accuracy possible for both targets. From the results of Chapter 4 it is easy to check that the optimal sensor configuration for single target positioning with 3 sensors is the one in which the range vectors form an orthogonal axis system. For the two target problem, the most simple solution is trivial, since one of the possible optimal sensor formations corresponds to a circular formation of radius $r = \sqrt{2} \cdot d/2$, where d is the distance between targets, in which the sensors are regularly distributed, and where the centre of the sensor formation is over the mid point of the segment that joins both targets. Moreover, the sensors are placed in the plane that is orthogonal to this segment. Thus, the range vectors form an orthogonal system with respect to each of the targets and then the FIM determinants at the target points are the theoretical maximum $|FIM| = n^3/(3^3\sigma^3)\ m^{-6}$. An equivalent solution would be obtained if the pyramids formed by the sensor positions and each target are rotated an arbitrary angle around the target positions, with the new sensor positions defined by the cut of the horizontal plane with the edges of the pyramids. These cuts determine the new sensor positions similarly as it was studied in Chapter 4. All these infinite solutions will provide the maximum accuracy for both targets too. It is clear that these solutions are optimal for 2 targets and any number of sensors, not only 3, for constant covariance and no constraints. A graphical example for 4 sensors and 2 targets is shown in Figure 5.2. It is important to remark that for this solution it is necessary to have some prior knowledge about the target positions because if all the sensors are in the same plane it is not possible to distinguish which target is above or under the sensor network.

5.3.2 Gaussian error with distance-dependent covariance

In the distance-dependent covariance error scenario some constraints must be imposed on the sensor placement so that the sensors do not collapse over the target position to reduce the distance-dependent added error as much as possible. It is important to remark at this point that if no constraints are imposed on the sensor network and the sensors can be placed freely in the 3D space,

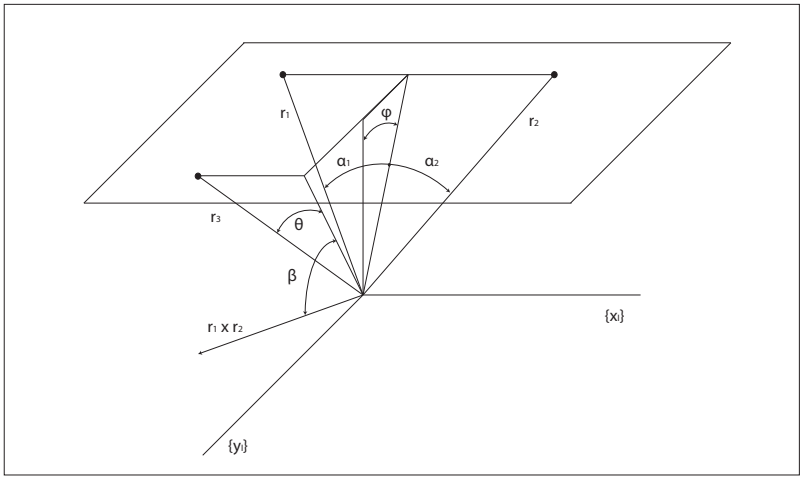

Figure 5.3: Notation adopted for the 3 sensor network problem.

the optimality criteria of the logarithm of the FIM determinant is not concave, and some numerical and stochastic methods must be used together with the gradient descendent algorithm to find the optimal solutions, which could not be considered global optimal solutions. Thus only specific scenarios with well defined constraints can be analysed for the problem at hand. For example, if the sensors are placed at the same (or a fixed) distance from the target, i.e., the sensors are placed over a sphere centred at the target position, then the solution is the same commented above for the constant covariance scenario. In the following analysis, the concavity of the logarithm of the FIM determinant is studied when the sensors must be placed in a plane, as it is usual for the application scenario of underwater target positioning by a surface sensor network.

Equation (5.7) for 3 surface sensors and distance-dependent covariance error yields

$$|FIM| = \frac{1}{\sigma^6} \frac{\sin^2(\alpha_{12}) \cos^2(\beta_{12,3})}{\left(1+\eta r_1^\gamma\right)^2 \left(1+\eta r_2^\gamma\right)^2 \left(1+\eta r_3^\gamma\right)^2} \tag{5.12}$$

For the sake of simplicity we rewrite (5.12) with the notation shown in Figure 5.3. We must take into account that the sensors lie in a plane, and therefore the range distances can be rewritten as a function of the angles shown in the set-up of Figure 5.3. Then, the logarithm of (5.12) becomes

$$\log|FIM| = \log \frac{\sin^2(\alpha)\cos^2(\beta)\cos^2(\theta)}{\left(1+\eta\left(z_q \frac{\sqrt{1+\tan^2(\phi)}}{\cos(\alpha_1)}\right)^\gamma\right)^2 \left(1+\eta\left(z_q \frac{\sqrt{1+\tan^2(\phi)}}{\cos(\alpha_2)}\right)^\gamma\right)^2 \left(1+\eta\left(\frac{z_q}{\cos(\theta)\sin(\beta+\phi)}\right)^\gamma\right)^2} \tag{5.13}$$

with $\sin(\alpha_{12}) = \sin(\alpha_1 + \alpha_2) = \sin(\alpha)$, $\cos(\beta_{12,3}) = \cos(\beta)\cos(\theta)$, and

$$r_1 = z_q \frac{\sqrt{1+\tan^2(\phi)}}{\cos(\alpha_1)} \qquad r_2 = z_q \frac{\sqrt{1+\tan^2(\phi)}}{\cos(\alpha_2)} \qquad r_3 = \frac{z_q}{\cos(\theta)\sin(\beta+\phi)}$$

To demonstrate the concavity of (5.13) we must compute the Hessian matrix with respect to each of the angles shown in Fig. 5.3. If the Hessian matrix is definite negative then (5.13) is a concave function with respect to the set-up adopted and we can use gradient descendent optimization tools to determine the optimal sensor configuration. Moreover, if it is possible to demonstrate the concavity of the function $\log|FIM|$ then we can use these techniques to determine the optimal sensor configuration for multiple target positioning. First, we compute the Jacobian, that after some simplifications yields

$$\nabla \log|FIM| = \left(\frac{\partial \log|FIM|}{\partial \alpha_1} \quad \frac{\partial \log|FIM|}{\partial \alpha_2} \quad \frac{\partial \log|FIM|}{\partial \beta} \quad \frac{\partial \log|FIM|}{\partial \theta} \quad \frac{\partial \log|FIM|}{\partial \phi} \right)^T \tag{5.14}$$

where

$$\frac{\partial \log|FIM|}{\partial \alpha_1} = \frac{2\cos(\alpha)}{\sin(\alpha)} - \frac{2\gamma\eta\left(z_q\sqrt{1+\tan^2(\phi)}\right)^{\gamma}\frac{\sin(\alpha_1)}{\cos^{\gamma+1}(\alpha_1)}}{1+\eta\left(z_q\frac{\sqrt{1+\tan^2(\phi)}}{\cos(\alpha_1)}\right)^{\gamma}}$$

$$\frac{\partial \log|FIM|}{\partial \alpha_2} = \frac{2\cos(\alpha)}{\sin(\alpha)} - \frac{2\gamma\eta\left(z_q\sqrt{1+\tan^2(\phi)}\right)^{\gamma}\frac{\sin(\alpha_2)}{\cos^{\gamma+1}(\alpha_2)}}{1+\eta\left(z_q\frac{\sqrt{1+\tan^2(\phi)}}{\cos(\alpha_2)}\right)^{\gamma}}$$

$$\frac{\partial \log|FIM|}{\partial \beta} = \frac{-2\sin(\beta)}{\cos(\beta)} + \frac{2\gamma\eta\left(\frac{z_q}{\cos(\theta)}\right)^{\gamma}\frac{\cos(\beta+\phi)}{\sin^{\gamma+1}(\beta+\phi)}}{1+\eta\left(\frac{z_q}{\cos(\theta)\sin(\beta+\phi)}\right)^{\gamma}}$$

$$\frac{\partial \log|FIM|}{\partial \theta} = \frac{-2\sin(\theta)}{\cos(\theta)} + \frac{2\gamma\eta\left(\frac{z_q}{\sin(\beta+\phi)}\right)^{\gamma}\frac{\sin(\theta)}{\cos^{\gamma+1}(\theta)}}{1+\eta\left(\frac{z_q}{\cos(\theta)\sin(\beta+\phi)}\right)^{\gamma}}$$

$$\begin{aligned}\frac{\partial \log|FIM|}{\partial \phi} = &- \frac{2\gamma\eta\left(z_q\sqrt{1+\tan^2(\phi)}\right)^{\gamma}\frac{\tan(\phi)}{\cos^{\gamma}(\alpha_1)}}{1+\eta\left(z_q\frac{\sqrt{1+\tan^2(\phi)}}{\cos(\alpha_1)}\right)^{\gamma}} \\ &- \frac{2\gamma\eta\left(z_q\sqrt{1+\tan^2(\phi)}\right)^{\gamma}\frac{\tan(\phi)}{\cos^{\gamma}(\alpha_2)}}{1+\eta\left(z_q\frac{\sqrt{1+\tan^2(\phi)}}{\cos(\alpha_2)}\right)^{\gamma}} + \frac{2\gamma\eta\left(\frac{z_q}{\cos(\theta)}\right)^{\gamma}\frac{\cos(\beta+\phi)}{\sin^{\gamma+1}(\beta+\phi)}}{1+\eta\left(\frac{z_q}{\cos(\theta)\sin(\beta+\phi)}\right)^{\gamma}}\end{aligned}$$

For the simplifications done in the computation of the Jacobian it must be noticed that $\sin(\alpha) \neq 0$, $\cos(\beta) \neq 0$, and $\cos(\theta) \neq 0$, because two sensors cannot be placed at the same point and sensors and target cannot be placed all in the same plane. The Hessian matrix, after some lengthy computations

that are omitted, yields

$$\mathcal{H} = \begin{pmatrix} \mathcal{H}_{1,1} & \frac{-2}{\sin^4(\alpha_1)} & 0 & 0 & \mathcal{H}_{1,5} \\ \frac{-2}{\sin^4(\alpha_1)} & \mathcal{H}_{2,2} & 0 & 0 & \mathcal{H}_{2,5} \\ 0 & 0 & \mathcal{H}_{3,3} & \mathcal{H}_{3,4} & \mathcal{H}_{3,5} \\ 0 & 0 & \mathcal{H}_{4,3} & \mathcal{H}_{4,4} & \mathcal{H}_{4,5} \\ \mathcal{H}_{5,1} & \mathcal{H}_{5,2} & \mathcal{H}_{5,3} & \mathcal{H}_{5,4} & \mathcal{H}_{5,5} \end{pmatrix} \tag{5.15}$$

where

$$\mathcal{H}_{1,1} = -\frac{2}{\sin^4(\alpha)} - \frac{2\gamma\eta\left(z_q\sqrt{1+\tan^2(\phi)}\right)^{\gamma}\left(1+\gamma\sin^2(\alpha_1)+\eta\left(z_q\frac{\sqrt{1+\tan^2(\phi)}}{\cos(\alpha_1)}\right)^{\gamma}\right)}{\cos^{\gamma+2}(\alpha_1)\left(1+\eta\left(z_q\frac{\sqrt{1+\tan^2(\phi)}}{\cos(\alpha_1)}\right)^{\gamma}\right)^2}$$

$$\mathcal{H}_{1,5} = -\frac{2\gamma^2\eta\left(z_q\sqrt{1+\tan^2(\phi)}\right)^{\gamma}\frac{\sin(\alpha_1)}{\cos^{\gamma+1}(\alpha_1)}\tan(\phi)}{\left(1+\eta\left(z_q\frac{\sqrt{1+\tan^2(\phi)}}{\cos(\alpha_1)}\right)^{\gamma}\right)^2}$$

$$\mathcal{H}_{2,2} = -\frac{2}{\sin^4(\alpha)} - \frac{2\gamma\eta\left(z_q\sqrt{1+\tan^2(\phi)}\right)^{\gamma}\left(1+\gamma\sin^2(\alpha_2)+\eta\left(z_q\frac{\sqrt{1+\tan^2(\phi)}}{\cos(\alpha_2)}\right)^{\gamma}\right)}{\cos^{\gamma+2}(\alpha_2)\left(1+\eta\left(z_q\frac{\sqrt{1+\tan^2(\phi)}}{\cos(\alpha_2)}\right)^{\gamma}\right)^2}$$

$$\mathcal{H}_{2,5} = -\frac{2\gamma^2\eta\left(z_q\sqrt{1+\tan^2(\phi)}\right)^{\gamma}\frac{\sin(\alpha_2 1)}{\cos^{\gamma+1}(\alpha_2)}\tan(\phi)}{\left(1+\eta\left(z_q\frac{\sqrt{1+\tan^2(\phi)}}{\cos(\alpha_2)}\right)^{\gamma}\right)^2}$$

$$\mathcal{H}_{3,3} = -\frac{2}{\cos^2(\beta)} - \frac{2\gamma\eta z_q^{\gamma}\left(1+\gamma\cos^2(\beta+\phi)+\eta\left(\frac{z_q}{\cos(\theta)\sin(\beta+\phi)}\right)^{\gamma}\right)}{\cos^{\gamma}(\theta)\sin^{\gamma+2}(\beta+\phi)\left(1+\eta\left(\frac{z_q}{\cos(\theta)\sin(\beta+\phi)}\right)^{\gamma}\right)^2}$$

$$\mathcal{H}_{3,4} = \frac{2\gamma^2\eta z_q^{\gamma}\cos(\beta+\phi)\sin(\theta)}{\sin^{\gamma+1}(\beta+\phi)\cos^{\gamma+1}(\theta)\left(1+\eta\left(\frac{z_q}{\cos(\theta)\sin(\beta+\phi)}\right)^{\gamma}\right)^2}$$

$$\mathcal{H}_{3,5} = -\frac{2\gamma\eta z_q^{\gamma}\left(1+\gamma\cos^2(\beta+\phi)+\eta\left(\frac{z_q}{\cos(\theta)\sin(\beta+\phi)}\right)^{\gamma}\right)}{\cos^{\gamma}(\theta)\sin^{\gamma+2}(\beta+\phi)\left(1+\eta\left(\frac{z_q}{\cos(\theta)\sin(\beta+\phi)}\right)^{\gamma}\right)^2}$$

$$\mathcal{H}_{4,3} = \mathcal{H}_{3,4}$$

$$\mathcal{H}_{4,4} = -\frac{2}{\cos^2(\theta)} - \frac{2\gamma\eta z_q^{\gamma}\left(1+\gamma\sin^2(\theta)+\eta\left(\frac{z_q}{\cos(\theta)\sin(\beta+\phi)}\right)^{\gamma}\right)}{\cos^{\gamma+2}(\theta)\sin^{\gamma}(\beta+\phi)\left(1+\eta\left(\frac{z_q}{\cos(\theta)\sin(\beta+\phi)}\right)^{\gamma}\right)^2}$$

$$\mathcal{H}_{4,5} = \frac{2\gamma^2\eta z_q^{\gamma}\cos(\beta+\phi)\sin(\theta)}{\sin^{\gamma+1}(\beta+\phi)\cos^{\gamma+1}(\theta)\left(1+\eta\left(\frac{z_q}{\cos(\theta)\sin(\beta+\phi)}\right)^{\gamma}\right)^2}$$

$$\mathcal{H}_{5,1} = \mathcal{H}_{1,5}$$

$$\mathcal{H}_{5,2} = \mathcal{H}_{2,5}$$

$$\mathcal{H}_{5,3} = \mathcal{H}_{3,5}$$

$$\mathcal{H}_{5,4} = \mathcal{H}_{4,5}$$

$$\mathcal{H}_{5,5} = -\frac{2\eta\gamma\left(z_q\sqrt{1+\tan^2(\phi)}\right)^{\gamma}\left(1+\gamma\sin^2(\phi)+\eta\left(z_q\frac{\sqrt{1+\tan^2(\phi)}}{\cos(\alpha_1)}\right)^{\gamma}\right)}{\cos^{\gamma}(\alpha_1)\cos^2(\phi)\left(1+\eta\left(z_q\frac{\sqrt{1+\tan^2(\phi)}}{\cos(\alpha_1)}\right)^{\gamma}\right)^2}$$

$$-\frac{2\eta\gamma\left(z_q\sqrt{1+\tan^2(\phi)}\right)^{\gamma}\left(1+\gamma\sin^2(\phi)+\eta\left(z_q\frac{\sqrt{1+\tan^2(\phi)}}{\cos(\alpha_2)}\right)^{\gamma}\right)}{\cos^{\gamma}(\alpha_2)\cos^2(\phi)\left(1+\eta\left(z_q\frac{\sqrt{1+\tan^2(\phi)}}{\cos(\alpha_2)}\right)^{\gamma}\right)^2}$$

$$-\frac{2\gamma\eta z_q^{\gamma}\left(1+\gamma\cos^2(\beta+\phi)+\eta\left(\frac{z_q}{\cos(\theta)\sin(\beta+\phi)}\right)^{\gamma}\right)}{\cos^{\gamma}(\theta)\sin^{\gamma+2}(\beta+\phi)\left(1+\eta\left(\frac{z_q}{\cos(\theta)\sin(\beta+\phi)}\right)^{\gamma}\right)^2}$$

For the analysis of concavity we have to take into account that $\alpha_1, \alpha_2 \in [-\pi/2, \pi/2]$, $\beta \in [-\pi/2, \pi/2]$, and $\phi, \theta \in [0, \pi/2]$, as it can be seen in Fig. 5.3. For negative definite matrices, all principal minors have to be in alternation of signs, i.e., the upper left 1 by 1 corner of (5.15) must be negative, the upper left 2 by 2 corner of (5.15) must be positive, the upper left 3 by 3 corner of (5.15) must be negative, and so on. We can check easily that

$$M_1 = \mathcal{H}_{1,1} < 0$$

$$M_2 = \mathcal{H}_{1,1}\cdot\mathcal{H}_{2,2} - \mathcal{H}_{1,2}^2 > 0;$$

$$M_3 = \mathcal{H}_{1,1}\cdot\mathcal{H}_{2,2}\cdot\mathcal{H}_{3,3} - \mathcal{H}_{1,2}^2\cdot\mathcal{H}_{3,3} = \mathcal{H}_{3,3}\cdot M_2 < 0;$$

$$M_4 = \left(\mathcal{H}_{1,1}\cdot\mathcal{H}_{2,2} - \mathcal{H}_{1,2}^2\right)\cdot\left(\mathcal{H}_{3,3}\cdot\mathcal{H}_{4,4} - \mathcal{H}_{3,4}^2\right) > 0$$

$$M_5 = |\mathcal{H}| < 0$$

Therefore (5.15) is definite negative and $\log|FIM|$ for a three sensor formation is a concave

function, so we can use convex optimization tools to determine the sensor formation that provides the maximum determinant possible over the target position and, moreover, to use Pareto optimization techniques to determine the optimal sensor configuration for a multiobjective problem.

Similarly to the constant covariance scenario, in a multiple target positioning problem the maximum log determinant cannot be achieved for all targets at the same time, so a tradeoff solution must be adopted. Again, this is true except for the special case of two targets when the sensors are placed in the horizontal plane that is perpendicular to the segment that joins both targets in its mid point. In this case an unique optimal sensor configuration provides the maximum possible accuracy for both targets. Thus the FIM determinant at the target points is the maximum possible. As abovementioned, this solution is optimal for 2 targets and any number of sensors, not only 3. It is important to remark again that for this solution it is necessary to have some prior knowledge about the target positions because if all the sensor are in the same plane it is not possible to distinguish which target is above or under the sensor network.

Once the concavity for a 3 sensor network problem is defined we must tackle the general problem of an arbitrary number of sensors and targets. In this situation it is not possible to prove the convexity (concavity) of the problem due to the complexity of the first and second derivatives of the logarithm of the FIM determinant, but from the above result together with the discussion on the convexity of the functions adopted for the problem at hand in [12], Chapter 3 and the work in [85] on the D-optimality criterion, we can think of extending the concavity result for 3 sensors to a formation with an arbitrary number of sensors, so that Pareto optimization and convex optimization techniques can be used to determine the optimal sensor configuration for multiple target positioning.

It is important to remark at this point that although the previous analysis shows the concavity of the logarithm of the FIM determinant with respect to the angles that the range vectors form between them, for more than 3 sensors and multiple targets the optimization process using these variables becomes so complex. For this reason, the optimization procedure of the following sections will be done in the Cartesian space considering the Cartesian coordinates of each sensor as the design variables. The logarithm of the FIM determinant is not a concave function with respect to these variables, but with the knowledge that the maximum is unique, and that this maximum is well defined for a single target, we have tools to determine if the solution provided by the optimization process achieves desired conditions and if it is close to the optimal value that would be obtained for a single target.

5.4 Gradient optimization algorithm for sensor placement

In this section the gradient optimization algorithm with which the optimal sensor formations are computed is presented.

Maximizing a convex combination of the logarithms of the determinants of the different FIMs, as a consequence of the Pareto-optimality conditions described in Appendix B, yields the most appropriate sensor formation geometry for the multiple underwater target positioning problem:

$$\bar{p}^* = arg \max_{\bar{p}} \sum_{k=1}^{m} \log |FIM_k| \tag{5.16}$$

where m is the number of targets involved in the multiple target positioning task, $|FIM_k|$ is the FIM determinant of target k, and $\bar{p}$ is the vector of sensor positions.

One simple method to find the optimal formation is the gradient optimization method. To use it,

we compute the derivative of the logarithm of the FIM determinant of each target with respect to all sensor coordinates. For the sake of simplicity, the computation of the derivatives is not shown here. For details on the computation of these partial derivatives, see Appendix C.

Once the gradients have been computed for each target, they are combined to update the sensor configuration so as to yield an increase in the specified convex combination of the logarithms of the FIM determinants. This computation is recursive, until the optimal position is found. For the single target positioning problem, an adequate initial guess for the solution is for example any regular distribution around the target. Checking that this algorithm behaves well for single target positioning is easy, for an analytical solution to the optimal sensor positions is available in Chapter 4. For the multiple target localization problem, the initial guess will be a regular distribution around the mass centre of the target group, with all the targets inside the sensor formation. The Armijo rule is used for the sensor placement update phase, yielding the following iterative gradient optimization algorithm.

1. For each target, (5.6) is computed for the current sensor formation at iteration t, from which $|FIM_\lambda|$, the convex combination of the logarithms of the determinants given by $|FIM_\lambda|[t] = \sum_{k=1}^{m} \lambda_k \log |FIM|_k [t]$, follows for a specific choice of $\lambda_k; k = 1, 2, ..m, \lambda_1 + ... + \lambda_m = 1$, where m is the number of targets.

2. The gradient of $|FIM_\lambda|[t]$ is computed, yielding $\nabla_{i,\xi} |FIM_\lambda|[t]$ with $\xi = x, y, z$ and $i = 1, ..., n$.

3. The sensor positions are updated according to the gradients: $p_{i,\xi}[t+1] = p_{i,\xi}[t] + \mu^{\zeta[t]} \nabla_{i,\xi} |FIM_\lambda|[t]$, with $\mu \in 0, 1$, $\zeta[0] = 1$, and $\zeta[t] = \zeta[t-1] + 1$.

4. If $|FIM_\lambda|[t+1] > |FIM_\lambda|[t]$, then $p_i[t+1] = \left[p_{i,x}[t+1], p_{i,y}[t+1], p_{i,z}[t+1]\right]^T$ becomes the new set of sensor positions, $\zeta[t+1] = \zeta[t] + 1$, and the iteration goes back to step 1.

5. If $|FIM_\lambda|[t+1] < |FIM_\lambda|[t]$, then there is no improvement in the convex combination of the determinants, $\zeta[t] = 0$, the iterative algorithm stops, and $p_i[t]$ is considered to be the optimal configuration for the current target position.

The above cycle is only run once if the targets are stationary. Notice the unrealistic assumption that the positions of the targets are known in advance. This is done to simplify the problem and to first fully understand its solution before the realistic scenario where the positions of the targets are known with error can be tackled, in this respect, see Section 5.6.

In a practical situation where the targets are in motion, the surface sensor network must adapt its optimal configuration as the mission unfolds. Clearly, this requires that three different, intertwined processes be activated as follows:

i) *multiple target position estimation*, albeit with a possibly large error, using the current sensor configuration and resorting to a dedicated non-linear filter (e.g. Extended Kalman filter);

ii) *optimal sensor configuration computation*, based on the data provided by the previous process and the algorithm described above;

iii) *coordinated motion control* to actually drive the moving sensors to the optimal positions determined in ii).

We thus envision the situation where the algorithm described (or its modification in Section 5.6) is run during each cycle of the positioning system in i). Interestingly enough, we can also think of a

situation where the different iterates of process ii) can be used to yield set points for the autonomous sensor network to move to, effectively guiding them collectively to the optimal configuration that is being computed.

The advantage of using a gradient optimization method is its simplicity. As it will be seen later, based on the simulations done so far, the method has proven to be quite satisfactory. However, should there be a need for a more refined method, the sensor network positions given by the gradient algorithm can be used as initial estimates in the new method.

It is not hard to envision situations where different "levels of importance" and therefore different localization accuracies are required for the elements in a group of targets. It is obvious that the geometry of the sensor network will impact on the accuracy with which the position of each of the targets can be computed. In the case of multiple targets, improving the accuracy in the estimate of one target may at times be done only in detriment of the accuracy of the other estimates. There are therefore tradeoffs that must be examined carefully. An example of a multi-target localization problem can be briefly described as follows: "given m targets and n sensors, determine, if possible, a geometric configuration for the sensors that will maximize the accuracy with which the position of target i can be estimated, while keeping the accuracy of the other target estimates above a desired threshold level".

5.4.1 Simulation examples on optimal sensor placement

The rest of this section contains the results of simulations that illustrate the potential of the method developed for optimal sensor placement when multiple targets are involved.

Example 5.1: 3 targets, 6 sensors and constant covariance.

As an introductory step, only the case where the targets have equal Pareto weights, that is, $\lambda_1 = \lambda_2 = ... = \lambda_m$, is considered. All the targets have the same importance (weight) in the mission so they must be localized with the largest global accuracy possible, it is, $\lambda_i = 1/m$ with $i = 1, \cdots, m$ where m is the number of targets. To determine the optimal configuration the algorithm explained above is run for a stationary group of targets. Once the optimal formation is obtained, the accuracy with which each of the targets is positioned is compared with the one that would be obtained for the corresponding target working in isolation to check if the targets are positioned with correct accuracy. The error is modelled with $\sigma = 0.1\ m$, and $\eta = 0$.

We consider a formation composed of 6 sensors and 3 targets to be positioned. The target positions have been generated with a pseudo-random algorithm, and they are listed in Table 5.1 together with the sensor positions of the optimal configuration.

Table 5.1: Target positions and optimal sensor positions for $\lambda_1 = \lambda_2 = \lambda_3 = 1/3$.

	q_1	q_2	q_3	p_1	p_2	p_3	p_4	p_5	p_6
$\{x_I\}(m)$	292.2	−464	178.7	1653.8	−149.7	−1832.9	−1841	−220	1826.9
$\{y_I\}(m)$	459.5	349.1	−257.7	1365.1	1299	1216.5	−642	−2137	−764.1
$\{z_I\}(m)$	155.7	434	−243.1	−1400	797.5	−1425.6	1754.7	−1757	1757.3

With this formation the determinants are $|FIM|_1 = 7.8386 \cdot 10^6\ m^{-6}$, $|FIM|_2 = 7.8284 \cdot 10^6\ m^{-6}$, and $|FIM|_3 = 7.9015 \cdot 10^6\ m^{-6}$. We can notice how a large accuracy is obtained for each target and how the FIM determinants are very close to the optimal one that would be obtained for a single

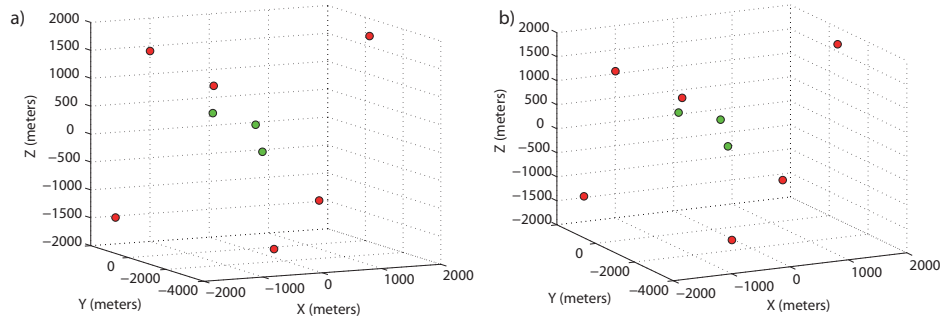

Figure 5.4: Optimal sensor configurations for 6 sensors and 3 targets with $\eta = 0$, (a) with $\lambda_1 = 0.33$, $\lambda_2 = 0.33$, and $\lambda_3 = 0.33$ and (b) with $\lambda_1 = 0.05$, $\lambda_2 = 0.05$, and $\lambda_3 = 0.9$.

target working in isolation, $|FIM|_{opt} = n^3/(3^3 \cdot \sigma^6) = 8 \cdot 10^6\ m^{-6}$. Their corresponding CRB traces are $tr(CRB)_1 = 0.0152\ m^2$, $tr(CRB)_2 = 0.0152\ m^2$, and $tr(CRB)_3 = 0.0151\ m^2$, being the theoretical minimum $tr(CRB)_{opt} = 0.015\ m^2$. In Figure 5.4 (a) it is shown this optimal formation (red points) and the targets (green points).

Therefore it is possible to obtain large FIM determinants for all the targets at the same time, so for most of the different Pareto weights that could be defined (for the 3 targets) the optimal formation is the one shown in Figure 5.4 (a). The formation only changes slightly for extreme cases, for example, in Figure 5.4 (b) one target must be localized with large accuracy while the accuracies of the others can be degraded. In this example the Pareto weights are $\lambda_1 = 0.05$, $\lambda_2 = 0.05$, and $\lambda_3 = 0.9$. Therefore it must be defined a formation that provides the maximum accuracy possible for two targets while keeping the very large accuracy of target 3. This formation can be seen in Table 5.2 and in Figure 5.4 (b)

Table 5.2: Target positions and optimal sensor positions for $\lambda_1 = 0.05$, $\lambda_2 = 0.05$, and $\lambda_3 = 0.9$.

	q_1	q_2	q_3	p_1	p_2	p_3	p_4	p_5	p_6
$\{x_I\}(m)$	292.2	−464	178.7	1602.5	−144	−1836.5	−1929	−381	1869
$\{y_I\}(m)$	459.5	349.1	−257.7	1207.1	1132	1096.4	−806.4	−2142.6	−826
$\{z_I\}(m)$	155.7	434	−243.1	−1437	540.6	−1256.6	1731.1	−1748.3	1744

The determinants are $|FIM|_1 = 7.7807 \cdot 10^6\ m^{-6}$, $|FIM|_2 = 7.5883 \cdot 10^6\ m^{-6}$ and $|FIM|_3 = 7.9822 \cdot 10^6\ m^{-6}$. It can be noticed how the determinant of target 3 is almost the optimal one, $|FIM|_{opt} = 8 \cdot 10^6\ m^{-6}$, while the determinants of targets 1 and 2, although lower, are large and close to the optimal one too. The traces of the CRB matrices are $tr(CRB)_1 = 0.0153\ m^2$, $tr(CRB)_2 = 0.0155\ m^2$, and $tr(CRB)_3 = 0.015\ m^2$, being the theoretical minimum $tr(CRB)_{opt} = 0.015\ m^2$.

Thus, for constant covariance it is possible to achieve a large accuracy for all the targets at the same time if there are no constraints on the sensor placement. Of course, the accuracy required for each target will be mission-dependent. It is important to remark at this point that for the multiple target positioning problem with constant covariance the distance between targets does not condition the optimal sensor configuration. As it was commented in Chapter 3, the optimal sensor formation only depends on the geometric configuration of the targets. If the distance between targets is increased while its geometric configuration is kept, then the optimal sensor formation will be the same with the appropriate change of scale. This issue was studied in detail in Chapter 3 where some

examples were shown to illustrate this behaviour. In the distance-dependent covariance scenario the distance affects dramatically the resultant sensor formation. ■

Example 5.2: 3 targets, 6 sensors and distance-dependent covariance.

The tradeoffs are clearer in the distance-dependent covariance scenario because the increase in the accuracy of one target only can be done in detriment of the accuracy of the other targets. This fact is studied in detail in Section 5.5 for surface sensor networks, because in this latter case the optimality criteria is concave, as it was demonstrated in Section 5.3.2. In the problem at hand, the criterion is not concave because of the distance-dependent added error; and the gradient descendent method detailed in Section 5.4 must be combined with numerical and stochastic methods to find an optimal configuration, that can or not be the global one. For these reasons, the study of the tradeoffs related with the variation of the Pareto weights is done for surface sensor networks. The aim of this example is to shed light on the tradeoffs involved in a multiple target positioning task in 3D space.

The same situation of 6 sensors and 3 targets is studied for the case in which the error covariance is distance-dependent, with $\eta = 0.01$ and $\gamma = 1$. The targets are placed at the same points of the above example to compare the different solutions obtained for different weights and different error models. The target positions and the optimal sensor configuration, for the case in which the weights are the same for all the targets, are shown in Table 5.3.

Table 5.3: Target positions and optimal sensor positions for $\lambda_1 = \lambda_2 = \lambda_3 = 0.33$.

	q_1	q_2	q_3	p_1	p_2	p_3	p_4	p_5	p_6
$\{x_I\}(m)$	292.2	−464	178.7	271	−445	119.5	−443.5	266	178
$\{y_I\}(m)$	459.5	349.1	−257.7	420.6	359.9	−203.5	335.8	450.6	−212.9
$\{z_I\}(m)$	155.7	434	−243.1	165.1	425.5	−216.1	431.6	125.1	−190

With the defined formation the determinants are $|FIM|_1 = 4.8148 \cdot 10^3\ m^{-6}$, $|FIM|_2 = 1.5542 \cdot 10^3\ m^{-6}$, and $|FIM|_3 = 230.9\ m^{-6}$. Their corresponding CRB traces are $tr(CRB)_1 = 0.5059\ m^2$, $tr(CRB)_2 = 2.2319\ m^2$, and $tr(CRB)_3 = 2.8021\ m^2$. We cannot compare these determinants with an optimal value because with distance-dependent covariance the optimal value for a single target depends on the constraints imposed to the sensor formation, and when several targets must be positioned the accuracy degrades substantially. The sensors try to reduce the distance to the targets as much as possible to minimize the distance-dependent added error, and it is clear that this is not possible for all the targets at the same time. Thus, a tradeoff solution must be adopted. Moreover, in the example the distance between targets and sensors is limited to 20 m to avoid that the sensors be placed so close from a target. In Figure 5.5 (a) it is shown this optimal formation (red points) and the targets (green points) where the sensor formation is split into pairs of sensors focused on one target each.

A second scenario is studied in which two targets must be localized with large accuracy (one with larger accuracy than the other) and the third one does not require a large accuracy. Thus, the weights are $\lambda_1 = 0.1$, $\lambda_2 = 0.4$, and $\lambda_3 = 0.5$. The optimal sensor positions are stated in Table 5.4.

The FIM determinants for each of the targets are $|FIM|_1 = 101\ m^{-6}$, $|FIM|_2 = 0.1034 \cdot 10^4\ m^{-6}$ and $|FIM|_3 = 2.1955 \cdot 10^4\ m^{-6}$. We can notice how targets 2 and 3 are positioned with larger accuracy than target 1, and how the accuracy of target 3 is larger than the accuracy of target 2. Their corresponding CRB traces are $tr(CRB)_1 = 1.6446\ m^2$, $tr(CRB)_2 = 1.5314\ m^2$, and $tr(CRB)_3 = 0.1245\ m^2$. Moreover, the FIM determinant of target 1 is significantly reduced with respect to the

Table 5.4: Target positions and optimal sensor positions for $\lambda_1 = 0.1$, $\lambda_2 = 0.4$, and $\lambda_3 = 0.5$.

	q_1	q_2	q_3	p_1	p_2	p_3	p_4	p_5	p_6
$\{x_I\}(m)$	292.2	−464	178.7	241	−425	176.6	−423.7	266	135.1
$\{y_I\}(m)$	459.5	349.1	−257.7	−220.6	359.9	−208.8	315.7	433.6	−225.7
$\{z_I\}(m)$	155.7	434	−243.1	−165.1	425.5	−249.6	431.6	125.1	−165

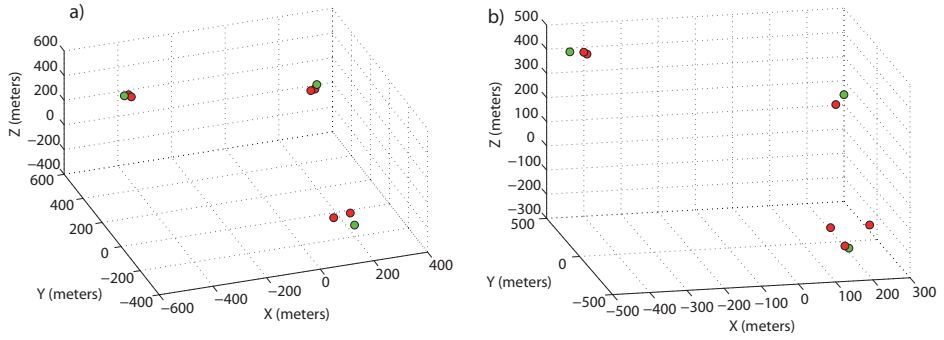

Figure 5.5: Optimal sensor configuration for 3 targets and 6 sensors, with distance-dependent covariance and $\lambda_1 = 0.33$, $\lambda_2 = 0.33$, and $\lambda_3 = 0.33$ in (a), and $\lambda_1 = 0.1$, $\lambda_2 = 0.4$, and $\lambda_3 = 0.5$ in (b).

previous example to increase the determinant of target 3. In Figure 5.5 (b) this optimal formation is shown and it is possible to notice how 3 sensors are close to target 3, 2 sensors are close to target 2, and 1 sensor is close to target 1, to obtain the desired accuracies for each of the targets. ■

From the previous examples we can conclude that it is possible to achieve a large accuracy for all the targets at the same time in a constant covariance scenario. We can notice how in the solution for the distance-dependent covariance case the sensors are closer to the targets to reduce the added error. Alternative and different examples could be obtained for different weights, number of sensors and/or number of targets. It is important to notice that the sensors take positions close to the targets because of the large distances between targets.

5.5 Gradient optimization algorithm for surface sensor placement

In many situations of interest, a number of human divers or AUVs may be required to work scattered over a certain area, executing different tasks or cooperating towards the execution of a common task. It is not hard to envision situations where different "levels of importance" and therefore different localization accuracies are required for the elements in a group of underwater targets. In the case of human divers, for example, in a 2 diver scenario one of the divers may be executing a very demanding and risky task, while the other is carrying out an easy, routine task. In this situation, the surface sensor network should "focus its attention" on the first target, effectively imposing strict requirements on the accuracy with which its position must be estimated, while relaxing the level of localization accuracy required for the second target. This situation may be inverted during the mission, so the formation should be able to reconfigure itself accordingly. It is obvious that the geometry of the sensor network will impact on the accuracy with which the position of each of the

targets can be computed.

The sensors are constrained to lie in the plane $z = 0$, at the sea surface. One simple method to find the optimal formation is the gradient optimization method used until this point. To use it, we compute the derivative of the logarithm of the FIM determinant of each target with respect to the sensor coordinates in the $\{x_I y_I\}$ plane. Then, the computation of the derivatives of the logarithm of (5.6) is carried out with respect to the p_{ix} and p_{iy} coordinates of a generic sensor i. The computation of these derivatives is shown in Appendix C.

It is at this stage that the power of multi-objective Pareto optimization must be brought into the picture, because, as explained in Section 5.3, (5.17) is a concave function for surface sensor networks. Clearly, in order to fully understand the problem we must compute the corresponding set of Pareto-optimal points and make decisions accordingly. See the presentation in Appendix B. As explained before, this can be done by computing

$$\overline{p}^* = arg \max_{\overline{p}} |FIM_\lambda| \tag{5.17}$$

over all possible sensor positions, and for all $\lambda = [\lambda_1, \lambda_2, ..., \lambda_m]$ such that $\lambda_1 + ... + \lambda_m = 1$. In practice a grid of points is adopted for vector λ. The maximization above is done by resorting to the gradient optimization algorithm introduced before.

For simplicity of explanation, a theoretical 2 target positioning problem with 6 sensors and distance-dependent covariance is studied although the procedure would be the same for more targets and a different number of sensors. The computation of the optimal solutions of this particular case is studied in detail in Example 5.4.

Because only two targets are involved, the Pareto-optimal curve is parametrized by a single parameter $\lambda \in [0, 1]$. For simplicity of notation, we use the same symbol for this scalar as well as for vector λ. The meaning will be clear from the context. We assume that $\lambda_1 = \lambda$ and $\lambda_2 = 1 - \lambda$. When λ varies from 0 to 1, the weight of one of the targets changes accordingly. Thus, in the extreme cases of 0 and 1 the solutions degenerate into those two of the single target localization problems for target 2 and 1, respectively. Two normalized curves that show the tradeoffs in the determinants of the Fisher information matrices for each of the targets (with the sensor geometry obtained by running the gradient optimization algorithm) are plotted in Fig. 5.6. The solid line corresponds to the Pareto curve for the maximization of $|FIM_\lambda|$, whereas the dotted line shows the corresponding FIM determinants. The two curves are normalized between 0 and 1.

Notice in Fig. 5.6 how the cost function $|FIM_\lambda|$ provides a concave Pareto curve (solid line), as expected for a maximization problem. As explained before, this is a consequence of the fact that in this case the criterion for each target is indeed concave. The dotted line shows the corresponding evolution of the FIM determinants. Notice that the curve is not concave, thus supporting the statement that the determinants of the FIMs are not adequate criteria to be maximized jointly (in the Pareto-optimal sense).

Fig. 5.6 shows how the accuracy of the measurements changes for different values of λ. At this point it is important to remark that if the measurement error does not depend on the distance between targets and sensors, that is, $\eta = 0$, it is possible to obtain sensor locations for which the accuracies obtained for each of the targets simultaneously are close to the optimal ones that would be obtained if the targets were operating in isolation. This follows from the shape of the Pareto curve when $\eta = 0$, not shown here. For example, with $\lambda = 0.5$ the performance achievable in the localization of targets 1 and 2 simultaneously does not degrade substantially when compared to the best performance achievable for the two targets isolated. Of course the acceptable level of degradation in performance is problem-dependent. When the measurement error is distance-

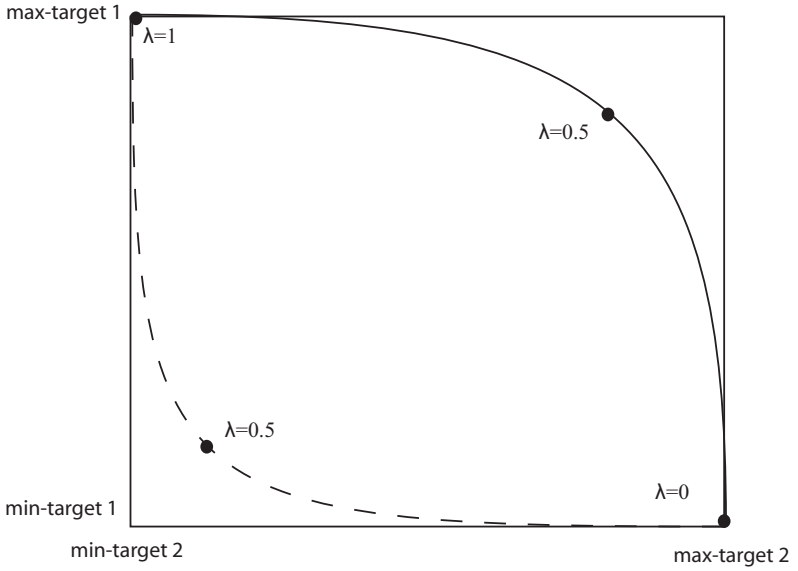

Figure 5.6: Pareto curve (solid line) for a 2 target localization problem, using 6 sensors for $\eta = 0.05$, and the corresponding FIM determinants (dotted line) for different values of the Pareto scalarization weights in λ.

dependent, the situation changes drastically because of the "steepness" of the Pareto curve. For example, when $\lambda = 0.5$ the performance that can be simultaneously achieved for both targets degrades substantially. The tradeoffs involved are clear.

5.5.1 Simulation examples on optimal sensor placement

This subsection contains the results of simulations that illustrate the potential of the method developed for optimal surface sensor placement when multiple targets are involved. The initial guess for the gradient optimization algorithm is of great importance to avoid local minima or divergence. Experience has shown that a regular formation around the centre of mass of the group of targets, keeping the targets inside the formation, is an appropriate initial guess. Starting from this initial guess, several examples of multi-target positioning are shown next. In the forthcoming examples we consider that all the targets are placed in the same plane, it is, at the same depth. The reason to adopt this condition is to be able to show graphically the tradeoffs involved with the representation of $|FIM|_{\mathcal{D}}$, $\mathcal{D} \in \Re^2$ as in Chapters 2 and 3, and to be able to analyse the accuracy with which each target is positioned. The approach would be exactly the same for different target depths.

Example 5.3: 4 sensors, 2 targets and constant covariance.

In this example the targets are placed at a depth of 100 meters at the positions $q_1 = [150,\ 0,\ -100]^T\ m$ and $q_2 = [-150,\ 0,\ -100]^T\ m$. In Figure 5.7 it is shown the optimal sensor formation when the targets have equal Pareto weights, $\lambda_1 = \lambda_2 = 0.5$. In this case the distance between sensors and targets does not condition the solution, so the sensors can be placed such that a large accuracy is obtained for both targets. The formation is placed according to Table 5.5.

The FIM determinants obtained for each target are $|FIM|_1 = 2.2722 \cdot 10^6\ m^{-6}$ and $|FIM|_2 =$

Table 5.5: Target positions and optimal sensor positions for $\lambda_1 = \lambda_2 = 0.5$.

	q_1	q_2	p_1	p_2	p_3	p_4
$\{x_I\}(m)$	-150	150	191.3	0	-191.3	0
$\{y_I\}(m)$	0	0	0	300.4	0	-300.4
$\{z_I\}(m)$	-100	-100	0	0	0	0

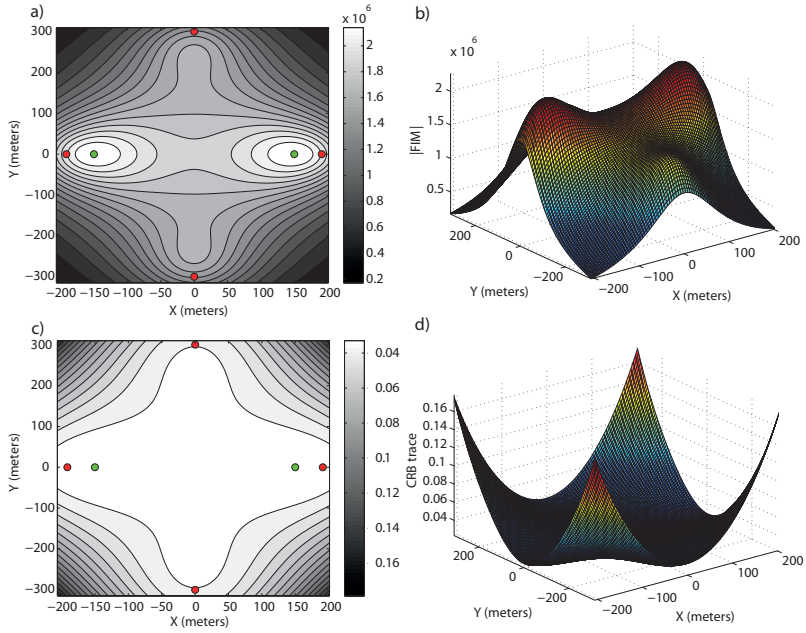

Figure 5.7: Optimal sensor configurations with $\eta = 0$ for 4 sensors and 2 targets, and $\lambda = 0.5$. $|FIM|_{\mathcal{D}}$, $\mathcal{D} \in \Re^2$ (a); FIM determinant for each point in the plane where the targets lie (b); $CRB_{\mathcal{D}}$ (c); and Value of the CRB in the targets plane (d). Sensors in red and targets in green.

$2.2722 \cdot 10^6\ m^{-6}$, that are very close to the optimal one, $|FIM|_{opt} = n^3/(3^3\sigma^6) = 2.37 \cdot 10^6\ m^{-6}$. Therefore it is possible to achieve large accuracy for both targets at the same time.

This same example is studied when the Pareto weights are different, $\lambda_1 = 0.9$ and $\lambda_2 = 0.1$, and the optimal sensor formation is shown in Figure 5.8 and in Table 5.6.

Table 5.6: Target positions and optimal sensor positions for $\lambda_1 = 0.9$ and $\lambda_2 = 0.1$.

	q_1	q_2	p_1	p_2	p_3	p_4
$\{x_I\}(m)$	-150	150	108.6	-101.4	-101.4	108.6
$\{y_I\}(m)$	0	0	90.4	114.3	-114.3	-90.4
$\{z_I\}(m)$	-100	-100	0	0	0	0

The FIM determinants are $|FIM|_1 = 2.3688 \cdot 10^6\ m^{-6}$ and $|FIM|_2 = 2.2712 \cdot 10^6\ m^{-6}$. We can notice how the FIM determinant of target 1 is almost the optimal one. However the FIM determinant of target 2 is close to the optimal one too, and therefore it is always possible to obtain large accuracy for multiple targets in the constant covariance scenario. ■

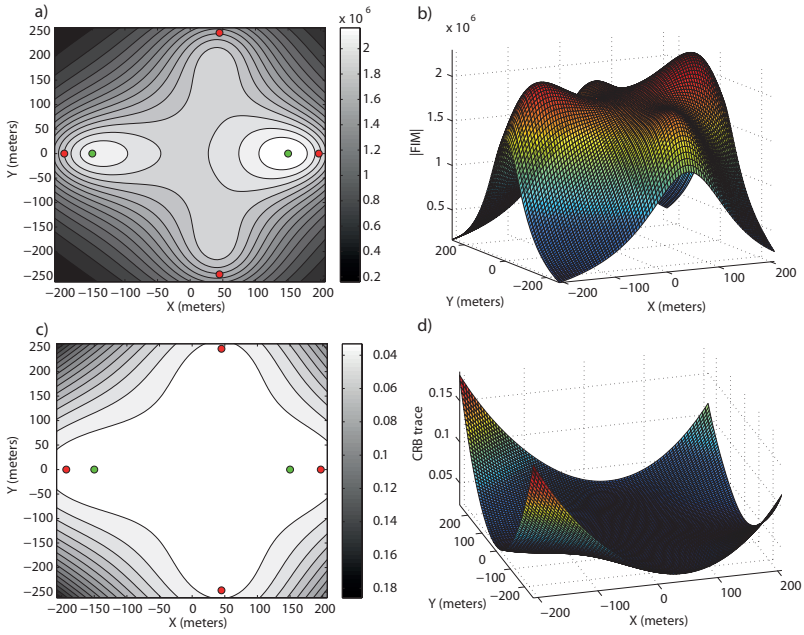

Figure 5.8: Optimal sensor configurations with $\eta = 0$ for 4 sensors and 2 targets, and $\lambda = 0.9$. $|FIM|_{\mathcal{D}}$, $\mathcal{D} \in \Re^2$ (a); FIM determinant for each point in the plane where the target lies (b); $CRB_{\mathcal{D}}$ (c); and Value of the CRB in the targets plane (d). Sensors in red and targets in green.

Example 5.4: 6 sensors, 2 targets and distance-dependent covariance.

In this second example we consider a 6 sensor formation for a two target positioning problem in which the targets are again at positions $q_1 = [150,\ 0,\ -100]^T\ m$ and $q_2 = [-150,\ 0,\ -100]^T\ m$. In Figure 5.9 and in Table 5.7 it is shown the optimal sensor formation when the targets have equal Pareto weights, $\lambda_1 = \lambda_2 = 0.5$.

Table 5.7: Target positions and optimal sensor positions for $\lambda_1 = \lambda_2 = 0.5$.

	q_1	q_2	p_1	p_2	p_3	p_4	p_5	p_6
$\{x_I\}(m)$	−150	150	193.8	91.3	−150.5	−193.8	−91.3	150.5
$\{y_I\}(m)$	0	0	40	57.5	67.1	−40	−57.5	−67.1
$\{z_I\}(m)$	−100	−100	0	0	0	0	0	0

In this case, in contrast to what was seen in the previous example, the distance affects the optimal sensor configuration and the accuracy with which each target can be localized is substantially degraded. We can notice how the 6 sensors are split into two formations of 3 sensors, each formation close to one of the targets. The FIM determinants are $|FIM|_1 = 8.4030\ m^{-6}$ and $|FIM|_2 = 8.4030\ m^{-6}$, that are quite smaller than in the previous example due to the added distance-dependent error.

Now it is studied the case in which the Pareto weights are different, $\lambda_1 = 0.8$ and $\lambda_2 = 0.2$, and the optimal sensor formation is shown in Figure 5.10 and in Table 5.8. We can see how the

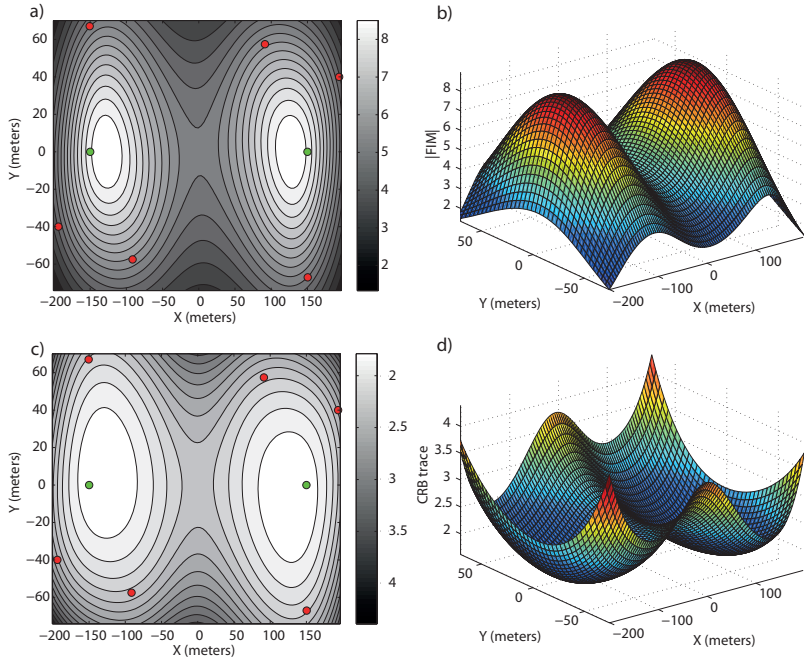

Figure 5.9: Optimal sensor configurations with $\eta = 0.05$ for 6 sensors and 2 targets, and $\lambda = 0.5$. $|FIM|_{\mathcal{D}}$, $\mathcal{D} \in \Re^2$ (a); FIM determinant for each point in the plane where the targets lie (b); $CRB_{\mathcal{D}}$ (c); and Value of the CRB in the targets plane (d). Sensors in red and targets in green.

sensor formation is focused on target 1 to increase its accuracy. The FIM determinants are now $|FIM|_1 = 14.0237\ m^{-6}$ and $|FIM|_2 = 4.5465\ m^{-6}$.

Table 5.8: Target positions and optimal sensor positions for $\lambda_1 = 0.8$ and $\lambda_2 = 0.2$.

	q_1	q_2	p_1	p_2	p_3	p_4	p_5	p_6
$\{x_I\}(m)$	−150	150	195.2	106.1	−148.4	−148.8	104.1	193.6
$\{y_I\}(m)$	0	0	51.2	58.9	58.4	−57.8	−57.1	−53.2
$\{z_I\}(m)$	−100	−100	0	0	0	0	0	0

Therefore it is clear that for distance-dependent covariance error a tradeoff solution must be adopted because the distance affects dramatically the precision with which each target is localized. ■

Now some more examples are shown briefly for more than 2 targets.

In Fig. 5.11 (a), $|FIM|_{\mathcal{D}}; \mathcal{D} \in \Re^2$ is mapped for a 6 sensor network, 3 targets, and $\eta = 0$ (constant covariance error). The maximum values of the function are over the target positions, close to the optimal values that would be obtained in a single target positioning problem, as seen in Fig. 5.11 (b). We can notice how the sensors are spread around the centre of mass of the targets. In Fig. 5.11 (c) the same formation of 6 sensors is used for a 4 target positioning problem. Again the maximum values are over the target positions and their values are close to the optimal ones, Figure 5.11 (d). Thus for constant covariance error it is possible to obtain a sensor formation that provides

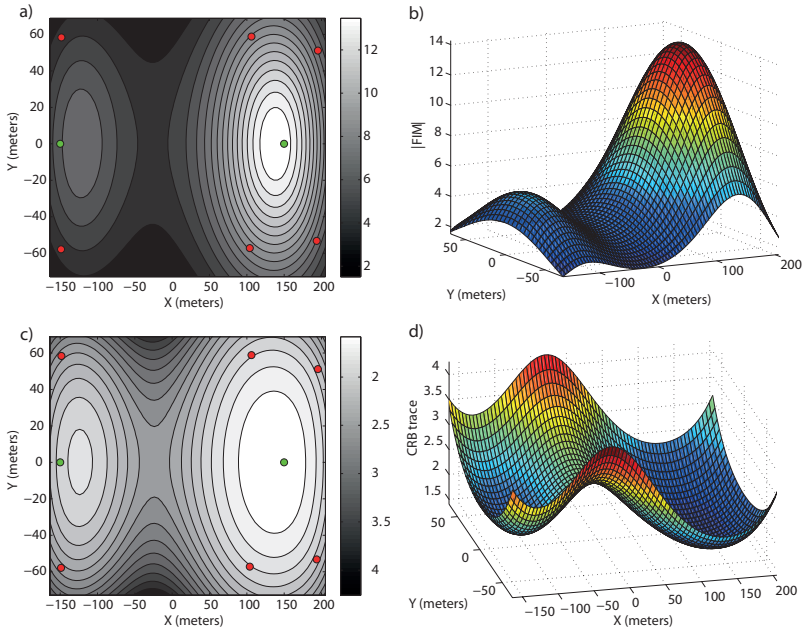

Figure 5.10: Optimal sensor configurations with $\eta = 0.05$ for 6 sensors and 2 targets, and $\lambda = 0.8$. $|FIM|_{\mathcal{D}}$, $\mathcal{D} \in \Re^2$ (a); FIM determinant for each point in the plane where the targets lie (b); $CRB_{\mathcal{D}}$ (c); and Value of the CRB in the targets plane (d). Sensors in red and targets in green.

for all the targets an accuracy close to the one that would be obtained for a single target working in isolation, as it was seen in detail in Example 5.3.

In Fig. 5.12 (a),$|FIM|_{\mathcal{D}}; \mathcal{D} \in \Re^2$ is mapped for a 6 sensor network, 3 targets, and $\eta = 0.1$ (distance-dependent covariance error). In this case, the position where the maximum of $|FIM|_{\mathcal{D}}$ occurs is strongly affected by the distance-dependent added error. It is possible to notice how the accuracy is similar for the three targets, Fig. 5.12 (b), but the FIM determinant obtained is dramatically affected by the distance-dependent added noise. In Fig. 5.12 (c), $|FIM|_{\mathcal{D}}; \mathcal{D} \in \Re^2$ is mapped for a 7 sensor formation and 4 targets, with $\eta = 0.1$. Again, the maximum values of the function are close to the targets, Fig. 5.12 (d), and the sensors spread themselves in an organized manner around the targets. For the choice of identical weights adopted, the most adequate configuration with 7 sensors and 4 targets is such that the accuracy with which two of the targets can be located is larger than the others because it is not possible to obtain the same good accuracy for all the targets and a tradeoff solution must be chosen. Should such a solution prove unsuitable, a complete analysis of the tradeoffs involved using the set-up with different target weights would be required.

5.6 Optimal sensor placement with uncertain target location

We now address the situation where the targets to be positioned are known to lie in well defined uncertainty regions. The objective is to obtain an expedite numerical solution for the problem at hand. We assume the uncertainty in each target position is described by a given probability distribution function and we seek to maximize, by proper sensor placement, the average value of the

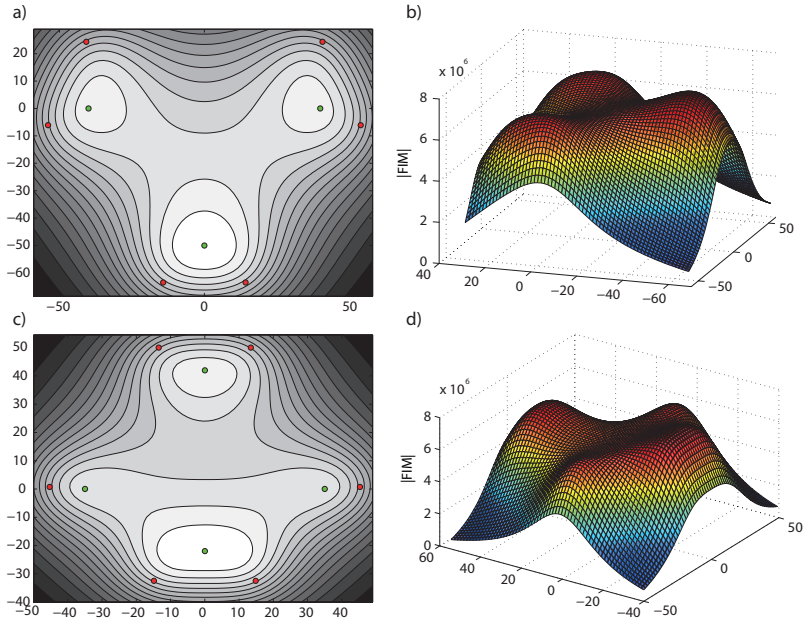

Figure 5.11: Optimal sensor configurations with $\eta = 0$ for 6 sensors and 3 targets, (a) and (b), and 4 targets, (c) and (d). $|FIM|_{\mathcal{D}}$ around the target positions in (a) and (c). Value of the FIM determinant in the plane of the target positions in (b) and (d). Sensors in red and targets in green. Lighter regions correspond to larger values of $|FIM|_{\mathcal{D}}$.

determinant of the FIM for the targets.

In what follows, $p_{i\xi}$; $i = 1, 2, ..., n$; $\xi = x, y, z$ denotes the $\xi - th$ coordinate of sensor i located at position p_i and $\overline{p} = [p_1^T, ..., p_n^T]^T$, $q_{k\xi}$; $k = 1, 2, ..., m$; $\xi = x, y, z$ denotes the $\xi - th$ coordinate of target k located at position q_k and $\overline{q} = [q_1^T, ..., q_m^T]^T$. We further denote by $\varphi(\overline{q})$; $\overline{q} \in \Re^{m\times 3}$ the probability density functions with support $D_{\overline{q}} \in \Re^3$ that describe the uncertainty in the position of the targets in region D. With this notation, the problem of optimal sensor placement can be cast in the form of finding a vector $\overline{p}^*$ such that

$$\overline{p}^* = arg \max_{\overline{p}} \int_D \log |FIM(\overline{p}, \overline{q})| \cdot \varphi(\overline{q})\, d\overline{q} \tag{5.18}$$

where we used the notation $|FIM(\overline{p}, \overline{q})|$ to clearly show the dependence of the FIM on the target and sensor locations. However, in the following $\log |FIM(\overline{p}, \overline{q})|$ will often be denoted simply as $|FIM_\lambda|$, as mentioned on the previous sections. In a real situation, $\varphi(\overline{q})$ will depend on the type of mission carried out by the targets. If the target k operates mostly in the centre of its working area, $\varphi(q_k)$ can for example assume the form of a truncated, radially-symmetric probabilistic Gaussian distribution centred at an appropriate point. On the other hand, if only the work area is known and the target k can operate anywhere inside it, $\varphi(q_k)$ can be taken as the unity function inside that area. Depending on the knowledge about the targets, each $\varphi(q_k)$, $k = 1, \cdots, m$, may be a different probability density function. In the most general set-up, the region D must be taken as the union of a number of disjoint regions $D_k; k = 1, 2, .., m$, where D_k is the work area of target k.

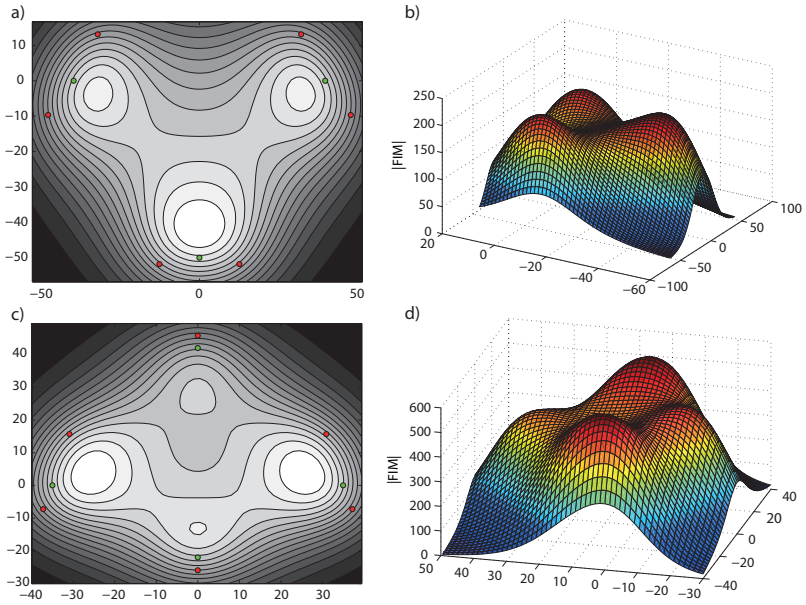

Figure 5.12: Optimal sensor configurations with $\eta = 0.1$ for 6 sensors and 3 targets, (a) and (b), and 7 sensors and 4 targets, (c) and (d). $|FIM|_{\mathcal{D}}$ around the target positions in (a) and (c). Value of the FIM determinant in the plane of the target positions in (b) and (d). Sensors in red and targets in green. Lighter regions correspond to larger values of $|FIM|_{\mathcal{D}}$.

It now remains to solve the optimization problem defined above. As explained later, we opted to use a gradient-based method to do so. To this effect, it is important to compute the derivatives of the integral in (5.18) with respect to the sensor coordinates, that is,

$$\frac{\partial}{\partial p_{i\xi}} \int_{D} |FIM_{\lambda}| \, \varphi(\overline{q}) d\overline{q} \tag{5.19}$$

for $i = 1, 2, ..., n$ and $\xi = x, y, z$.

To proceed with the computations, the integral and derivative operations are interchanged: the derivatives are explicitly determined first and the integration over region D is performed afterwards. The derivative can be computed in a recursive way using the equations of Appendix C for any number of targets. In what regards the computation of the triple integral over the region D of interest, however, this is virtually impossible to do analytically. The computation of the triple integral was obtained numerically using a Monte Carlo method. Finally, the solution of (5.18) is obtained using the gradient optimization method detailed in Section 5.4. Again, to overcome the possible occurrence of local maxima or the divergence of the algorithm, the initial guess in the iterative algorithm must be chosen with care. In the examples that we studied we found it useful and expedite to adopt as an initial guess the solution for the multiple target positioning problem described in this chapter, with the hypothetical targets placed at the centre of their corresponding work areas. It is important to stress that the solution to (5.18) depends strongly on the probability density function adopted for each of the target positions (e.g. a truncated, radially-symmetric probabilistic Gaussian distribution or a radially-symmetric step distribution, [39]).

5.6.1 Optimal sensor placement solutions in 3D

In this section an optimal sensor configuration scenario is studied to illustrate the methodology developed to define optimal sensor networks for multiple target positioning when the target positions are described by probability density functions. The simple examples studied search to shed light on the problem at hand, it does not pretend to be an exhaustive study but an explanation on how to apply the methodology developed in this chapter. For this reason the most simple scenario of two target positioning is considered although the procedure would be exactly the same for any number of sensors and targets.

In the problem at hand it is considered that the prior knowledge about the target positions is that they are placed inside two given volumes, so that the probability distribution functions that define the target positions inside these volumes are step-like distributions. Once the sensors are placed on the optimal positions that maximize the average log determinant, the target positions are known with larger accuracy than the prior one and then the sensors could track the movements of the targets to improve and to maintain large accuracy over the target positions.

We can think of a different problem with the same statement and solution. If we have a static sensor network and the work areas of the targets are known *a priori*, then the optimal sensor network is the one that maximizes the average logarithm of the FIM determinants inside these work areas. This problem is equivalent to position a single target that follows a known preplanned trajectory with a static sensor network.

The constant and distance-dependent covariance error cases are studied. The uncertainty regions for the two targets are defined by parallelepipeds whose dimensions are $80 \times 80 \times 80\ m^3$ defined by the limits $A_1 = [-250,\ -170;\ -40,\ 40;\ -40,\ 40]\ m$ and $A_2 = [170,\ 250;\ -40,\ 40;\ -40,\ 40]\ m$, where $A = [x_{min},\ x_{max};\ y_{min},\ y_{max};\ z_{min},\ z_{max}]\ m$.

Example 5.5: Constant covariance.

In this first example it is possible to define a sensor network that provides a very large accuracy inside the volumes of interest. The optimization process provides the optimal formation defined in Table 5.9.

Table 5.9: Target positions and optimal sensor positions for constant covariance.

	p_1	p_2	p_3	p_4	p_5	p_6
$\{x_I\}(m)$	289.8	0.2	−290.7	−290.8	−2.6	290.1
$\{y_I\}(m)$	−20	456.5	−18.6	−143.1	−590.8	−144
$\{z_I\}(m)$	261.7	−117.2	263.3	−222.1	151.6	−220.5

This formation provides $|FIM|_{max} = 8 \cdot 10^6\ m^{-6}$ and $|FIM|_{min} = 7.8037 \cdot 10^6\ m^{-6}$ as maximum and minimum FIM determinants inside the volumes of interest, respectively. We can notice how the maximum is the theoretical optimal FIM determinant and how the minimum is very close to this optimal value too. The average FIM determinant in the work areas is given by $|FIM|_{avg} = 7.9467 \cdot 10^6\ m^{-6}$, showing how the average accuracy is very close to the optimal one, providing a very good positioning of the targets inside the areas of interest. The maximum and minimum CRB trace are $tr(CRB)_{max} = 0.0153\ m^2$ and $tr(CRB)_{min} = 0.015\ m^2$, respectively, being the latter the theoretical optimal CRB trace.

Therefore it is possible to define optimal sensor configurations that provide large accuracy, close to the optimal one, inside the volumes of interest for constant covariance error. ■

Example 5.6: Distance-dependent covariance.

In this second example, where $\eta = 0.05$ and $\gamma = 1$, the sensor network that provides the largest accuracy inside the volumes of interest is defined by the points in Table 5.10.

Table 5.10: Target positions and optimal sensor positions for $\eta = 0.05$ and $\gamma = 1$.

	p_1	p_2	p_3	p_4	p_5	p_6
$\{x_I\}(m)$	208.7	−0.2	−209.1	−209.6	−2.4	208.8
$\{y_I\}(m)$	4.6	370.6	5.1	−5	−474.1	−4.7
$\{z_I\}(m)$	28	−92.9	27.7	−27.1	120.1	−27.7

This formation provides as maximum and minimum FIM determinants inside the volumes of interest $|FIM|_{max} = 270.6958\ m^{-6}$ and $|FIM|_{min} = 2.6213\ m^{-6}$, respectively. We can notice how the FIM determinants are quite smaller than the ones obtained in Example 5.5, and how the difference between the maximum and minimum value is large because of the distance-dependent added error. The average FIM determinant inside the work areas is given by $|FIM|_{avg} = 3.2662\ m^{-6}$, showing how the average accuracy is seriously affected by the error model considered. The maximum and minimum CRB trace are $tr(CRB)_{max} = 6.0312\ m^2$ and $tr(CRB)_{min} = 2.2129\ m^2$, respectively.

Therefore it is possible to define optimal sensor configurations that provide an homogeneus accuracy inside the volumes of interest, maximizing as much as possible the average log determinant. Of course, the accuracy required for each target will be mission-dependent. ■

5.6.2 Sensors lying on a plane: Underwater target positioning

In Chapter 4 it was commented that an interesting problem arises when the targets are known to lie anywhere in one or several volumes in the water column and one is free to distribute the sensors at the sea surface and at the sea-bottom. At this point, an interesting question arises: given the experimental conditions, should we place all the sensors in one plane (sea surface or sea-bottom), or distribute them between the two planes? In what follows we show, via a design example, how the circle of ideas exploited in the previous section can be used to solve this problem.

Suppose that 2 underwater targets operate inside a rectangular parallelepiped each, the two volumes with dimensions 80x60x60 meters and geometrical centre at 100 m depth. The limits of the areas are $A_1 = [-120,\ -40;\ -30,\ 30;\ -30,\ 30]\ m$ and $A_2 = [40,\ 120;\ -30,\ 30;\ -30,\ 30]\ m$, where the areas are defined by $A = [x_{min},\ x_{max};\ y_{min},\ y_{max};\ z_{min},\ z_{max}]\ m$. The sea bottom is 200 m deep. We consider two possible arrangements for a 6 sensor network. In the first case, depicted in Figure 5.13 (a), all sensors are placed at the sea surface. In the second case, illustrated in Figure 5.13 (b), 3 of the sensors are placed at the surface, while the others are placed at the sea-bottom.

Example 5.7: Constant covariance

We have seen in the examples along this chapter that for constant covariance it is possible to obtain sensor configurations that provide large accuracy for all the points in the region of interest. In this example we determine the surface sensor network that maximizes the average log determinant over the above areas and then we compare the accuracy obtained by the latter formation with the accuracy that provides the network for which 3 of the sensors are placed at the sea surface, while the others are placed on the sea-bottom.

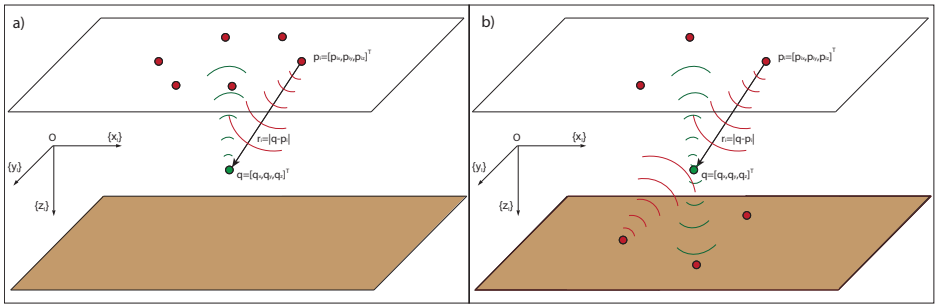

Figure 5.13: Maximization of the average FIM determinant inside a volume, with all the sensors placed in the same plane (a), or with the sensors distributed among two different parallel planes (b).

The first scenario tackles the arrangement of Figure 5.13 (a), a surface sensor network. The resultant sensor formation is placed at points shown in Table 5.11.

Table 5.11: Target positions and optimal sensor positions for constant covariance.

	p_1	p_2	p_3	p_4	p_5	p_6
$\{x_I\}(m)$	135.4	−1.5	−134.9	−135.5	1	134
$\{y_I\}(m)$	33.7	405.6	33.1	−33.6	−406.7	−32.9
$\{z_I\}(m)$	100	100	100	100	100	100

This resultant configuration provides inside the work areas a maximum and minimum FIM determinants given by $|FIM|_{max} = 8 \cdot 10^6\ m^{-6}$ and $|FIM|_{min} = 5.7 \cdot 10^6\ m^{-6}$, respectively, with an average value of $|FIM|_{avg} = 7.5241 \cdot 10^6\ m^{-6}$. We can notice how the maximum determinant corresponds to the theoretical optimal value and how the minimum determinant is large and close to the optimal value, providing a large average accuracy inside the volumes of interest. The maximum and minimum CRB trace are $tr(CRB)_{max} = 0.0193\ m^2$ and $tr(CRB)_{min} = 0.015\ m^2$, respectively.

Now we consider the arrangement depicted in Figure 5.13 (b). The optimal sensor is shown in Table 5.12.

Table 5.12: Target positions and optimal sensor positions for constant covariance.

	p_1	p_2	p_3	p_4	p_5	p_6
$\{x_I\}(m)$	122.2	−0.6	−122.7	−122.9	−0.2	122.1
$\{y_I\}(m)$	27.4	373	27.3	−27	−371.4	−26.9
$\{z_I\}(m)$	100	−100	100	−100	100	−100

The maximum and minimum FIM determinant are now $|FIM|_{max} = 8 \cdot 10^6\ m^{-6}$ and $|FIM|_{min} = 7.6994 \cdot 10^6\ m^{-6}$, respectively, with an average value of $|FIM|_{avg} = 7.8979 \cdot 10^6\ m^{-6}$. We can notice how the maximum determinant is again the theoretical optimal determinant, but in this case the minimum determinant is very close to this theoretical optimal value providing a very large accuracy over the work areas. The maximum and minimum CRB trace are $tr(CRB)_{max} = 0.0154\ m^2$ and $tr(CRB)_{min} = 0.015\ m^2$, respectively.

Therefore, for the constant covariance case, it is clear that if it is possible to place the sensor network in two different parallel planes the accuracy over the volumes of interest is improved in a

great manner.

Example 5.8: Distance-dependent covariance

The same two scenarios of Example 5.7 are now studied considering that the measurement error is distance-dependent and modelled by the parameters $\eta = 0.05$ and $\gamma = 1$.

The first scenario studies the optimal surface sensor formation of Figure 5.13 (a). After the optimization process the resultant optimal formation is the one shown in Table 5.13.

Table 5.13: Target positions and optimal sensor positions for $\eta = 0.05$ and $\gamma = 1$.

	p_1	p_2	p_3	p_4	p_5	p_6
$\{x_I\}(m)$	107.6	21.9	−88.7	−89.8	20.1	106.1
$\{y_I\}(m)$	43.9	61.6	47.8	−46.9	−61.8	−45.6
$\{z_I\}(m)$	100	100	100	100	100	100

This resultant configuration provides inside the work volumes a maximum and minimum FIM determinants given by $|FIM|_{max} = 87.2283\ m^{-6}$ and $|FIM|_{min} = 1.3473\ m^{-6}$, respectively, with an average value of $|FIM|_{avg} = 19.5355\ m^{-6}$. The maximum and minimum CRB trace are $tr(CRB)_{max} = 3.9155\ m^2$ and $tr(CRB)_{min} = 0.6920\ m^2$, respectively. We can notice how the accuracy over the areas of interest is seriously affected by the distances involved in the problem.

The second scenario of Figure 5.13 (b) in which 3 sensors are at the sea surface and the other 3 sensors are at the sea-bottom is studied now. The optimal sensor formation is listed in Table 5.14.

Table 5.14: Target positions and optimal sensor positions for $\eta = 0.05$ and $\gamma = 1$.

	p_1	p_2	p_3	p_4	p_5	p_6
$\{x_I\}(m)$	6	18.2	−24.4	−3.7	−15.9	18.4
$\{y_I\}(m)$	5.4	73.1	71.7	2.4	−71.2	−71.7
$\{z_I\}(m)$	−100	100	−100	100	−100	100

This resultant configuration provides inside the work volumes a maximum and minimum FIM determinants given by $|FIM|_{max} = 42.7823\ m^{-6}$ and $|FIM|_{min} = 6.1053\ m^{-6}$, respectively, with an average value of $|FIM|_{avg} = 20.4632\ m^{-6}$. The maximum and minimum CRB trace are $tr(CRB)_{max} = 2.1255\ m^2$ and $tr(CRB)_{min} = 0.9682\ m^2$, respectively. We can check how the maximum determinant is smaller in this latter case, however the minimum FIM determinant is larger and the average determinant is larger too. Therefore, although the maximum accuracy is reduced, the average accuracy and the minimum accuracy are larger, moreover, the FIM determinant inside the volumes of interest is more homogeneous than in the previous scenario.

Therefore, for distance-dependent covariance, the optimal formation will be clearly mission-dependent. If the maximum accuracy possible for some given points is searched then the first scenario is the correct one, but if we need an homogeneous accuracy for all the points inside the work volumes then the second scenario is the appropriate one.

5.7 Conclusions

We studied the problem of determining the optimal configuration of a sensor network that will, in a well defined sense, maximize the range-related information available for multiple underwater target positioning. To this effect, we assumed that the range measurements were corrupted by white Gaussian noise with distance-dependent covariance. In contrast to what has so far been published in the literature, we explicitly addressed the localization problem in 3D using a sensor array located at the sea surface (2D). Furthermore, we incorporate directly into the problem formulation the fact that multiple targets must be localized simultaneously. At the core of the techniques used are key concepts and methods from Pareto optimization and estimation theory. From a mathematical standpoint, the key problem that we solved was that of maximizing, by proper choice of the sensor geometric configuration, convex combinations of the logarithms of the determinants of the Fisher Information Matrices corresponding to estimation problems for each target separately. This was done by resorting to an iterative optimization algorithm. The methodology developed allows for an in depth study of the tradeoffs that are inherent to a multiple target localization problem. Simulation examples show clearly how the optimal sensor location depends on the size of the area in which the targets operate, on the type of measurement noise, and on the "level of importance" attached to each of the targets; the latter aims to capture the fact that tradeoffs are inevitable, and therefore different levels of accuracy may be required in the localization of the different targets.

Chapter 6

SINGLE TARGET POSITIONING IN 3D SCENARIOS WITH BEARING-ONLY MEASUREMENTS

6.1 Introduction

In previous chapters the general problem of single and multiple target positioning with range measurements in 2D and 3D scenarios has been studied, and analytical and numerical solutions of optimal sensor placements have been derived, paying special attention to the practical scenario of underwater target positioning by surface sensors. In the chapter at hand this analysis is extended to single underwater target positioning with noisy angle measurements. The chapter is focused on the underwater target positioning problem because this practical scenario allows for a well defined analytical solution.

As it has been explained along this work, a key element in the operation of some classes of AUVs is the availability of reliable underwater positioning systems to localize one or more vehicles simultaneously based on information received on-board a support ship or an autonomous surface system. The info thus obtained is at times used to follow the state of progress of a particular mission or, if reliable acoustic modems are available, to relay it as a navigation aid to the navigation systems existent on-board the AUV. In this sense, we address the problem of single target positioning based on measurements of the azimuth (bearing, in 2D scenarios) and elevation angles between an underwater target and a set of sensors, obtained via acoustic devices. In what follows we will refer to these measurements in 3D as AE (azimuth-elevation) measurements or, for simplicity, with an obvious abuse of notation, simply as bearing measurements. Speaking in loose terms, we are interested in determining the optimal configuration (formation) of a sensor network that will, in a well defined sense, maximize the AE-related information available for underwater target positioning. To this effect, we assume that the AE measurements are corrupted by white Gaussian noise, the variance of which is distance-dependent. The computation of the target position may be done by resorting to triangulation algorithms, based on the nature of the measurements.We recall that the

triangulation problem has been widely studied in the computer vision field, and that there exist many examples of algorithms to compute the position of a target using angle measurements; see for example [34] and [43] for an example of the design of motion-planning and sensor assignment strategies to track multiple targets with a mobile sensor network by resorting to triangulation.

When compared with other possible techniques commonly used for underwater target positioning, the problem of determining the optimal sensor placement for target localization using AE-only measurements is of special interest because no information flows from the sensor network to the target, and therefore its solution does not require the exchange of information between the target and the sensor network. Thus, AE-based strategies allow for the sensor network to observe without being detected itself. A problem of this type was studied in [57] for an unmanned underwater vehicle tracking an underwater target while avoiding detection. Given a localization strategy, the optimal sensor configuration can be ascertained by examining the corresponding Fisher Information Matrix (FIM) or its inverse, the so-called Cramer-Rao Bound (CRB) matrix. In this chapter, we use the trace of the CRB matrix as an indicator of the performance that is achievable with a given sensor configuration. Minimizing this quantity yields the most appropriate sensor formation geometry. It is important to remark that in many studies published in the literature on ground and marine robots, the determinant of the FIM is often used as an indicator of the type of positioning performance that can be achieved. For the problem that we tackle in this chapter this indicator is not adequate, as will be shown in Section 6.5. This is a simple consequence of the fact that the AE-measurements enter the FIM in such a way as to render its determinant extremely large for certain trigonometric configurations. However, the large value of the determinant is misleading since it corresponds to close-to-singular configurations of the network. This issue does not arise in 2D applications, see [10]. For interesting related work, the reader is also referred to [56], [15], [36], [53] and [61].

Motivated by previous results published in the literature, we address the problem of finding the optimal geometric configuration of a sensor formation for the localization of an underwater target, based on AE-only measurements. The optimality conditions for a generic sensor formation are defined, and the explicit optimal geometric configuration of a sensor formation based on AE-only measurements is studied for two different scenarios:

- The case in which the sensors lie on a sphere centred at the target position, which provides a simple example of how to define optimal sensor configurations for a given set of (physical or mission-related) constraints imposed on the sensor formation.
- The application scenario in which a surface-based sensor formation is defined for the localization of an underwater target. Notice that in this scenario the sensors are restricted to lie at the sea surface. A problem of this type was previously studied in [99], where a method to determine the optimal two-dimensional spatial placement of multiple sensors participating in a robot perception task was introduced. One of the scenarios considered was that of localizing an underwater vehicle, with the locations of the acoustic receivers constrained to lie in a horizontal plane.

The key contributions of the present chapter are threefold: i) global solutions to the optimal sensor configuration problem in 3D are obtained analytically *in the cases where the sensor network is restricted to lie on a sphere centred at the target position or on a plane*, the latter capturing the situation where the sensors are deployed at the sea surface; ii) in striking contrast to what is customary in the literature, where zero mean Gaussian processes with fixed variances are assumed for the measurements, the *variances are now allowed to depend explicitly on the distances between target and sensors*. This allows us to address explicitly the important fact (rooted in first physics principles) that the measurement noise may increase in a non-linear manner with distance; finally,

iii) the solutions derived are extended to the case where *a priori* knowledge about the target in 3D is given in terms of a probability density function. In this latter case it is virtually impossible to make a general analytical characterization of the optimal solutions, and one must resort to numerical search methods. At this stage, an in-depth understanding of the types of solutions obtained for the ideal case in which the target position is known in advance is of the utmost importance to compute an initial guess for the optimal sensor placement algorithm adopted.

The document is organized as follows. Section 6.2 derives the FIM for AE-measurements when the measurement noise is Gaussian, with distance-dependent variance. The optimal Fisher Information Matrix that minimizes the trace of the corresponding CRB matrix is computed in Section 6.3. The optimal sensor configuration is defined explicitly for the case in which the sensors lie on a sphere centred at the target position in Section 6.4. In Section 6.5, the optimal sensor placement is computed in the context of a sensor network restricted to lie on a plane and two illustrative scenarios are shown as examples. In Section 6.6, the optimal sensor placement problem is solved for the case where the prior knowledge about the target in 3D is given in terms of a probability density function. Finally, the conclusions are included in Section 6.7.

6.2 The Fisher Information Matrix and the Cramer-Rao Lower Bound

The same notation of previous chapters is adopted. In what follows, $\{I\}$ denotes an inertial frame with unit axis $\{x_I\}$, $\{y_I\}$, and $\{z_I\}$ defined according to the notation that is customary in marine systems, see Fig. 6.1. Let $q = [q_x, q_y, q_z]^T$ be the position of the target to be positioned in $\{I\}$. Further denote by $p_i = [p_{ix}, p_{iy}, p_{iz}]^T$; $i = 1, 2, .., n$, the position vector of the $i-th$ acoustic sensor, also in $\{I\}$, where n is the number of sensors. Define $\overline{r_i}(q)$ as the range vector from the $i-th$ sensor to the target located at q, and let $r_i(q) = |q - p_i|$ (abbv. r_i), where $|\cdot|$ denotes the Euclidean norm, denote the corresponding vector length (that is, range between the sensor and the target).

To each of the acoustic sensors at the surface we attach a parallel translation of $\{I\}$. Furthermore, for each sensor $i = 1, 2, .., n$ we define $z_i(q) = (\alpha_i, \beta_i)^T$, where α_i and β_i are the AE angles that define the direction of the target with respect to the sensor location. As is customary, the elevation β is the angle between the range vector and the $\{x_I y_I\}$ plane, while the azimuth α is the angle between the projection of the range vector in the $\{x_I y_I\}$ plane and the $\{x_I\}$ axis; see Fig. 6.1. Stated mathematically,

$$\begin{aligned} \alpha_i &= atan2\left(q_y - p_{iy}, q_x - p_{ix}\right) \\ \beta_i &= atan2\left(q_z - p_{iz}, \sqrt{(q_x - p_{ix})^2 + \left(q_y - p_{iy}\right)^2}\right) \end{aligned} \tag{6.1}$$

where *atan*2 is a variation of the arctangent function to distinguish between diametrically opposite directions. We denote by z_i the measurements of the actual AE angles α_i and β_i in $z_i(q)$, corrupted by additive noise $\left(\omega_{\alpha i}, \omega_{\beta i}\right)^T$.

For analytical tractability, it is commonly assumed that measurement errors can be described as Gaussian, zero mean additive noise with constant covariance. See for example [99], where different noise covariances are taken for different range sensors, but the covariances are constant. Clearly, the latter assumption is artificial, in view of the simple fact that the "level of noise" is distance dependent. We can assume that the measurement noise can be modelled by a zero-mean Gaussian process with an added term that depends on the distance (range) between the sensor and the target.

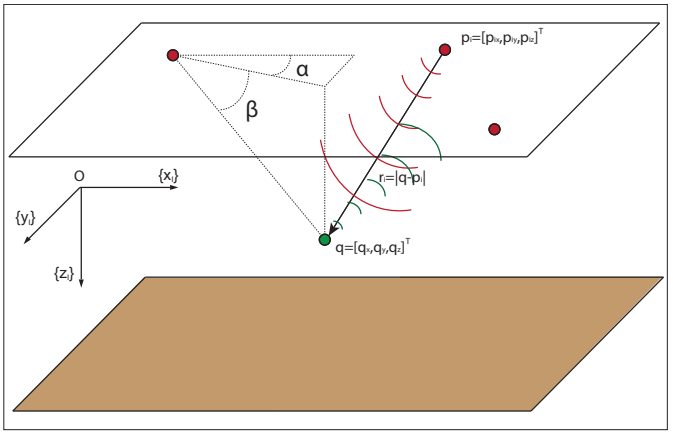

Figure 6.1: Elevation and azimuth angles measured in the inertial coordinate frame used in marine systems.

A similar error model is considered in [42] for range measurements. Stated mathematically, for an arbitrary sensor i the associated measurement noise ω_i is given by

$$\omega_i = \left(\omega_{\alpha i}, \omega_{\beta i}\right)^T = \left(\omega_{\alpha_0} \cdot \left(1 + \eta r_i^{\gamma}\right), \omega_{\beta_0} \cdot \left(1 + \eta r_i^{\gamma}\right)\right)^T \tag{6.2}$$

where ω_α and ω_β are noises associated with the azimuth and elevation angle measurements, respectively, ω_{β_0} and ω_{α_0} are zero mean Gaussian processes described by the probability density function $N(0, \Sigma_0)$ with $\Sigma_0 = \sigma^2 \cdot I$, I is the identity matrix, r is range, and η and γ are modelling parameters of the distance-dependent noise component. For simplicity of exposition, and without loss of generality, the noises in the measurements of α_i and β_i are assumed to have identical distributions. We further assume that the distributions are identical for all sensors.

Define $z(q) = \left(z_1(q)^T, ..., z_n(q)^T\right)^T$, $z = \left(z_1^T, ..., z_n^T\right)^T$, and $\omega = \left(\omega_1^T, ..., \omega_n^T\right)^T$. With this notation, the collection of all AE angle measurements obtained from all the sensors can be written as

$$z = z(q) + \omega \tag{6.3}$$

or equivalently, in component form

$$z_i = (\alpha_i, \beta_i)^T + \left(\omega_{\alpha i}, \omega_{\beta i}\right)^T \tag{6.4}$$

where ω is a Gaussian process with covariance matrix

$$\Sigma = \delta\left(\left(\sigma_\alpha^2 \cdot \left(1 + \eta r_1^{\gamma}\right)^2, \sigma_\beta^2 \cdot \left(1 + \eta r_1^{\gamma}\right)^2\right), ..., \left(\sigma_\alpha^2 \cdot \left(1 + \eta r_n^{\gamma}\right)^2, \sigma_\beta^2 \cdot \left(1 + \eta r_n^{\gamma}\right)^2\right)\right) \tag{6.5}$$

with $\Sigma \in \Re^{2nx2n}$ and δ is the operator *diag* that converts a vector into a square diagonal matrix whose diagonal components are the array elements.

Stated in simple terms, the FIM captures the amount of information that measured data provide about an unknown parameter (or vector of parameters) to be estimated. Under known assumptions, the FIM is the inverse of the Cramer-Rao Bound matrix (abbv. CRB), which lower bounds the covariance of the estimation error that can possibly be obtained with any unbiased estimator. Thus, "minimizing the CRB" may yield (by proper estimator selection) a decrease of uncertainty in the

parameter estimation.

Formally, let $\hat{q}(z)$ be any unbiased estimator of q, that is, a mapping $\hat{q} : \Re^n \rightarrow \Re^3$ between the observations z and the target position space such that $E\{\hat{q}\} = q$ for all $q \in \Re^3$, where $E\{\cdot\}$ denotes the average operator. Let $p_q(z)$ be the likelihood function that defines the probability of obtaining the observation z given that the true target position is q. It is well known that under some regularity conditions on $p_q(z)$ the following inequality holds:

$$Cov\{\hat{q}\} \geq FIM(q)^{-1} = CRB(q) \tag{6.6}$$

where

$$Cov\{\hat{q}\} = E\{(\hat{q} - q)(\hat{q} - q)^T\}, \tag{6.7}$$

FIM (q) (often abbreviated simply as FIM) is the Fisher Information Matrix defined as

$$FIM(q) = E\left\{(\nabla_q \log p_q(z))(\nabla_q \log p_q(z))^T\right\}, \tag{6.8}$$

and $CRB(q)$ is the Cramer-Rao Bound matrix. In the above, $\nabla_q \log p_q$ denotes the gradient of the log of the likelihood function with respect to the unknown parameter q. Taking the trace of both sides of the covariance inequality yields

$$var\{\hat{q}\} := tr(Cov\{\hat{q}\}) = tr(E\{(\hat{q} - q)(\hat{q} - q)^T\}) \geq tr(CRB(q)) \tag{6.9}$$

that sets a lower bound on the mean-square error of any unbiased estimator.

From the above notation, following standard procedures, the FIM is computed from the likelihood function

$$p_q(z) = \frac{1}{(2\pi)^{\frac{n}{2}} |\Sigma|^{\frac{1}{2}}} \exp\left\{-\frac{1}{2}(z - z(q))^T \Sigma^{-1} (z - z(q))\right\} \tag{6.10}$$

where n is the number of receivers, z is the vector of measured angles, and $z(q)$ the vector of actual angles. From (6.8),

$$FIM = E\left\{\nabla_q \log p_q \cdot \nabla_q \log p_q^T\right\} = F^T \Sigma^{-1} F, \tag{6.11}$$

with

$$F = \begin{bmatrix} \frac{-\sin(\alpha_1)}{r_1 \cos(\beta_1)} & \frac{\cos(\alpha_1)}{r_1 \cos(\beta_1)} & 0 \\ \frac{-\sin(\beta_1)\cos(\alpha_1)}{r_1} & \frac{-\sin(\beta_1)\sin(\alpha_1)}{r_1} & \frac{-\cos(\beta_1)}{r_1} \\ \vdots & \vdots & \vdots \\ \frac{-\sin(\alpha_n)}{r_n \cos(\beta_n)} & \frac{\cos(\alpha_n)}{r_n \cos(\beta_n)} & 0 \\ \frac{-\sin(\beta_n)\cos(\alpha_n)}{r_n} & \frac{-\sin(\beta_n)\sin(\alpha_n)}{r_n} & \frac{-\cos(\beta_n)}{r_n} \end{bmatrix} \tag{6.12}$$

where $F \in \Re^{2nx3}$ and $CRB = FIM^{-1}$. In this context, the optimal sensor placement strategy for a single vehicle localization problem is obtained by minimizing the trace of the CRB.

6.3 Optimal Fisher Information Matrix

To compute the trace of the CRB matrix it is convenient to introduce the following three vectors in $\Re^{2n}$:

$$\mathrm{X} = \left[\begin{array}{cccc} \frac{F(1,1)}{\sigma\left(1+\eta r_1^{\gamma}\right)} & \frac{F(2,1)}{\sigma\left(1+\eta r_1^{\gamma}\right)} & \cdots & \frac{F(n-1,1)}{\sigma\left(1+\eta r_n^{\gamma}\right)} \quad \frac{F(n,1)}{\sigma\left(1+\eta r_n^{\gamma}\right)} \end{array} \right],$$

$$\Upsilon = \left[\begin{array}{cccc} \frac{F(1,2)}{\sigma\left(1+\eta r_1^{\gamma}\right)} & \frac{F(2,2)}{\sigma\left(1+\eta r_1^{\gamma}\right)} & \cdots & \frac{F(n-1,2)}{\sigma\left(1+\eta r_n^{\gamma}\right)} \quad \frac{F(n,2)}{\sigma\left(1+\eta r_n^{\gamma}\right)} \end{array} \right], \tag{6.13}$$

$$\mathrm{Z} = \left[\begin{array}{cccc} \frac{F(1,3)}{\sigma\left(1+\eta r_1^{\gamma}\right)} & \frac{F(2,3)}{\sigma\left(1+\eta r_1^{\gamma}\right)} & \cdots & \frac{F(n-1,3)}{\sigma\left(1+\eta r_n^{\gamma}\right)} \quad \frac{F(n,3)}{\sigma\left(1+\eta r_n^{\gamma}\right)} \end{array} \right].$$

The latter should be viewed as vectors of a Hilbert space with elements in $\Re^{2n}$, endowed with an inner product structure $<,>$. This allows for the computation of the length of a vector and also for the angle between two vectors. Namely, given X and Υ in $\Re^{2n}$, then $|\mathrm{X}|^2 =< \mathrm{X}, \mathrm{X} >$ and $< \mathrm{X}, \Upsilon >= |\mathrm{X}||\Upsilon| \cos(\theta_{\mathrm{X}\Upsilon})$, from which it follows that the angle $\theta_{\mathrm{X}\Upsilon}$ between vectors X and Υ is given by $\theta_{\mathrm{X}\Upsilon} = \cos^{-1}(< \mathrm{X}, \Upsilon > /(|\mathrm{X}||\Upsilon|))$.

With this notation, the FIM becomes

$$FIM = \left(\begin{array}{ccc} \mathrm{X}\cdot\mathrm{X} & \mathrm{X}\cdot\Upsilon & \mathrm{X}\cdot\mathrm{Z} \\ \mathrm{X}\cdot\Upsilon & \Upsilon\cdot\Upsilon & \Upsilon\cdot\mathrm{Z} \\ \mathrm{X}\cdot\mathrm{Z} & \Upsilon\cdot\mathrm{Z} & \mathrm{Z}\cdot\mathrm{Z} \end{array} \right) = \left(\begin{array}{ccc} |\mathrm{X}|^2 & |\mathrm{X}|\,|\Upsilon| \cos\left(\theta_{\mathrm{X}\Upsilon}\right) & |\mathrm{X}|\,|\mathrm{Z}| \cos\left(\theta_{\mathrm{X}\mathrm{Z}}\right) \\ |\mathrm{X}|\,|\Upsilon| \cos\left(\theta_{\mathrm{X}\Upsilon}\right) & |\Upsilon|^2 & |\Upsilon|\,|\mathrm{Z}| \cos\left(\theta_{\Upsilon\mathrm{Z}}\right) \\ |\mathrm{X}|\,|\mathrm{Z}| \cos\left(\theta_{\mathrm{X}\mathrm{Z}}\right) & |\Upsilon|\,|\mathrm{Z}| \cos\left(\theta_{\Upsilon\mathrm{Z}}\right) & |\mathrm{Z}|^2 \end{array} \right), \tag{6.14}$$

from which it follows that

$$\begin{aligned} tr\left(CRB\right) = tr\left(FIM^{-1}\right) = & \frac{|\Upsilon|^2 |\mathrm{Z}|^2 \left(1 - \cos^2\left(\theta_{\Upsilon\mathrm{Z}}\right)\right)}{|FIM|} \\ & + \frac{|\mathrm{X}|^2 |\mathrm{Z}|^2 \left(1 - \cos^2\left(\theta_{\mathrm{X}\mathrm{Z}}\right)\right)}{|FIM|} + \frac{|\Upsilon|^2 |\mathrm{X}|^2 \left(1 - \cos^2\left(\theta_{\mathrm{X}\Upsilon}\right)\right)}{|FIM|}, \end{aligned} \tag{6.15}$$

where $\theta_{\mathrm{X}\Upsilon}$, $\theta_{\mathrm{X}\mathrm{Z}}$ and $\theta_{\Upsilon\mathrm{Z}}$ are the angles defined by vectors X and Υ, X and Z, and Υ and Z, respectively, and $|FIM|$ denotes the determinant of the FIM. Straightforward computations show that

$$|FIM| = |\mathrm{X}|^2 \cdot |\Upsilon|^2 \cdot |\mathrm{Z}|^2 \cdot \Theta, \tag{6.16}$$

where

$$\Theta = 1 + 2\cos\left(\theta_{\Upsilon\mathrm{Z}}\right)\cos\left(\theta_{\mathrm{X}\mathrm{Z}}\right)\cos\left(\theta_{\mathrm{X}\Upsilon}\right) - \cos^2\left(\theta_{\Upsilon\mathrm{Z}}\right) - \cos^2\left(\theta_{\mathrm{X}\mathrm{Z}}\right) - \cos^2\left(\theta_{\mathrm{X}\Upsilon}\right) \tag{6.17}$$

Notice how $tr\left(CRB\right)$ has been expressed in terms of the norms of vectors X, Υ, and Z and the angles $\theta_{\mathrm{X}\Upsilon}$, $\theta_{\mathrm{X}\mathrm{Z}}$, and $\theta_{\Upsilon\mathrm{Z}}$ between them. The latter depend on the variables $\alpha_i, \beta_i, r_i; i = 1, 2, ...n$, that define the positions of the sensors with respect to the target. Formally, in order to seek conditions that the optimal sensor configurations must satisfy in order to minimize $tr\left(CRB\right)$, one could compute the derivatives of $tr\left(CRB\right)$ with respect to α_i, β_i, and r_i and equate them to zero. This task is tedious and will not shed light on the form of the optimal sensor configurations. We therefore follow a different approach. To this effect, we rewrite (6.15) as

$$tr(CRB) = f_{FIM}^1 + f_{FIM}^2 + f_{FIM}^3 = \frac{\left(1 - \cos^2\left(\theta_{\Upsilon\mathrm{Z}}\right)\right)}{|\mathrm{X}|^2\,\Theta} + \frac{\left(1 - \cos^2\left(\theta_{\mathrm{X}\mathrm{Z}}\right)\right)}{|\Upsilon|^2\,\Theta} + \frac{\left(1 - \cos^2\left(\theta_{\mathrm{X}\Upsilon}\right)\right)}{|\mathrm{Z}|^2\,\Theta} \tag{6.18}$$

where the definitions of f_{FIM}^1, f_{FIM}^2, and f_{FIM}^3 are obvious. We also define the auxiliary cost function

$$f^*(CRB) = f^{1*}_{FIM} + f^{2*}_{FIM} + f^{3*}_{FIM} = \frac{1}{|\mathrm{X}|^2} + \frac{1}{|\Upsilon|^2} + \frac{1}{|\mathrm{Z}|^2} \tag{6.19}$$

Consider now the problem of minimizing $f^*(CRB)$ by proper choice of α_i, β_i, and $r_i; i = 1, 2, ..., n$, and let α_i^*, β_i^*, and $r_i^*; i = 1, 2, ..., n$, be a minimizing solution. Let X^*, Υ^*, and Z^* be the corresponding vectors in $\Re^{2n}$. Suppose also that the corresponding angles $\theta^*_{\mathrm{X}\Upsilon}$, θ^*_{XZ}, and $\theta^*_{\Upsilon\mathrm{Z}}$ satisfy

$$\cos(\theta^*_{\mathrm{X}\Upsilon}) = \cos(\theta^*_{\mathrm{XZ}}) = \cos(\theta^*_{\Upsilon\mathrm{Z}}) = 0. \tag{6.20}$$

Then, as will shown next, α_i^*, β_i^*, and $r_i^*; i = 1, 2, ..., n$ minimize also (6.18). To see this, consider each of the three functions in (6.18) independently. Take for example the function f^1_{FIM}. Clearly, if the angles $\theta^*_{\mathrm{X}\Upsilon}$, θ^*_{XZ}, and $\theta^*_{\Upsilon\mathrm{Z}}$ are equal to $k \cdot \pi/2$, where k is any odd natural number, then they satisfy (6.20) and the above function takes the value $f^1_{FIM} = 1/|\mathrm{X}|^2$. We now show that this is its minimum possible value. In fact, suppose that a smaller value can be obtained, which clearly requires that

$$\frac{\left(1 - \cos^2(\theta_{\Upsilon\mathrm{Z}})\right)}{\Theta} < 1. \tag{6.21}$$

The above inequality is equivalent to

$$0 < 2\cos(\theta_{\Upsilon\mathrm{Z}})\cos(\theta_{\mathrm{XZ}})\cos(\theta_{\mathrm{X}\Upsilon}) - \cos^2(\theta_{\mathrm{XZ}}) - \cos^2(\theta_{\mathrm{X}\Upsilon}). \tag{6.22}$$

Notice, however that because $\cos^2(\theta_{\mathrm{XZ}}) + \cos^2(\theta_{\mathrm{X}\Upsilon}) \geq 2\cos(\theta_{\mathrm{XZ}})\cos(\theta_{\mathrm{X}\Upsilon})$ and $0 \leq |\cos(\theta_{\Upsilon\mathrm{Z}})| \leq 1$, it follows that

$$\cos^2(\theta_{\mathrm{XZ}}) + \cos^2(\theta_{\mathrm{X}\Upsilon}) \geq 2\cos(\theta_{\Upsilon\mathrm{Z}})\cos(\theta_{\mathrm{XZ}})\cos(\theta_{\mathrm{X}\Upsilon})$$

which contradicts (6.22). Therefore,

$$\frac{\left(1 - \cos^2(\theta_{\Upsilon\mathrm{Z}})\right)}{\Theta} \geq 1, \tag{6.23}$$

and its minimum value of 1 is obtained when all the angles are equal to $k \cdot \pi/2$, with k being an odd natural number. By applying the same reasoning to the other terms in the trace of the CRB in (6.18) it follows, under the assumptions stated, that the optimal FIM is a diagonal matrix, that is,

$$FIM = \begin{pmatrix} \mathrm{XX} & \mathrm{X}\Upsilon & \mathrm{XZ} \\ \mathrm{X}\Upsilon & \Upsilon\Upsilon & \Upsilon\mathrm{Z} \\ \mathrm{XZ} & \Upsilon\mathrm{Z} & \mathrm{ZZ} \end{pmatrix} = \sum_{i=1}^{n} \begin{bmatrix} A_i & 0 & 0 \\ 0 & B_i & 0 \\ 0 & 0 & C_i \end{bmatrix} \tag{6.24}$$

with

$$A_i = \frac{\sin^2(\alpha_i)}{r_i^2\cos^2(\beta_i)\cdot\sigma^2\cdot\left(1+\eta r_i^\gamma\right)^2} + \frac{\sin^2(\beta_i)\cos^2(\alpha_i)}{r_i^2\cdot\sigma^2\cdot\left(1+\eta r_i^\gamma\right)^2},$$

$$B_i = \frac{\cos^2(\alpha_i)}{r_i^2\cos^2(\beta_i)\cdot\sigma^2\cdot\left(1+\eta r_i^\gamma\right)^2} + \frac{\sin^2(\beta_i)\sin^2(\alpha_i)}{r_i^2\cdot\sigma^2\cdot\left(1+\eta r_i^\gamma\right)^2},$$

$$C_i = \frac{\cos^2(\beta_i)}{r_i^2\cdot\sigma^2\cdot\left(1+\eta r_i^\gamma\right)^2}.$$

With the above assumption on the general form that the simplified FIM matrix will take, we now introduce a simple general procedure to derive conditions for optimal sensor placement that lend

themselves to clear geometric interpretations. To this effect, define $A = \sum_{i=1}^{n} A_i$, $B = \sum_{i=1}^{n} B_i$, $C = \sum_{i=1}^{n} C_i$. With this notation, the problem at hand can be converted into that of computing

$$\overline{p}^{*} = arg\min_{\overline{p}} tr\,(CRB) = arg\min_{\overline{p}} tr\left(FIM^{-1}\right) = arg\min_{\overline{p}}\left(\frac{1}{A}+\frac{1}{B}+\frac{1}{C}\right) \tag{6.25}$$

where $\overline{p} = [p_1^T, ..., p_n^T]^T$, and $\overline{p}^{*}$ are the optimal sensor positions expressed in spherical coordinates, that is, $p_i^T = [\alpha_i, \beta_i, r_i]$. Notice that the sensor positions $\overline{p}^{*}$ must satisfy the additional constraint imposed by inequality (6.20), i.e., the angles $\theta_{X\Upsilon}$, θ_{XZ}, and $\theta_{\Upsilon Z}$ must be equal to $k \cdot \pi/2$ for some odd natural number k which, as explained, makes the off-diagonal elements of (6.24) equal to 0.

Formally, the conditions that an optimal sensor configuration must satisfy may now be obtained by computing the derivatives of (6.25) with respect to α_i, β_i, and r_i; $i = 1, 2, ..., n$ and equating them to 0. The candidate solutions must also satisfy (6.20). This will naturally yield multiple optimal sensor configurations for single target positioning if no extra constraints are placed on the sensor configuration. To make the problem tractable, it is therefore important to impose configuration constraints rooted in operational considerations. In what follows, the methodology adopted is illustrated with two representative design examples: i) first, by considering that the sensors are restricted to lie at the same distance from the target, that is, $r_i = r$ for all $i = 1, \cdots, n$, and ii) second, by considering that the sensors are restricted to lie in a horizontal plane, i. e., $q_z - p_{iz} = q_z$ where q_z is the target depth and $p_{iz} = 0$. The latter example captures the very important situation where the sensors are placed at the sea surface. The procedure adopted can of course be used to deal with other types of constraints on sensor placement.

6.4 Sensors placed at a fixed distance from the target

This section shows how the incorporation of physical or mission-related constraints on the positions of the sensors leads to a methodology to determine a solution to the optimal sensor placement that eschews tedious computations and lends itself to a simple geometric interpretation. To this effect, we consider the situation where all the sensors are placed on a sphere centred at the target position, that is, the distances from the sensors to the target are equal. With this assumption, $r_i = r; i = 1, \cdots, n$, where r is the radius of the sphere. In this case, the diagonal elements of the optimal Fisher Information Matrix (6.24) can be written as

$$\begin{aligned}
A &= \frac{1}{r^2\cdot\sigma^2\cdot(1+\eta r^{\gamma})^2}\sum_{i=1}^{n}\left(\frac{\sin^2(\alpha_i)}{\cos^2(\beta_i)} + \sin^2(\beta_i)\cos^2(\alpha_i)\right) = \Gamma A^{*},\\
B &= \frac{1}{r^2\cdot\sigma^2\cdot(1+\eta r^{\gamma})^2}\sum_{i=1}^{n}\left(\frac{\cos^2(\alpha_i)}{\cos^2(\beta_i)} + \sin^2(\beta_i)\sin^2(\alpha_i)\right) = \Gamma B^{*},\\
C &= \frac{1}{r^2\cdot\sigma^2\cdot(1+\eta r^{\gamma})^2}\sum_{i=1}^{n}\cos^2(\beta_i) = \Gamma C^{*},
\end{aligned} \tag{6.26}$$

where $\Gamma = \frac{1}{r^2\cdot\sigma^2\cdot(1+\eta r^{\gamma})^2}$ is constant and the same for all sensors in the formation and A^{*}, B^{*}, C^{*} are defined in the obvious manner. With the notation introduced, the problem of optimal sensor

placement can be cast in the form of finding a vector $\overline{p}^*$ such that

$$\overline{p}^* = arg \min_{\overline{p}} tr(CRB) = arg \min_{\overline{p}} \left(\frac{1}{A^*} + \frac{1}{B^*} + \frac{1}{C^*} \right) \tag{6.27}$$

It is important to notice that for this scenario the optimal solutions corresponding to constant or distance-dependent measurement noise covariances are identical. In fact, the solutions depend only on the azimuth and elevation angles of each sensor with respect to the target location, and the distance between target and sensors does not affect the solutions (distance is the constraint parameter). This fact does not hold true in the practical scenario of surface sensor networks, as will be shown in Section 6.5, where the optimal solutions depend explicitly on the range distances between target and sensors and on the noise model. At this point, the derivatives of (6.27) with respect to α_i and β_i must be computed and equated to 0. Straightforward manipulations yield

$$\frac{\partial (tr\,(CRB))}{\partial \alpha_i} = 2 \cos(\alpha_i) \sin(\alpha_i) \cdot \left(\frac{1}{\cos^2(\beta_i)} - \sin^2(\beta_i) \right) \left(A^{*2} - B^{*2} \right) = 0, \tag{6.28}$$

$$\begin{aligned} \frac{\partial (tr\,(CRB))}{\partial \beta_i} =& 2 \sin(\beta_i) \left(\left(\frac{\sin^2(\alpha_i)}{\cos^3(\beta_i)} + \cos(\beta_i) \cos^2(\alpha_i) \right) \frac{1}{A^{*2}} + \right. \\ & \left. \frac{1}{B^{*2}} \left(\frac{\cos^2(\alpha_i)}{\cos^3(\beta_i)} + \cos(\beta_i) \sin^2(\alpha_i) \right) - \left(\frac{\cos(\beta_i)}{C^{*2}} \right) \right) = 2 \sin(\beta_i)\, \Phi = 0, \end{aligned} \tag{6.29}$$

where the definition of Φ is clear from the context. By examining (6.28) and (6.29) it is possible to define several configurations. For this reason, and because the purpose of this section is to derive a general methodology to obtain optimal sensor configurations under suitable constraints on sensor placement we will illustrate the procedure by examining solutions that are relatively easy to obtain. Clearly, (6.28) is satisfied if at least one of the following conditions holds: i) $\cos(\alpha_i) = 0$; ii) $\sin(\alpha_i) = 0$; iii) $A^{*2} = B^{*2}$. Similarly, (6.29) is satisfied if i) $\Phi = 0$ or ii) $\sin(\beta_i) = 0$. The last condition is not studied in detail because, if all the sensors are placed such that $\sin(\beta_i) = 0$, it can be shown that the condition yields a local maximum for $tr(CRB)$.Thus, in what follows, we consider that the optimality condition for (6.29) is $\Phi = 0$. However, it is important to keep in mind that alternative optimal solutions could be defined by combination of different optimal formations. Let us now examine the conditions corresponding to (6.28).

If $\cos(\alpha_i) = 0$ for all sensors in the formation, then this means that all sensors are placed in the same vertical plane, $\{y_I z_I\}$, and therefore (6.29) becomes:

$$\cos^4(\beta_i) = \frac{C^{*2} B^{*2}}{A^{*2}(B^{*2} - C^{*2})}. \tag{6.30}$$

The above equation only holds for a single value of $\cos^4(\beta_i)$ since A^{*2}, B^{*2}, and C^{*2} are constant for a given optimal configuration and (6.30) must be satisfied for every sensor in the formation. Thus, (6.30) implies that the elevation angle for all elements of the sensor network must be $\pm\beta$ which, together with $\cos(\alpha_i) = 0$; $i = 1, \cdots, n$, defines 4 feasible optimal points for sensor placement. Clearly, this solution cannot be generalized for an arbitrary number of sensors. Furthermore, the analysis of $tr(CRB)$ with the previous conditions shows that this solution yields a local maximum and is equivalent to having $\sin(\beta_i) = 0$ for $i = 1, \cdots, n$; thus, the solution is discarded.

Consider now the case where $\sin(\alpha_i) = 0$ for each sensor in the formation. In this case, the

sensors are placed in the vertical plane $\{x_I z_I\}$ and (6.29) yields

$$\cos^4(\beta_i) = \frac{C^{*2}A^{*2}}{B^{*2}(A^{*2} - C^{*2})}. \tag{6.31}$$

A similar reasoning to that used in the previous case allows for the conclusion that this solution must also be discarded.

Finally if $\cos(\alpha_i) = 0$ or $\sin(\alpha_i) = 0$ holds for every sensor, the solution only defines a small number of optimal points for the sensor placement, so the solution cannot be generalized for an arbitrary number of sensors. Moreover, for this solution $A^* = B^*$. Therefore, $A^* = B^*$ is one of the conditions that an optimal sensor network must satisfy. Moreover, this solution can be easily generalized for an arbitrary number of sensors. Analyzing (6.30) with $A^* = B^* = D^*$ for some D^* yields

$$C^{*2} = D^{*2}\frac{\cos^4(\beta_i)}{1 + \cos^4(\beta_i)} \tag{6.32}$$

It must be noticed that (6.32) must hold for each and every sensor for a given optimal formation, since A^*, B^*, and C^* are constant for that given formation. Equation (6.32) can be rewritten as,

$$C^{*2} = D^{*2}\frac{1}{1 + \Omega} \tag{6.33}$$

where $\Omega = \frac{1}{\cos^4(\beta_i)}$. Considering that an arbitrary sensor i can be under or above the target, the angle β_i can take values between $[-\pi/2, \pi/2]$. In the interval $[-\pi/2, 0]$, Ω is strictly decreasing and thus $\frac{1}{1+\Omega}$ is strictly increasing, so that (6.33) only holds for a single value of the elevation angle $\beta = \beta_1^*$, the same angle for all the sensors placed under the target position. In the interval $[0, \pi/2]$, Ω is strictly increasing and thus $\frac{1}{1+\Omega}$ is strictly decreasing, so that, in the same way as before, (6.33) only holds for a single value of the elevation angle $\beta = \beta_2^*$, the same for all the sensors placed above the target position. Furthermore, since A^*, B^*, and C^* are fixed for a given sensor formation then $\beta_1^* = -\beta_2^*$. It is clear that a given value of β defines a circumference on the sphere where the sensors lie, with the radius (and height, $q_z - p_{iz}$) depending on the given angle β. Thus, from $\beta_1^* = -\beta_2^*$, the sensors are placed in two parallel planes over two circumferences centred at the target projections over these planes.

To define β regardless of the sensor distribution over the resulting circumferences, we proceed by adding the square root of (6.33), with $D^* = A^*$, to the square root of (6.33) with $D^* = B^*$. When doing so, all the terms in α_i are cancelled and one obtains

$$2n\cos^2(\beta_i) = \left(\frac{n}{\cos^2(\beta)} + n\sin^2(\beta)\right)\sqrt{\frac{\cos^4(\beta)}{1 + \cos^4(\beta)}} \tag{6.34}$$

Equation (6.34) has a single valid solution, $\beta = 42.40$ degrees, and thus the radius of the two parallel circumferences is equal to $r \cdot \cos(\beta)$. From the above, the values of A, B and C, and therefore the norms of the vectors X, ϒ and Z, are well defined. Once these values of the norms of the vectors are well defined, the extra conditions to be specified are that $A^* = B^*$ and that the off-diagonal

elements of the FIM are equal to 0 (or equivalently $\cos(\theta_{XY}) = \cos(\theta_{XZ}) = \cos(\theta_{YZ}) = 0$), that is:

$$\begin{aligned} FIM_{12} &= \sum_{i=1}^{n} \frac{\sin(\alpha_i)\cos(\alpha_i)}{r_i^2\cos^2(\beta_i)\cdot\sigma^2\cdot\left(1+\eta r_i^{\gamma}\right)^2} + \sum_{i=1}^{n} \frac{\sin^2(\beta_i)\cos(\alpha_i)\sin(\alpha_i)}{r_i^2\cdot\sigma^2\cdot\left(1+\eta r_i^{\gamma}\right)^2} = \\ &= \left(\frac{1}{r^2\cos^2(\beta)\cdot\sigma^2\cdot(1+\eta r^{\gamma})^2} + \frac{\sin^2(\beta)}{r^2\cdot\sigma^2\cdot(1+\eta r^{\gamma})^2}\right)\sum_{i=1}^{n}\cos(\alpha_i)\sin(\alpha_i) = 0 \\ FIM_{13} &= \sum_{i=1}^{n} \frac{\sin(\beta_i)\cos(\beta_i)\cos(\alpha_i)}{r_i^2\cdot\sigma^2\cdot\left(1+\eta r_i^{\gamma}\right)^2} = \frac{\sin(\beta)\cos(\beta)}{r^2\cdot\sigma^2\cdot(1+\eta r^{\gamma})^2}\sum_{i=1}^{n}\cos(\alpha_i) = 0 \\ FIM_{23} &= \sum_{i=1}^{n} \frac{\sin(\beta_i)\cos(\beta_i)\sin(\alpha_i)}{r_i^2\cdot\sigma^2\cdot\left(1+\eta r_i^{\gamma}\right)^2} = \frac{\sin(\beta)\cos(\beta)}{r^2\cdot\sigma^2\cdot(1+\eta r^{\gamma})^2}\sum_{i=1}^{n}\sin(\alpha_i) = 0 \end{aligned} \tag{6.35}$$

A simple and elegant solution that satisfies the two above extra conditions is obtained by noticing the orthogonality relations for sines and cosines from Fourier analysis [37],

$$\begin{aligned} &\sum_{i=1}^{n}\cos(\alpha_i) = \sum_{i=1}^{n}\sin(\alpha_i) = \sum_{i=1}^{n}\sin(\alpha_i)\cos(\alpha_i) = 0 \\ &\sum_{i=1}^{n}\cos^2(\alpha_i) = \sum_{i=1}^{n}\sin^2(\alpha_i) = \tfrac{n}{2} \end{aligned} \tag{6.36}$$

so we can take a regularly distributed formation on the circumferences, with the sensors placed along one or both of them. Using classical terminology, the sensor formation must be first and second moment balanced. Therefore, with this configuration the minimum trace of the CRB is obtained for this scenario.

6.5 Surface sensor network for underwater target positioning

In real situations, the sensors cannot be placed at will, either due to physical or mission constraints. As an interesting application scenario, we tackle the case where the sensors are restricted to lie in the horizontal plane $z = 0$ and search for the minimum of the trace of the CRB. It will be shown an explicit result that lends itself to an intuitive geometric interpretation without constraint in the number of sensors used for the network.

It is clear that the angles β_i, with $i = 1, .., n$, must take values between 0 and $\pi/2$, because the sensors lie in the horizontal plane, above the target. It is also easy to check that the value of each β_i determines the distance r_i between the target and the $i-th$ sensor because $r_i = q_z/sin(\beta_i)$, where q_z is the target depth. Thus, r_i depends directly on β_i, and therefore the derivatives of the trace of the CRB with respect to α_i and β_i must be computed. Straightforward manipulations yield

$$\frac{\partial(tr(CRB))}{\partial\alpha_i} = 2\cos(\alpha_i)\sin(\alpha_i)\sin^2(\beta_i)\cdot\left(\frac{1}{\cos^2(\beta_i)} - \sin^2(\beta_i)\right)\left(A^2 - B^2\right) = 0 \tag{6.37}$$

$$\frac{\partial\left(tr\left(CRB\right)\right)}{\partial\beta_i}=\left(\frac{\sin^3\left(\beta_i\right)\sin^2\left(\alpha_i\right)}{\cos^3\left(\beta_i\right)}+2\sin^3\left(\beta_i\right)\cos\left(\beta_i\right)\cos^2\left(\alpha_i\right)+\frac{\sin\left(\beta_i\right)\sin^2\left(\alpha_i\right)}{\cos\left(\beta_i\right)}\right)\frac{1}{A^2}+$$

$$\frac{1}{B^2}\left(\frac{\sin^3\left(\beta_i\right)\cos^2\left(\alpha_i\right)}{\cos^3\left(\beta_i\right)}+\frac{\sin\left(\beta_i\right)\cos^2\left(\alpha_i\right)}{\cos\left(\beta_i\right)}+2\sin^3\left(\beta_i\right)\cos\left(\beta_i\right)\sin^2\left(\alpha_i\right)\right)+$$

$$\left(\frac{-\sin^3\left(\beta_i\right)\cos\left(\beta_i\right)+\sin\left(\beta_i\right)\cos^3\left(\beta_i\right)}{C^2}\right)+\frac{\eta\gamma\left(q_z/\sin\left(\beta_i\right)\right)^\gamma}{\tan\left(\beta_i\right)\left(1+\left(q_z/\sin\left(\beta_i\right)\right)^\gamma\right)}\left[\frac{\cos^2\left(\beta_i\right)}{C^2}\right.$$

$$\left.+\left(\frac{\sin^2\left(\alpha_i\right)}{\cos^2\left(\beta_i\right)}+\sin^2\left(\beta_i\right)\cos^2\left(\alpha_i\right)\right)\frac{1}{A^2}+\left(\frac{\sin^2\left(\alpha_i\right)}{\cos^2\left(\beta_i\right)}+\sin^2\left(\beta_i\right)\cos^2\left(\alpha_i\right)\right)\frac{1}{B^2}\right]=0 \tag{6.38}$$

We now examine (6.37) and (6.38). From (6.37) it is easy to check that one of the following conditions must hold: i) $\cos\left(\alpha_i\right)=0$; ii) $\sin\left(\alpha_i\right)=0$; iii) $A-B=0$.

Following a similar procedure to that of the previous section, the analysis of (6.38) with the previous conditions shows that if $\cos\left(\alpha_i\right)=0$ for each sensor in the formation the solution is not optimal, so this solution is discarded. The same occurs if $\sin\left(\alpha_i\right)=0$ for each sensor in the formation, and so this solution is discarded too. If $\cos\left(\alpha_i\right)=0$ or $\sin\left(\alpha_i\right)=0$ for each sensor in the formation, (6.38) implies that the only feasible solution is that $A=B$. Therefore, $A=B$ is one of the conditions that an optimal surface sensor network must satisfy. Analysing (6.38) with $A=B=D$ yields

$$C^2=D^2\left(\frac{N_1+N_2}{M_1+M_2}\right) \tag{6.39}$$

where

$$N_1=\cos^4\left(\beta_i\right)\sin^3\left(\beta_i\right)-\sin\left(\beta_i\right)\cos^6\left(\beta_i\right)$$

$$N_2=-\cos^5\left(\beta_i\right)\frac{\eta\gamma\left(q_z/\sin\left(\beta_i\right)\right)^\gamma}{\tan\left(\beta_i\right)\left(1+\left(q_z/\sin\left(\beta_i\right)\right)^\gamma\right)}$$

$$M_1=\sin^3\left(\beta_i\right)+2\cos^4\left(\beta_i\right)\sin^3\left(\beta_i\right)+\cos^2\left(\beta_i\right)\sin\left(\beta_i\right)$$

$$M_2=\frac{\eta\gamma\left(\cos\left(\beta_i\right)+\cos^3\left(\beta_i\right)\sin^2\left(\beta_i\right)\right)\left(q_z/\sin\left(\beta_i\right)\right)^\gamma}{\tan\left(\beta_i\right)\left(1+\left(q_z/\sin\left(\beta_i\right)\right)^\gamma\right)}$$

and A, B, and C (and therefore D) are constant for a given sensor configuration. This equation allows us to determine the optimal sensor configuration for underwater target positioning when the sensors are placed on the same plane. An in-depth analysis of

$$f\left(\beta_i\right)=\left(\frac{N_1+N_2}{M_1+M_2}\right) \tag{6.40}$$

reveals that (6.39) can be satisfied for a maximum of two different values of β_i at the same time, for given values of A, B, and C. An equivalent angle β_i for a group of sensors indicates that they are placed at points belonging to a circumference around the target projection on the plane $z=0$. Therefore, the sensors are placed on a circumference around the target projection if the solution is

only one β_i or on two concentric circumferences around the target projection if the optimal formation is defined by two different values of β_i. A numerical analysis of these two possible solutions shows that the minimum trace is obtained if the sensors are all placed in the same circumference, therefore $\beta_i = \beta$. The value of β, and therefore the radius of the circumference where the sensors must be placed, can be obtained by solving (6.39). Then the sensors are all placed at the same distance from the target, i.e., $r_i = r$ for $i = 1, \cdots, n$, and the two extra conditions defined by $A = B$ and (6.35) are satisfied, as in the previous example, with the orthogonality relations for sines and cosines from Fourier analysis (6.36), so the formation must be first and second moment balanced. Clearly, the solution depends on β, q_z, and the noise measurement model.

6.5.1 Simulation examples with known target position

Based on (6.39) we now study two different scenarios that illustrate the potential of the methods developed for optimal sensor positioning. In the first scenario one wishes to find the sensor configuration that yields the minimum CRB trace when the noise covariance is distance-independent, that is, $\eta = 0$. The second scenario shows how the optimal formation changes when the noise covariance is distance-dependent, that is, $\eta \neq 0$. In the second scenario, the optimal formation depends directly on the modelling parameters η and γ, and on the target depth q_z. The values of $q_z = 50\ m$ and $\sigma = 0.05\ m^2$ will be constant in the forthcoming examples. Clearly, in order for the information about the optimal configurations to be useful, one must check if the trace of the CRB matrix meets the desired specifications. To this effect, and for comparison purposes, the trace of the CRB matrix obtained for a number of hypothetical target points (based on a fixed optimal sensor configuration corresponding to a well-defined scenario) will at times be computed by allowing these points to be on a grid in a finite spatial region $\mathcal{D}$. This will allow us to evaluate how good the sensor formation is in terms of yielding accurate localization of the real target, in comparison with the performance localization accuracy that is possible for any hypothetical target (different from the real target) positioned anywhere in $\mathcal{D}$. For the sake of clarity, and with an obvious abuse of notation, we will refer to that trace of the CRB, viewed as a function of its argument in $\mathcal{D}$, simply as $tr(CRB)_{\mathcal{D}}$. In this chapter, $\mathcal{D}$ will always be a rectangle in $\Re^2$.

Example 6.1: Distance independent covariance error.

Analysing (6.39) with $\eta = 0$ gives

$$C^2 = D^2 \frac{\cos^4(\beta)\sin^2(\beta) - \cos^6(\beta)}{1 + 2\cos^4(\beta)\sin^2(\beta)} \tag{6.41}$$

The value of β, and therefore the radius of the circumference where the sensors must stay is obtained from (6.41). The sensors are placed in a circumference centred at the target projection on the plane $z = 0$, therefore all the radii are the same, that is, $r_i = r$ for $i = 1, ..., n$. To define β irrespective of the sensor distribution over the resulting circumference, we proceed by adding the square root of (6.41), with $D = A$, to the square root of (6.41) with $D = B$, all the terms in α_i are cancelled and one obtains

$$2C = (A + B)\sqrt{\frac{\cos^4(\beta)\sin^2(\beta) - \cos^6(\beta)}{1 + 2\cos^4(\beta)\sin^2(\beta)}} \tag{6.42}$$

Straightforward computations yield

$$2\cos^2(\beta)\sqrt{1+2\cos^4(\beta)\sin^2(\beta)} = \left(1+\cos^2(\beta)\sin^2(\beta)\right)\sqrt{\sin^2(\beta)-\cos^2(\beta)} \tag{6.43}$$

whose only valid solution is $\beta = 54.86$ degrees. At this point, we can compare this optimal elevation angle with the one obtained in Section 6.4 for a sensor network placed over a sphere, that was equal to 42.40 degrees. We can check how the optimal elevation angle is different depending on the constraints imposed to the sensor network. This difference on the two optimal elevation angles can be negligible or very important depending on the target depth or the limit distance considered in the mission scenario. For example, for a limit distance or depth of 50 meters, the optimal formation of Section 6.4 has a radius of 54.76 meters, and the surface network of the example at hand, a radius of 32.69 meters. In this case the difference between formations can be considered not so important for a practical situation. However if we consider a limit distance or target depth equal to 500 meters, the radius are 547.60 and 326.94 meters, and the difference between formations is almost 220 meters, a very significant difference. Moreover, for the scenario of Section 6.4 the optimal elevation angle is the same for constant and distance-dependent covariance error. In the problem at hand, the noise model is a crucial factor to determine the optimal configuration, and the solution will change depending on the noise model considered, as shown next.

Clearly, the optimal elevation angle β is not enough to specify the optimal location of the sensors. The extra conditions to be specified are that $A = B$ and (6.35). As abovementioned these conditions are met if the sensors are first and second moment balanced, so we can take a regularly distributed formation around the circumference. This is exactly the configuration obtained in [10] for 2D, under the explicit *a priori* condition that all sensors be placed at the same distance from the target. We thus examine the example where the sensors are regularly distributed around a circumference centred at the target projection on the surface plane. This solution can be observed in Fig. 6.2 a) where the optimal formation and the CRB trace for each point in $\Re^2$ at the target depth ($tr(CRB)_{\mathcal{D}}$) are shown on the left-hand side (lighter regions correspond to hypothetical target points with lower values of the trace of the corresponding CRB matrices). On the right-hand side of Fig. 6.2 a) it is possible to observe the value of the trace and how its minimum is reached over the target position.

In Fig. 6.3 we show a comparison between the FIM determinant and the trace of the CRB for the different possible values of β, with $\beta_i = \beta$ for all sensors, for a regular distribution of sensors around the target projection. Notice that there are configurations that yield very large values of the determinant of the FIM but that differ from the one which provides the minimum trace of the CRB, as introduced in Section 6.1. Moreover, these large values correspond to configurations of the network that are clearly inadequate, e.g., they are close to configurations where all the sensors are placed at the same point, coincident with the target projection on the surface plane. It is for this reason that the trace of the CRB is used as indicator to analyse the performance of an arbitrary formation for AE-only measurements in 3D space. ■

Example 6.2: Distance-dependent covariance error.

Following the reasoning of the previous example, the radius of the circumference can be obtained easily by adequately manipulating (6.39). We can define an optimal formation where the sensors are regularly distributed around the target projection.

The only valid solution of (6.39) yields the size of the optimal formation for single target positioning. In Fig. 6.2 b), the optimal formation is shown for a value of η different from 0, $\eta = 0.05$, and $\gamma = 2$. The optimal radius is defined by an angle $\beta = 63.18$ degrees. Notice how

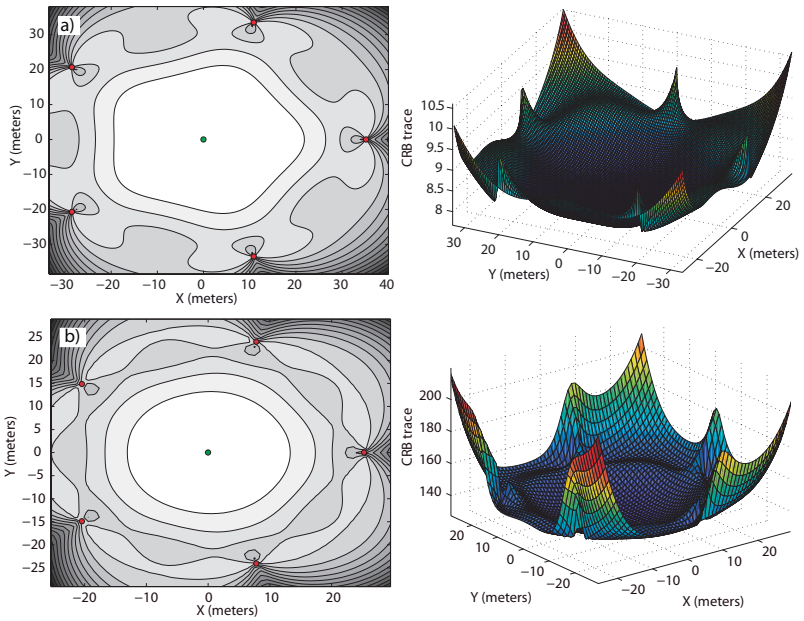

Figure 6.2: Optimal surface sensor formations for a target depth of 50 meters, $\sigma = 0.05\ m^2$ and different values of η. a) $\eta = 0$, b) $\eta = 0.05$. Lighter regions indicate higher accuracy in the 2D plots of $tr(CRB)_{\mathcal{D}}$.

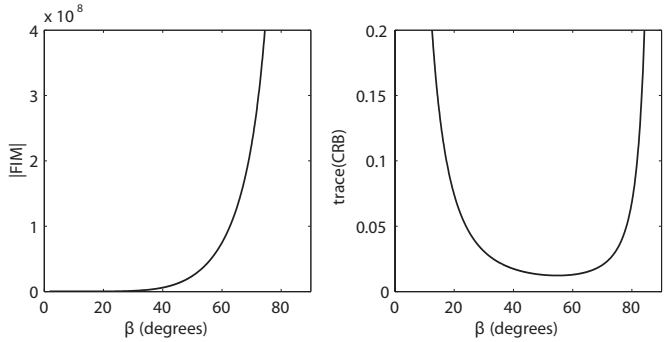

Figure 6.3: FIM determinant versus Cramer-Rao Bound for β between 0 and $\pi/2$ considering a circular formation centred at the target projection on the surface plane.

the formation size becomes smaller when the noise between target and sensors increases, to reduce the distance-dependent measurement noise component. The formation tends to concentrate itself around the projection of the target on the surface plane for increasing values of η and γ to reduce the impact of the distance-dependent measurement noise. This shows that it is critical to have an adequate noise model, for the optimal sensor formation is strongly noise-dependent. ■

6.6 Uncertainty in the target location

At this point, following what is commonly reported in the literature, we have started by addressing the problem of optimal sensor placement given an assumed position for the target. In a practical situation, the position of the target is only known with uncertainty and this problem must be tackled directly. However, in this case it is virtually impossible to make a general analytical characterization of the optimal solutions, and one must resort to numerical search methods. At this stage, an in-depth understanding of the types of solutions obtained for the ideal case is of key importance to compute an initial guess for the optimal sensor placement algorithm adopted. The objective is to obtain a numerical solution when the target is known to lie in a well defined uncertainty region, and we assume the uncertainty in the target position is described by a given probability distribution function and seek to minimize, by proper sensor placement, the average value of the trace of the CRB matrix for the target.

In what follows, $p_{i\xi}$; $i = 1, 2, ..., n; \xi = \alpha, \beta, r$, denotes the AE-measurements and range of sensor i located at position $p_i^T = [\alpha_i, \beta_i, r_i]$, and $\overline{p} = [p_1^T, ..., p_n^T]^T$. We further denote by $\varphi(q)\,; q \in \Re^3$ a probability density function with support $D \in \Re^3$ that describes the uncertainty in the position of the target in region D. With this notation, the problem of optimal sensor placement can be cast in the form of finding a vector $\overline{p}^*$ such that

$$\overline{p}^* = arg \min_{\overline{p}} \int_D tr\,(CRB(\overline{p}, q)) \cdot \varphi(q)\, dq \tag{6.44}$$

where we used the notation $CRB(\overline{p}, q)$ to clearly show the dependence of the trace of the CRB on the target and sensor locations. However, in the following $CRB(\overline{p}, q)$ will often be denoted simply as CRB. In a real situation, $\varphi(q)$ will depend on the type of mission carried out by the underwater target. If the target operates mostly in the centre of the working area, $\varphi(q)$ can for example assume the form of a truncated, radially-symmetric probabilistic Gaussian distribution centred at an appropriate point. On the other hand, if only the work area is known and the target can operate anywhere inside it, $\varphi(q)$ can be taken as the unity function inside that area.

To proceed, $tr\,(CRB(\overline{p}, q))$ must be computed in the equation above. At this point it is important to remark that, given the complexity of the optimal sensor placement problem at hand, the only viable solution is a numerical one. It now remains to solve the optimization problem defined above. As explained later, and similarly to the approach followed in previous chapters, we opted to use a gradient-based method to do so. To this effect, it is important to compute the derivatives of the integral in (6.44) with respect to the sensor coordinates, that is,

$$\frac{\partial}{\partial p_{i\xi}} \int_D tr\,(CRB(\overline{p}, q))\, \varphi(q) dq \tag{6.45}$$

for $i = 1, 2, ..., n$ and $\xi = \alpha, \beta, r$. To proceed with the computations, the integral and the derivative

operations are interchanged: the derivatives are explicitly determined first and the integration over region D is performed afterwards. After lengthy computations, the derivatives of $tr\,(CRB(\overline{p}, q))$ are well defined, see Appendix D for details.

The seemingly complex form of the derivatives, shown in Appendix D stems from the fact that $tr(CRB)$ is defined explicitly and from the complexity of the FIM expression, (6.11). However, with the notation adopted, each of the derivatives of $tr(CRB)$ with respect to the coordinates of a specific sensor can be computed in a recursive manner.

In what concerns the computation of the triple integral over the region D of interest, we opted to do it numerically using a Monte Carlo method. Finally, a solution of (6.44) can be obtained using a gradient optimization method with the Armijo rule (see [12] and the references therein). To overcome the occurrence of local minima or the divergence of the algorithm, the initial guess in the iterative algorithm must be chosen with care. In the examples that we studied we found it useful and expedite to adopt as an initial guess the solution for the single target positioning problem described in previous sections, with an hypothetical single target placed at the centre of the work area. It is important to stress that the solution to (6.44) depends strongly on the probability density function adopted for the target position q.

6.6.1 Simulation examples with uncertain target location

The methodology developed is now illustrated with the help of several examples that address the problem of optimal surface-sensor placement for uncertain underwater target positioning. Therefore the main constraint imposed to the problem is that the range distances depend explicitly on the angles β_i, with $i = 1, \cdots, n$, i.e., $r_i = q_z / \sin(\beta_i)$, where q_z is the target depth. Different problem scenarios are studied both for constant and distance-dependent covariance error.

Scenario 1: In this first scenario the target is known to be working inside an area defined by a circumference of a 50 m radius, at a constant depth of 50 meters. A 5 sensor network is used for the positioning task and the sensors are restricted to lie in the surface plane.

Example 6.3: The first example of this scenario corresponds to a constant covariance positioning problem with $\sigma = 0.1$ m. After the optimization method described above it is found that the optimal surface formation is the one described in Figure 6.4. We can notice in Figure 6.4 (a) how the formation keeps a regular distribution around the work area with an optimum radius of 39.9 m; and in Figure 6.4 (b) how an homogeneous trace of the CRB matrix is obtained inside the area of interest, keeping an equivalent accuracy for all the points inside the area. The sensors are placed regularly around the target projection forming a regular pentagon. The maximum and minimum values of the CRB trace inside the area of interest are 53.51 m^2 and 31.33 m^2, respectively. Despite of the difference between the maximum and minimum values of the CRB trace, the average value inside the working area is 36.41 m^2, so the average accuracy is close to the optimal one, and thus for most points the accuracy is closer to the minimum value of the CRB trace.

Example 6.4: This example corresponds to a distance-dependent covariance problem, with $\eta = 0.05$ and $\gamma = 1$. We can notice in Figure 6.5 (a) the difference of this optimal formation with respect to the optimal one of Example 6.3 shown in Figure 6.4 (a). The optimal formation is defined by a radius of 36.12 m with the sensors distributed regularly around the target projection. We can notice in Figure 6.5 (b) how the values of the trace of the CRB matrices are larger due to the added distance-dependent error. The maximum and minimum values of the CRB trace inside the work area are 326.94 m^2 and 128.05 m^2, respectively. However an homogeneous accuracy over the area of interest is obtained, with an average value of 180.17 m^2, that shows that for most of the points of the area of interest an accuracy close to the minimum one is obtained. ■

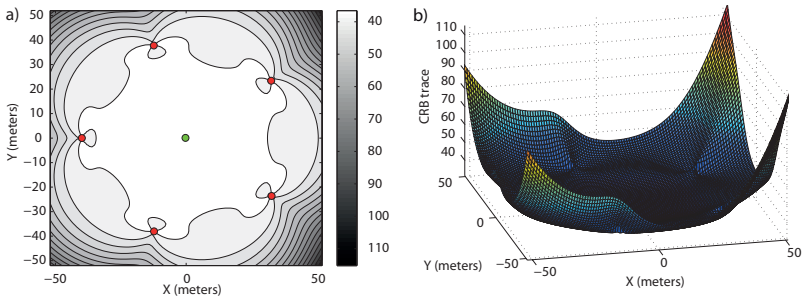

Figure 6.4: Optimal surface sensor formations for a target depth of 50 meters, $\sigma^2 = 0.01\ m^2$ and $\eta = 0$. Lighter regions indicate higher accuracy in the 2D plots of $tr(CRB)_{\mathcal{D}}$.

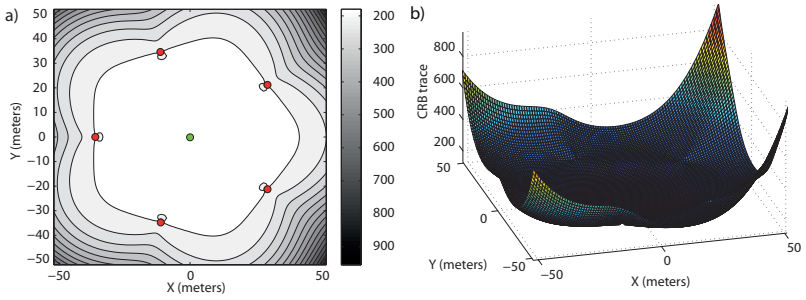

Figure 6.5: Optimal surface sensor formations for a target depth of 50 meters, $\sigma^2 = 0.01\ m^2$ and $\eta = 0.05$. Lighter regions indicate higher accuracy in the 2D plots of $tr(CRB)_{\mathcal{D}}$.

Scenario 2: In this second scenario the target is placed inside an area of $60 \times 60 \times 60\ m^3$ centred at the origin of the inertial coordinate frame, but there is no additional knowledge about the target position so the distribution function is a step-like distribution. The target is positioned by a 6 sensor network at the sea surface as shown in the set-up of Figure 6.6 (a). Again both situations with constant and distance-dependent covariance are studied.

Example 6.5: This example deals with a constant covariance error with $\sigma = 0.05\ m$. No figures are shown because it is not possible to show adequately the accuracy in a figure when a volume is studied. The optimal sensor formation that maximizes the accuracy inside the working volume takes a shape similar to a circumference, with an approximate radius of 41 meters. The sensor positions, in Cartesian coordinates, are shown in Table 6.1.

Table 6.1: Optimal sensor positions for constant covariance.

	p_1	p_2	p_3	p_4	p_5	p_6
$\{x_I\}(m)$	35.48	0.07	−35.33	−35.3	0.07	35.48
$\{y_I\}(m)$	20.37	40.80	20.37	−20.52	−40.96	−20.52
$\{z_I\}(m)$	50	50	50	50	50	50

The minimum and maximum CRB trace values obtained inside the volume are $tr(CRB)_{min} = 2.44\ m^2$ and $tr(CRB)_{max} = 18.62\ m^2$, respectively, with an average value of $tr(CRB)_{avg} = 8.11\ m^2$, providing a large accuracy for most points inside the region of interest.

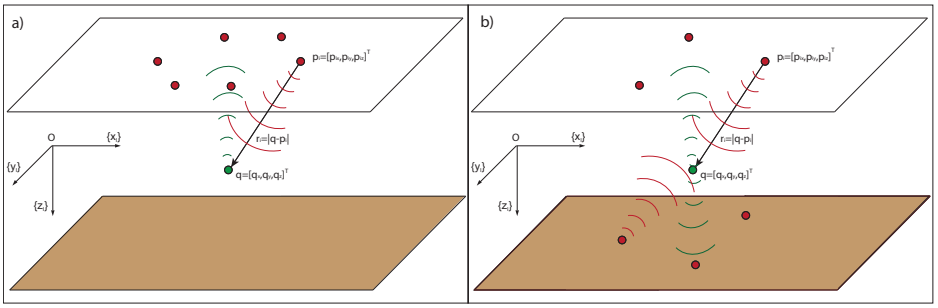

Figure 6.6: Sensor formations for an uncertainty volume of $60 \times 60 \times 60$ m^3, (a) surface sensor network, and (b) sensor network split into two formations, one at the sea surface and another at the sea bottom.

Example 6.6: In the second example of this scenario the error is considered to be distance-dependent, with $\sigma = 0.05$, $\eta = 0.1$ and $\gamma = 1$. After the gradient optimization the optimal sensor network is placed at the positions listed in Table 6.2.

Table 6.2: Optimal sensor positions for $\sigma = 0.05$, $\eta = 0.1$ and $\gamma = 1$.

	p_1	p_2	p_3	p_4	p_5	p_6
$\{x_I\}(m)$	32.76	0.04	−32.69	−32.68	0.04	32.76
$\{y_I\}(m)$	18.91	37.80	18.91	−18.87	−37.77	−18.87
$\{z_I\}(m)$	50	50	50	50	50	50

We can notice how the formation is smaller than that of Example 6.5 to reduce the impact of the distance-dependent added error, with the network keeping a formation similar to a circumference of an approximate radius of 37 meters. The minimum and maximum CRB trace inside the volume of interest are $tr(CRB)_{min} = 49.39$ m^2 and $tr(CRB)_{max} = 2.17 \cdot 10^3$ m^2, respectively, with an average value of $tr(CRB)_{avg} = 591.05$ m^2, that shows that, in this example, the accuracy is dramatically affected by the added distance-dependent error component. ■

Scenario 3: We now tackle the same situation of Scenario 2 but the sensor network can be placed in two different planes, it is, one subnetwork on the sea surface, and another subnetwork on the sea bottom, shown in the set-up of Figure 6.6 (b).

Example 6.7: This example is again with constant covariance, $\eta = 0$ and $\sigma = 0.05$ m. After the optimization process, in which 3 sensors are constrained to lie at the sea surface, i.e., 50 meters above the centre of the volume of interest, and the other 3 sensors are constrained to lie at the sea bottom, at 50 meters under the centre of the volume of interest, the optimal formation is such that the sensor are placed, in Cartesian coordinates, at the positions stated in Table 6.3.

Table 6.3: Optimal sensor positions for constant covariance.

	p_1	p_2	p_3	p_4	p_5	p_6
$\{x_I\}(m)$	21.98	−0.04	−22.15	−22.23	−0.08	22.14
$\{y_I\}(m)$	12.841	25.68	12.84	−12.7	−25.38	−12.74
$\{z_I\}(m)$	−50	50	−50	50	−50	50

We can notice that the formation shape, although split in two formations, is very similar to the

one obtained in the previous scenario but with an approximate radius of 26 meters. However, in this case the minimum and maximum CRB trace are $tr(CRB)_{min} = 2.23\ m^2$ and $tr(CRB)_{max} = 7.27\ m^2$, respectively, with an average value of $tr(CRB)_{avg} = 5.13\ m^2$, that shows how the accuracy, for the constant covariance case, increases when the formation consists of two formations, one at the sea surface and another at the sea bottom. We can check how the maximum value of the CRB trace is smaller with respect to Example 6.5 and how the average CRB trace is very close to the minimum value.

Example 6.8: Finally, this one tackles the distance-dependent covariance problem, with $\sigma = 0.05\ m$, $\eta = 0.1$, and $\gamma = 1$. In this case the optimal formation is the one in which the sensors take the positions shown in Table 6.4.

Table 6.4: Optimal sensor positions for $\sigma = 0.05\ m$, $\eta = 0.1$, and $\gamma = 1$.

	p_1	p_2	p_3	p_4	p_5	p_6
$\{x_I\}(m)$	19.74	0.14	−19.28	−19.41	0.21	19.70
$\{y_I\}(m)$	11.16	22.66	11.14	−11.16	−22.66	−11.14
$\{z_I\}(m)$	−50	50	−50	50	−50	50

Again the formation shape is similar to that obtained in Example 6.6, but with an approximate radius of 22 meters. The minimum and maximum CRB trace are now $tr(CRB)_{min} = 39.36\ m^2$ and $tr(CRB)_{max} = 414.77\ m^2$, respectively, with an average value of $tr(CRB)_{avg} = 214.09\ m^2$. We can notice how the maximum CRB trace is significantly reduced with respect to the value obtained in Example 6.6. The average value is again smaller, showing that a very good average accuracy is obtained inside the volume of interest. Finally, the minimum value of CRB trace is also smaller. Thus a more homogeneous accuracy inside the area with a significantly smaller error is obtained for this example with the sensors split in two formations, one at the sea surface and the other at the sea bottom. ■

Therefore, for an unknown target location it is clear that the average accuracy inside the working area is improved if we can place the sensors in two different parallel planes.

6.7 Conclusions

We studied the problem of determining optimal configurations of sensor networks that will, in a well defined sense, maximize the AE-related information available for underwater target positioning. To this effect, we assumed that the measurements were corrupted by white Gaussian noise, the variance of which is distance-dependent. The Fisher Information Matrix and the minimization of the trace of the CRB matrix were used to determine the optimal sensor configurations. Explicit analytical results were obtained for both distance-dependent and distance-independent noise. In the application scenario of underwater target positioning by a surface sensor network, we have shown that the optimal formation lies on a circumference around the target projection and that a "regularly distributed formation" around this target provides an optimal configuration, the size of which depends on the measurement noise model and the target depth. The methodology was then extended to deal with uncertainty in the target location, because in a practical situation the target position is only known with uncertainty. Simulation examples illustrated the concepts developed in different application scenarios, showing that the optimal configuration of the sensors depends explicitly on the intensity of the measurement noise, the constraints imposed to the sensor configuration, the target depth, and the probabilistic distribution that defines the prior uncertainty in the target position.

Chapter 7

UNDERWATER TARGET POSITIONING WITH A SINGLE SURFACE SENSOR

7.1 Introduction

The developments studied in previous chapters exploit the geometric configuration of acoustic sensors in order to define the position of an underwater target from range or bearings measurements. These ranges or bearings are measured at different locations that make it possible to determine the target position. However, in this chapter an alternative approach is used, a single sensor that employs both the spatial and temporal diversity in order to extract position information. In particular, and speaking in loose terms, we are interested in determining the optimal movements or trajectory of a single mobile sensor that will, in a well defined sense, maximize the range-related information available for underwater target positioning. To this effect, we assume that the range measurements are corrupted by white Gaussian noise. The actual computation of the target position may be done by resorting to trilateration algorithms as mentioned in previous chapters.

There is a great interest in reducing the number of beacons involved in the acoustic navigation/positioning system, as they usually involve deployment, calibration and recovery time which is money and time consuming. The concept of underwater navigation using ranges to a single beacon/transponder has received increasing attention in the marine robotics community. An early reference can be found in [8] where the target motion analysis (TMA) with unknown marine systems using sonar measurements is discussed, i.e., the estimation of the position and velocity of a target ship, given a sequence of measurements, is studied, or [83] where the observability requirements are obtained for three-dimensional maneuvering target tracking with bearings-only measurements. Another early work on this trend is the work of Larsen who came up with the term Synthetic Long Baseline navigation [49], [50]. Observability is the key issue, and several works have addressed this [82], [86], [30], [68], [31], [75], [41], [19], [29]. More recently, several works have addressed the problem from diverse perspectives, and pointed out its relationship with the multiple vehicle

navigation problem.

Some interesting examples are [35] in which the author develops a computer algorithm based on least squares and a Kalman Filter for single beacon navigation that can be integrated in the architecture of an AUV, [48] where multiple asynchronous ranges from a transponder are manipulated to create a long baseline of virtual transponders in different locations at a single point in time so that an underwater vehicle can compute its global location in the same way that it would do using multiple transponders, [23] in which a continuous time adaptive localization algorithm that permits a mobile agent to estimate the location of a stationary source is developed, or [26] where the simultaneous navigation of multiple underwater vehicles is done using a surface-ship acting as a moving transponder with a maximum likelihood framework. Another interesting work can be found on [76] where the estimation of an underwater vehicle position with a single beacon is studied in the presence of unknown ocean currents. The idea behind this work is the combination of DR information with a sequence of range measurements taken at different instants of time to determine the target position, target velocity and current velocity with a Kalman Filter. Note that this problem is also closely related to the classic source localization problem in underwater acoustics [40].

A dual to this problem is the tracking of an underwater target with a single range measuring device. An important question in positioning with sensor networks is about the minimum number of beacons that can be used to perform an underwater target positioning task. A single range measurement does not contain enough information to determine the target position, so we cannot compute a position fix. Instead of a static surface sensor network, one could think of a surface vehicle that, by moving in convenient trajectories, exploits its spatial diversity while measuring ranges to the underwater platform in order to determine its position. Therefore, in this chapter the study of the optimal trajectories that a single sensor must follow, in order to maximize the accuracy with which a target is localized, is tackled. Some previous works go back to the work of [70] where optimal control theory is used to determine the course of a constant speed observer by minimization of a criterion based on the FIM with a mixed analytical and numerical procedure. In [69] a fixed target location is estimated from a sequence of noisy bearings measurements, and the optimal trajectories for bearings-only target localization are based on the maximization of the determinant of the FIM subject to some constraints. The optimal solutions are determined numerically. In [77] a single LBL acoustic transponder is used for AUV positioning. The localization algorithm is based on a least square root method that estimates the AUV position and current velocity. In [14] a navigation system to remove the accumulated position errors of an underwater system is described. Finally, in [78] some algorithms to position an AUV based on one moving beacon are described. The navigation systems are composed of AUV on-board reckoning systems and an acoustic positioning system with LBL with a moving beacon. The AUV position is computed with a Kalman Filter and the algorithm for mobile beacon trajectory is presented.

The key contributions of the present chapter are threefold: i) two different approaches to determine the optimal sensor trajectories are studied, the first one when only the next best measurement of the current trajectory is computed, and the second one when the whole trajectory is optimized to maximize the positioning accuracy, ii) a general solution is obtained analytically and numerically for the positioning of a static underwater target with the above approaches, and finally iii), the results are extended to the scenario in which the target moves at a constant speed.

The chapter is organized as follows. In Section 7.2 the optimal sensor trajectory problem is formulated and the assumptions made for the computation of the optimal trajectories are established. In Section 7.3 the three first optimal range measurements are determined analytically, so that the initial target estimation be defined with the maximum possible accuracy. Section 7.4 contains the derivation of optimal sensor trajectories for two different approaches, i) when only the next best

measurement point for the current sensor trajectory must be determined and ii) when the whole trajectory must be optimized, both for the case where the target is static. Simulation examples are included. In Section 7.5 the above analysis is extended to the scenario in which the target moves at a constant speed, and some simulation examples are included too. Finally, Section 7.6 contains the conclusions.

7.2 Problem formulation

For a given target positioning problem, the optimal sensor trajectory depends strongly on the constraints imposed by the task itself (e.g. maximum number of measurements used for the computation of the FIM and type of sensor that can be used) and the environment (e.g. ambient noise). In fact, an inadequate sensor trajectory may yield large positioning errors. Therefore it is of the utmost importance to define the constraints and assumptions considered for the problem at hand:

- The variance of the measurement error ω is constant and equal to σ.
- The USV must localize a single static target or a mobile target with constant speed.
- The target position is *a priori* known and it is considered to be placed at the origin of the inertial coordinate frame.
- The initial USV position is arbitrary because it actually does not condition the final optimal solution.
- The target is positioned with a fixed number of measurements, i.e., the amount of memory used to storage the measurements is limited and the FIM is computed with a fixed given number of range measurements.
- The acoustic signals are emitted at constant intervals of time Δt and there exists a delay between the emission by the pinger on board the USV and the answer from the target, so the reception of the answer is at a different point from the emission point, see Fig 7.1.
- The sensor, or USV, moves with constant speed $V(t) = V$.
- It is considered that the range measured by the sensor is the distance between the target and the position of the sensor at the moment of the reception of the acoustic signal.

Some of the above issues can be observed in Figure 7.1. We can notice how the sensor (red) emits the acoustic signal at the moment E_k and the answer from the target (green) is received by the sensor at R_k, with d_k being the distance between the two above points. This distance d_k depends on the velocity of sound in water, on the sensor speed V, and on the range distances r'_k and r_k that define the go and back way travel of the acoustic signal. The emission point E_k defines the point p'_k, the reception point R_k defines the $k-th$ measurement point p_k, and the range distance measured for the FIM computation is considered to be r_k, i.e., the distance between the target position q and the point p_k. In this theoretical framework it is considered that r'_k and r_k, and therefore p'_k and p_k, are known, so we can define analytically the distance d_k that separates the emission and reception points. If we consider that c_s is the speed of sound in water we can write:

$$\frac{d_k}{V} = \frac{r'_k}{c_s} + \frac{r_k}{c_s} \tag{7.1}$$

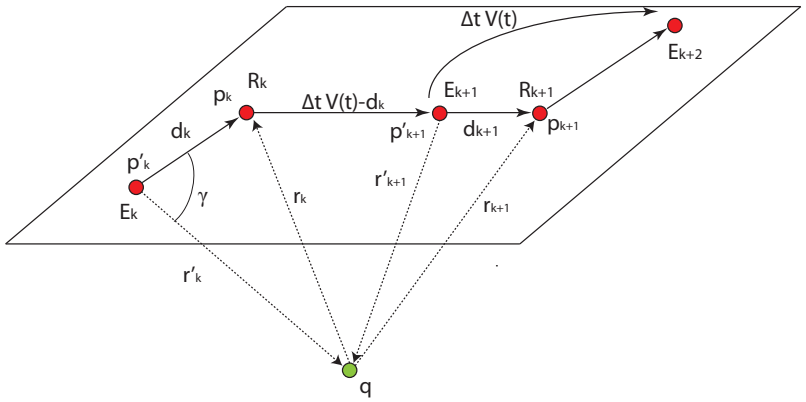

Figure 7.1: Problem set-up: the acoustic signal is emitted at the points E_k and received by the sensor at the points R_k. The range distance measured to define the FIM is the range distance of the way back of the acoustic signal from the target to the sensor, r_k.

Moreover, if γ is the angle defined by r'_k and d_k, from the theorem of the cosine we can express r_k as

$$r_k^2 = r'^2_k + d_k^2 + 2d_k r'_k \cos(\gamma) \tag{7.2}$$

with

$$\gamma = \arccos\left(\frac{\langle\left(q - p'_k\right)\left(p'_k - p_{k-1}\right)\rangle}{r'_k \cdot (\Delta tV - d_{k-1})}\right) \tag{7.3}$$

where <> denotes the inner product between its operands, see Fig. 7.1. Then we can rewrite (7.1) as

$$\frac{d_k}{V} - \frac{r'_k}{c_s} = \frac{\sqrt{r'^2_k + d_k^2 + 2d_k r'_k \cos(\gamma)}}{c_s} \tag{7.4}$$

Now taking the square of both sides and rewriting the equation we find,

$$d_k = \frac{2r'_k}{c_s}\left(\frac{\cos(\gamma)}{c_s} - \frac{1}{V}\right)\left(\frac{1}{c_s^2} - \frac{1}{V^2}\right)^{-1} \tag{7.5}$$

so the measurement points may be explicitly defined considering only the orientation angles α_i taken by the surface sensor at the R_k points and the already known information.

Given a target positioning problem, the optimal sensor trajectory can be ascertained by examining the corresponding Cramer-Rao Lower Bound (CRLB) or Fisher Information Matrix (FIM). We focus on the computation of the CRLB (or, equivalently the FIM) for the problem at hand. In particular, the determinant of the FIM is used as an indicator of the performance that is achievable with a given sensor trajectory. Maximizing this quantity yields the most appropriate sensor movements.

The FIM is defined as the expected value of the logarithm of the derivative of the maximum likelihood function, that yields

$$FIM = \frac{1}{\sigma^2}\sum_{i=1}^{n}\begin{pmatrix} (u_{i,x})^2 & \left(u_{i,y}\right)(u_{i,x}) & (u_{i,z})(u_{i,x}) \\ (u_{i,x})\left(u_{i,y}\right) & \left(u_{i,y}\right)^2 & (u_{i,z})\left(u_{i,y}\right) \\ (u_{i,x})(u_{i,z}) & \left(u_{i,y}\right)(u_{i,z}) & (u_{i,z})^2 \end{pmatrix} \tag{7.6}$$

where $u_{ij} = \frac{\partial \|q_i - p_i\|}{\partial q_{i,j}}$, for $i \in \{1, ..., n\}$ and $j \in \{x, y, z\}$, $p_i = R_i$, and q_i corresponds to the target position at the moment in which the measurement i is taken, i.e, the position in which the target sends the acoustic signal to the surface sensor, that could be a position fix or not depending on the scenario studied.

7.3 Initial target estimation: Three first range measurements

The number of ranges needed to determine the position of a target is of the utmost importance, in the most general scenario, 3 non-collinear ranges in two-dimensional scenarios, and 4 non-coplanar ranges in three-dimensional scenarios are needed to determine a position fix. In a practical situation, such as the underwater target positioning with surface sensors, the target is known to be under the sea surface, so 3 non-collinear range measurements are enough.

In this section the three first measurement points that provide an initial target position estimation and that maximize the FIM determinant given a constant advance speed and a constant sample time are determined analytically. For this initial scenario the notation introduced in [6] for the FIM determinant is used for simplicity reasons, that becomes,

$$|FIM| = \frac{1}{\sigma^6}\sum_{j\le k\le l}^{n}\left(\left(u_j \times u_k\right)\cdot u_l\right)^2 = \frac{1}{\sigma^6}\sum_{j\le k\le l}^{n}\sin^2\left(\alpha_{jk}\right)\cos^2\left(\beta_{jk,l}\right) \tag{7.7}$$

where

$$u_j = [u_{jx}, u_{jy}, u_{jz}]^T = \left[\begin{array}{ccc} \frac{\partial|q-p_j|}{\partial q_x} & \frac{\partial|q-p_j|}{\partial q_y} & \frac{\partial|q-p_j|}{\partial q_z} \end{array}\right]^T; \tag{7.8}$$

$j \in \{1, ..., n\}$; identical definitions apply to the indices k, l; α_{jk} is the angle formed by the vectors u_j and u_k, and $\beta_{jk,l}$ is the angle that the vector u_l forms with the resultant vector of the cross product between u_j and u_k. The optimal sensor configuration is the one which maximizes the logarithm of (7.7).

We consider 3 range measurements, constant covariance, and the target placed at the origin of the inertial coordinate frame, so that (7.7) can be rewritten as

$$|FIM| = \frac{1}{\sigma^6}\frac{\left((p_1 \times p_2)\cdot p_3\right)^2}{r_1^2 r_2^2 r_3^2} \tag{7.9}$$

where p_1, p_2, p_3 are the three points in which the range measurements are taken, as defined in Section 7.2. The point p_1 is an arbitrary point, the sensor velocity V is constant, and the time between two consecutive emissions of acoustic signals by the surface sensor Δt is also constant, so points p_2 and

p_3 can be rewritten as

$$p_2 = \begin{bmatrix} p_{1x} + (V\Delta t - d_1 + d_2)\cos(\alpha_2) \\ p_{1y} + (V\Delta t - d_1 + d_2)\sin(\alpha_2) \\ q_z \end{bmatrix}^T$$

$$p_3 = \begin{bmatrix} p_{1x} + (V\Delta t - d_1 + d_2)\cos(\alpha_2) + (V\Delta t - d_2 + d_3)\cos(\alpha_3) \\ p_{1y} + (V\Delta t - d_1 + d_2)\sin(\alpha_2) + (V\Delta t - d_2 + d_3)\sin(\alpha_3) \\ q_z \end{bmatrix}^T$$

where α_2 and α_3 are the angles that line that joins p_1 and p_2 and the line that joins p_2 and p_3 form with respect to the $\{x_I\}$ axis, respectively, and d_1 and d_2 are the distances between the point in which the acoustic signal is emitted by the surface sensor and the point in which the response from the target is received, as it was defined in Figure 7.1. As mentioned above, the point in which the signal is received is considered to be the measurement point. For simplicity reasons, and without loss of generality, we consider that the initial measurement point is such that $p_{1x} = p_{1y}$.

The angles α_2 and α_3 must be chosen so that their values maximize the logarithm of (7.9). To define these angles the cross and dot product of (7.9) can be expanded as

$$(p_1 \times p_2) \cdot p_3 = q_z(p_{1y}p_{3x} - p_{2y}p_{3x} + p_{2x}p_{3y} - p_{1x}p_{3y} + p_{1x}p_{2y} - p_{2x}p_{1y}) =$$

$$= q_z \cdot ((V\Delta t - d_1 + d_2)(V\Delta t - d_2 + d_3) + (V\Delta t - d_1 + d_2)d_3 +$$

$$+(V\Delta t - d_2 + d_3)d_2 + d_2d_3)\,(\cos(\alpha_2)\sin(\alpha_3) - \sin(\alpha_2)\cos(\alpha_3))$$

The range distances r_2 and r_3 can be written in terms of r_1 and the angles α_2 and α_3,

$$r_2^2 = r_1^2 + (V\Delta t - d_1 + d_2)^2 + 2p_{1x}(V\Delta t - d_1 + d_2)(\cos(\alpha_2) + \sin(\alpha_2))$$

$$r_3^2 = r_1^2 + (V\Delta t - d_1 + d_2)^2 + 2p_{1x}(V\Delta t - d_1 + d_2)(\cos(\alpha_2) + \sin(\alpha_2))$$

$$+ 2p_{1x}(V\Delta t - d_2 + d_3)(\cos(\alpha_3) + \sin(\alpha_3)) + 2(V\Delta t - d_1 + d_2)$$

$$\cdot (V\Delta t - d_2 + d_3)(\cos(\alpha_2)\cos(\alpha_3) + \sin(\alpha_2)\sin(\alpha_3))$$

Moreover, we have that

$$p_{1x}^2 + p_{1y}^2 + q_z^2 = r_1^2 \Longrightarrow p_{1x} = p_{1y} = \sqrt{\frac{r_1^2 - q_z^2}{2}}$$

With the above notation the derivatives of (7.9) with respect to α_2 and α_3 can be computed analytically to obtain the optimality conditions for the single target positioning problem with 3 range measurements by a single mobile surface sensor. These derivatives, after some straightforward

computations, yield,

$$\frac{\partial |FIM|}{\partial \alpha_i} = \frac{2((p_1 \times p_2) \cdot p_3) \cdot \partial((p_1 \times p_2) \cdot p_3) r_1^2 r_2^2 r_3^2}{r_1^4 r_2^4 r_3^4} + \frac{((p_1 \times p_2) \cdot p_3)^2 r_1^2 \left(\partial r_2^2 \cdot r_3^2 + r_2^2 \cdot \partial r_3^2\right)}{r_1^4 r_2^4 r_3^4} = 0 \tag{7.10}$$

with $i = 2, 3$, and

$$\frac{\partial((p_1 \times p_2) \cdot p_3)}{\partial \alpha_2} = q_z \cdot ((V\Delta t - d_1 + d_2)(V\Delta t - d_2 + d_3) + (V\Delta t - d_1 + d_2)d_3 + (V\Delta t - d_2 + d_3)d_2 + d_2 d_3)\,(-\sin(\alpha_2)\sin(\alpha_3) - \cos(\alpha_2)\cos(\alpha_3))$$

$$\frac{\partial((p_1 \times p_2) \cdot p_3)}{\partial \alpha_3} = q_z \cdot ((V\Delta t - d_1 + d_2)(V\Delta t - d_2 + d_3) + (V\Delta t - d_1 + d_2)d_3 + (V\Delta t - d_2 + d_3)d_2 + d_2 d_3)\,(\cos(\alpha_2)\cos(\alpha_3) + \sin(\alpha_2)\sin(\alpha_3))$$

$$\frac{\partial r_2^2}{\partial \alpha_2} = 2p_{1x}\,(\Delta t V - d_1 + d_2)\,(\cos(\alpha_2) - \sin(\alpha_2))$$

$$\frac{\partial r_2^2}{\partial \alpha_2} = 0$$

$$\frac{\partial r_3^2}{\partial \alpha_2} = 2p_{1x}\,(\Delta t V - d_1 + d_2)\,(\cos(\alpha_2) - \sin(\alpha_2)) + 2\,(\Delta t V - d_1 + d_2) \cdot (\Delta t V - d_2 + d_3)\,(\cos(\alpha_2)\sin(\alpha_3) - \sin(\alpha_2)\cos(\alpha_3))$$

$$\frac{\partial r_3^2}{\partial \alpha_3} = 2p_{1x}\,(\Delta t V - d_2 + d_3)\,(\cos(\alpha_3) - \sin(\alpha_3)) + 2\,(\Delta t V - d_1 + d_2) \cdot (\Delta t V - d_2 + d_3)\,(\sin(\alpha_2)\cos(\alpha_3) - \cos(\alpha_2)\sin(\alpha_3))$$

If we now combine (7.10) for both α_2 and α_3 it implies that

$$(V\Delta t - d_1 + d_2)(\cos(\alpha_2) - \sin(\alpha_2))(r_2^2 + r_3^2) + r_2^2(V\Delta t - d_1 + d_2)(\cos(\alpha_3) - \sin(\alpha_3)) = 0 \tag{7.11}$$

Therefore, with (7.11), we can compute the 2 next measurement points to maximize the FIM determinant.

7.4 Static target positioning

In this section we define the points or the trajectory that a moving surface sensor must follow in order to maximize the accuracy with which a static underwater target is localized. The computation of the optimal trajectory is done with two different approaches: i) when the immediate best next measurement point for the current sensor trajectory is computed to update the FIM after the elimination of the oldest one, and ii) when the whole trajectory, for a given number of range measurements, is optimized. As commented in Section 7.2, it is considered that the FIM is computed with a limited and constant number of range measurements, i.e., in the first scenario the new measurement substitutes the oldest one of the n measurement points with which the FIM is computed, and in the second scenario the optimal trajectory is computed recursively for the n measurement points considering that the initial point of the new trajectory is the last point of the old one.

7.4.1 Next optimal range measurement

Once the mission is running and we have an initial estimation of the target position, it is necessary to determine the next measurement point, i. e., the direction that the single tracker must take in order to maximize the FIM determinant and thus to minimize the positioning error. If we have a given number of measurements and we want to know the next one, for a given velocity and sample time, it is easy to define the analytical expression that provides this optimal value because the new FIM determinant will have only one unknown parameter, the new angle α_{k+1} that defines the sensor movement direction. As mentioned above, the single tracker computes the FIM with a given number of measurements, therefore it is necessary to delete the oldest measurement to be able to update the FIM. The sensor speed V and the sampling time Δt are known, so the new measurement point p_{k+1} can be written as:

$$p_{k+1} = \begin{bmatrix} p_k + (V\Delta t - d_k + d_{k+1})\cos(\alpha_{k+1}) \\ p_k + (V\Delta t - d_k + d_{k+1})\sin(\alpha_{k+1}) \\ q_z \end{bmatrix}^T$$

where d_k and d_{k+1} are defined according to Section 7.2.

The derivative of the FIM determinant with respect to the new direction angle α_{k+1} can be obtained easily and quickly. We consider that FIM_k^* is the FIM computed with the current k known range measurements except the oldest one that has been deleted, and FIM_{k+1} the updated FIM that has been computed with the new range measurement obtained from a point to be defined. This new and unknown FIM yields,

$$FIM_{k+1} = FIM_k^* + FIM'_{k+1} \tag{7.12}$$

where

$$FIM'_{k+1} = \frac{1}{\sigma^2}\begin{pmatrix} \frac{p_{k+1,x}^2}{r_{k+1}^2} & \frac{p_{k+1,x}p_{k+1,y}}{r_{k+1}^2} & \frac{p_{k+1,x}p_{k+1,z}}{r_{k+1}^2} \\ \frac{p_{k+1,x}p_{k+1,y}}{r_{k+1}^2} & \frac{p_{k+1,y}^2}{r_{k+1}^2} & \frac{p_{k+1,y}p_{k+1,z}}{r_{k+1}^2} \\ \frac{p_{k+1,x}p_{k+1,z}}{r_{k+1}^2} & \frac{p_{k+1,y}p_{k+1,z}}{r_{k+1}^2} & \frac{p_{k+1,z}^2}{r_{k+1}^2} \end{pmatrix}$$

Thus, the problem to solve can be defined as,

$$\alpha_{k+1}^* = arg\max_{\alpha_{k+1}} |FIM_{k+1}| \tag{7.13}$$

The derivative of (7.13) with respect to α_{k+1} can be computed by decomposing the determinant by its adjoints:

$$\frac{\partial |FIM_{k+1}|}{\partial \alpha_{k+1}} = \sum_{i,j}^{n} (-1)^{i+j} |Adj_{i,j}(FIM_{k+1})| \cdot \Theta(i,j) \tag{7.14}$$

where $\Theta(i,j) = \frac{\partial FIM_{k+1}(i,j)}{\partial \alpha_{k+1}}$ and $|Adj_{i,j}(FIM_{k+1})|$ is the determinant of the adjoint matrix of FIM_{k+1} with respect to the element (i,j). The derivatives of each FIM_{k+1} element with respect to α_{k+1} are actually the derivatives of each element of the matrix FIM'_{k+1} with respect to α_{k+1}. With this clarification, these derivatives are defined next:

$$\frac{\partial |FIM_{k+1}(1,1)|}{\partial \alpha_{k+1}} = \frac{-2\left(p_{kx} + \upsilon \cos(\alpha_{k+1})\right) \upsilon \sin(\alpha_{k+1}) r_{k+1}^2 - \left(p_{kx} + \upsilon \cos(\alpha_{k+1})\right)^2 \partial\left(r_{k+1}^2\right)}{r_{k+1}^4}$$

$$\frac{\partial |FIM_{k+1}(2,2)|}{\partial \alpha_{k+1}} = \frac{-2\left(p_{ky} + \upsilon \sin(\alpha_{k+1})\right) \upsilon \cos(\alpha_{k+1}) r_{k+1}^2 - \left(p_{ky} + \upsilon \sin(\alpha_{k+1})\right)^2 \partial\left(r_{k+1}^2\right)}{r_{k+1}^4}$$

$$\frac{\partial |FIM_{k+1}(3,3)|}{\partial \alpha_{k+1}} = \frac{-q_z^2 \partial\left(r_{k+1}^2\right)}{r_{k+1}^4}$$

$$\frac{\partial |FIM_{k+1}(1,2)|}{\partial \alpha_{k+1}} = \frac{\left(-\left(p_{ky} + \upsilon \sin(\alpha_{k+1})\right) \sin(\alpha_{k+1}) + \left(p_{kx} + \upsilon \cos(\alpha_{k+1})\right) \cos(\alpha_{k+1})\right) \upsilon r_{k+1}^2}{r_{k+1}^4}$$
$$- \frac{\left(p_{kx} + \upsilon \cos(\alpha_{k+1})\right)\left(p_{ky} + \upsilon \sin(\alpha_{k+1})\right) \partial\left(r_{k+1}^2\right)}{r_{k+1}^4}$$

$$\frac{\partial |FIM_{k+1}(1,3)|}{\partial \alpha_{k+1}} = \frac{-\upsilon \sin(\alpha_{k+1}) q_z r_{k+1}^2 - \left(p_{kx} + \upsilon \cos(\alpha_{k+1})\right) q_z \partial\left(r_{k+1}^2\right)}{r_{k+1}^4}$$

$$\frac{\partial |FIM_{k+1}(2,3)|}{\partial \alpha_{k+1}} = \frac{-\upsilon \cos(\alpha_{k+1}) q_z r_{k+1}^2 - \left(p_{ky} + \upsilon \sin(\alpha_{k+1})\right) q_z \partial\left(r_{k+1}^2\right)}{r_{k+1}^4}$$

where

$$\partial\left(r_{k+1}^2\right) = \frac{\partial r_{k+1}^2}{\partial \alpha_{k+1}} = 2\left(-p_{kx} \sin(\alpha_{k+1}) + -p_{ky} \cos(\alpha_{k+1})\right)$$

$$\upsilon = (V\Delta t - d_k + d_{k+1})$$

Making (7.14) equal to 0 we can find the angle that makes the determinant of FIM_{k+1} maximum. It can be seen that although (7.14) depends only on α_{k+1} and an analytical solution may be defined from this equation, the computation of the optimal solution is not immediate. In a practical situation, the optimal value of α_{k+1} can be obtained by using the gradient of the FIM determinant, i.e., to use (7.14) at the current sensor position to define the movement direction. In fact, the solution that the gradient provides is very close to the one given by the analytical procedure.

Some examples of optimal sensor trajectories for a static target position are now studied for different values of the velocity of the single tracker, the sampling time or the number of points with which the FIM is constructed.

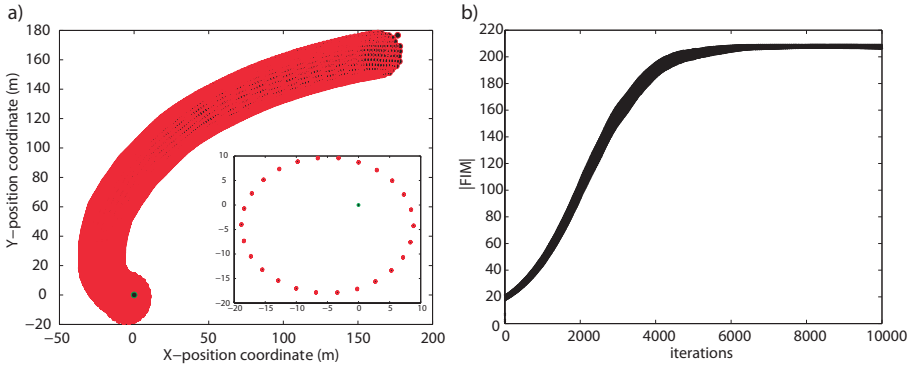

Figure 7.2: (a) Trajectory followed by the sensor to reach the optimal trajectory that provides the maximum FIM determinant. In the lower right corner, the final optimal trajectory is shown in detail. (b) FIM determinant computed at each iteration of the algorithm, i.e., for each new measurement point.

7.4.2 Simulation examples

For each of the following examples we consider that the optimal trajectories are computed for $n = 5$ range measurements but the procedure will be very similar for any number of measurements. The sensor starts at the position $p_1 = [170, 170, 200]^T$ m and the target is placed at the origin of the inertial coordinate frame, so that the target is placed at a depth of 200 m.

Example 7.1: $V = 3\ m/s$ and $\Delta t = 3\ s$

In this first example the constant speed $V = 3\ m/s$ and the sampling time $\Delta t = 3\ s$ are considered. In Figure 7.2 (a) the trajectory followed by the sensor during the simulation is shown. It can be noticed how the sensor describes circumferences while it is getting closer to the target position. In the lower right corner of Figure 7.2 (a) we can see the last 100 points of the simulation that correspond to the stationary of the optimal trajectory, i.e., the trajectory that the sensor is repeating if we continue simulating because this trajectory provides the largest accuracy possible for the approach adopted. The values of V and Δt determine the number of points (or equivalently, time) needed to reach the optimal trajectory, as it will be seen in the forthcoming examples. The optimal trajectory is a circumference of 15 meters of radius around the target projection on the horizontal plane, moreover, the size of this circumference depends directly on the sensor speed V, the sampling time Δt, and the number of points n used for the computation of the FIM. It is interesting to comment, although it is not shown, that the radius of the optimal trajectory increases with the number of measurements used for the computation of the FIM. In Figure 7.2 (b) the FIM determinant computed at each iteration of the algorithm is shown. It is easy to notice how the accuracy increases during the simulation because the sensor describes a trajectory closer to the optimal one. After 7000 iterations the FIM determinant has a constant value that means that the sensor has reached its optimal trajectory. ■

Example 7.2: $V = 5\ m/s$ and $\Delta t = 5\ s$

For this example the velocity $V = 5\ m/s$ and the sampling time $\Delta t = 5\ s$ are considered. In this case 2000 points are simulated because the values of V and Δt are larger, and then the optimal trajectory is reached in less iterations than in the previous example.

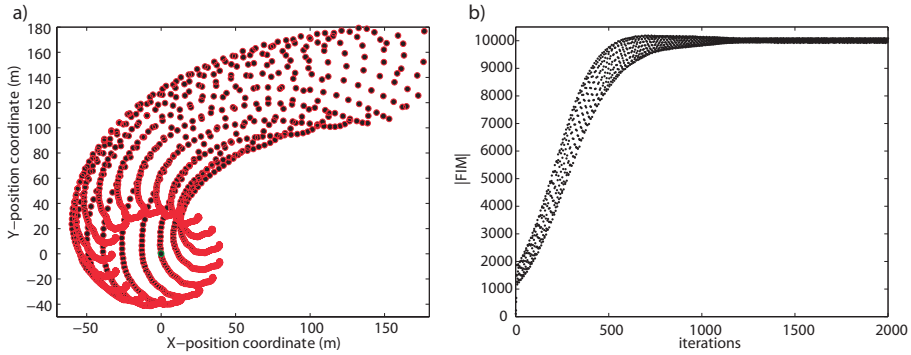

Figure 7.3: (a) Trajectory followed by the sensor to reach the optimal trajectory that provides the maximum FIM determinant. (b) FIM determinant computed at each iteration of the algorithm, i.e., for each new measurement point.

In Figure 7.3 (a) we can observe the trajectory followed by the sensor until the optimal trajectory and the maximum FIM determinant are defined. In this case we can notice how this optimal trajectory is reached in less iterations than in the previous example, in around 1000 iterations. Again we can check how this final trajectory is a circumference around the target projection on the horizontal plane, but the circumference has around 35 meters of radius, in contrast to the 15 meters of the previous example. Thus, with larger values of V and Δt the final trajectory follows a larger circumference and it is computed with less iterations of the algorithm. In Figure 7.3 (b) the FIM determinant computed at each iteration of the algorithm is shown again. The accuracy increases during the simulation because the sensor describes trajectories closer to the optimal one. After approximately 1000 iterations, the FIM determinant has its maximum value, i.e., the sensor has reached its optimal trajectory. In this example, the FIM determinant obtained is quite larger than in the previous example, around 50 times larger, so it shows that it is adequate that V and Δt be large enough so that the optimal trajectory can be followed with a lower number of iterations and it provides larger positioning accuracy (FIM determinant). Of course, the election of V, Δt and n will be mission-dependent. ■

7.4.3 Optimal trajectory

In this approach, we now determine the optimal trajectory to be followed by the sensor so that the next n range measurements maximize the positioning accuracy of the underwater target. Therefore, in contrast to the previous approach, the whole trajectory of n points is optimized and we have a new target position estimate each $n \cdot \Delta t$ seconds. The same assumptions about the sensor speed V, sampling time Δt, target q, and noise ω still hold for the scenario at hand, the only difference is that the optimization procedure deals with n range measurements to be computed, not just one.

The solution may be computed analytically from the derivatives of the FIM determinant with respect to the angles α_i, $i = 2, \cdots, n$, that determine the distance and relative orientation of two consecutive measurements. It is clear that, considering that the initial sensor position is known, we have $n-1$ variables α_i, $i = 2, \cdots, n$, and $n-1$ derivatives with respect to these angles α_i, so that we have an equation system with the same number of equations and unknowns. The complexity of this approach resides in the fact that the process to obtain the solution of this equation system is complex and tedious. Moreover, we must resort to numerical methods to solve it. Therefore,

the commented derivatives are used for a gradient optimization algorithm. These derivatives can be defined, similarly to the previous section, as follows,

$$\frac{\partial |FIM|}{\partial \alpha_i} = \sum_{j,k}^{3} (-1)^{j+k} |Adj_{j,k}(FIM)| \cdot \frac{\partial FIM(j,k)}{\partial \alpha_i} \tag{7.15}$$

where $|Adj_{j,k}(FIM)|$ is the determinant of the adjoint matrix of the FIM with respect to the element (j,k). Details are omitted but the procedure is very similar to that explained in Section 7.4.1. The optimal solution is obtained with a gradient optimization algorithm with the Armijo rule. As it will be explained in the forthcoming examples, it is interesting to notice that this approach provides optimal trajectories very similar to those obtained in the previous examples. The difference lies in that, for the approach at hand, the optimal trajectories are defined in quite less iterations of the algorithm, and then, in a practical situation, the optimal trajectory would be reached faster.

At this point, it is interesting to mention that if the values of V, Δt and n are the optimal ones for the target depth so that the maximum theoretical FIM determinant can be obtained, the same solution defined in Chapter 4 for surface sensor networks is recovered.

7.4.4 Simulation examples

Now some examples of optimal sensor trajectories are studied. For comparison purposes with Section 7.4.2, the number of range measurements with which the FIM is computed will be $n = 5$, but the procedure would be very similar for any number of measurements. The initial sensor position is $p_1 = [170, 170, 200]^T$ m and the target is placed at the origin of the inertial coordinate frame, at a depth of 200 m. For each iteration of the algorithm explained above, the first point of the new trajectory of 5 points is the last one of the previous iteration, so for each iteration the next 4 measurement points are planned. The algorithm is recursively executed 30 times, so 120 points are computed. Although this algorithm needs less iterations to compute the optimal trajectory, and this trajectory is reached with less measurement points, the computation of the solution is more complex.

Example 7.3: $V = 3\ m/s$ and $\Delta t = 3\ s$

A constant speed $V = 3\ m/s$ and a sampling time $\Delta t = 3\ s$ are considered. In Figure 7.4 (a) the trajectory followed by the sensor is shown. In this case the final trajectory is reached faster compared to the result obtained in Example 7.1. We can notice how the optimal trajectory is not exactly a circumference, the optimal measurement points are concentrated in two concentric circumferences around the target projection, and the sensor moves between them in the optimal trajectory. However, their size is very close to that of the circumference of Example 7.1. In the left upper corner of Figure 7.4 (a) the optimal trajectory is shown for the last 80 measurement points.

In Figure 7.4 (b) the FIM determinant computed for each of the 30 iterations of the algorithm is shown. We can notice how the maximum FIM determinant obtained is the same of Example 7.1, but it is obtained with less iterations, and in a practical situation, the optimal trajectory would be reached faster. ■

Example 7.4: $V = 5\ m/s$ and $\Delta t = 5\ s$

For this second example the velocity of the sensor and the sampling time are both considered to be equal to 5, being the dual of Example 7.2. In Figure 7.5 (a) it is shown the trajectory followed

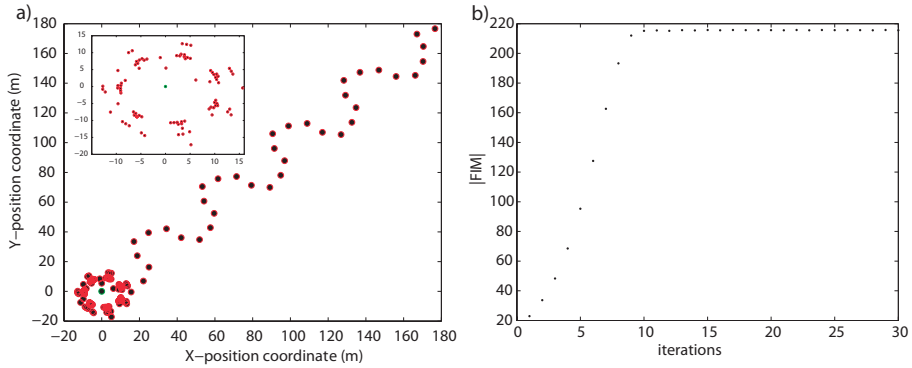

Figure 7.4: (a) Trajectory followed by the sensor to reach the optimal trajectory that provides the maximum FIM determinant. (b) FIM determinant computed at each iteration of the algorithm, i.e., for each new 5 measurement points.

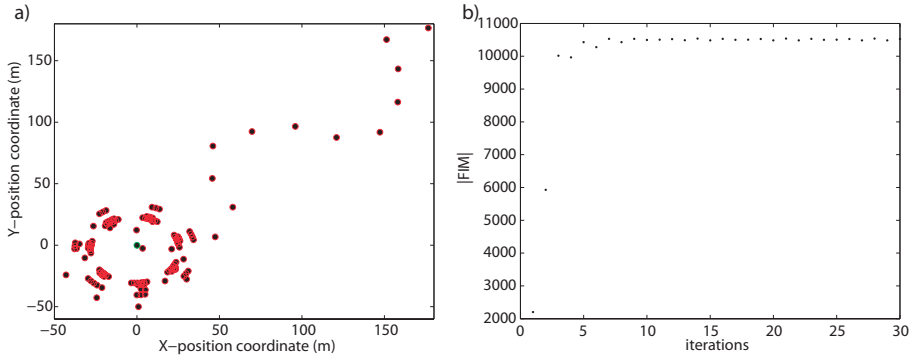

Figure 7.5: (a) Trajectory followed by the sensor to reach the optimal trajectory that provides the maximum FIM determinant. (b) FIM determinant computed at each iteration of the algorithm, i.e., for each new 5 measurement points.

by the sensor. We can notice again how the final trajectory is not a circumference, and the sensor moves between 2 circumferences. Again, this optimal trajectory is computed in less iterations than in Example 7.2, so in a practical scenario the maximum accuracy would be obtained faster and with less iterations of the optimization algorithm. Compared to the above Example 7.3, the final trajectory defines circumferences of a larger radius, similarly to what happened in the examples of Section 7.4.1. In Figure 7.5 (b) The FIM determinant obtained for each iteration of the algorithm is shown. We can notice how the FIM determinant is larger than in the previous example, so for larger values of V and Δt the determinant of the FIM increases too. Moreover, the maximum FIM determinant is obtained in less iterations of the algorithm. Again the accuracy is similar to that obtained in Example 7.2, but the optimal trajectory is computed with a very significant less number of algorithm iterations and measurement points. ■

Therefore we can conclude that, for a static target, although both approaches provide the same maximum FIM determinant and therefore the same positioning accuracy for similar mission constraints, the latter approach computes the optimal trajectory in less iterations, and the optimal

trajectory is reached with a few sensor movements and less measurement points. Despite of this, this algorithm is more complex to implement and the computation of the optimal solution may take more time than in the first approach, whose implementation is quite easier and faster.

7.5 Moving target positioning

The previous scenario is now extended to the problem of positioning an underwater target that is not static. The target is considered to be moving in a straight line with a constant velocity, which must be slower than that of the sensor. The latter assumption is a necessary condition so that the sensor be able to track the target correctly. The two above different approaches are studied, i) when the next best measurement is computed and then the FIM is updated with this new range measurement deleting the oldest one, and ii) when the trajectory for a given number n of future measurements is planned to be optimal.

7.5.1 Next optimal range measurement

In this approach the immediate next measurement that maximizes the accuracy is computed, considering a limited number of range measurements with which the FIM is computed, similarly as it was studied in Section 7.4.1 for a static target. To obtain a good positioning accuracy the sensor speed must be quite larger than the target one, moreover, as it will be studied in Section 7.5.3, planning the trajectory for a given number of measurements, instead of just the next one, provides a much better solution.

The target position is now defined by $q = [V_t \cdot \Delta t, 0, 0]^T \ m$, where V_t is the target speed. With this assumption the FIM becomes,

$$FIM = \frac{1}{\sigma^2} \sum_{i=1}^{n} \begin{pmatrix} (u_{i,x})^2 & \left(u_{i,y}\right)(u_{i,x}) & (u_{i,z})(u_{i,x}) \\ (u_{i,x})\left(u_{i,y}\right) & \left(u_{i,y}\right)^2 & (u_{i,z})\left(u_{i,y}\right) \\ (u_{i,x})(u_{i,z}) & \left(u_{i,y}\right)(u_{i,z}) & (u_{i,z})^2 \end{pmatrix} \tag{7.16}$$

where $u_{ij} = \frac{\partial \|q_i - p_i\|}{\partial q_{i,j}}$, for $i \in \{1, ..., n\}$ and $j \in \{x, y, z\}$, and q_i corresponds to the target position at the moment in which the measurement i is taken, i.e, the position in which the target sends the acoustic signal to the surface sensor. The next measurement point is defined as in previous sections:

$$p_{k+1} = \begin{bmatrix} p_k + (V\Delta t - d_k + d_{k+1})\cos(\alpha_{k+1}) \\ p_k + (V\Delta t - d_k + d_{k+1})\sin(\alpha_{k+1}) \\ q_z \end{bmatrix}^T$$

Again, we opted for a recursive procedure to compute the derivative of the new FIM determinant with respect to the new direction angle α_{k+1}. The matrix FIM_k^* is the FIM computed with the current n known range measurement except the oldest one, and FIM_{k+1} is the FIM computed by adding the new range measurement to FIM_k^*. Then the updated and unknown optimal FIM yields,

$$FIM_{k+1} = FIM_k^* + FIM'_{k+1} \tag{7.17}$$

where

$$FIM'_{k+1} = \frac{1}{\sigma^2}\sum_{i=1}^{n}\begin{pmatrix} (u_{i,x})^2 & (u_{i,y})(u_{i,x}) & (u_{i,z})(u_{i,x}) \\ (u_{i,x})(u_{i,y}) & (u_{i,y})^2 & (u_{i,z})(u_{i,y}) \\ (u_{i,x})(u_{i,z}) & (u_{i,y})(u_{i,z}) & (u_{i,z})^2 \end{pmatrix} \tag{7.18}$$

with $i = k + 1$. Thus the problem to solve can be cast as

$$\alpha^*_{k+1} = arg\max_{\alpha_{k+1}} |FIM_{k+1}| \tag{7.19}$$

The derivative of (7.19) with respect to α_{k+1} can be computed by decomposing the determinant by its adjoints:

$$\frac{\partial |FIM_{k+1}|}{\partial \alpha_{k+1}} = \sum_{i,j}^{n}(-1)^{i+j}|Adj_{i,j}(FIM_{k+1})| \cdot \Theta(i,j) \tag{7.20}$$

where $\Theta(i,j) = \frac{\partial FIM_{k+1}(i,j)}{\partial \alpha_{k+1}}$, and $|Adj_{i,j}(FIM_{k+1})|$ is the determinant of the adjoint matrix of FIM_{k+1} with respect to the element (i,j). The derivatives of each FIM_{k+1} element with respect to α_{k+1} are actually the derivatives of each element of FIM'_{k+1} with respect to α_{k+1}. These derivatives are computed as explained in Section 7.4.1, so the details are omitted to avoid tedious repetition of the same arguments. An analytical solution may be defined but we opted to use the gradient (7.20) to define the sensor movements for simplicity reasons.

It is important to remark that this approach is useful and provides good results when the sensor speed V is quite larger than the target velocity, V_t. If the difference is not significant enough, then the present approach will not be adequate, and planning the optimal trajectory would be a much better approach, as it is studied in the next examples.

7.5.2 Simulation examples

Different examples are now studied to show the performance of the above algorithm when a moving target must be localized. Similarly to the examples seen in Section 7.4, a constant speed $V = 5\ m/s$ and a sampling time $\Delta t = 5\ s$ are considered. The initial sensor position is $p_1 = [170, 170, 200]^T\ m$ and the target is initially placed at the origin of the inertial coordinate frame, at a depth of 200 m. The algorithm is run for the next 5000 points, so 5000 iterations are carried out.

Example 7.5: $V_t = 0.1\ m/s$, $V = 5\ m/s$ and $\Delta t = 5\ s$

The target moves with a constant speed $V_t = 0.1\ m/s$ along the $\{x_I\}$-axis. In Figure 7.6 (a) we can see the trajectory described by the sensor to maximize the positioning accuracy and how the sensor tracks the target movements describing circumferences around its projection on the horizontal plane. It is interesting how the optimal trajectory described by the sensor is very similar to that shown in Example 7.2 for a static target, with the difference that in the example at hand, the optimal trajectory is moving accordingly to the target displacement. In the capture of the upper right corner of Figure 7.6 (a), the trajectory for the last 100 simulated points is shown to demonstrate how the sensor is moving around the target position. As aforementioned, this good result is possible due to V is much larger than V_t. In Figure 7.6 (b) the FIM determinant obtained for each iteration of the algorithm is shown. We can notice how the FIM determinant is very close to the value obtained for a static target in Example 7.2, but in this case the final value is not a fix value, it is within a range of values due to the target and sensor movements. We can see how the optimal trajectory is reached in around 2000

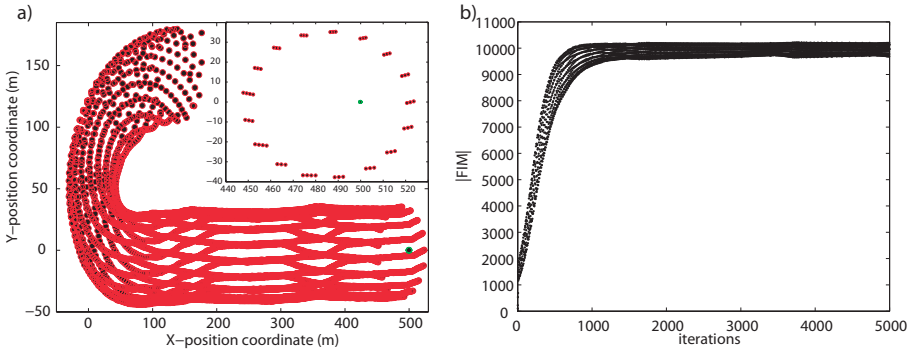

Figure 7.6: (a) Trajectory followed by the sensor to reach the optimal trajectory that provides the maximum FIM determinant. (b) FIM determinant computed at each iteration of the algorithm.

iterations of the optimization algorithm. ■

Example 7.6: $V_t = 1\ m/s$, $V = 5\ m/s$ and $\Delta t = 5\ s$

This example aims at showing the problem presented by this approach when the target velocity increases, so the difference between target and sensor speeds is reduced. Now the target speed is ten times larger than in the previous example, but five times smaller than that of the sensor. There is still a great difference between speeds but the sensor does not behave well as it has no reaction margin to compensate the target movements, so it cannot follow a correct trajectory. Henceforth, this approach is not adequate for this particular case.

In Figure 7.7 (a) we can see the trajectory described by the sensor. In the upper right corner of Figure 7.7 (a) the last 100 measurement points are shown in detail. It is interesting how the trajectory described by the sensor diverges from the target trajectory and how it becomes very different from what it could be expected, or what it was obtained in the previous example. The solution obtained comes from the fact that the target speed is very large (or the difference between speeds small) for the approach adopted so that planning only the next measurement is not enough to describe a correct trajectory to track and localize the underwater target. Therefore this approach gives a non-optimal trajectory because the sensor is not able to track the target.

In Figure 7.7 (b) the FIM determinant is shown for each iteration of the algorithm. The FIM determinant has a large initial value compared to the final one. As already mentioned, the sensor trajectory diverges from that of the target, reducing quickly the FIM determinant. Thus, we can conclude that this approach, for the mission constraints considered, is not adequate. ■

Therefore, it is clear that if the target speed is much smaller than the sensor speed this approach provides satisfactory results, but if the difference between those velocities is not significant, the final trajectory is not as accurate as it should be. For this latter scenario, planning the trajectory for the next n future measurements provides a better result, close to the optimal one that would be obtained for a static target.

Example 7.7: $V_t = 1\ m/s$, $V = 5\ m/s$ and $\Delta t = 5\ s$ and 15 measurements.

If we cannot increase the sensor speed or decrease the target speed, and our design constraints

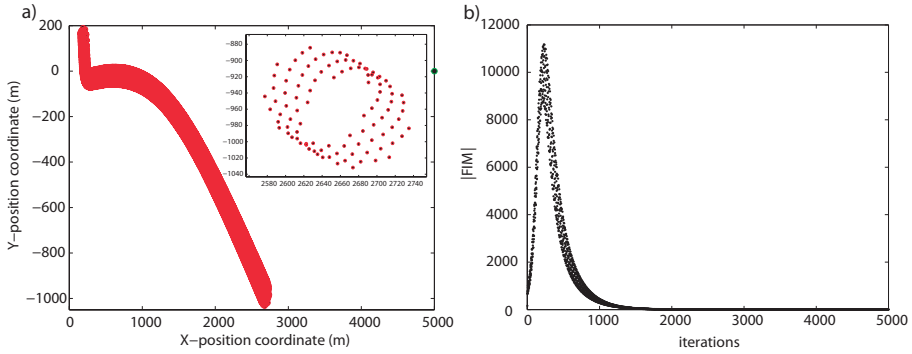

Figure 7.7: (a) Trajectory followed by the sensor trying to obtain the maximum FIM determinant. (b) FIM determinant computed at each iteration of the algorithm.

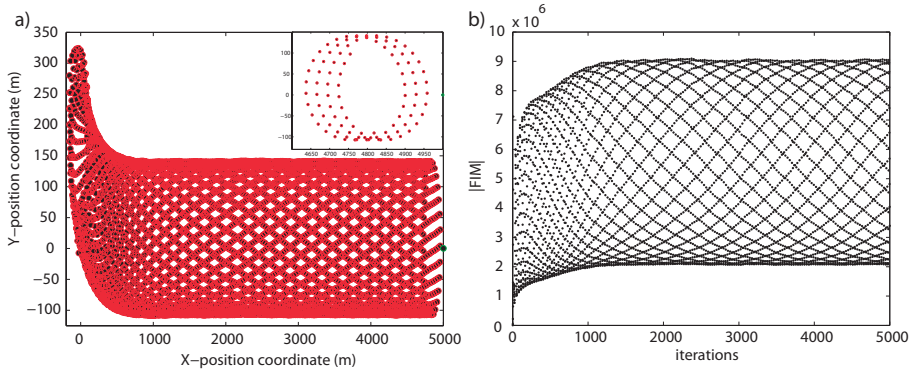

Figure 7.8: (a) Trajectory followed by the sensor to reach the optimal trajectory that provides the maximum FIM determinant. (b) FIM determinant computed for each iteration of the algorithm.

with respect to the target and sensor velocities are similar to those seen on the previous example, a simple manner to (partially) avoid the abovementioned problem is to compute the FIM with a large number of range measurements. By doing so the sensor can describe a larger trajectory and a larger FIM determinant can be obtained. For the example at hand, we consider that the FIM is computed with the last 15 range measurements.

In Figure 7.8 (a) the optimal trajectory is shown. It can be noticed how the trajectory described by the sensor is a sequence of circumferences following the target trajectory. Although this trajectory implies a good positioning accuracy and the sensor is able to track the target, the difference of speeds is still large for this approach and the tracking of the target is not adequately performed. The latter can be seen on the capture of the upper left corner of Figure 7.8 (a), where the last 100 measurement points are shown. It can be seen how the sensor is always behind the target and the circumferences described are not around the target projection on the horizontal plane. The maximum positioning accuracy would be obtained if the sensor was turning around the target, so the target is not tracked with the largest accuracy that could be obtained for 15 range measurements, moreover, this is a very large number of range measurements for the computation of the FIM. In Fig. 7.8 (b) the FIM determinant obtained at each iteration of the optimization algorithm is shown. The accuracy obtained is large and the value is kept within a margin of accuracy during the tracking of the target, although

a large number of measurements is required to obtain this result. Of course, if the variability on the accuracy shown in Fig. 7.8 (b) is tolerable or not will be mission-dependent. ■

Therefore, from the three examples shown it is clear that this approach is only valid when the target moves much slower than the sensor or when the number of measurements used to compute the FIM is very large. In any other case, other strategies are more adequate.

7.5.3 Optimal trajectory

In this scenario we find again an equation system of $n-1$ equations and $n-1$ unknowns if an analytical solution for the set of orientation angles α_i to be defined is searched in a similar manner as in Section 7.4.3. These equations may be easily defined by computing the derivatives of the determinant of (7.16) with respect to the angles α_i, $i = 2, \cdots, n$, in the same way as it was defined in (7.15). Therefore an analytical solution may be defined, although the procedure is complex and it is necessary to resort to numerical methods to find the solution. For the above reason we opted again for a gradient optimization method for the computation of the optimal trajectories. Details are omitted to avoid tedious repetition of the same arguments commented in previous sections and we proceed to the study of some examples.

7.5.4 Simulation examples

The same examples of Section 7.5.2 are now studied for comparison purposes of both methodologies. For this reason, a constant speed $V = 5\ m/s$ and a sampling time $\Delta t = 5\ s$ are considered. The initial sensor position is $p_1 = [170, 170, 200]^T\ m$ and the target is initially placed at the origin of the inertial coordinate frame, at a depth of 200 m.

Example 7.8: $V_t = 0.1\ m/s$, $V = 5\ m/s$ and $\Delta t = 5\ s$

For this first example the target velocity is $V_t = 0.1\ m/s$. In Figure 7.9 (a) the optimal trajectory followed by the sensor to track the target is shown. Similarly to Example 7.6, the sensor tracks adequately the target since there is a great difference of speeds and the trajectory can be planned without problems. In the lower right corner of Figure 7.9 (a) the last 100 measurement points are shown in detail, so we can see how the sensor is describing circumferences around the target position in a similar manner as if the target was in a position fix. In Figure 7.9 (b) the FIM determinant is shown and it can be noticed that the accuracy obtained is larger than in Example 7.5, and it is very close to the one obtained for a static target in Example 7.3. Although for both examples the trajectory followed by the sensor is correct and provides a large positioning accuracy, in this case the FIM determinant is larger because the trajectory is optimized for a given number of measurements, not just one. Moreover, the optimal trajectory is reached in less iterations than in Example 7.5. ■

Example 7.9: $V_t = 1\ m/s$, $V = 5\ m/s$ and $\Delta t = 5\ s$

This second example shows the advantage of using this approach when the target speed is larger, i.e., the difference between target and sensor speeds is smaller. In Figure 7.10 (a) the trajectory described by the sensor to track the target is shown. We can notice how in this example, in contrast to the result of Example 7.6, the sensor adequately tracks the target describing circumferences around the target projection on the horizontal plane, similarly to that obtained in the previous example. In

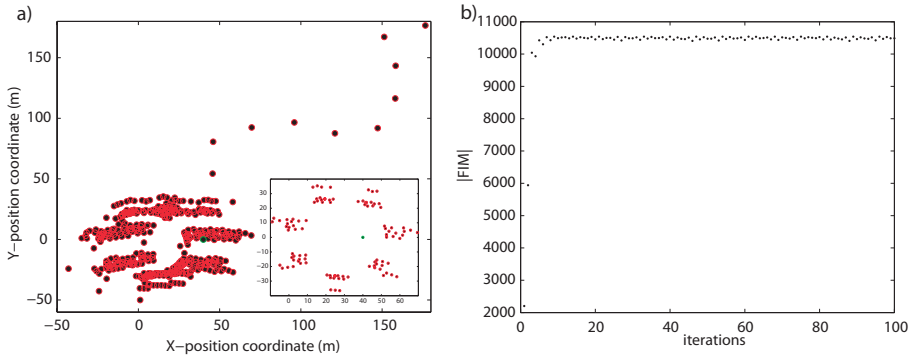

Figure 7.9: (a) Trajectory followed by the sensor to reach the optimal trajectory that provides the maximum FIM determinant. (b) FIM determinant computed at each iteration of the algorithm, i.e., for each new 5 measurement points.

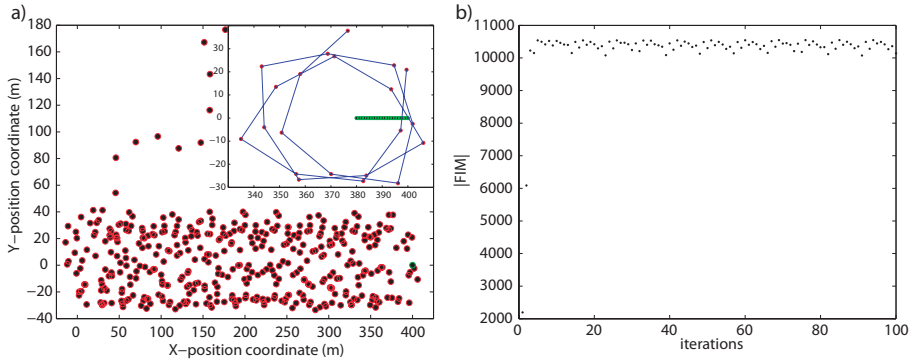

Figure 7.10: (a) Trajectory followed by the sensor to reach the optimal trajectory that provides the maximum FIM determinant. (b) FIM determinant computed at each iteration of the algorithm, i.e., for each new 5 measurement points.

the upper right corner the last 30 measurement points are shown, and these circumferences described by the sensor around the target can be seen in detail. We can notice in Figure 7.10 (b) how the FIM determinant obtained is very similar to the one obtained in the previous example and the one of Example 7.4. Moreover, we can see how the accuracy is much larger than in Example 7.6. ■

Therefore when the target is moving, it is clear that planning a number of future measurement points is a better strategy than planning just the next one, so that a good positioning accuracy can be obtained.

7.6 Conclusions

In this chapter the problem of single underwater target positioning by a single surface sensor has been studied. The analysis of optimal sensor trajectories exploits the spatial and temporal diversity of the measurements taken by the surface sensor and it has been done for two different scenarios,

initially i) for a static target placed at a known position, and then ii) for a mobile target that is moving in a straight line with constant velocity. Two different approaches for the computation of the optimal trajectories have been tested considering a fixed number *n* of range measurements with which the FIM is computed. The first approach deals with the computation of the next measurement point that maximizes the current FIM determinant, and once this optimal point is determined, the sensor is driven to this position in which a new range measurement is taken and the FIM is updated, deleting the oldest range measurement. The second approach optimizes the whole trajectory for the number of range measurements considered, so in contrast to the previous approach, the sensor trajectory is computed each *n* measurements, instead of recomputing it after each new range measurement. The examples showed that for a static target both approaches provide similar accuracies and optimal trajectories. However, for a mobile target, it was clear that the second approach was more reliable, providing a similar solution to that defined for a static target, and with so much larger accuracy than the first approach.

Chapter 8

CONCLUSIONS

This work has addressed several estimation problems relevant to the positioning of underwater targets. The problems however, are also of practical importance in other different fields such as indoor, urban, and space navigation, whenever GPS measurements are not available, or unreliable, and one wants to use an alternative range-based local navigation system. Therefore, the sensor configurations that maximize the estimation accuracy have been theoretically defined to be applied in a practical scenario.

This work offered a characterization of the solutions to the problem of optimal acoustic sensor placement for single target positioning in 2D and 3D spaces, with special emphasis on the application scenario of underwater target positioning in 3D by a surface sensor network.

By assuming that the range measurements between the target and the acoustic sensors were corrupted by white Gaussian noise, the variance of which was distance-dependent, conditions were derived under which a sensor network maximizes the range-related information available for positioning. This was done by exploiting tools from estimation theory whereby the problem to be solved was converted into that of maximizing the determinant of a conveniently defined Fisher Information Matrix (FIM). The core result obtained was an analytic characterization of the conditions that must be met by a generic n sensor network in order for it to be optimal. This result was instrumental in deriving strategies to deal with practical situations where, depending on the mission at hand, the sensor network should satisfy several constraints.

One of the practical scenarios studied was an underwater target positioning, in which the sensor network might be completely underwater or at the surface, or even configured such that a sub-group of sensors is at the sea surface and the remaining sub-group is close to the sea-bottom. The relationship between optimal solutions in 2D and 3D spaces was clarified. It was further shown that the optimal sensor configuration lends itself to an interesting geometrical interpretation and that the spreading of the sensor configuration depends explicitly on the intensity of the range measurement noise and the probabilistic distribution that defines the prior uncertainty in the target position. Examples illustrated the application of the methodology in a number of applications-relevant scenarios.

The previous analysis was extended to the problem of determining the optimal configuration of a sensor network that will, in a well defined sense, maximize the range-related information available for multiple underwater target positioning. To this effect, we assumed again that the

range measurements were corrupted by white Gaussian noise with distance-dependent covariance. In contrast to what has so far been published in the literature, we explicitly addressed the localization problem both in 2D and 3D using a sensor array located in 2D and 3D spaces too. The special scenario of a surface sensor network (2D) was studied for underwater target positioning in the 3D positioning problems. Furthermore, we incorporated directly in to the problem formulation the fact that multiple targets must be simultaneously localized.

At the core of the techniques used are key concepts and methods from Pareto optimization and estimation theory. From a mathematical standpoint, the key problem that we solved was that of maximizing, by proper choice of the sensor geometric configuration, convex combinations of the logarithms of the determinants of the Fisher Information Matrices corresponding to estimation problems for each target separately. This was done by resorting to an iterative optimization algorithm. The methodology developed allowed for an in depth study of the tradeoffs that are inherent to a multiple target localization problem. Simulation examples showed clearly how the optimal sensor location depends on the size of the area in which the targets operate, the type of measurement noise, and the "level of importance" attached to each of the targets; the latter aims to capture the fact that tradeoffs are inevitable, and therefore different levels of accuracy may be required in the localization of the different targets. The analysis was extended to the situation in which the prior knowledge about the targets is described by probability distribution functions and it was shown that the spreading of the sensor configuration depends explicitly on the intensity of the range measurement noise and the probabilistic distribution that defines the prior uncertainty in the target positions.

The special scenario in which the target positioning is performed by angle measurements in 3D was studied as a natural extension of the previous methodology. The measurements of the azimuth and elevation angles were considered to be corrupted by white Gaussian noise, the variance of which was distance-dependent, and conditions were derived under which a sensor network maximizes the angle-related information available for positioning. The optimal formations and conclusions obtained for this problem were very similar to those of the range-measurement problem, so only a brief analysis has been developed to avoid tedious repetition of the same arguments exploited in the range-measurement problems.

Finally the problem of underwater target positioning using a single surface sensor was addressed. For this problem two different approaches were studied. The first one i) when just the next measurement point, and thus the next sensor movement, must be chosen so as the new FIM determinant be maximum considering the past measured ranges, and the second one ii) in which the next n measurements are planned so as they maximize the FIM determinant. Both approaches were studied for a static and a moving target, showing that for a static target both approaches provide similar optimal trajectories; however, for the second approach the optimal trajectory is reached faster. In the case of a moving target, the examples showed that planning the trajectory *a priori* is a much better alternative that implies similar results to those obtained for a static target. For the next best measurement approach, the results were not as accurate as it could be expected, and this approach only provides satisfactory results if the sensor speed is much larger than the target one, or if the FIM is computed with a large number of range measurements. Consequently, it was clear that for a moving target it was necessary to plan the trajectory to obtain a good positioning accuracy.

To sum up, in this work the problem of single and multiple target localization has been studied both in 2D and 3D. Analytical and numerical solutions for optimal sensor placement and optimal sensor trajectory, depending on whether a sensor network or just a single sensor is used, have been defined. Moreover, the problem in which the covariance error can be distance-dependent has been tackled as well. The potential of the methodology developed has been illustrated with multiple

examples for the different problems and scenarios, with special emphasis on the application scenario of underwater target localization by acoustic sensors.

There are several topics that were not addressed in the report and warrant further research.

8.1 Future Work: Multiple Target Tracking and Cooperative Navigation

In the last few years there has been an increasing interest in the use of multiple underwater vehicles to work in cooperative missions and tasks. The use of multiple vehicles presents many potential advantages compared with a single vehicle. For instance, operations such as searching or surveying can be developed in less time, in addition the area coverage can be increased depending on the number of vehicles employed. In this sense, fleets of underwater gliders have started to be used to gather oceanographic data, and groups of AUVs have been used to perform surveying and de-mining missions successfully, showing the potential on using multiple vehicles simultaneously.

Central to these kind of tasks are the navigation capabilities of each vehicle and its navigation systems, that in a classical scenario can be possibly aided with some underwater acoustic positioning system. This scenario can be improved in a great manner if inter vehicle communications and ranging are used in order to increase the overall group navigation performance. A group of underwater robots might be able to navigate with higher precision, as compared to each individual vehicle navigation system, if they can communicate certain information with all the vehicles or with their neighbours.

This leads to the concept of cooperative navigation, where there is a synergy between the navigation systems of the multiple vehicles operating simultaneously, allowing them to navigate better than they would do on their own. There has been some theoretical and experimental works on this direction but it is expected to see many more in the near future, see for example [21], [17], [28], [72], [93]. There are many fundamental theoretical and practical questions that still need to be addressed. Particularly important in the underwater environment is the characterization of the communication requirements in terms of bandwidths and communication topologies that are needed in order to achieve a certain navigation performance [33].

Bibliography

[1] J. S. Abel. Optimal sensor placement for passive source localization. In *Proceedings of the IEEE International Conference on Acoustics, Speech, and Signal Processing, ICASSP*, Albuquerque, NM, 1990.

[2] M. Alam, V. Cevher, J.H. McClellan, G.D. Larson, and W.R. Scott. Optimal Maneuvering of Seismic Sensors for Localization of Subsurface Targets. *IEEE Transactions on Geoscience and Remote Sensing*, vol. 45, num. 5, p. 1247-1257, 2007.

[3] A. Alcocer, P. Oliveira, and A. Pascoal. Study and Implementation of an EKF GIB-based Underwater Positioning System. *IFAC Journal of Control Engineering Practice*, Vol. 15, no. 6, pp. 689-701, Elsevier, 2007.

[4] A. Alcocer. Positioning and Navigation Systems for Robotic Underwater Vehicles. *PhD Thesis*, Instituto Superior Tecnico, Lisbon, Portugal, 2009.

[5] A. Alcocer, P. Oliveira, and A. Pascoal. Underwater Acoustic Positioning Systems Based on Buoys with GPS. In *Proceedings of Eigth European Conference on Underwater Acoustics (ECUA'06)*, Carvoeiro, Portugal, June 2006.

[6] S.E. Aranda, S. Martinez, and F. Bullo. On optimal sensor placement and motion coordination for target tracking. In *Proceedings of the IEEE Int. Conf. on Robotics and Automation (ICRA'05)*, Barcelona, Spain, pages 4544-4549, 2005.

[7] Y. Bar-Shalom, X.R. Li, and T. Kirubarajan. *Estimation with Application to Tracking and Navigation*. John Wiley, New York, NY, 2001.

[8] R. Been, W.L. de Koning, and J.H. de Vlieger. On improving target motion analysis trough own ship maneuvering. *Digital Signal Processing* -91, Elsevier, 1991.

[9] A. Birk, G. Antonelli, A. Caiti, G. Casalino, G. Indiveri, A. Pascoal, and A. Caffaz. The CO3AUVs (COoperative COgnitive COntrol for Autonomous Underwater Vehicles) Project: overview and current progresses. In *Proceedings of OCEANS 2011*, Santander, Spain, 2011.

[10] A.N. Bishop, B. Fidan, B.D.O. Anderson, K. Dogancay, and P.N. Pathirana. Optimality Analysis of Sensor-Target Geometries in Passive Localization: Part 1 - Bearing-Only Localization. In *Proceedings of the 3rd International Conference on Intelligent Sensors, Sensor Networks, and Information Processing (ISSNIP'07)*, pages 7-12, Melbourne, Australia, 2007.

[11] A.N. Bishop, B. Fidan, B.D.O. Anderson, K. Dogancay, and P.N. Pathirana. Optimality Analysis of Sensor-Target Geometries in Passive Localization: Part 2 - Time-of-Arrival Based Localization. In *Proceedings of the 3rd International Conference on Intelligent Sensors, Sensor Networks, and Information Processing (ISSNIP'07)*, pages 13-18, Melbourne, Australia, 2007.

[12] S. Boyd, and L. Vandenberghe. *Convex Optimization*, Cambridge University Press 2004.

[13] D. Carta. Optimal estimation of undersea acoustic transponder locations. In *Proc. OCEANS'78*, volume 10, pages 466–471, 1978.

[14] T. Casey, B. Guimond, and J. Hu. Underwater Vehicle Positioning Based on Time of Arrival Measurements from a Single Beacon. In *Proc. OCEANS 2007*, sept. 29 - Oct. 4, 2007.

[15] J. Chaffee, and J. Abel. GDOP and the Cramer-Rao bound. *in Proc. IEEE Symposium on Position Location and Navigation*, Las Vegas, NV, USA, 1994.

[16] K. Chakrabarty, S.S. Iyengar, H. Qi, and E. Cho. Coding theory framework for target location in distributed sensor networks. In *Proceedings International Conference on Information Technology: Coding and Computing*, pages 130 - 134, 2001.

[17] S.G. Chappell, J.C. Jalbert, P. Pietryka, and J. Duchesney. Acoustic communication between two autonomous underwater vehicles. In *Proc. of the 1994 Symposium on Autonomous Underwater Vehicle Technology (AUV'94)*, pages 462– 469, July 1994.

[18] S.-R. Chioma Ibeawuchi. Optimum sensor placement for source localization and monitoring from received signal strength. *PhD Thesis*, University of Iowa, 2010.

[19] F. Cretollier, and P. Morvan. Use of a Rangemeter in Advanced and Modular Subsea Positioning Solutions. In *Proc. of MCMC2006 - 7th Conference on Manoeuvring and Control of Marine Craft*, Lisbon, Portugal, 2006.

[20] Y. Cui, and S.S. Ge. Autonomous vehicle positioning with gps in urban canyon environments. *IEEE Transactions on Robotics and Automation*, 19:15–25, February 2003.

[21] J. Curcio, J. Leonard, J. Vaganay, A. Patrikalakis, A. Bahr, D. Battle, H. Schmidt, and M. Grund. Experiments in Moving Baseline navigation using autonomous surface craft. In *Proc. IEEE OCEANS'05*, Washington, D.C., 2005.

[22] N.O. Cunha, and E. Polak. Constrained Minimization under Vector-Valued Criteria in Topological Spaces. *Math. Theory Contr., Proc. USC Conf., A.V. Balakrishnan and L. W. Neustad*, Eds. New York: Academic, pp. 96-108, 1967.

[23] S. Dasgupta S. Dandach, B. Fidan, and B. Anderson. Adaptive Source Localization by Mobile Agents. In *Proceedings of the 45th IEEE Conference on Decision and Control (CDC'06)*, San Diego, USA, pages 2045–2050, December 2006.

[24] J.E. Dennis, and R.B. Schnabel. *Numerical Methods for Unconstrained Optimization and Nonlinear Equations*. SIAM, 1996.

[25] K. Dogancay, and H. Hmam. On optimal sensor placement for time-difference-of-arrival localization utilizing uncertainty minimization. In *Proceedings of 17th European Signal Processing Conference (EUSIPCO 2009)* Glasgow, Scotland, August 24-28, 2009.

[26] R. Eustice, L. Whitcomb, H. Singh, and M. Grund. Experimental Results in Synchronous-Clock One-Way-Travel-Time AcousticNavigation for Autonomous Underwater Vehicles. In *Proc. of the 2007 IEEE International Conference on Robotics and Automation (ICRA'07)*, Roma, Italy, April 2007.

[27] N. Fairfield, G. Kantor, and D. Wettergreen. Real-time slam with octree evidence grids for exploration in underwater tunnels. *Journal of Field Robotics, Special Issue on SLAM in the Field*, 24(1-2):03–21, February 2007.

[28] E. Fiorelli, N.E. Leonard, P. Bhatta, D. Paley, R. Bachmayer, and D.M. Fratantoni. Multi-AUV Control and Adaptive Sampling in Monterey Bay. *IEEE Journal of Oceanic Engineering*, 31(4):935–948, October 2006.

[29] A. Gadre. Observability Analysis in Navigation Systems with an Underwater Vehicle Application. *PhD thesis*, Virginia Polytechnic Institute and State University, January 2007.

[30] A. Gadre, and D. Stilwell. Toward Underwater Navigation Based on Range Measurements From a Single Location. In *Proc. IEEE International Conference on Robotics and Automation (ICRA'04)*, New Orleans, LA, pages 4472–4477, 2004.

[31] A. Gadre, and D. Stilwell. A Complete Solution to Underwater Navigation In the Presence of Unknown Currents Based On Range Measurements From a Single Location. In *Proceedings of the IEEE/RSJ International Conference on Intelligent Robotics and Systems (IROS'05)*, Edmonton AB, Canada, 2005.

[32] R. Ghabcheloo, A. Aguiar, A. Pascoal, C. Silvestre, I. Kaminer, and J. Hespanha. Coordinated path-following in the presence of communication losses and time delays. *SIAM - Journal on Control and Optimization*, Vol. 48, No. 1, pp. 234-265, 2009.

[33] R. Ghabcheloo, A. Aguiar, A. Pascoal, and C. Silvestre. Coordinated pathfollowing control of multiple auvs in the presence of communication failures and time delays. In *Proc. of MCMC2006 - 7th Conference on Manoeuvring and Control of Marine Craft*, Lisbon, Portugal, 2006.

[34] R.I. Hartley, and P. Sturm. Triangulation. *Computer Vision and Image Understanding*, Volume 68, Issue 2, November 1997, Pages 146-157.

[35] J. Hartsfield. Single transponder range only navigation geometry (strong) applied to remus autonomous under water vehicles. *Master's thesis*, Massachusetts Institute of Technology and the Woods Hole Oceanographic Institution, August 2005.

[36] M. Hawkes, and A. Nehorai. Acoustic vector-sensor beamforming and capon direction estimation. *IEEE Trans. on Signal Processing*, Vol. 46, nº9, September 1998.

[37] K.B. Howell. *Principles of Fourier Analysis.* CRC Press, 2001.

[38] M.M. Hunt, W.M. Marquet, D.A. Moller, K.R. Peal, W.K. Smith, and R.C. Spindell. An Acoustic Navigation System. *Technical Report WHOI-74-6*, Woods Hole Oceanographic Institution, Woods Hole, Massachusetts 02543 USA, December 1974.

[39] J.T. Isaacs, D.J. Klein, and J.P. Hespanha. Optimal sensor placement for time difference of arrival localization. In *Proceedings of the 48th IEEE Conference on Decision and Control (CDC'09)*, Shanghai, 2009.

[40] S. Jesus, M. Porter, Y. Stephane, X. Demoulin, O. Rodriguez, and E. Coelho. Single Hydrophone Source Localization. *IEEE Journal of Oceanic Engineering*, 25(3):337–346, 2000.

[41] J. Jouffroy, and J. Reger. An algebraic perspective to single-transponder underwater navigation. In *Proc. of the 2006 IEEE International Conference on Control Applications (ICCA'06)*, Munich, Germany, October 2006.

[42] D.B. Jourdan, and N. Roy. Optimal Sensor Placement for Agent Localization. *ACM Transactions on Sensor Networks (TOSN)*, Volume 4,Article No. 13, 2008.

[43] S. Kamath, E. Meisner, and V. Isler. Triangulation Based Multi Target Tracking with Mobile Sensor Networks. *In IEEE Int. Conf. on Robotics and Automation (ICRA'07)*, Roma, Italy, pages 4544-4549, April 2007.

[44] K.W.K. Lui, and H.C. So. A study of two-dimensional sensor placement using time-difference-of-arrival measurements. Digital Signal Processing 19, 2009.

[45] P. Khargonekar, and M. Rotea. Multiple Objective Optimal Control of Linear Systems: The Quadratic Norm Case. *IEEE Transactions on Automatic Control*, Vol. 36, No.1, January 1991, pp. 14-24.

[46] J.C. Kinsey, R. Eustice, and L.L. Whitcomb. Survey of Underwater Vehicle Navigation: Recent Advances and New Challenges. In *Proc. of MCMC2006 -7th Conference on Manoeuvring and Control of Marine Craft*, Lisbon, Portugal, 2006.

[47] A.M. Ladd, K.E. Bekris, A.P. Rudys, D.S. Wallach, and L.E. Kavraki. On the feasibility of using wireless ethernet for indoor localization. *IEEE Transactions on Robotics and Automation*, 20:555–559, June 2004.

[48] C. LaPointe. Virtual long baseline (vlbl) autonomous underwater vehicle navigation using a single transponder. *Master's thesis*, Massachusetts Institute of Technology and the Woods Hole Oceanographic Institution, June 2006.

[49] M.B. Larsen. Autonomous Navigation of Underwater Vehicles. *PhD thesis*, Department of Automation, Technical University of Denmark, February 2001.

[50] M.B. Larsen. Synthetic long baseline navigation of underwater vehicles. In *Proc. IEEE OCEANS'00*, Providence, RI, USA, pages 2043–2050, September 2000.

[51] J. Leonard, A. Bennett, C. Smith, and H. Feder. Autonomous underwater vehicle navigation. *MIT Marine Robotics Laboratory Technical Memorandum* 98-1. 1998.

[52] N. Levanon. Lowest GDOP in 2-D scenarios. *IEE Proceedings-Radar, Sonar and Navigation* vol.147, no.3, pp.149-155, 2000.

[53] T. Li, and A. Nehorai. Maximum likelihood direction-of-arrival estimation of underwater acoustic signals containing sinusoidal components. *IEEE Trans. on Signal Processing*, Volume 59, Issue: 11, 5302 - 53141, 2011 .

[54] J.R. Magnus, and H. Neudecker. *Matrix Differential Calculus With Applications in Statistics and Econometrics*. Wiley Series in Probability and Statistics, Chichester, 1988.

[55] Martinez, S. and Bullo, F. Optimal Sensor Placement and Motion Coordination for Target Tracking. *Automatica*, 42(4):661–668, 2006.

[56] J.B. McKay, and M. Pachter. Geometry optimization for GPS navigation. *in Proc. IEEE Conference on Decision and Control (CDC'97)*, San Diego, CA, USA, 1997.

[57] D.L. Midlebrook. Bearing-Only Tracking Automation for a Single Unmanned Underwater Vehicle. *Master Thesis*, Department of Mechanical Engineering, Massachusetts Institute of Technology, 2007.

[58] P. H. Milne. *Underwater Acoustic Positioning Systems*. Gulf Publishing, Houston, 1983.

[59] A. R. Mohan Rao, and G. Anandakumar. Optimal placement of sensors for structural system identification and health monitoring using a hybrid swarm intelligence technique. *Smart Mater. Struct.* 16, 2007.

[60] M.C. Moreau, E.P. Davis, J.R. Carpenter, D. Kelbel, G.W. Davis, and P. Axelrad. Results from the gps flight experiment on the high earth orbit amsatoscar-40 spacecraft. In *Proceedings of the ION GPS*, 2002.

[61] D. Moreno-Salinas, A. Pascoal, A. Alcocer, and J. Aranda. Optimal Sensor Placement for Underwater Target Positioning with Noisy Range Measurements. In *Proceedings of the 8th IFAC Conference on Control Applications in Marine Systems, CAMS 2010*, Rostock, Germany, 2010.

[62] D. Moreno-Salinas, A. Pascoal, and J. Aranda. Optimal Sensor Placement for Underwater Positioning with Uncertainty in the Target Location. *2011 IEEE International Conference on Robotics and Automation (ICRA 2011)*, Shanghai, China, 2011.

[63] D. Moreno-Salinas, A. Pascoal, and J. Aranda. Optimal Sensor Placement for Multiple Underwater Target Localization with Acoustic Range Measurements. *2011 IFAC World Congress*, Milano, Italy, 2011.

[64] D. Moreno-Salinas, A. Pascoal, and J. Aranda. Surface Sensor Networks for Underwater Vehicle Positioning with Bearings-Only Measurements. *2012 IEEE/RSJ International Conference on Intelligent Robots and Systems (IROS 2012)*, Vila-Moura, Portugal, 2012.

[65] M. Morgado, P. Oliveira, C. Silvestre, and J. Vasconcelos. USBL/INS Integration Technique for Underwater Vehicles. In *In Proc. of MCMC2006 - 7th Conference on Manoeuvring and Control of Marine Craft*, Lisbon, Portugal, 2006.

[66] J. Neering, C. Fischer, M. Bordier, and N. Maizi. Optimal sensor configuration for passive position estimation. In *Position, Location and Navigation Symposium, 2008 IEEE/ION*, pages 951 - 960, 5-8, May, 2008.

[67] S. Nordebo, and M. Gustafsson. On the Design of Optimal Measurements for Antenna Near-Field Imaging Problems. *Mathematical modelling of wave phenomena: 2nd Conference on Mathematical Modelling of Wave Phenomena. AIP Conference Proceedings*, Volume 834, pp. 234-249 (2006).

[68] E. Olson, J. Leonard, and S. Teller. Robust range-only beacon localization. In *IEEE Journal of Oceanic Engineering*, 31(4):949–958, October 2006.

[69] Y. Oshman, and P. Davidson. Optimization of observer trajectories for bearings-only target localization. *IEEE Transactions on Aerospace and Electronic Systems*, vol. 35, NO. 3, July 1999.

[70] J.M. Passerieux, and D. Van Cappel. Optimal observer maneuver for bearings-only tracking. *IEEE Transactions on Aerospace and Electronic Systems*, Vol. 34, NO. 5, July 1998.

[71] N. Patwari, A. O. Hero III, and J. A. Costa. Learning Sensor Location from Signal Strength and Connectivity. *Secure Localization and Time Synchronization for Wireless Sensor and Ad Hoc Networks, Advances in Information Security*, Volume 30, Part I, 57-81, 2007.

[72] D. Popaf, A. Sandersont, R. Komerskat, S. Mupparapd, D. Blidberg, and S. Chappelf. Adaptive sampling algorithms for multiple autonomous underwater vehicles. In *Proc. IEEE/OES Autonomous Underwater Vehicles AUV'04*, 2004.

[73] N. Priyantha. The Cricket Indoor Location System. *PhD thesis*, Massachusetts Institute of Technology, June 2005.

[74] J. Rosa. Optimal sensor placement for multiple underwater target positioning. *Master Thesis*, Instituto Superior Tecnico, Lisboa, Portugal, 2011.

[75] A. Ross, and J. Jouffroy. Remarks on the observability of single beacon underwater navigation. In *Int. Symp. on Unmanned Untethered Submersible Technology (UUST'05)*. Durham, NH., 2005.

[76] J. Saude, and P. Aguiar. Single Beacon Acoustic Navigation for an AUV in the Presence of Unknown Ocean Currents. In *Proc. of the 8th IFAC International Conference on Manoeuvring and Control of Marine Craft (MCMC'09)*, Brazil, 2009

[77] A.P. Scherbatyuk. The AUV positioning using ranges from one transponder LBL. In *Proc. OCEANS 95*, 9-12 October, 1995.

[78] A.P. Scherbatyuk, and F.S. Dubrovin. Some algorithms of AUV positioning based on one moving beacon. In *IFAC Workshop on Navigation, Guidance and Control of Underwater Vehicles*, Porto, Portugal, 10-12 April, 2012.

[79] M. Schikora, D. Bender, D. Cremers, and W. Koch. Passive Multi-Object Localization and Tracking Using Bearing Data. In *13th Conference on Information Fusion (FUSION)*, 2010.

[80] R. Sim and N. Roy. Global A-Optimal Robot Exploration in SLAM. In *Proceedings of the 2005 IEEE International Conference on Robotics and Automation, 2005 (ICRA'05)*, pages: 661 - 666, 2005.

[81] S. Smith, and D. Kronen. Experimental results of an inexpensive short baseline acoustic positioning system for AUV navigation. In *Proceedings of MTS/IEEE Conference OCEANS 97*, Halifax, NS, pages 714–720, 1997.

[82] T. Song. Observability of Target Tracking with Range-Only Measurements. *IEEE Journal of Oceanic Engineering*, 24(3):383–387, 1999.

[83] T. Song. Observability of Target Tracking with Bearings-Only Measurements. *IEEE Transactions on Aerospace and Electronic Systems*, Vol. 32, NO. 4, October 1996.

[84] Tao Jia, and R. M. Buehrer. A New Cramer-Rao Lower Bound for TOA-based Localization. 2008.

[85] D. Ucinsky. *Optimal measurement methods for distributed parameter system identification*. CRC Press, 2005.

[86] J. Vaganay, P. Baccou, and B. Jouvencel. Homing by acoustic ranging to a single beacon. In *Proc. IEEE OCEANS'00*, Providence, RI, USA, pages 1457–1461, September 2000.

[87] H.L. Van Trees. *Detection, Estimation, and Modulation Theory, Vol. 1*. Wiley, 2001.

[88] K. Vickery. Acoustic positioning systems. A practical overview of current systems. In *Proceedings of the 1998 Workshop on Autonomous Underwater Vehicles*, Fort Lauderdale, FL, USA., pages 5–17, August 1998.

[89] K. Vickery. Acoustic positioning systems. New concepts-the future. In *Proceedings of the 1998 Workshop on Autonomous Underwater Vehicles*, Fort Lauderdale, FL, USA., pages 103–110, August 1998.

[90] T.L. Vincent, and W.J. Grantham. *Optimality in Parametric Systems*. New York: Wiley, 1981.

[91] M.P. Vitus, and C.J. Tomlin. Sensor Placement for Improved Robotic Navigation. 2010.

[92] L.L. Whitcomb, D.R. Yoerger, and H. Singh. Combined Doppler/LBL Based Navigation of Underwater Vehicles. In *Proc. 11th UUST*, Durham, New Hampshire, USA, August 1999.

[93] R. Williams. Design and experimental evaluation of an autonomous surface craft to support auv operations. *Master's thesis*, Massachusetts Institute of Technology, February 2007.

[94] B. Yang, and J. Scheuing. Cramer-Rao Bound and optimum sensor array for source location from time differences of arrival. In *Proceedings of the IEEE International Conference on Acoustics, Speech, and Signal Processing, 2005 (ICASSP '05)*, pages iv/961 - iv/964 Vol. 4, 18-23, March, 2005.

[95] B. Yang. Different sensor placement strategies for TDOA based localization. In *Proceedings of IEEE International Conference on Acoustics, Speech and Signal Processing (ICASSP'07)*, Volume 2, pages II-1093 - II-1096, 2007.

[96] D. Yoerger, and D. Mindell. Precise navigation and control of an ROV at 2200 meters depth. In *Proceedings of Intervention/ROV 92*, San Diego, USA, June 1992.

[97] J.W. Youngberg. *Method for extending GPS to Underwater Applications*. US Patent 5,119,341, June 2 1992, 1992.

[98] N. Zayats, and D.M. Steinberg. Optimal design of experiments when factors affect detection capability. *Pakistan Journal of Statistics*, Vol.26(1), 15-37, 2010.

[99] H. Zhang. Two-dimensional optimal sensor placement. In *Proceedings of the IEEE Trans. Syst., Man, Cybern.*, 25, 5, 1995.

Appendix A

THE INFORMATION INEQUALITY

In this Appendix it is computed the Fisher Information Matrix when the measurement error is modelled by Gaussian, zero mean additive noise with an added term that depends on the distance between the two objects that exchange range data.

Let $q = [q_x, q_y, q_z]^T$ in 3D, or $q = [q_x, q_y]^T$ in 2D, be the position of an arbitrary target; $p_i = [p_{ix}, p_{iy,}]^T$ or $p_i = [p_{ix}, p_{iy,}, p_{iz}]^T$, with $i = 1, 2, .., n$, the position of the *i-th* acoustic ranging sensor, and ω_i the corresponding measurement noise. Stated mathematically,

$$\omega = (I + \eta\delta(r(q)^\gamma)) \cdot \omega_0 \tag{A.1}$$

where ω is measurement noise, ω_0 is a zero mean Gaussian process $N(0, \Sigma_0)$ with $\Sigma_0 = \sigma^2 \cdot I$, I is the identity matrix, $r(q)$ is the vector of actual ranges (abbv. r), and η and γ are the modelling parameters for the distance-dependent noise component. In the above, δ is the operator *diag*, that either converts a square matrix into a vector consisting of its diagonal elements, or converts a vector into a square diagonal matrix whose diagonal components are the array elements. With these assumptions, the measurement noise covariance matrix is given by

$$\begin{aligned}
\Sigma = E\left\{\omega \cdot \omega^T\right\} &= E\left\{(I + \eta\delta(r(q)^\gamma))\,\omega_0 \cdot \omega_0^T\,(I + \eta\delta(r(q)^\gamma))^T\right\} = \\
&= (I + \eta\delta(r(q)^\gamma))\,E\left\{\omega_0 \cdot \omega_0^T\right\}(I + \eta\delta(r(q)^\gamma))^T = \\
&= (I + \eta\delta(r(q)^\gamma))\sum_0 (I + \eta\delta(r(q)^\gamma)) = \sigma^2\,(I + \eta\delta(r(q)^\gamma))^2
\end{aligned} \tag{A.2}$$

We denote by z_i the measurements of the actual range $r_i(q)$, corrupted by additive noise ω_i. With the above notation, the measurement model adopted is given by

$$z_i = |q - p_i| + \omega_i = r_i(q) + \omega_i \tag{A.3}$$

Stated in simple terms, the FIM captures the amount of information that measured data provide

about an unknown parameter (or vector of parameters) to be estimated. Under known assumptions, the FIM is the inverse of the CRLB, which lower bounds the covariance of the estimation error that can possibly be obtained with any unbiased estimator. Thus, *minimizing the CRLB* may yield (by proper estimator selection) a decrease of uncertainty in the parameter estimation. We therefore focus on the computation of the CRLB (or, equivalently the FIM) for the problem at hand.

Formally, let $\hat{q}(z)$ be any unbiased estimator of q, that is, a mapping $\hat{q} : \Re^n \rightarrow \Re^3$ between the observations z and the target position space such that $E\{\hat{q}\} = q$ for all $q \in \Re^3$, where $E\{\cdot\}$ denotes the average operator. Let $p_q(z)$ be the likelihood function that defines the probability of obtaining the observation z given that the true target position is q. It is well known that under some regularity conditions on $p_q(z)$ the following inequality holds:

$$Cov\{\hat{q}\} \geq FIM(q)^{-1} = CRB(q) \tag{A.4}$$

where

$$Cov\{\hat{q}\} = E\{(\hat{q} - q)(\hat{q} - q)^T\}, \tag{A.5}$$

FIM (q) (often abbreviated simply as FIM) is the Fisher Information Matrix defined as

$$FIM(q) = E\left\{(\nabla_q \log p_q(z))(\nabla_q \log p_q(z))^T\right\}, \tag{A.6}$$

and $CRB(q)$ is the Cramer-Rao Bound matrix. In the above, $\nabla_q \log p_q$ denotes the gradient of the log of the likelihood function with respect to the unknown parameter q. Taking the trace of both sides of the covariance inequality yields

$$var\{\hat{q}\} := tr(Cov\{\hat{q}\}) = tr(E\{(\hat{q} - q)(\hat{q} - q)^T\}) \geq tr(FIM(q))^{-1} \tag{A.7}$$

that sets a lower bound on the mean-square error of any unbiased estimator.

Equipped with the above notation and tools of estimation theory, and following standard procedures, the FIM corresponding to the problem of range-based single target positioning in 2D or 3D can be computed from the likelihood function $p_q(z)$ given by

$$p_q(z) = \frac{1}{(2\pi)^{\frac{n}{2}} |\Sigma|^{\frac{1}{2}}} \exp\left\{-\frac{1}{2}(z - r(q))^T \Sigma^{-1} (z - r(q))\right\} \tag{A.8}$$

where n is the number of receivers, $z = [z_1, z_2, ..., z_n]^T$ consists of n measured ranges, and $r(q)$ are the actual ranges. Taking the logarithm of (A.8) yields

$$\log p_q = -\log\left((2\pi)^{\frac{m}{2}} |\Sigma|^{\frac{1}{2}}\right) - \frac{1}{2}(z - r(q))^T \Sigma^{-1} (z - r(q)) \tag{A.9}$$

At this point it is necessary to introduce some concepts in Matrix Differential Calculus and Derivations to derive (A.9) with respect to q. For this purpose it is necessary to determine the gradient of the function $f : \Re^n \rightarrow \Re$ given by

$$f(x) := \frac{1}{2}(r - r(x))^T \Sigma^{-1} (r - r(x)) \tag{A.10}$$

where Σ is taken as a constant and $r(x) = \begin{bmatrix} r_1(x) & \dots & r_n(x) \end{bmatrix} \in \Re^n$ is the vector of range measurements between x and the landmarks whose coordinates are defined by p_i, i.e., with

components $r_i(x) = \|x - p_i\|$, with $i \in \{1, \cdots, n\}$. The first differential of f yields

$$\begin{aligned} df(x) &= \frac{1}{2} d(r - r(x))^T \Sigma^{-1} (r - r(x)) + \frac{1}{2} (r - r(x))^T \Sigma^{-1} d(r - r(x)) = \\ &= -\frac{1}{2} dr(x)^T \Sigma^{-1} (r - r(x)) - \frac{1}{2} (r - r(x))^T \Sigma^{-1} dr(x) = -(r - r(x))^T \Sigma^{-1} dr(x) \end{aligned} \tag{A.11}$$

The differential of $r(x)$ is given by the differential of its components, $dr(x) = \begin{bmatrix} dr_1(x) & \cdots & dr(x) \end{bmatrix}^T$, $dr_i(x) = d\|x - p_i\|$ where

$$\begin{aligned} d\|x - p_i\| &= d\left((x - p_i)^T (x - p_i)\right)^{\frac{1}{2}} = \frac{1}{2}\left((x - p_i)^T (x - p_i)\right)^{-\frac{1}{2}} d\left((x - p_i)^T (x - p_i)\right) = \\ &= \frac{1}{2r_i(x)} 2(x - p_i)^T dx = \frac{1}{r_i(x)} (x - p_i)^T dx \end{aligned} \tag{A.12}$$

Then,

$$dr(x) = \begin{bmatrix} \frac{1}{r_1(x)} (x - p_1)^T dx \\ \vdots \\ \frac{1}{r_n(x)} (x - p_n)^T dx \end{bmatrix} = \begin{bmatrix} \frac{1}{r_1(x)} & \cdots & 0 \\ \vdots & \ddots & \vdots \\ 0 & \cdots & \frac{1}{r_n(x)} \end{bmatrix} \begin{bmatrix} (x - p_1)^T \\ \vdots \\ (x - p_n)^T \end{bmatrix} dx = \delta(r(x))^{-1} C^T dx \tag{A.13}$$

and

$$df(x) = -(r - r(x))^T \Sigma^{-1} dr(x) = -(r - r(x))^T \Sigma^{-1} \delta(r(x))^{-1} C^T dx \tag{A.14}$$

which has the form $df(x) = a^T dx$. According to the *First Identification Theorem* in [54], the gradient of the MLR cost function is given by

$$\nabla f(x) = -C\delta(r(x))^{-1} \Sigma^{-1} (r - r(x)). \tag{A.15}$$

From the above results and considering that $\nabla_q r(q) = \left[\nabla_q r_1(q) \ldots \nabla_q r_n(q)\right]$,

$$\nabla r_i(q) = \frac{1}{2}(q^T q - 2p_i^T q + p_i^T p_i)^{-\frac{1}{2}}(2q^T - 2p_i^T) = \frac{1}{r_i(q)}(q - p_i)^T = \delta(r)^{-1}(q 1_m^T - p)^T = \delta(r)^{-1} C^T$$

where $C = (q 1_m^T - p) \in \Re^{nxm}$, n is the number of sensors, $m = 3$ in 3D problems and $m = 2$ in 2D problems, and p is the vector with the sensor positions, the latter being defined in $\Re^{nxm}$. Making $\Sigma^{-1} = B^2$, the derivative of (A.9) with respect to q yields

$$\begin{aligned} \nabla_q \log p_q &= -\frac{1}{2} \nabla_q \left[(z - r(q))^T \Sigma^{-1} (z - r(q))\right] = \\ &= (z - r(q))^T \Sigma^{-1} \partial r(q) = (z - r(q))^T B \cdot B \cdot \delta(r)^{-1} C^T \end{aligned} \tag{A.16}$$

It is not necessary to derive B with respect to q because the noise model depends on the actual range, not the measured one. The FIM is computed from the expected value of the covariance matrix

of (A.16):

$$FIM = I(\theta) = E\left\{\nabla_\theta \log p_\theta \cdot \nabla_\theta \log p_\theta^T\right\} = E\left\{C\delta(r)^{-1}B^2\left(z - r(q)\right)\left(z - r(q)\right)^T B^2\delta(r)^{-1}C^T\right\} =$$

$$= C\delta(r)^{-1}B^2 \cdot E\left\{\left(z - r(q)\right)\left(z - r(q)\right)^T\right\} \cdot B^2\delta(r)^{-1}C^T =$$

$$= C\delta(r)^{-1}B^2 \cdot (I + \eta\delta(r^\beta))E\left\{\omega_0\omega_0^T\right\} \cdot (I + \eta\delta(r^\beta))^T B^2\delta(r)^{-1}C^T =$$

$$= C\delta(r)^{-1}B^2 \cdot \sigma^2 \cdot I \cdot (I + \eta\delta(r^\beta))^2 \cdot B^2\delta(r)^{-1}C^T = C(\delta(r)\Sigma\delta(r))^{-1}C^T$$

Then the expression of the FIM yields,

$$FIM = E\left\{\nabla_q \log p_q \nabla_q \log p_q^T\right\} = C\left(\delta(r)\Sigma\delta(r)\right)^{-1}C^T \tag{A.17}$$

Thus the expression of the FIM with distance-dependent covariance is well defined and it has an structure very similar to the one with constant covariance.

Appendix B

PARETO-OPTIMALITY

For the sake of completeness, this Appendix contains a very brief introduction to some key concepts and results on multiobjective optimization and Pareto-optimality. The exposition is largely based on the summary in [45].

Because we are interested in the problem of multi-target positioning, we are naturally led to adopt a multiobjective optimization strategy. We adopt the concept of Pareto optimality introduced below. Let $\mathcal{X}$ be an arbitrary non-empty set and let $f_i : \mathcal{X} \to \mathcal{R}_+ : i = 1, 2, ..., n$ be n nonnegative functionals defined on $\mathcal{X}$. A point $x^0 \in \mathcal{X}$ is said to be Pareto-optimal with respect to the vector-valued criterion $f := (f_1, f_2, ..., f_n)$ if there does not exist $x \in \mathcal{X}$ such that

$$f_i(x) \leq f_i(x^0) \text{ for all } i = 1, 2, ..., n$$

and

$$f_k(x) < f_k(x^0) \text{ for some } k \in 1, 2, .., n$$

From the above it follows that if one wishes to find points $x \in \mathcal{X}$ such that, in some sense, x jointly minimizes all the components of f, then one must examine the Pareto-optimal points. It is interesting to point that in the literature on economics a Pareto-optimal outcome is one such that *no person could be made better off without having someone else worse off.*

When Pareto-optimal solutions do exist, in general they are not unique. The determination of the Pareto-optimal set for a given multiobjective problem plays a key role in that it allows for a thorough study of the tradeoffs involved in the problem at hand. The next scalarization result in [22] is of crucial importance in characterizing this set.

Scalarization result. Suppose that $\mathcal{X}$ is a normed linear space and that each component of $f := (f_1, f_2, ..., f_n)$ is a convex function on $\mathcal{X}$. Let

$$\Lambda := \{\lambda \in \mathcal{R}^n : \lambda_i \geq 0, \lambda_1 + \lambda_2 + ... + \lambda_n = 1\}$$

and for each $\lambda \in \Lambda$ consider the following scalar-valued optimization problem:

$$\inf\{\lambda^T f(x) : x^0 \in \mathcal{X}\} \tag{B.1}$$

Suppose that $x^0 \in \mathcal{X}$ is Pareto-optimal with respect to the vector-valued criterion $f := (f_1, f_2, ..., f_n)$. Then, there exists $\lambda \in \Lambda$ such that x_0 is a solution to the scalar optimization problem above. Conversely, given $\lambda \in \Lambda$ if the scalar optimization problem has at most one solution $x^0 \in \mathcal{X}$, then x^0 is Pareto-optimal with respect to $f(x)$.

The above result yields a powerful methodology to compute all Pareto-optimal points. In this work, the scalar functions f_i are related to the logarithms of the determinants of the Fisher Information Matrices corresponding to each of the targets being localized (notice that we wish to maximize the determinants jointly, rather than minimize them; in this case, however, an obvious modification of the result above applies).

Appendix C

GRADIENT OF THE FIM DETERMINANT

This Appendix contains the derivatives of the logarithm of the FIM determinant with respect to the position coordinates of the $i-th$ sensor used in Chapter 4 and Chapter 5 for the gradient optimization algorithm. For the sake of completeness the FIM is defined again,

$$FIM = C(\delta(r)\Sigma\delta(r))^{-1}C^T \tag{C.1}$$

where $C = (q1_n^T - p) \in \Re^{3xn}$, $1_n \in \Re^{nx1}$ is a vector of 1s, and p is the vector of sensor positions, the latter being defined in $\Re^{3xn}$, and with

$$\Sigma = \sigma^2 \left(I + \eta\delta(r(q)^\gamma)\right)^2 = \delta\left(\sigma^2 \cdot \left(1 + \eta r_1^\gamma\right)^2, \cdots, \sigma^2 \cdot \left(1 + \eta r_n^\gamma\right)^2\right) \tag{C.2}$$

Expanding (C.1) we find,

$$FIM = \frac{1}{\sigma^2}\sum_{i=1}^{n}\begin{pmatrix} \frac{(q_x-p_{ix})^2}{r_i^2}\Gamma_i^2 & \frac{(q_x-p_{ix})(q_y-p_{iy})}{r_i^2}\Gamma_i^2 & \frac{(q_x-p_{ix})(q_z-p_{iz})}{r_i^2}\Gamma_i^2 \\ \frac{(q_x-p_{ix})(q_y-p_{iy})}{r_i^2}\Gamma_i^2 & \frac{(q_y-p_{iy})^2}{r_i^2}\Gamma_i^2 & \frac{(q_y-p_{iy})(q_z-p_{iz})}{r_i^2}\Gamma_i^2 \\ \frac{(q_x-p_{ix})(q_z-p_{iz})}{r_i^2}\Gamma_i^2 & \frac{(q_y-p_{iy})(q_z-p_{iz})}{r_i^2}\Gamma_i^2 & \frac{(q_z-p_{iz})^2}{r_i^2}\Gamma_i^2 \end{pmatrix} \tag{C.3}$$

where $\Gamma_i = 1/\left(1 + \eta r_i^\gamma\right)$ for $i \in \{1, ..., n\}$. For the sake of simplicity the FIM described in (C.3) is rewritten as,

$$FIM = \begin{bmatrix} FIM_{11} & FIM_{12} & FIM_{13} \\ FIM_{12} & FIM_{22} & FIM_{23} \\ FIM_{13} & FIM_{23} & FIM_{33} \end{bmatrix} \tag{C.4}$$

where the meaning of each FIM element is clear from the context.

The FIM determinant can be written now,

$$\begin{aligned} |FIM| =& FIM_{11}FIM_{22}FIM_{33} + 2FIM_{12}FIM_{13}FIM_{23} \\ &- FIM_{23}^2FIM_{11} - FIM_{13}^2FIM_{22} - FIM_{12}^2FIM_{33} \end{aligned} \tag{C.5}$$

and the derivative of its logarithm with respect to ξ, where $\xi = p_{ix}, p_{iy}, p_{iz}$, becomes

$$\frac{\partial \log |FIM|}{\partial \xi_i} = \frac{1}{|FIM|}\frac{\partial |FIM|}{\partial \xi_i} \tag{C.6}$$

where

$$\begin{aligned} \frac{\partial |FIM|}{\partial \xi_i} =& \frac{\partial FIM_{11}}{\partial \xi_i}FIM_{22}FIM_{33} + \frac{\partial FIM_{22}}{\partial \xi_i}FIM_{11}FIM_{33} + \frac{\partial FIM_{33}}{\partial \xi_i}FIM_{22}FIM_{11} + \\ & 2\frac{\partial FIM_{12}}{\partial \xi_i}FIM_{23}FIM_{13} + 2\frac{\partial FIM_{13}}{\partial \xi_i}FIM_{23}FIM_{12} + 2\frac{\partial FIM_{23}}{\partial \xi_i}FIM_{12}FIM_{13} \\ & - \frac{\partial FIM_{11}}{\partial \xi_i}FIM_{23}^2 - 2\frac{\partial FIM_{23}}{\partial \xi_i}FIM_{23}FIM_{11} - \frac{\partial FIM_{22}}{\partial \xi_i}FIM_{13} - \\ & - 2\frac{\partial FIM_{13}}{\partial \xi_i}FIM_{13}FIM_{22} - \frac{\partial FIM_{33}}{\partial \xi_i}FIM_{12} - 2\frac{\partial FIM_{12}}{\partial \xi_i}FIM_{12}FIM_{33} \end{aligned} \tag{C.7}$$

To finalize with the analysis of the derivatives of the log FIM determinant with respect to the sensor position coordinates it only remains to define the derivatives of the elements of the FIM with respect to these variables, so that the whole derivative be defined explicitly. We define next the derivative of each FIM component with respect to p_{ix}, p_{iy}, p_{iz}, respectively.

$$\frac{\partial FIM_{11}}{\partial p_{ix}} = \left(\frac{-2\,(q_x - p_{ix})\left(\left(q_y - p_{iy}\right)^2 + (q_z - p_{iz})^2 \right)}{r_i^4} \right) \cdot \Gamma_i^2 + \frac{(q_x - p_{ix})^2}{r_i^2} \cdot \frac{\partial \Gamma_i^2}{\partial p_{ix}}$$

$$\frac{\partial FIM_{11}}{\partial p_{iy}} = \left(\frac{2\,(q_x - p_{ix})^2 \left(q_y - p_{iy}\right)}{r_i^4} \right) \cdot \Gamma_i^2 + \frac{(q_x - p_{ix})^2}{r_i^2} \cdot \frac{\partial \Gamma_i^2}{\partial p_{iy}}$$

$$\frac{\partial FIM_{11}}{\partial p_{iz}} = \left(\frac{2\,(q_x - p_{ix})^2 (q_z - p_{iz})}{r_i^4} \right) \cdot \Gamma_i^2 + \frac{(q_x - p_{ix})^2}{r_i^2} \cdot \frac{\partial \Gamma_i^2}{\partial p_{iz}}$$

$$\frac{\partial FIM_{22}}{\partial p_{ix}} = \left(\frac{2\left(q_y - p_{iy}\right)^2 (q_x - p_{ix})}{r_i^4} \right) \cdot \Gamma_i^2 + \frac{\left(q_y - p_{iy}\right)^2}{r_i^2} \cdot \frac{\partial \Gamma_i^2}{\partial p_{ix}}$$

$$\frac{\partial FIM_{22}}{\partial p_{iy}} = \left(\frac{-2\left(q_y - p_{iy}\right)\left((q_x - p_{ix})^2 + (q_z - p_{iz})^2\right)}{r_i^4} \right) \cdot \Gamma_i^2 + \frac{\left(q_y - p_{iy}\right)^2}{r_i^2} \cdot \frac{\partial \Gamma_i^2}{\partial p_{iy}}$$

$$\frac{\partial FIM_{22}}{\partial p_{iz}} = \left(\frac{2\left(q_y - p_{iy}\right)^2 \left(q_z - p_{iz}\right)}{r_i^4} \right) \cdot \Gamma_i^2 + \frac{\left(q_y - p_{iy}\right)^2}{r_i^2} \cdot \frac{\partial \Gamma_i^2}{\partial p_{iz}}$$

$$\frac{\partial FIM_{33}}{\partial p_{ix}} = \left(\frac{2\left(q_z - p_{iz}\right)^2 \left(q_x - p_{ix}\right)}{r_i^4} \right) \cdot \Gamma_i^2 + \frac{\left(q_z - p_{iz}\right)^2}{r_i^2} \cdot \frac{\partial \Gamma_i^2}{\partial p_{ix}}$$

$$\frac{\partial FIM_{33}}{\partial p_{iy}} = \left(\frac{2\left(q_z - p_{iz}\right)^2 \left(q_y - p_{iy}\right)}{r_i^4} \right) \cdot \Gamma_i^2 + \frac{\left(q_z - p_{iz}\right)^2}{r_i^2} \cdot \frac{\partial \Gamma_i^2}{\partial p_{iy}}$$

$$\frac{\partial FIM_{33}}{\partial p_{iz}} = \left(\frac{-2\left(q_z - p_{iz}\right)\left(\left(q_x - p_{ix}\right)^2 + \left(q_y - p_{iy}\right)^2\right)}{r_i^4} \right) \cdot \Gamma_i^2 + \frac{\left(q_z - p_{iz}\right)^2}{r_i^2} \cdot \frac{\partial \Gamma_i^2}{\partial p_{iz}}$$

$$\frac{\partial FIM_{12}}{\partial p_{ix}} = \left(\frac{\left(q_y - p_{iy}\right)\left(\left(q_x - p_{ix}\right)^2 - \left(q_y - p_{iy}\right)^2 - \left(q_z - p_{iz}\right)^2\right)}{r_i^4} \right) \cdot \Gamma_i^2 + \frac{\left(q_x - p_{ix}\right)\left(q_y - p_{iy}\right)}{r_i^2} \cdot \frac{\partial \Gamma_i^2}{\partial p_{ix}}$$

$$\frac{\partial FIM_{12}}{\partial p_{iy}} = \left(\frac{\left(q_x - p_{ix}\right)\left(-\left(q_x - p_{ix}\right)^2 + \left(q_y - p_{iy}\right)^2 - \left(q_z - p_{iz}\right)^2\right)}{r_i^4} \right) \cdot \Gamma_i^2 + \frac{\left(q_x - p_{ix}\right)\left(q_y - p_{iy}\right)}{r_i^2} \cdot \frac{\partial \Gamma_i^2}{\partial p_{iy}}$$

$$\frac{\partial FIM_{12}}{\partial p_{iz}} = \left(\frac{2\left(q_x - p_{ix}\right)\left(q_y - p_{iy}\right)\left(q_z - p_{iz}\right)}{r_i^4} \right) \cdot \Gamma_i^2 + \frac{\left(q_x - p_{ix}\right)\left(q_y - p_{iy}\right)}{r_i^2} \cdot \frac{\partial \Gamma_i^2}{\partial p_{iz}}$$

$$\frac{\partial FIM_{13}}{\partial p_{ix}} = \left(\frac{\left(q_z - p_{iz}\right)\left(\left(q_x - p_{ix}\right)^2 - \left(q_y - p_{iy}\right)^2 - \left(q_z - p_{iz}\right)^2\right)}{r_i^4} \right) \cdot \Gamma_i^2 + \frac{\left(q_x - p_{ix}\right)\left(q_z - p_{iz}\right)}{r_i^2} \cdot \frac{\partial \Gamma_i^2}{\partial p_{ix}}$$

$$\frac{\partial FIM_{13}}{\partial p_{iy}} = \left(\frac{2\left(q_x - p_{ix}\right)\left(q_y - p_{iy}\right)\left(q_z - p_{iz}\right)}{r_i^4} \right) \cdot \Gamma_i^2 + \frac{\left(q_x - p_{ix}\right)\left(q_z - p_{iz}\right)}{r_i^2} \cdot \frac{\partial \Gamma_i^2}{\partial p_{iy}}$$

$$\frac{\partial FIM_{13}}{\partial p_{iz}} = \left(\frac{\left(q_x - p_{ix}\right)\left(-\left(q_x - p_{ix}\right)^2 - \left(q_y - p_{iy}\right)^2 + \left(q_z - p_{iz}\right)^2\right)}{r_i^4} \right) \cdot \Gamma_i^2 + \frac{\left(q_x - p_{ix}\right)\left(q_z - p_{iz}\right)}{r_i^2} \cdot \frac{\partial \Gamma_i^2}{\partial p_{iz}}$$

$$\frac{\partial FIM_{23}}{\partial p_{ix}} = \left(\frac{2\left(q_x - p_{ix}\right)\left(q_y - p_{iy}\right)\left(q_z - p_{iz}\right)}{r_i^4} \right) \cdot \Gamma_i^2 + \frac{\left(q_y - p_{iy}\right)\left(q_z - p_{iz}\right)}{r_i^2} \cdot \frac{\partial \Gamma_i^2}{\partial p_{ix}}$$

$$\frac{\partial FIM_{23}}{\partial p_{iy}} = \left(\frac{(q_z - p_{iz})\left(-(q_x - p_{ix})^2 + \left(q_y - p_{iy}\right)^2 - (q_z - p_{iz})^2 \right)}{r_i^4} \right) \cdot \Gamma_i^2 + \frac{\left(q_y - p_{iy}\right)(q_z - p_{iz})}{r_i^2} \cdot \frac{\partial \Gamma_i^2}{\partial p_{iy}}$$

$$\frac{\partial FIM_{23}}{\partial p_{iz}} = \left(\frac{\left(q_y - p_{iy}\right)\left(-(q_x - p_{ix})^2 - \left(q_y - p_{iy}\right)^2 + (q_z - p_{iz})^2 \right)}{r_i^4} \right) \cdot \Gamma_i^2 + \frac{\left(q_y - p_{iy}\right)(q_z - p_{iz})}{r_i^2} \cdot \frac{\partial \Gamma_i^2}{\partial p_{iz}}$$

and finally,

$$\frac{\partial \Gamma_i^2}{\partial p_{ix}} = \frac{2\eta\gamma r_i^{\gamma-2}(q_x - p_{ix})}{\sigma^2 (1 + \eta r^\gamma)^3}$$

$$\frac{\partial \Gamma_i^2}{\partial p_{iy}} = \frac{2\eta\gamma r_i^{\gamma-2}\left(q_y - p_{iy}\right)}{\sigma^2 (1 + \eta r^\gamma)^3}$$

$$\frac{\partial \Gamma_i^2}{\partial p_{iz}} = \frac{2\eta\gamma r_i^{\gamma-2}(q_z - p_{iz})}{\sigma^2 (1 + \eta r^\gamma)^3}$$

Therefore the derivatives of the logarithm of the FIM determinant with respect to p_{ix}, p_{iy}, p_{iz} are well defined and can be used explicitly for the gradient optimization algorithm of Chapter 4 and Chapter 5.

Appendix D

GRADIENT OF THE TRACE OF THE CRLB MATRIX

This Appendix contains the derivatives of the trace of the CRB with respect to the angles α_i and β_i of the $i-th$ acoustic sensor. These derivatives are used in Chapter 6 for the gradient optimization algorithm to determine the optimal sensor placement for single target positioning with AE-measurements with uncertainty in the target location. For the sake of completeness the FIM for AE-measurements is defined again,

$$FIM = E\left\{\nabla_q \log p_q \cdot \nabla_q \log p_q^T\right\} = F^T \Sigma^{-1} F, \tag{D.1}$$

with

$$\Sigma = \delta\left(\left(\sigma_\alpha^2 \cdot (1+\eta r^\gamma)^2, \sigma_\beta^2 \cdot (1+\eta r^\gamma)\right)^T\right) \tag{D.2}$$

and

$$F = \begin{bmatrix} \frac{-\sin(\alpha_1)}{r_1 \cos(\beta_1)} & \frac{\cos(\alpha_1)}{r_1 \cos(\beta_1)} & 0 \\ \frac{-\sin(\beta_1)\cos(\alpha_1)}{r_1} & \frac{-\sin(\beta_1)\sin(\alpha_1)}{r_1} & \frac{-\cos(\beta_1)}{r_1} \\ \vdots & \vdots & \vdots \\ \frac{-\sin(\alpha_n)}{r_n \cos(\beta_n)} & \frac{\cos(\alpha_n)}{r_n \cos(\beta_n)} & 0 \\ \frac{-\sin(\beta_n)\cos(\alpha_n)}{r_n} & \frac{-\sin(\beta_n)\sin(\alpha_n)}{r_n} & \frac{-\cos(\beta_n)}{r_n} \end{bmatrix} \tag{D.3}$$

where $F \in \Re^{2nx3}$, $\Sigma \in \Re^{2nx2n}$, and $CRB = FIM^{-1}$. The sensors are considered to be placed at the sea surface so that the range distance r_i of the $i-th$ sensor can be rewritten as $r_i = q_z/\sin(\beta_i)$, where q_z is the target depth and β_i is the elevation angle, as described in Chapter 6. For the sake of simplicity the FIM described in (D.1) is rewritten as,

$$FIM = \begin{bmatrix} FIM_{11} & FIM_{12} & FIM_{13} \\ FIM_{12} & FIM_{22} & FIM_{23} \\ FIM_{13} & FIM_{23} & FIM_{33} \end{bmatrix} \tag{D.4}$$

where

$$FIM_{11} = \sum_{i=1}^{n}\left(\frac{\sin^2(\alpha_i)\sin^2(\beta_i)}{q_z^2\cos^2(\beta_i)\cdot\sigma^2\cdot\left(1+\eta\left(\frac{q_z}{\sin(\beta_i)}\right)^{\gamma}\right)^2}+\frac{\sin^4(\beta_i)\cos^2(\alpha_i)}{q_z^2\cdot\sigma^2\cdot\left(1+\eta\left(\frac{q_z}{\sin(\beta_i)}\right)^{\gamma}\right)^2}\right)$$

$$FIM_{22} = \sum_{i=1}^{n}\left(\frac{\cos^2(\alpha_i)\sin^2(\beta_i)}{q_z^2\cos^2(\beta_i)\cdot\sigma^2\cdot\left(1+\eta\left(\frac{q_z}{\sin(\beta_i)}\right)^{\gamma}\right)^2}+\frac{\sin^4(\beta_i)\sin^2(\alpha_i)}{q_z^2\cdot\sigma^2\cdot\left(1+\eta\left(\frac{q_z}{\sin(\beta_i)}\right)^{\gamma}\right)^2}\right)$$

$$FIM_{33} = \sum_{i=1}^{n}\left(\frac{\cos^2(\beta_i)\sin^2(\beta_i)}{q_z^2\cdot\sigma^2\cdot\left(1+\eta\left(\frac{q_z}{\sin(\beta_i)}\right)^{\gamma}\right)^2}\right)$$

$$FIM_{12} = \sum_{i=1}^{n}\left(\frac{\sin(\alpha_i)\cos(\alpha_i)\sin^2(\beta_i)}{q_z^2\cos^2(\beta_i)\cdot\sigma^2\cdot\left(1+\eta\left(\frac{q_z}{\sin(\beta_i)}\right)^{\gamma}\right)^2}+\frac{\sin^4(\beta_i)\cos(\alpha_i)\sin(\alpha_i)}{q_z^2\cdot\sigma^2\cdot\left(1+\eta\left(\frac{q_z}{\sin(\beta_i)}\right)^{\gamma}\right)^2}\right)$$

$$FIM_{13} = \sum_{i=1}^{n}\left(\frac{\cos(\beta_i)\sin^3(\beta_i)\cos(\alpha_i)}{q_z^2\cdot\sigma^2\cdot\left(1+\eta\left(\frac{q_z}{\sin(\beta_i)}\right)^{\gamma}\right)^2}\right)$$

$$FIM_{23} = \sum_{i=1}^{n}\left(\frac{\cos(\beta_i)\sin^3(\beta_i)\sin(\alpha_i)}{q_z^2\cdot\sigma^2\cdot\left(1+\eta\left(\frac{q_z}{\sin(\beta_i)}\right)^{\gamma}\right)^2}\right)$$

With the above notation, the trace of the CRB matrix yields

$$tr(CRB) = \frac{FIM_{22}FIM_{33}-FIM_{23}^2}{|FIM|}+\frac{FIM_{11}FIM_{33}-FIM_{13}^2}{|FIM|}+\frac{FIM_{11}FIM_{22}-FIM_{12}^2}{|FIM|} \quad \text{(D.5)}$$

and its derivatives with respect to ξ, where $\xi = \alpha_i, \beta_i$, become

$$\begin{aligned}\frac{\partial tr(CRB)}{\partial \xi_i} =& \left(\frac{\partial FIM_{22}}{\partial \xi_i}FIM_{33}+\frac{\partial FIM_{33}}{\partial \xi_i}FIM_{22}-2\frac{\partial FIM_{23}}{\partial \xi_i}FIM_{23}\right.\\ &+\frac{\partial FIM_{11}}{\partial \xi_i}FIM_{33}+\frac{\partial FIM_{33}}{\partial \alpha_i}FIM_{11}-2\frac{\partial FIM_{13}}{\partial \alpha_i}FIM_{13}+\frac{\partial FIM_{11}}{\partial \xi_i}FIM_{22} \quad \text{(D.6)}\\ &\left.+\frac{\partial FIM_{22}}{\partial \xi_i}FIM_{11}-2\frac{\partial FIM_{12}}{\partial \xi_i}FIM_{12}\right)|FIM|^{-1}+tr(CRB)\cdot\frac{\partial |FIM|}{\partial \xi_i}|FIM|^{-1}\end{aligned}$$

where

$$\frac{\partial |FIM|}{\partial \xi_i} = \frac{\partial FIM_{11}}{\partial \xi_i} FIM_{22} FIM_{33} + \frac{\partial FIM_{22}}{\partial \xi_i} FIM_{11} FIM_{33} + \frac{\partial FIM_{33}}{\partial \xi_i} FIM_{22} FIM_{11}$$

$$+ 2\frac{\partial FIM_{12}}{\partial \xi_i} FIM_{23} FIM_{13} + 2\frac{\partial FIM_{13}}{\partial \xi_i} FIM_{23} FIM_{12} + 2\frac{\partial FIM_{23}}{\partial \xi_i} FIM_{12} FIM_{13}$$

$$- \frac{\partial FIM_{11}}{\partial \xi_i} FIM_{23}^2 - 2\frac{\partial FIM_{23}}{\partial \xi_i} FIM_{23} FIM_{11} - \frac{\partial FIM_{22}}{\partial \xi_i} FIM_{13}$$

$$- 2\frac{\partial FIM_{13}}{\partial \xi_i} FIM_{13} FIM_{22} - \frac{\partial FIM_{33}}{\partial \xi_i} FIM_{12} - 2\frac{\partial FIM_{12}}{\partial \xi_i} FIM_{12} FIM_{33} \tag{D.7}$$

To finalize with the analysis of the derivatives of the trace of the CRB matrix with respect to the angles α_i and β_i it only remains to define the derivatives of the elements of the FIM with respect to these angles, so that the whole derivatives be defined explicitly. We define next the derivative of each FIM component with respect to α_i and β_i, respectively.

$$\frac{\partial FIM_{11}}{\partial \alpha_i} = \left(\frac{2\sin(\alpha_i)\cos(\alpha_i)\sin^2(\beta_i)}{\cos^2(\beta_i)} - 2\sin(\alpha_i)\cos(\alpha_i)\sin^4(\beta_i) \right) \cdot \Gamma_i^2$$

$$\frac{\partial FIM_{11}}{\partial \beta_i} = \left(\frac{2\sin(\beta_i)\sin^2(\alpha_i)}{\cos(\beta_i)} - \frac{2\sin^3(\beta_i)\sin^2(\alpha_i)}{\cos^3(\beta_i)} + 4\sin^3(\beta_i)\cos(\beta_i)\cos^2(\alpha_i) \right) \cdot \Gamma_i^2$$

$$+ \left(\frac{\sin^2(\alpha_i)\sin^2(\beta_i)}{\cos^2(\beta_i)} + \sin^4(\beta_i)\cos^2(\alpha_i) \right) \cdot \frac{\partial \Gamma_i^2}{\partial \beta_i}$$

$$\frac{\partial FIM_{22}}{\partial \alpha_i} = \left(-\frac{2\sin(\alpha_i)\cos(\alpha_i)\sin^2(\beta_i)}{\cos^2(\beta_i)} + 2\sin(\alpha_i)\cos(\alpha_i)\sin^4(\beta_i) \right) \cdot \Gamma_i^2$$

$$\frac{\partial FIM_{22}}{\partial \beta_i} = \left(\frac{2\sin(\beta_i)\cos^2(\alpha_i)}{\cos(\beta_i)} - \frac{2\sin^3(\beta_i)\cos^2(\alpha_i)}{\cos^3(\beta_i)} + 4\sin^3(\beta_i)\cos(\beta_i)\sin^2(\alpha_i) \right) \cdot \Gamma_i^2$$

$$+ \left(\frac{\cos^2(\alpha_i)\sin^2(\beta_i)}{\cos^2(\beta_i)} + \sin^4(\beta_i)\sin^2(\alpha_i) \right) \cdot \frac{\partial \Gamma_i^2}{\partial \beta_i}$$

$$\frac{\partial FIM_{33}}{\partial \alpha_i} = 0$$

$$\frac{\partial FIM_{33}}{\partial \beta_i} = \left(2\sin(\beta_i)\cos^3(\beta_i) - 2\cos(\beta_i)\sin^3(\beta_i) \right) \cdot \Gamma_i^2 + \left(\cos^2(\beta_i)\sin^2(\beta_i) \right) \cdot \frac{\partial \Gamma_i^2}{\partial \beta_i}$$

$$\frac{\partial FIM_{12}}{\partial \alpha_i} = \left(\frac{\left(\cos^2(\alpha_i) - \sin^2(\alpha_i)\right)\sin^2(\beta_i)}{\cos^2(\beta_i)} + \left(\cos^2(\alpha_i) - \sin^2(\alpha_i)\right)\sin^4(\beta_i) \right) \cdot \Gamma_i^2$$

$$\frac{\partial FIM_{12}}{\partial \beta_i} = \Gamma_i^2 \cdot \left(\frac{2\sin(\beta_i)\sin(\alpha_i)\cos(\alpha_i)}{\cos(\beta_i)} + 4\sin^3(\beta_i)\cos(\beta_i)\cos(\alpha_i)\sin(\alpha_i) \right.$$

$$\left. - \frac{2\sin^3(\beta_i)\sin(\alpha_i)\cos(\alpha_i)}{\cos^3(\beta_i)} \right) + \sin(\alpha_i)\cos(\alpha_i)\left(\frac{\sin^2(\beta_i)}{\cos^2(\beta_i)} + \sin^4(\beta_i) \right) \frac{\partial \Gamma_i^2}{\partial \beta_i}$$

$$\frac{\partial FIM_{13}}{\partial \alpha_i} = -\sin^3(\beta_i)\cos(\beta_i)\sin(\alpha_i) \cdot \Gamma_i^2$$

$$\frac{\partial FIM_{13}}{\partial \beta_i} = \cos(\alpha_i)\left(3\sin^2(\beta_i)\cos^2(\beta_i) - \sin^4(\beta_i)\right) \cdot \Gamma_i^2 + \sin^3(\beta_i)\cos(\beta_i)\cos(\alpha_i) \cdot \frac{\partial \Gamma_i^2}{\partial \beta_i}$$

$$\frac{\partial FIM_{23}}{\partial \alpha_i} = -\sin^3(\beta_i)\cos(\beta_i)\cos(\alpha_i) \cdot \Gamma_i^2$$

$$\frac{\partial FIM_{23}}{\partial \beta_i} = \sin(\alpha_i)\left(3\sin^2(\beta_i)\cos^2(\beta_i) - \sin^4(\beta_i)\right) \cdot \Gamma_i^2 + \sin^3(\beta_i)\cos(\beta_i)\sin(\alpha_i) \cdot \frac{\partial \Gamma_i^2}{\partial \beta_i}$$

and finally,

$$\frac{\partial \Gamma_i^2}{\partial \beta_i} = \frac{2\eta\gamma\left(\frac{q_z}{\sin(\beta_i)}\right)^\gamma}{q_z^2\sigma^2\tan(\beta_i)\left(1 + \eta\left(\frac{q_z}{\sin(\beta_i)}\right)^\gamma\right)^3}$$

Therefore the derivatives of the CRB trace with respect to α_i and β_i are well defined and can be used explicitly for the gradient optimization algorithm of Chapter 6 to define optimal sensor networks for underwater positioning with uncertain target location.